DOT-HS-805-370

IMPROVEMENT OF MATHEMATICAL MODELS FOR SIMULATION OF VEHICLE HANDLING

Volume 7: Technical Manual for the General Simulation

R. Garrott
R. A. Scott

College of Engineering
The University of Michigan
Ann Arbor, Michigan 48109

Contract No. DOT HS-7-01715
Contract Amt. $135,900

March 1980
FINAL REPORT

Prepared For
U.S. DEPARTMENT OF TRANSPORTATION
National Highway Traffic Safety Administration
Washington, D.C. 20590

Technical Report Documentation Page

1. Report No.	2. Government Accession No.	3. Recipient's Catalog No.
DOT-HS-805-370		

4. Title and Subtitle	5. Report Date
Improvement of Mathematical Models for Vehicle Handling. Vol. 7. Technical Manual for the General Simulation.	March 1, 1980
	6. Performing Organization Code
7. Author(s)	8. Performing Organization Report No.
W. R. Garrott and R. A. Scott	
9. Performing Organization Name and Address	10. Work Unit No. (TRAIS)
The University of Michigan Ann Arbor, Michigan 48109	11. Contract or Grant No. DOT-HS-7-01715
	13. Type of Report and Period Covered FINAL REPORT 9/30/77 to 4/30/80
12. Sponsoring Agency Name and Address National Highway Traffic Safety Administration U.S. Department of Transportation Trans. Point Bldg., Washington, D.C.	14. Sponsoring Agency Code

15. Supplementary Notes

16. Abstract

This volume is the technical manual for the general simulation. Mathematical modelling of the vehicle and of the human driver is presented in detail, as are differences between the APL simulation and the current one. Information on model validation and operating costs are also given. A comparison between two mathematical models of tire behaviour is made. Extensive output for open and closed loop maneuvers is presented and analyzed.

17. Key Words	18. Distribution Statement
Vehicle Handling. Simulation. Vehicle Modeling.	Document is available to public through the National Technical Information Service, Springfield, VA 22161.

19. Security Classif. (of this report)	20. Security Classif. (of this page)	21. No. of Pages	22. Price
Unclassified	Unclassified	278	

Form DOT F 1700.7 (8-72) Reproduction of completed page authorized

METRIC CONVERSION FACTORS

Approximate Conversions to Metric Measures

Symbol	When You Know	Multiply by	To Find	Symbol
		LENGTH		
in	inches	*2.5	centimeters	cm
ft	feet	30	centimeters	cm
yd	yards	0.9	meters	m
mi	miles	1.6	kilometers	km
		AREA		
in^2	square inches	6.5	square centimeters	cm^2
ft^2	square feet	0.09	square meters	m^2
yd^2	square yards	0.8	square meters	m^2
mi^2	square miles	2.6	square kilometers	km^2
	acres	0.4	hectares	ha
		MASS (weight)		
oz	ounces	28	grams	g
lb	pounds	0.45	kilograms	kg
	short tons (2000 lb)	0.9	tonnes	t
		VOLUME		
tsp	teaspoons	5	milliliters	ml
Tbsp	tablespoons	15	milliliters	ml
fl oz	fluid ounces	30	milliliters	ml
c	cups	0.24	liters	l
pt	pints	0.47	liters	l
qt	quarts	0.95	liters	l
gal	gallons	3.8	liters	l
ft^3	cubic feet	0.03	cubic meters	m^3
yd^3	cubic yards	0.76	cubic meters	m^3
		TEMPERATURE (exact)		
°F	Fahrenheit temperature	5/9 (after subtracting 32)	Celsius temperature	°C

*1 in = 2.54 (exactly). For other exact conversions and more detailed tables, see NBS Misc. Publ. 286, Units of Weights and Measures, Price $2.25, SD Catalog No. C13.10:286.

Approximate Conversions from Metric Measures

Symbol	When You Know	Multiply by	To Find	Symbol
		LENGTH		
mm	millimeters	0.04	inches	in
cm	centimeters	0.4	inches	in
m	meters	3.3	feet	ft
m	meters	1.1	yards	yd
km	kilometers	0.6	miles	mi
		AREA		
cm^2	square centimeters	0.16	square inches	in^2
m^2	square meters	1.2	square yards	yd^2
km^2	square kilometers	0.4	square miles	mi^2
ha	hectares (10,000 m^2)	2.5	acres	
		MASS (weight)		
g	grams	0.035	ounces	oz
kg	kilograms	2.2	pounds	lb
t	tonnes (1000 kg)	1.1	short tons	
		VOLUME		
ml	milliliters	0.03	fluid ounces	fl oz
l	liters	2.1	pints	pt
l	liters	1.06	quarts	qt
l	liters	0.26	gallons	gal
m^3	cubic meters	35	cubic feet	ft^3
m^3	cubic meters	1.3	cubic yards	yd^3
		TEMPERATURE (exact)		
°C	Celsius temperature	9/5 (then add 32)	Fahrenheit temperature	°F

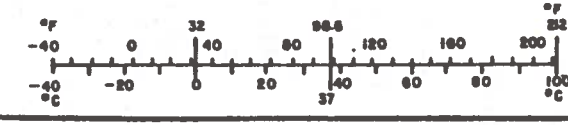

TABLE OF CONTENTS

Acknowledgment

The authors gratefully acknowledge the contributions of the Contract Technical Manager, Dr. Joseph Kanianthra. His advice and encouragement were very helpful. Also, many useful discussions with Paul Fancher and Charles MacAdam are gratefully acknowledged.

CHAPTER ONE

INTRODUCTION

The current report is concerned with the mathematical modelling and simulation of vehicle handling and human driver behavior. Early work in this area has been thoroughly reviewed by Bohn [1.1]. Of particular note is the development of a mathematical model for open-loop dynamics by McHenry and Deleys ([1.2], [1.3]). This model was made operational on a hybrid computer at the Bendix Research Laboratories (see Refs. [1.4] and [1.5]), and it later evolved into the National Highway Traffic Safety Administration Hybrid Computer Vehicle Handling Program (HVHP). This model together with recent improvments is set up at the Applied Physics Laboratory of the John's Hopkins University,and is described in detail in the Report of Bohn and Keenan [1.6] . An account of the original HVHP model can be found in Jindra [1.7].

The present report involves further work along the above lines. Under Contract No. DOT-HS-7-01715 an all-digital simulation was developed for handling open-loop and closed-loop maneuvers up to and including the limit regime. A goal was extensive modularization, so that difficulties in possible future program development would be minimized. The simulation consists of two main parts, namely, a vehicle model called IDSFC and a general purpose driver module called DRIVER. Interfacing between the driver module and the vehicle model is handled by 4 subroutines which can be readily altered to use the driver module with different vehicle models.

The vehicle model IDSFC involves the following degrees of freedom:

Sprung Mass. Specification of the sprung mass requires 3 translational and 3 rotational degrees of freedom.

Front Unsprung Masses. The degrees of freedom allowed are 2 wheel hops, 2 wheel spins, 2 wheel rotations about the kingpins, and 1 steering connecting rod displacement. To reduce costs, the steering system is handled statically.

Rear Unsprung Masses.

A. Solid Rear Axle. The degrees of freedom allowed are 1 rear suspension deflection, 1 real axle roll, and 2 wheel spins.

B. Independent Rear Suspensions. The degrees of freedom allowed are 2 rear suspension deflections and 2 wheel spins.

The mathematical representation of the vehicle model involves 30 first-order nonlinear differential equations and approximately 250 algebraic equations. The digital program contains 30 subroutines and both single precision and double precision versions are available.

The vehicle simulation capabilities are basically as follows:

(1) Straight-line braking/acceleration, cornering without braking/acceleration and cornering with braking/acceleration are allowed.

(2) Maneuvers up to and including the limit range can be studied in that (i) Nonlinear terms in the kinematics are retained (ii) These terms are activated by model level switches and can be deleted for less severe maneuvers, thereby

decreasing running costs. These switches can also be employed if the user wishes to do studies on the effects of various nonlinearities. The tire and suspension forces and moments are modeled into the nonlinear range.

(3) For system and user flexibility, two methods are provided for computing tire forces and moments, namely, (i) The APL-CALSPAN model which is based on curves fitted to the measured data. (ii) A Partial Data Deck model which directly uses the measured data.

(4) An antilock capacity, which can be activated by a model level switch, is available.

(5) Both solid rear axle and independent rear suspensions are allowed.

(6) Front wheel drive, rear wheel drive, and four wheel drive are available.

(7) Separate braking at each wheel is permissible.

(8) An interactive capability is provided, which is activated by a model level switch.

Control input to the vehicle model is through the general purpose driver module DRIVER, the main features of which are as follows:

(1) Driver controls steering, braking, and drive torque inputs to the vehicle model.

(2) There are 5 pre-programmed open-loop maneuvers available, namely:

(a) Sinusoidal steer with trapezoidal braking.

(b) Trapezoidal steer with trapezoidal braking.

(c) Double trapezoidal steer with trapezoidal braking.

(d) Trapezoidal steering with a sinusoidal perturbation with trapezoidal braking.

(e) Sinusoidal steering sweep with no braking.

In addition, the driver module will accept:

(i) Any open-loop maneuver supplied by the user in tabular form.

(ii) Any open-loop maneuver specified by a user supplied subroutine.

(3) The driver module can operate in a closed-loop mode following a desired path. Four control strategies are available, namely:

(a) A "crossover" model for a straight line path.

(b) A "crossover" model for an arbitrary path.

(c) A preview-predictor model which uses a geometric predictor.

(d) A preview-predictor model which uses a 3 degree-of-freedom vehicle model as a predictor.

(4) The driver module permits a mixed-mode operation which allows combined open and closed loop control.

(5) An obstacle avoidance strategy using the preview-predictor models is available.

Volume 4 of the series is a USER'S GUIDE for the general simulation, and Volume 5 is a PROGRAMER'S GUIDE for the vehicle simulation.

References For Chapter One.

1.1. P. F. Bohn, "Modeling and Simulation in Vehicle Handling Research", Proc. Symp. on Vehicle Safety Research Integration, pp. 143-169, DOT HS-820-306, May, 1973.

1.2 R. R. McHenry and N. J. Deleys, "Vehicle Dynamics in Single Vehicle Accident, Validation and Extensions of a Computer Simulation", Cornell Areonautical Laboratory Rept. NO. VJ-2251-V-3, Dec. 1968.

1.3 R. R. McHenry and N. J. Deleys, "Automobile Dynamics - A Computer Simulation of Three-Dimensional Motions for Use in Studies of Braking Systems and of the Driving Task", Cornell Aeronautical Laboratory Rept. NO. VJ-2251-V-7, August 1970.

1.4 "Vehicle Handling", Final Report, Vol. II, DOT HS-800-282, April, 1970.

1.5 "Computer Simulation of Vehicle Handling", DOT HS-800-789, Sept. 1972.

1.6. P. F. Bohn, and R. J. Keenan, "Improved Hybrid Computer Vehicle Handling Program", Applied Physis Laboratory, The Johns Hopkins University, CP 049 A, Oct. 1978.

1.7. F. Jindra, "Mathematical Model of Four-Wheel Vehicle for Hybrid Computer Vehicle Handling Program, DOT-HS-801-800, Ultrasystems, Inc., Oct. 1975.

CHAPTER TWO

MATHEMATICAL MODEL OF THE VEHICLE

§2.1. Introduction. This chapter presents the mathematical model of the vehicle that is implemented in the digital program: IDSFC (Improved Digital Simulation Fully Comprehensive). The modeling is to a large degree the same as that implemented on the Applied Physics Laboratory/Johns Hopkins University Hybrid Computer and described in References (1.1), (1.6) and (1.7).

Section 2.2. describes the physical representation of the vehicle. Section 2.3 gives the mathematical equations and the nomenclature used. Section 2.4 gives in detail the differences between the current modeling and that of the Applied Physics Laboratory.

§2.2. Physical Representation of the Vehicle

Seventeen degrees of freedom are involved in the vehicle modeling. Fig. 2.1 shows the basic configuration employed for the case of a solid rear suspension. Fig. 2.2 gives more detail on the solid rear suspension.

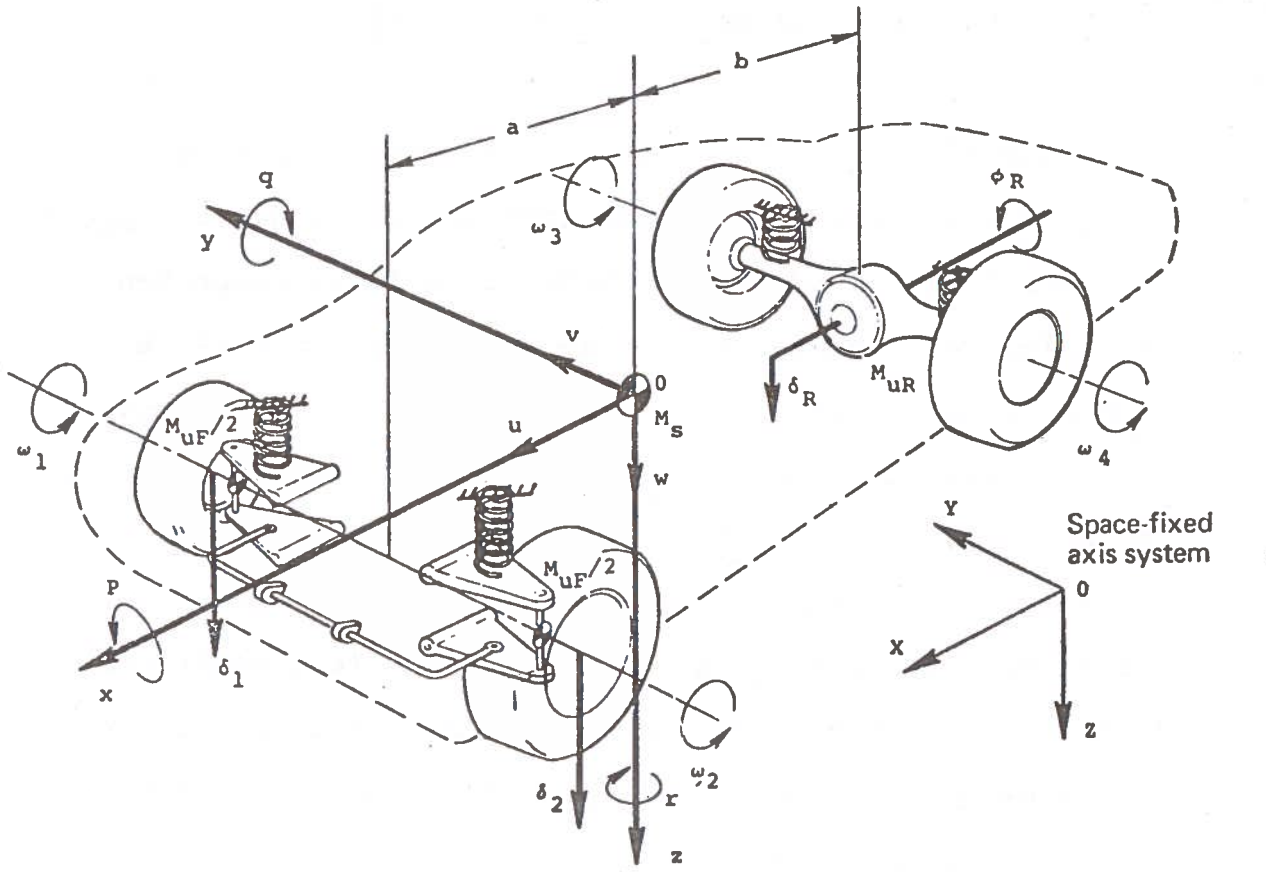

Fig. 2.1. Vehicle Configuration for a Solid Rear Suspension.

The degrees of freedom used are:

Sprung Mass. Specification of the sprung mass requires 3 translational and 3 rotational degrees of freedom.

Front Unsprung Masses. The degrees of freedom allowed are 2 wheel hops, 2 wheel spins, 2 wheel rotations about the king-pins and 1 steering connecting rod displacement. (To reduce costs, the steering system is handled statically.)

Rear Unsprung Masses.

A. Solid Rear Axle. The degrees of freedom allowed are 1 rear suspension deflection, 1 real axle roll and 2 wheel spins.

B. Independent Rear Suspensions. The degrees of freedom

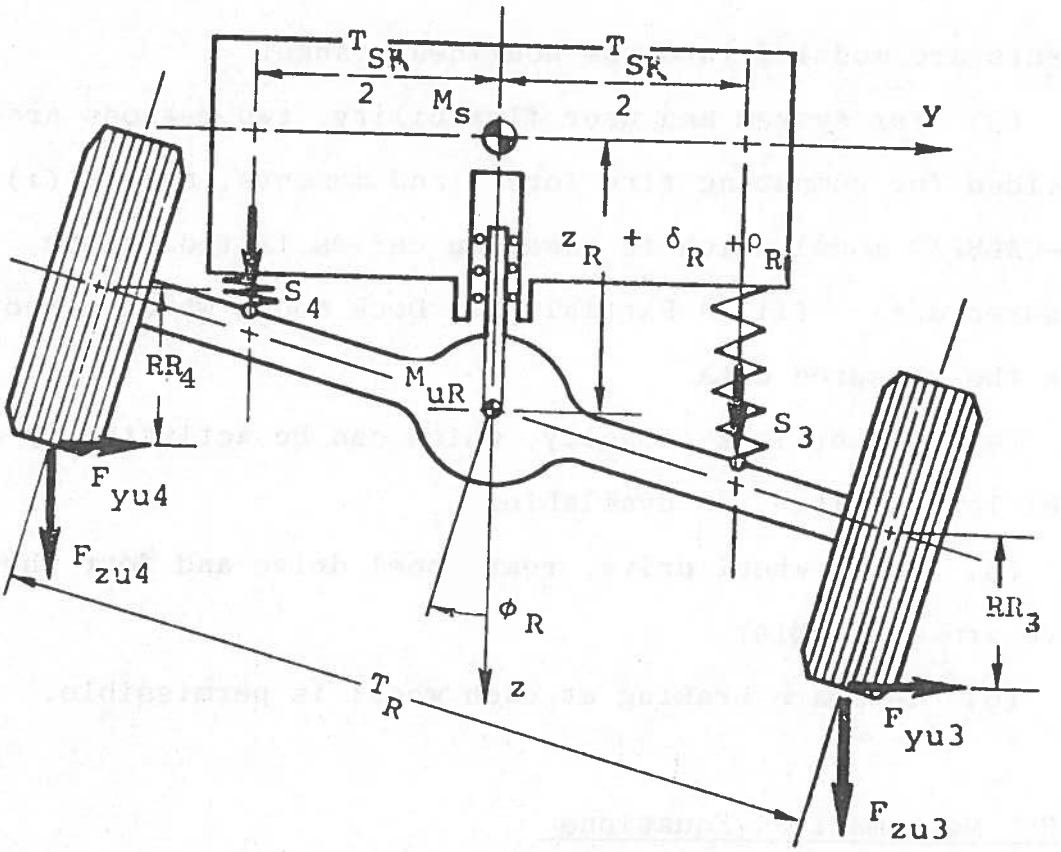

Fig. 2.2. Details of the Solid Rear Suspension.

allowed are 2 rear suspension defelections and 2 wheel spins.

Control commands are steering wheel displacement, acceleration and braking.

Additional features of IDSFC are:

(1) Maneuvers up to and including the limit range can be studied in that (i) Nonlinear terms in the kinematics are retained. (ii) These terms are activated by model level switches and can be deleted for less severe maneuvers, thereby decreasing running costs. These switches can also be employed if the user wishes to do studies on the effects of various nonlinearities. The tire and suspension forces and

moments are modeled into the nonlinear range.

(3) For system and user flexibility, two methods are provided for computing tire forces and moments, namely (i) The APL-CALSPAN model which is based on curves fitted to the measured data. (ii) A Partial Data Deck model which directly uses the measured data.

(4) An antilock capacity, which can be activated by a model level switch, is available.

(5) Front wheel drive, rear wheel drive and four wheel drive are available.

(6) Separate braking at each wheel is permissible.

§2.3. Mathematical Equations

In the sequel, equation numbers involving and S or an I refer to results valid for a solid rear suspension and an independent rear suspension, respectively. The items treated are as follows:

§2.3.1 : General Structure of the Equations.

§2.3.2 : Attitude and Position of the Vehicle.

§2.3.3 : Suspension Forces and Wheel Orientations.

§2.3.4 : Aerodynamic Forces and Moments.

§2.3.5 : Resultant Forces and Moments.

§2.3.6 : Steering Equations.

§2.3.7 : Tire Rolling Radii.

§2.3.8 : Tire Slip Angles and Contact Patch Velocities.

§2.3.9 : Wheel Spins and Longitudinal Slips.

§2.3.10 : Tire Camber Angles.

§2.3.11 : Tire Forces and Moments.

§2.3.12 : Brake and Drive Torques.

§2.3.13 : Center of Mass Accelerations.

§2.3.1. General Structure of the Equations

The equations of motion may be written in the form

$$[M]\begin{Bmatrix} \dot{u} \\ \dot{v} \\ \dot{w} \\ \dot{p} \\ \dot{q} \\ \dot{r} \\ \ddot{\delta}_1 \\ \ddot{\delta}_2 \\ \ddot{\delta}_R \\ \ddot{\phi}_R \end{Bmatrix} = \begin{Bmatrix} F(1) \\ F(2) \\ F(3) \\ F(4) \\ F(5) \\ F(6) \\ F(7) \\ F(8) \\ F(9) \\ F(10) \end{Bmatrix} \qquad (2.1S)$$

where:

$$F(1) = (vr-wq-g\sin\theta)\Sigma M + \Sigma F_{xs} + \Sigma F_{xu}$$
$$+ O_1(-2\rho_R M_{uR}\dot{\phi}_R r) + O_{12}[\rho_R M_{uR} p(\phi_R q-r)]$$
$$+ O_{16}(2\rho_R M_{uR}\phi_R\dot{\phi}_R q) + O_2[-\gamma_2' pr+\gamma_1(q^2+r^2)]$$
$$+ O_{245}\{-[(\delta_1+\delta_2)M_{uF}/2+M_{uR}\delta_R]pr\}$$
$$+ O_5\{-[M_{uF}(\dot{\delta}_1+\dot{\delta}_2)+2M_{uR}\dot{\delta}_R]q\} \qquad (2.2S)$$

$$F(2) = (wp-ur+g\cos\theta\sin\phi)\Sigma M + \Sigma F_{ys} + \Sigma F_{yu}$$
$$+ O_{12}\{-\rho_R M_{uR}[qr+\phi_R(p^2+r^2)]\}$$
$$+ O_{16}[-\rho_R M_{uR}\phi_R\dot{\phi}_R(2p+\dot{\phi}_R)]$$
$$+ O_2[-\gamma_1 pq-\gamma_2' qr] + O_{245}\{-[(\delta_1+\delta_2)M_{uF}/2$$
$$+M_{uR}\delta_R]qr\} + O_5\{[M_{uF}(\dot{\delta}_1+\dot{\delta}_2)+2M_{uR}\dot{\delta}_R]p\} \qquad (2.3S)$$

$$F(3) = M_S(uq-vp+g\cos\theta\cos\phi) + \Sigma F_{zs} - \sum_{i=1}^{4} S_i \qquad (2.4)$$

$$
\begin{aligned}
F(4) \;=\; & \gamma_2' \,(ur-wp-g\cos\theta\sin\phi) + \Sigma N_{\phi s} + \Sigma N_{\phi u} \\
& + O_{12}\{\rho_R M_{uR}[z_R qr + z_R \phi_R (p^2+r^2)]\} + O_{1245} \\
& \times \{\rho_R M_{uR}\delta_R[qr+\phi_R(p^2+r^2)]\} + O_{16}[\rho_R M_{uR} z_R \\
& \times \phi_R \dot{\phi}_R(2p+\dot{\phi}_R)] + O_{1456}[\rho_R M_{uR}\delta_R\phi_R\dot{\phi}_R(2p+\dot{\phi}_R)] \\
& + O_2[(I_{xz}+I'_{xz})pq + (I_y - I_z + I'_y)qr] \\
& + O_{245}\{[M_{uF}a(\delta_1+\delta_2)/2 - M_{uR}b\delta_R]pq + [M_{uF} \\
& \times z_F(\delta_1+\delta_2) + M_{uF}(\delta_1^{\,2}+\delta_2^{\,2})/2 + 2M_{uR}z_R\delta_R + M_{uR} \\
& \times \delta_R^{\,2}]qr\} + O_{25}[-M_{uF}T_F(\delta_1-\delta_2)(p^2+r^2)/4] \\
& + O_4\{-[M_{uF}(\delta_1+\delta_2)/2 + M_{uR}\delta_R]g\cos\theta\sin\phi\} \\
& + O_{45}\{[M_{uF}(\delta_1+\delta_2)/2 + M_{uR}\delta_R](ur-wp) - M_{uF} \\
& \times (\delta_1\dot{\delta}_1+\delta_2\dot{\delta}_2)p - 2M_{uR}\delta_R\dot{\delta}_R p\} + O_5\{-[M_{uF}z_F \\
& \times (\dot{\delta}_1+\dot{\delta}_2) + 2M_{uR}z_R\dot{\delta}_R]p\} \qquad (2.5S)
\end{aligned}
$$

$$
\begin{aligned}
F(5) \;=\; & \gamma_2' \,(vr-wq-g\sin\theta) + \Sigma N_{\theta s} + \Sigma N_{\theta u} + O_1 \\
& \times \{\rho_R M_{uR}[vr-wq-g\sin\theta - 2(z_R+\rho_R)\dot{\phi}_R r]\} + O_{12} \\
& \times \{\rho_R M_{uR}[-(\rho_R+2z_R)pr + (z_R+\rho_R)\phi_R pq - b(q^2+r^2)]\} \\
& + O_{1245}[\rho_R M_{uR}(-2\delta_R pr + \phi_R\delta_R pq)] + O_{145} \\
& \times (2\rho_R M_{uR}\delta_R\dot{\phi}_R r) + O_{1456}(2\rho_R M_{uR}\delta_R\phi_R\dot{\phi}_R q) \\
& + O_{15}\,(-2\rho_R M_{uR}\dot{\delta}_R q) + O_{16}[2\rho_R M_{uR}\phi_R\dot{\phi}_R q(z_R+\rho_R)] \\
& + O_2\, I_{xz}(r^2-p^2) + (I_z - I_x - I'_y)\, pr + I'_{xz} \\
& \times (q^2+r^2)] + O_{245}\,\{[-M_{uF}z_F(\delta_1+\delta_2) - M_{uF} \\
& \times (\delta_1^{\,2}+\delta_2^{\,2})/2 - 2M_{uR}z_R\delta_R - M_{uR}\delta_R^{\,2}]pr + [M_{uF}a \\
& \times (\delta_1+\delta_2)/2 - M_{uR}b\delta_R\,](q^2+r^2)\} + O_{25}\,[-M_{uF}T_F \\
& \times (\delta_1-\delta_2)pq/4] + O_4\{-[M_{uF}(\delta_1+\delta_2)/2 + M_{uR}\delta_R]
\end{aligned}
$$

$$x\ g\sin\theta\} + O_{45}\{[M_{uF}(\delta_1+\delta_2)/2+M_{uR}\delta_R](vr-wq)$$

$$- M_{uF}(\delta_1\dot{\delta}_1+\delta_2\dot{\delta}_2)q-2M_{uR}\delta_R\dot{\delta}_R q\} + O_5\{-[M_{uF}z_F$$

$$x\ (\dot{\delta}_1+\dot{\delta}_2)+2M_{uR}z_R\dot{\delta}_R]q\} \qquad (2.6S)$$

$$F(6) = \gamma_1(wp-ur+g\cos\theta\sin\phi) + \Sigma N_{\psi s} + \Sigma N_{\psi u}$$

$$+ O_1[\rho_R M_{uR}\phi_R(vr-wq-g\sin\theta)] + O_{12}\{\rho_R$$

$$x\ M_{uR}\phi_R\ [b(p^2-q^2)-(z_R+\rho_R)pr]+\rho_R M_{uR}bqr\}$$

$$+ O_{1245}(-\rho_R M_{uR}\phi_R\delta_R pr) + O_{126}(\rho_R^2 M_{uR}\phi_R^2 pq)$$

$$+ O_{15}(-2\rho_R M_{uR}\phi_R\dot{\delta}_R q) + O_{16}[\rho_R M_{uR}\phi_R\dot{\phi}_R(b\dot{\phi}_R$$

$$- 2\rho_R r+2\rho_R\phi_R q+2bp)] + O_2\ (I_x-I_y-\gamma_5')pq$$

$$- (I_{xz}+I_{xz}')qr] + O_{25}[M_{uF}T_F(\delta_1-\delta_2)pr/4]$$

$$+ O_{245}\{[-M_{uF}a(\delta_1+\delta_2)/2+M_{uR}b\delta_R]qr\}$$

$$+ O_5\{M_{uF}T_F(\dot{\delta}_1-\dot{\delta}_2)q/2+[M_{uF}a(\dot{\delta}_1+\dot{\delta}_2)$$

$$- 2M_{uR}b\dot{\delta}_R]p\} \qquad (2.7S)$$

$$F(7) = M_{uF}(uq-vp+g\cos\theta\cos\phi)/2 + F_{z1} + S_1$$

$$+ F_{J1} + F_{SWF} + O_2\ \{-M_{uF}[apr + \tfrac{1}{2}T_F qr-z_F$$

$$x\ (p^2+q^2)]/2\} + O_{245}[M_{uF}\delta_1(p^2+q^2)/2] \qquad (2.8)$$

$$F(8) = M_{uF}(uq-vp+g\cos\theta\cos\phi)/2 + F_{z2} + S_2$$

$$+ F_{J2} + F_{SWF} + O_2\{-M_{uF}[apr-T_F qr/2-z_F$$

$$x\ (p^2+q^2)]/2\} + O_{245}[M_{uF}\delta_2(p^2+q^2)/2] \qquad (2.9)$$

$$F(9) = M_{uR}(uq-vp+g\cos\theta\cos\phi) + F_{z3} + F_{z4} + S_3$$

$$+ S_4 + 2F_{SWR} + O_1(2\rho_R M_{uR}\dot{\phi}_R p) + O_{12}[\rho_R M_{uR}$$

$$x\ (\phi_R qr+p^2+q^2) + O_{16}(\rho_R M_{uR}\dot{\phi}_R^2) + O_2\{M_{uR}$$

$$x\ [bpr+z_R(p^2+q^2)]\} + O_{245}[M_{uR}\delta_R(p^2+q^2)] \qquad (2.10S)$$

$$F(10) = \Sigma N_{\phi R} + O_1\{\rho_R M_{uR}[ur-wp-g\cos\sin(\phi+\phi_R) + \phi_R(vp-uq)]\} + O_{12}\{\rho_R M_{uR}[-bpq+\rho_R\phi_R r^2 + (z_R+\rho_R)qr-\phi_R bpr-\phi_R z_R(p^2+q^2)-\rho_R\phi_R q^2]\} + O_{1245}\{\rho_R M_{uR}\delta_R[qr-\phi_R(p^2+q^2)]\} + O_{126}(-\rho_R^2 M_{uR}\phi_R^2 qr) + O_{15}(-2\rho_R M_{uR}\dot{\delta}_R p) + O_2\{I_R[\phi_R(q^2-r^2)-qr]\} \quad (2.11S)$$

$$\gamma_2' = M_{uF}z_F + M_{uR}z_R \quad (2.12)$$

$$I_y' = M_{uF}z_F^2 + M_{uR}z_R^2 \quad (2.13)$$

$$I_{xz}' = M_{uF}az_F - M_{uR}bz_R \quad (2.14)$$

$$\gamma_5' = M_{uF}(a^2-T_F^2/4) + M_{uR}b^2 \quad (2.14a)$$

$$\gamma_1 = M_{uF}a - M_{uR}b \quad (2.14b)$$

$$[M]\begin{Bmatrix} \dot{u} \\ \dot{v} \\ \dot{w} \\ \dot{p} \\ \dot{q} \\ \dot{r} \\ \ddot{\delta}_1 \\ \ddot{\delta}_2 \\ \ddot{\delta}_3 \\ \ddot{\delta}_4 \end{Bmatrix} = \begin{Bmatrix} F(1) \\ F(2) \\ F(3) \\ F(4) \\ F(5) \\ F(6) \\ F(7) \\ F(8) \\ F(9) \\ F(10) \end{Bmatrix} \quad (2.1I)$$

$$F(1) = (vr-wq-g\sin\theta)\Sigma M + \Sigma F_{xs} + \Sigma F_{xu} + O_2[-\gamma_2' pr+\gamma_1(q^2+r^2)] + O_{245}\{-(\delta_1+\delta_2)M_{uF}/2 + (\delta_3+\delta_4)M_{uR}/2\ pr\} + O_5\{-[M_{uF}(\dot{\delta}_1+\dot{\delta}_2) + M_{uR}(\dot{\delta}_3+\dot{\delta}_4)]q\} \quad (2.2I)$$

$$F(2) = (wp-ur+g\cos\theta\sin\phi)\Sigma M + \Sigma F_{ys} + \Sigma F_{yu} + O_2[-\gamma_1 pq-\gamma_2' qr] + O_{245}\{-[(\delta_1+\delta_2)M_{uF}/2 + (\delta_3+\delta_4)M_{uR}/2]qr\} + O_5\{[M_{uF}(\dot{\delta}_1+\dot{\delta}_2) + M_{uR}(\dot{\delta}_3+\dot{\delta}_4)]p\} \quad (2.3I)$$

$$F(4) = \gamma_2'(ur-wp-g\cos\theta\sin\phi) + \Sigma N_{\phi S} + \Sigma N_{\phi u} + O_2[(I_{xz}+I_{xz}')pq + (I_y-I_z+I_y')qr] + O_{245}\{[M_{uF}a(\delta_1+\delta_2)/2 - M_{uR}b(\delta_3+\delta_4)/2]pq + [M_{uF}z_F(\delta_1+\delta_2) + M_{uF}(\delta_1^2+\delta_2^2)/2 + M_{uR} \times z_R(\delta_3+\delta_4) + M_{uR}(\delta_3^2+\delta_4^2)/2]qr\} + O_{25}\{-[M_{uF}T_F(\delta_1-\delta_2) + M_{uR}T_R(\delta_3-\delta_4)] \times \frac{(p^2+r^2)}{4} + O_4\{-[M_{uF}(\delta_1+\delta_2)/2 + M_{uR} \times (\delta_3+\delta_4)/2]\ g\cos\theta\sin\phi\} + O_{45}\{[M_{uF} \times (\delta_1+\delta_2)/2 + M_{uR}(\delta_3+\delta_4)/2](ur-wp) - [M_{uF}(\delta_1\dot{\delta}_1+\delta_2\dot{\delta}_2) + M_{uR}(\delta_3\dot{\delta}_3+\delta_4\dot{\delta}_4)]p\} - O_5\{-[M_{uF}(\dot{\delta}_1+\dot{\delta}_2) + M_{uR}z_R(\dot{\delta}_3+\dot{\delta}_4)]p\} \quad (2.5I)$$

$$F(5) = \gamma_2'(vr-wq-g\sin\theta) + \Sigma N_{\theta s} + \Sigma N_{\theta u}$$
$$+ O_2[I_{xz}(r^2-p^2) + (I_z-I_x-I_y')pr + I_{xz}'$$
$$x\ (q^2+r^2)] + O_{245}\{[-M_{uF}z_F(\delta_1+\delta_2) - M_{uF}$$
$$x\ (\delta_1^2+\delta_2^2)/2 - M_{uR}z_R(\delta_3+\delta_4) - M_{uR}(\delta_{3+}^2\delta_3^2)/2]$$
$$x\ pr + [M_{uF}a(\delta_1+\delta_2)/2 - M_{uR}b(\delta_3+\delta_4)/2]$$
$$x\ (q^2+r^2)\} + O_{25}\{[-M_{uF}T_F(\delta_1-\delta_2) + M_{uR}T_R(\delta_3-\delta_4)]$$
$$x\ \frac{pq}{4}\} + O_4\{-[M_{uF}(\delta_1+\delta_2)/2 + M_{uR}(\delta_3+\delta_4)]/2$$
$$x\ g\sin\theta\} + O_{45}\{[M_{uF}(\delta_1+\delta_2)/2 + M_{uR}(\delta_3+\delta_4)/2]$$
$$x\ (vr-wq) - M_{uF}(\delta_1\dot{\delta}_1+\delta_2\dot{\delta}_2)q$$
$$- M_{uR}(\delta_3\dot{\delta}_3\ \delta_4\dot{\delta}_4)q\} + O_5\{-[M_{uF}z_F$$
$$x\ (\dot{\delta}_1+\dot{\delta}_2) + M_{uR}z_R(\dot{\delta}_3+\dot{\delta}_4)]q\} \qquad (2.6I)$$

$$F(6) = \gamma_1(wp-ur+g\cos\theta\sin\phi) + \Sigma N_{\psi s} + \Sigma N_{\psi u}$$
$$+ O_2\ (I_x-I_y-\gamma_5')pq$$
$$- (I_{xz}+I_{xz}')qr] + O_{25}[M_{uF}T_F(\delta_1-\delta_2)pr/4$$
$$+ M_{uR}T_R(\delta_3-\delta_4)pr/4]$$
$$+ O_{245}\{[-M_{uF}a(\delta_1+\delta_2)/2 + M_{uR}b(\delta_3+\delta_4)/2]qr\}$$
$$+ O_5\{M_{uF}T_F(\dot{\delta}_1-\dot{\delta}_2)q/2 + [M_{uF}a(\dot{\delta}_1+\dot{\delta}_2)$$
$$+ M_{uR}b(\dot{\delta}_3+\dot{\delta}_4)]p + M_{uR}T_R(\dot{\delta}_3-\dot{\delta}_4)q/2 \qquad (2.7I)$$

$$F(9) = M_{uR}(uq-vp+g\cos\theta\cos\phi) + F_{z3} + S_3$$
$$+ F_{J3} + F_{SWR} + O_2\{-M_{uR}[bpr-T_Rqr/2$$
$$- z_R\ x\ (p^2+q^2)]/2\} + O_{245}[M_{uR}\delta_3\ x\ (p^2+q^2)/2]$$
$$(2.10I)$$

$$F(10) = M_{uR}(uq-vp+g\cos\theta\cos\phi) + F_{z4} + S_4$$
$$+ F_{J4} + F_{SWR} + O_2\{-M_{uR}[bpr$$
$$- T_R qr/2 - z_R (p^2+q^2)]/2\}$$
$$+ O_{245}[M_{uR}\delta_4(p^2+q^2)/2] \qquad (2.11I)$$

The elements of the matrix M are as follows:

$$M(1,2) = M(1,3) = M(1,4) = M(1,7) = M(1,8) = M(1,9)$$
$$= M(1,10) = M(2,1) = M(2,3) = M(2,5)$$
$$= M(2,7) = M(2,8) = M(2,9) = M(3,1) = M(3,2)$$
$$= M(3,4) = M(3,5) = M(3,6) = M(3,7) = M(3,8)$$
$$= M(3,9) = M(3,10) = M(4,1) = M(4,3)$$
$$= M(4,5) = M(4,7) = M(4,8) = M(4,9) = M(5,2)$$
$$= M(5,3) = M(5,4) = M(5,7) = M(5,8) = M(5,9)$$
$$= M(5,10) = M(6,3) = M(6,7) = M(6,8)$$
$$= M(6,9) = M(7,1) = M(7,2) = M(7,6) = M(7,8)$$
$$= M(7,9) = M(7,10) = M(8,1) = M(8,2)$$
$$= M(8,6) = M(8,7) = M(8,9) = M8,10)$$
$$= M(9,1) = M(9,2) = M(9,6) = M(9,7) = M(9,8)$$
$$= M(10,1) = M(10,7) = M(10,8) = 0 \qquad (2.15)$$
$$M(1,1) = M(2,2) = \Sigma M \qquad (2.16)$$
$$M(5,1) = \gamma_2' + O_4[M_{uF}(\delta_1+\delta_2)/2+M_{uR}\delta_R] + O_1(\rho_R M_{uR}) \qquad (2.17S)$$

$$M(6,1) = O_1(\rho_R M_{uR}\phi_R) \tag{2.18S}$$

$$M(4,2) = -\gamma_2' + O_4[-M_{uF}(\delta_1+\delta_2)/2-M_{uR}\delta_R] \tag{2.19}$$

$$M(2,6) = M(6,2) = \gamma_1 \tag{2.20}$$

$$M(2,10) = M(10,2) = O_1(-\rho_R M_{uR}) \tag{2.21S}$$

$$M(3,3) = M_S \tag{2.22}$$

$$M(7,3) = M(8,3) = M(7,7) = M(8,8) = M_{uF}/2 \tag{2.23}$$

$$M(9,3) = M(9,9) = M_{uR} \tag{2.24S}$$

$$M(10,3) = M(9,4) = M(10,9) = O_1(-\rho_R M_{uR}\phi_R) \tag{2.25S}$$

$$M(2,4) = -M(1,5) = -\gamma_2' + O_{45}[-M_{uF}(\delta_1+\delta_2)/2-M_{uR}\delta_R] + O_1(-\rho_R M_{uR}) \tag{2.26S}$$

$$M(4,4) = I_x + I_y' + O_{45}\, M_{uF}z_F(\delta_1+\delta_2)+M_{uF}(\delta_1^2+\delta_2^2)/2 +2M_{uR}z_R\delta_R+M_{uR}\delta_R^2] + O_1(\rho_R M_{uR}z_R) + O_{145}(\rho_R M_{uR}\delta_R) \tag{2.27S}$$

$$M(6,4) = - I_{xz} - I_{xz}' + O_{45}[-M_{uF}a(\delta_1+\delta_2)/2+bM_{uR}\delta_R] \times O_1\,(\rho_R M_{uR}b) \tag{2.28S}$$

$$M(7,4) = - M(8,4) = M_{uF}T_F/4 \tag{2.29}$$

$$M(10,4) = I_R + O_1(\rho_R M_{uR}z_R+\rho_R^2 M_{uR}) + O_{145}(\rho_R M_{uR}\delta_R) \tag{2.30S}$$

$$M(5,5) = I_y + I_y' + O_{45}[M_{uF}z_F(\delta_1+\delta_2)+M_{uF}(\delta_1^2+\delta_2^2)/2 +2M_{uR}z_R\delta_R+M_{uR}\delta_R^2] + O_1[2M_{uR}\rho_R z_R+M_{uR}\rho_R^2] + O_{145}(2M_{uR}\rho_R\delta_R) \tag{2.31S}$$

$$M(6,5) = O_1\,(\rho_R M_{uR}\phi_R z_R+\rho_R^2 M_{uR}\phi_R) + O_{45}[-M_{uF}T_F(\delta_1-\delta_2)/4] + O_{145}(\rho_R M_{uR}\phi_R\delta_R) \tag{2.32S}$$

$$M(7,5) = M(8,5) = -M_{uF}a/2 \qquad (2.33)$$

$$M(9,5) = bM_{uR} \qquad (2.34S)$$

$$M(10,5) = O_1(-\rho_R M_{uR} b\phi_R) \qquad (2.35S)$$

$$M(1,6) = O_1(\rho_R M_{uR}\phi_R) \qquad (2.36S)$$

$$M(4,6) = -I_{xz} - I'_{xz} + O_{45}[-M_{uF}a(\delta_1+\delta_2)/2+M_{uR}b\delta_R]$$

$$M(5,6) = O_{45}[-M_{uF}T_F(\delta_1-\delta_2)/4] + O_1[\rho_R M_{uR}\phi_R z_R+\rho_R^2 M_{uR}\phi_R] + O_{145}(\rho_R M_{uR}\phi_R\delta_R) \qquad (2.38S)$$

$$M(6,6) = I_R + I_z + M_{uF}(a^2+T_F^2/4) + M_{uR}b^2 + O_{16}(M_{uR}\rho_R^2\phi_R^2) \qquad (2.39S)$$

$$M(10,6) = M(6,10) = O_1(\rho_R M_{uR} b) \qquad (2.40S)$$

$$M(4,10) = O_1(\rho_R M_{uR} z_R) + O_{14}(\rho_R M_{uR}\delta_R) \qquad (2.41S)$$

$$M(9,10) = O_{16}(-\rho_R M_{uR}\phi_R) \qquad (2.42S)$$

$$M(10,10) = I_R + O_1(M_{uR}\rho_R^2) \qquad (2.43S)$$

$$M(5,1) = \gamma'_2 + O_4\,[M_{uF}(\delta_1+\delta_2)/2 + M_{uR} \times (\delta_3+\delta_4)] \qquad (2.17I)$$

$$M(6,1) = 0 \qquad (2.18O)$$

$$M(2,10) = M(10,2) = 0 \qquad (2.21I)$$

$$M(9,3) = M(9,9) = M_{uR}/2 \qquad (2.24I)$$

$$M(10,3) = M_{uR}/2 \quad M(9,4) = M_{uR}T_R/4$$

$$M(10,9) = 0 \qquad (2.25I)$$

$$M(2,4) = -M(1,5) = -\gamma'_2 + O_{45}[-M_{uF}(\delta_1+\delta_2)/2 - M_{uR}(\delta_3-\delta_4)/2] \qquad (2.26I)$$

$$M(4,4) = I_x + I'_y + O_{45}[M_{uF}z_F(\delta_1+\delta_2) + M_{uF} \times (\delta_1^2+\delta_2^2)/2 + M_{uR}z_R(\delta_3+\delta_4) + M_{uR} \times (\delta_3^2+\delta_4^2)/2] \qquad (2.27I)$$

$$M(6,4) = -I_{xz} - I'_{xz} + O_{45}[-M_{uF}a(\delta_1+\delta_2)/2 + M_{uR}b(\delta_3+\delta_4)/2] \quad (2.28I)$$

$$M(10,4) = M_{uR}T_R/4 \quad (2.30I)$$

$$M(5,5) = I_y + I'_y + O_{45}[M_{uF}z_F(\delta_1+\delta_2) + M_{uF}(\delta_1^2+\delta_2^2)/2 + M_{uR}(\delta_3+\delta_4) + M_{uR}(\delta_3^2+\delta_4^2)/2] \quad (2.31I)$$

$$M(6,5) = O_{45}[-M_{uF}T_F(\delta_1-\delta_2)/4 - M_{uR}T_R(\delta_3-\delta_4)/4] \quad (2.32I)$$

$$M(9,5) = M_{uR}b/2 \quad (2.34I)$$

$$M(10,5) = M_{uR}b/2 \quad (2.35I)$$

$$M(1,6) = 0 \quad (2.36I)$$

$$M(4,6) = -I_{xz} - I'_{xz} + O_{45}[-M_{uF}a\,x (\delta_1+\delta_2)/2 + M_{uR}b(\delta_3+\delta_4)/2] \quad (2.37I)$$

$$M(5,6) = M(6,5) \quad (2.38I)$$

$$M(6,6) = I_z + M_{uF}(a^2+T_F^2/4) + M_{uR}(b^2+T_R^2/4) \quad (2.39I)$$

$$M(10,6) = M(6,10) = 0 \quad (2.40I)$$

$$M(4,10) = 0 \quad (2.41I)$$

$$M(9,10) = 0 \quad (2.42I)$$

$$M(10,10) = M_{uR}/2 \quad (2.43I)$$

Note that in the above equations if the pitch angle θ and the roll angle ϕ are assumed to be small, the program uses the approximations $\sin\theta \simeq \theta$, $\cos 0 \simeq 1$, $\sin\phi \simeq \phi$, $\cos\phi \simeq 1$.

§2.3.2. Attitude and Position of the Vehicle

a_{ij}, i, j = 1...3 are the elements of the transformation matrix from the sprung mass coordinate system to the inertial frame with the sequence ψ, θ, ϕ. They are given by

$$a_{11} = \cos\theta \cos\psi \tag{2.44}$$

$$a_{12} = -\cos\phi \sin\psi + \sin\phi \sin\theta \cos\psi \tag{2.45}$$

$$a_{13} = \sin\phi \sin\psi + \cos\phi \sin\theta \cos\psi \tag{2.46}$$

$$a_{21} = \cos\theta \sin\psi \tag{2.47}$$

$$a_{22} = \cos\phi \cos\psi + \sin\phi \sin\theta \sin\psi \tag{2.48}$$

$$a_{23} = -\cos\psi \sin\phi + \cos\phi \sin\theta \sin\psi \tag{2.49}$$

$$a_{31} = -\sin\theta \tag{2.50}$$

$$a_{32} = \cos\theta \sin\phi \tag{2.51}$$

$$a_{33} = \cos\theta \cos\phi \tag{2.52}$$

Kinematic variables are

$$\dot{\theta} = (q \cos\phi - r \sin\phi) \tag{2.53}$$

$$\dot{\theta} = p + (q\sin\phi + r\cos\phi) \tan\theta \tag{2.54}$$

$$\dot{\psi} = (q\sin\phi + r\cos\phi) \sec\theta \tag{2.55}$$

$$\dot{X} = (a_{11}u + a_{12}v + a_{13}w) \tag{2.56}$$

$$\dot{Y} = (a_{21}u + a_{22}v + a_{23}w) \tag{2.57}$$

$$\dot{Z} = (a_{31}u + a_{32}v + a_{33}w) \tag{2.58}$$

Note that if the pitch angle θ and the roll angle ϕ are assumed to be small, then the program makes the approximation $\sin\theta \simeq \theta, \cos\theta \simeq 1$, $\sin\phi \simeq \phi$, $\cos\phi \simeq 1$, and eqs. (2.53) to (2.58) are changed to:

$$\phi = (p + r\theta) \tag{2.59}$$

$$\theta = (q - r\phi) \tag{2.60}$$

$$\psi = (r + q\phi) \tag{2.61}$$

$$\dot{X} = (u \text{ COS } \psi - v \text{ SIN } \psi) \tag{2.62}$$

$$\dot{Y} = (u \text{ SIN } \psi + v \text{ COS } \psi) \tag{2.63}$$

$$\dot{Z} = (-u\theta + v\phi + w) \tag{2.64}$$

§2.3.3. Suspension Forces and Wheel Orientations

Front Wheels. The suspension forces S_i are decomposed as follows:

$$S_i = - F_{1i} - F_{2i} - F_{3i} + F_{4i} + F_{APi} + F_{ARi} \quad , \quad i = 1...2. \tag{2.65}$$

the F_{1i} are the Coulomb friction forces and are given by

$$\text{If } \dot{\delta}_i > (BPT)_i \quad , \quad F_{1i} = C'_{Fi} \quad , \quad i = 1,2 \tag{2.66}$$

$$\text{If } \dot{\delta}_i < -(BPT)_i \quad , \quad F_{1i} = -C'_{Fi} \quad , \quad i = 1,2 \tag{2.67}$$

Otherwise,

$$F_{1i} = C'_{Fi}\dot{\delta}_i/(BPT)_i \quad , \quad i = 1,2 \tag{2.68}$$

$$(BPT)_i = 2\,\Delta t\{C'_{Fi}\,(1/M_S+1/M_{uF}+a^2/I_y) + C'_{R(i+2)}(1/M_S+ab/I_y)\} \quad , \quad i = 1,2 \tag{2.68a}$$

Note that eqs. (2.66), (2.67) and (2.68) represents a model in which the friction is taken to act like viscous damping for small values of velocity. The F_{2i} are the spring forces and are given by:

$$\delta_{Si} = \delta_i + \delta_{INi} \quad , \quad i = 1...2 \tag{2.69}$$

For j such that $\chi_{i(j-1)} < \delta_{Si} < \chi_{ij}$, then

$$F_{2i} = F_{Spij} + (\delta_{Si} - \chi_{ij})(F_{Spi(j+1)} - F_{Spij})/(\chi_{i(j+1)} - \chi_{ij}) - K_{Fi}\,\delta_{INi} \quad , \quad 1 = 1...2 \tag{2.70}$$

NOTE: If j = 5, then:

$$F_{2i} = F_{Spij} + (\delta_{Si} - \chi_{i5})(F_{Spi5} - F_{Spi4})/(\chi_{i5}-\chi_{i4}) - K_{Fi}\delta_{INi} \quad , \quad i = 1...2 \tag{2.71}$$

$$K_{Fi} = (F_{Spi4} - F_{Spi2})/(\chi_{i4} - \chi_{i2}) \tag{2.72}$$

$$F_{BSi} = F_{2i} - K_{Fi}\delta_i \quad , \quad i = 1...2 \tag{2.73}$$

Note that eqs. (2.69) through (2.73) model the spring forces in a piecewise linear fashion with up to four segments. The F_{3i} are the shock absorber forces and are given by: For j such that $\dot{\chi}_{i(j-1)} < \dot{\delta}_i \leq \dot{\chi}_{ij}$, then

$$F_{3i} = F_{SHij} + (\dot{\delta}_i - \dot{\chi}_{ij})(F_{SHi(j+1)} - F_{SHij})/(\dot{\chi}_{i(j+1)} - \dot{\chi}_{ij}) \tag{2.74}$$

NOTE: If j = 5, then

$$F_{3i} = F_{SHi5} + (\dot{\delta}_i - \dot{\chi}_{i5})(F_{SHi5} - F_{SHi4})/(\dot{\chi}_{i5} - \dot{\chi}_{i4}) \quad , \quad i = 1,2 \tag{2.75}$$

Note that eqs. (2.74) and (2.75) model the shock absorber forces in a piecewise linear fashion with up to four segments. The F_{4i} are the auxiliary roll stiffness forces and are given by:

$$F_{4i} = (-1)^i R_F(\delta_1 - \delta_2)/T_F^2 \quad , \quad i = 1...2 \tag{2.76}$$

The F_{APi} are the antipitch forces and are given by

$$F_{APi} = (P_{i1} + P_{i2}\delta_i + P_{i3}\delta_i^2)(F_{xu} - F_{xINi}) \quad , \quad i = 1,2 \tag{2.77}$$

The F_{ARi} are the antiroll forces and are given by

$$F_{ARi} = (R_{i1} + R_{i2}\delta_i + R_{i3}\delta_i^2)(F_{yu} - F_{yINi}) \quad , \quad i = 1,2 \tag{2.78}$$

The wheel orientations are

$$\phi_{SA1} = \phi_{SAO1} + \sum_{j=0}^{5} C_{1j}\delta_{S1}^{j} \tag{2.79}$$

$$\phi_{SA2} = \phi_{SAO2} - \sum_{j=0}^{5} C_{2j}\delta_{S2}^{j} \tag{2.80}$$

$$\phi_1 = \sum_{j=0}^{5} C_{1j}\delta_{S1}^{j} + \Delta\phi_1 \mathrm{sgn}F_{S1} - \phi_{SA1}(1-\cos\psi_1) + K_{OT1}M_{x1} \tag{2.81}$$

$$\phi_2 = -\sum_{j=0}^{5} C_{2j}\delta_{S2}^{j} + \Delta\phi_2 \mathrm{sgn}F_{S2} - \phi_{SA2}(1-\cos\psi_2) + K_{OT2}M_{x2} \tag{2.82}$$

$$\psi_1 = \delta_{Fw1} + \sum_{j=0}^{5} D_{1j}\delta_{S1}^{j} + \Delta\psi_1 \tag{2.83}$$

$$\psi_2 = \delta_{Fw2} - \sum_{j=0}^{5} D_{2j}\delta_{S2}^{j} + \Delta\psi_2 \tag{2.84}$$

$$\theta_{S1} = \sum_{j=1}^{5} E_{1j}\delta_{S1}^{j} + \Delta\theta_1 \tag{2.85}$$

$$\theta_{S2} = \sum_{j=0}^{5} E_{2j}\delta_{S2}^{j} + \Delta\theta_2 \tag{2.86}$$

Rear Wheels with a Solid Axle. The suspension forces are decomposed into:

$$S_i = -F_{1i} - F_{2i} - F_{3i} + F_{4i} + F_{APi} + F_{ARi}, \quad i = 3\ldots4 \tag{2.87}$$

$$\text{If } \dot{\chi}_i > (BPT)_i, \; F_{1i} = C'_{Ri}, \; i = 3, 4 \tag{2.88}$$

$$\text{If } \dot{\chi} < -(BPT)_i, \; F_{1i} = -C'_{Ri}, \; i = 3,4 \tag{2.89}$$

where

$$\dot{\chi}_i = \dot{\delta}_R - (-1)^i T_{SR}\dot{\phi}_R/2, \quad i = 3,4 \tag{2.90}$$

Otherwise,

$$F_{1i} = C_i\dot{\chi}_i/(BPT)_i, \quad i = 3,4 \tag{2.91}$$

$$(BPT)_i = 2\Delta t\{C'_{Ri}(1/M_S + 1/M_{uR} + b^2/I_y) + C'_{F(i-2)}(1/M_S + ab/I_y)\} \quad , i = 3,4. \tag{2.91a}$$

The eqs. for F_{2i} remain unchanged except that δ_i is replaced by χ_i where

$$\chi_i = \delta_R - (-1)^i T_{SR}\phi_R/2 \quad , \quad i = 3, 4 \tag{2.92}$$

The eqs. for F_{3i} remain unchanged except that $\dot{\delta}_i$ is replaced by $\dot{\chi}_i$ as given by eq. (2.90). And:

$$F_{4i} = (-1)^i R_R\phi_R/T_{SR} \quad , \quad i = 3...4 \tag{2.93}$$

The eqs. for F_{APi} and F_{ARi} remain unchanged except that the δ_i are replaced by χ'_i where

$$\chi'_i = \delta_R - (-1)^i T_R\phi_R/2 \quad , \quad i = 3,4 \tag{2.94}$$

The wheel orientations are

$$\phi_3 = \phi_R \tag{2.95}$$

$$\phi_4 = \phi_R \tag{2.96}$$

$$\psi_3 = K_{RS}\phi_R + K_{SR}M_{z3} + K_{LR}F_{S3} \tag{2.97}$$

$$\psi_4 = K_{RS}\phi_R + K_{SR}M_{z4} + K_{LR}F_{S4} \tag{2.98}$$

<u>Rear Wheels with Independent Suspensions</u>. The suspension forces are decomposed into

$$S_i = -F_{1i} - F_{2i} - F_{3i} + F_{4i} + F_{APi} + F_{ARi} \quad , \quad i = 1...4 \tag{2.99}$$

$$\text{If } \dot{\delta}_i > (BPT)_i, F_{1i} = C'_{Ri} \quad , \quad i = 3,4 \tag{2.100}$$

$$\text{If } \dot{\delta}_i < -(BPT)_i \quad , \quad F_{1i} = -C'_{Ri} \quad , \quad i = 3,4 \tag{2.101}$$

Otherwise,

$$F_{1i} = C'_{Ri}\dot{\delta}_i/(BPT)_i \quad , \quad i = 3,4 \qquad (2.102)$$

$(BPT)_i$ is as in (2.91a)

F_{2i}, F_{3i} remain unchanged.

$$F_{4i} = (-1)^i R_R(\delta_3 - \delta_4)/T_R^2 \quad , \quad i = 3,4 \qquad (2.103)$$

F_{APi}, F_{ARi} remain unchanged.

The wheel orientations are

$$\phi_3 = \sum_{j=0}^{5} C_{3j}\,\delta_{S3}^j + K_{OT3}M_{x3} \qquad (2.104)$$

$$\phi_4 = -\sum_{j=0}^{5} C_{4j}\,\delta_{S4}^j + K_{OT4}M_{x4} \qquad (2.105)$$

$$\psi_3 = \sum_{j=0}^{5} D_{3j}\,\delta_{S3}^j + K_{SR}M_{ZR3} + K_{LR}F_{S3} \qquad (2.106)$$

$$\psi 4 = -\sum_{j=0}^{5} D_{4j}\,\delta_{S4}^j + K_{SR}M_{ZR4} + K_{LR}R_{S4} \qquad (2.107)$$

As a smoothing process the suspension forces are averaged according to the following scheme:

First Averaging

$$\bar{S}_i(t) = \tfrac{1}{2}(S_i(t) + S_i(t-\Delta t)) \qquad (2.108)$$

Second Averaging

$$\bar{\bar{S}}_i(t) = \tfrac{1}{2}(\bar{S}_i(t) + \bar{S}_i(t-\Delta t)) \qquad (2.109)$$

$$= \tfrac{1}{4}\left[S_i(t) + 2S_i(t-\Delta t) + S_i(t-2\Delta t)\right]$$

The weight components of the suspension forces are calculated by:

$$F_{SWF} = \left[(ST)_1 - \tfrac{1}{2}M_{uF}g\right]\cos\theta \qquad (2.110)$$

$$F_{SWR} = \left[(ST)_2 - \tfrac{1}{2}M_{uR}g\right]\cos\theta \qquad (2.111)$$

$$(ST)_1 = \tfrac{1}{2}g\left[M_{uF} + M_S b'/(a'+b')\right] \qquad (2.112)$$

$$(ST)_2 = \tfrac{1}{2}g\left[M_{uR} + M_S a'/(a'+b')\right] \qquad (2.113)$$

$$a' = a\cos\theta + z_F\sin\theta \qquad (2.114)$$

$$b' = b\cos\theta - z_R\sin\theta \qquad (2.115)$$

where in eqs. (2.110) throughout (2.115) θ is the initial value of θ for zero initial conditions.

§2.3.4. Aerodynamic Forces and Moments

The velocity of the cross-wind is given by:

For k such that $wd_{t1(k-1)} < X \leq wd_{t1k}$,

$$V_{yw} = wd_{t2(k-1)} + (X-wd_{t1(k-1)})(wd_{t2k} - wd_{t2(k-1)})/wd_{t1k}-wd_{t1(k-1)}) \quad , \tag{2.116}$$

Other aerodynamic quantities are

$$u_r = u - V_{yw}\sin\psi \tag{2.117}$$

$$v_r = v - V_{yw}\cos\psi \tag{2.118}$$

$$w_r = w \tag{2.119}$$

$$V_{CW} = \sqrt{u_r^2+v_r^2+w_r^2} \tag{2.120}$$

$$q_a = \frac{1}{2}\rho_a V_{CW}^2 \tag{2.121}$$

$$\tau = \sin^{-1}(\frac{v_r}{V_{CW}}), -3.14 \leq \tau \leq 3.14 \tag{2.122}$$

$$\bar{p} = (p-\omega_{xw}\cos\psi+\omega_{zw}\sin\theta)\ \frac{\ell}{u_r} \tag{2.123}$$

$$\bar{q} = (q+\omega_{xw}\sin\psi-\omega_{zw}\sin\phi)\ \frac{\ell}{u_r} \tag{2.124}$$

$$\bar{r} = (r-\omega_{zw})\ \frac{\ell}{u_r} \tag{2.125}$$

NOTE: If $u_r = 0, \bar{p}, \bar{q}, \bar{r} = 0$ (2.126)

$$\alpha = \tan^{-1}(\frac{w_r}{u_r}) \tag{2.127}$$

For k such that $dC_{x1(k-1)} < \alpha \leq dC_{x1k}$,

$$\Delta C_x = dC_{x2(k-1)} + (\alpha - dC_{x1(k-1)})(dC_{x2k} - dC_{x2(k-1)})/(dC_{x1k} - dC_{x1(k-1)}) \quad (2.128)$$

For k such that $C_{\tau 1(k-1)} < \tau \leq C_{\tau 1k}$,

$$f(RAC) = (C_{\tau 1(k-1)})/(C_{\tau 1k} - C_{\tau 1(k-1)}) \quad (2.129)$$

$$C_L = C_{\tau 2(k-1)} + f(RAC)(C_{\tau 2k} - C_{\tau 2(k-1)}) \quad (2.130)$$

$$C_M = C_{\tau 3(k-1)} + f(RAC)(C_{\tau 3k} - C_{\tau 3(k-1)}) \quad (2.131)$$

$$C_N = C_{\tau 4(k-1)} + f(RAC)(C_{\tau 4k} - C_{\tau 4(k-1)}) \quad (2.132)$$

$$C_X = C_{\tau 5(k-1)} + f(RAC)(C_{\tau 5k} - C_{\tau 5(k-1)}) \quad (2.133)$$

$$C_Y = C_{\tau 6(k-1)} + f(RAC)(C_{\tau 6k} - C_{\tau 6(k-1)}) \quad (2.134)$$

$$C_Z = C_{\tau 7(k-1)} + f(RAC)(C_{\tau 7k} - C_{\tau 7(k-1)}) \quad (2.135)$$

$$\Sigma F_{xs} = (C_X + \Delta C_X) q_a S_f \quad (2.136)$$

$$\Sigma F_{ys} = (C_Y + C_{y_p} \bar{p} + C_{y_r} \bar{r}) q_a S_f \quad (2.137)$$

$$\Sigma F_{zs} = (C_Z + C_{z_\alpha} \alpha + C_{z_q} \bar{q}) q_a S_f \quad (2.138)$$

$$d_{CG} = a - \frac{\ell}{2} \quad (2.139)$$

$$C'_L = \frac{\ell_v}{\ell} C_L + \frac{Z_{(O)}}{\ell} C_Y \quad (2.140)$$

$$C'_M = \frac{\ell_v}{\ell} C_M - \frac{d_{CG}}{\ell} C_Z - \frac{Z_{(O)}}{\ell} C_X \quad (2.141)$$

$$C'_N = \frac{\ell_v}{\ell} C_N + \frac{d_{CG}}{\ell} C_Y \quad (2.142)$$

$$\Sigma N_{\phi s} = (C_L' + C_{\ell_p} \bar{p} + C_{\ell_r} \bar{r}) q_a S_f \ell \tag{2.143}$$

$$\Sigma N_{\theta s} = (C_M' + C_{m_\alpha} \alpha + C_{m_q} \bar{q}) q_a S_f \ell \tag{2.144}$$

$$\Sigma N_{\psi s} = (C_N' + C_{n_p} \bar{p} + C_{n_r} \bar{r}) q_a S_f \ell \tag{2.145}$$

§2.3.5. Resultant Forces and Moments.

The resultant tire forces acting on the unsprung masses are given by, for i=1...4:

$$F_{xui} = -F'_{Ri}a_{31} + F_{Ci}(a_{11}\cos\alpha_{ci}+a_{21}\cos\beta_{ci}) \quad (2.146)$$
$$+ F_{Si}(-a_{11}\cos\beta_{ci}+a_{21}\cos\alpha_{ci})$$

$$F_{yui} = - F'_{Ri}a_{32} + F_{Ci}(a_{12}\cos\alpha_{ci}+a_{22}\cos\beta_{ci}) \quad (2.147)$$
$$+ F_{Si}(-a_{12}\cos\beta_{ci}+a_{22}\cos\alpha_{ci})$$

$$F_{zui} = - F'_{Ri}a_{33} + F_{Ci}(a_{13}\cos\alpha_{ci}+a_{23}\cos\beta_{ci}) \quad (2.148)$$
$$+ F_{Si}(-a_{13}\cos\beta_{ci}+a_{23}\cos\alpha_{ci})$$

Note: If the pitch and roll angles θ, ϕ are assumed small,

$$F_{xui} = F_{Ri}\theta + F_{Ci}\cos\psi_i - F_{Si}\sin\psi_i \quad (2.149)$$

$$F_{yui} = -F_{Ri}\phi + F_{Ci}\sin\psi_i + F_{Si}\cos\psi_i \quad (2.150)$$

$$F_{zui} = - F_{Ri} \quad (2.151)$$

$$\Sigma F_{xu} = \sum_{i=1}^{4} F_{xui} \quad (2.152)$$

$$\Sigma F_{yu} = \sum_{i=1}^{4} F_{yui} \quad (2.153)$$

where

$$\cos \alpha_{ywi} = a_{11}(-\sin\psi_i) + a_{12}(\cos\phi_i \cos\psi_i) + a_{13}(\sin\phi_i \cos\psi_i) \tag{2.154}$$

$$\cos \beta_{ywi} = a_{21}(-\sin\psi_i) + a_{22}(\cos\phi_i \cos\psi_i) + a_{23}(\sin\phi_i \cos\psi_i) \tag{2.155}$$

$$\cos \gamma_{ywi} = a_{31}(-\sin\psi_i) + a_{32}(\cos\phi_i \cos\psi_i) + a_{33}(\sin\phi_i \cos\psi_i) \tag{2.156}$$

$$\cos \alpha_{ci} = \frac{\cos\beta_{ywi}}{\sqrt{\cos^2\beta_{ywi} + \cos^2\alpha_{ywi}}} \tag{2.157}$$

$$\cos \beta_{ci} = \frac{-\cos\alpha_{ywi}}{\sqrt{\cos^2\beta_{ywi} + \cos^2\alpha_{ywi}}} \tag{2.158}$$

The resultant tire moments acting on the unsprung masses are given by:

$$\Sigma N_{\phi u} = (S_2-S_1)\frac{T_F}{2} + (S_4-S_3)\frac{T_{SR}}{2}$$

$$- F_{yu1}[z_F+RR_1\cos\gamma_{h1}-h_{FC}+O_4(\delta_1)]$$

$$- F_{yu2}[z_F+RR_2\cos\gamma_{h2}-h_{FC}+O_4(\delta_2)]$$

$$- (F_{yu3}+F_{yu4})[z_R+O_4(\delta_R)] + M_{x1} + M_{x2} \qquad (2.159S)$$

$$\Sigma N_{\theta u} = 2F_{SWF}a - 2F_{SWR}b + (S_1+S_2)a - (S_3+S_4)b$$

$$+ F_{xu1}[z_F+RR_1\cos\gamma_{h1}+O_4(\delta_1)]$$

$$+ F_{xu2}[z_F+RR_2\cos\gamma_{h2}+O_4(\delta_2)]$$

$$+ F_{xu3}[z_R+\frac{T_R}{2}\phi_R+RR_3\cos\gamma_{h3}+O_4(\delta_R)]$$

$$+ F_{xu4}[z_R-\frac{T_R}{2}\phi_R+RR_4\cos\gamma_{h4}+O_4(\delta_R)]$$

$$+ O_1[(F_{xu3}+F_{xu4})\rho_R] + O_7[(RR_1F_{zu1}+RR_2F_{zu2}$$

$$+RR_3F_{zu3}+RR_4F_{zu4})\sin\theta-I_{WF}(\dot{\omega}_1+\dot{\omega}_2)$$

$$- I_{WR}(\dot{\omega}_3+\dot{\omega}_4)] \qquad (2.160S)$$

$$\Sigma N_{\psi u} = F_{yu1}(a+RR_1\cos\alpha_{h1}) + F_{yu2}(a+RR_2\cos\alpha_{h2})$$
$$- F_{yu3}(b-RR_3\cos\alpha_{h3}) - F_{yu4}(b-RR_4\cos\alpha_{h4})$$
$$+ F_{xu2}(\frac{T_F}{2} - RR_2\cos\beta_{h2}) - F_{xu1}(\frac{T_F}{2}+RR_1\cos\beta_{h1})$$
$$+ F_{xu4}(\frac{T_R}{2} - RR_4\cos\beta_{h4}) - F_{xu3}(\frac{T_R}{2}+RR_3\cos\beta_{h3})$$
$$+ M_{z1} + M_{z2} + M_{z3} + M_{z4} + O_1[\rho_R\phi_R(F_{xu3}+F_{xu4})] \quad (2.161)$$

$$\Sigma N_{\phi R} = F_{zu3}(\frac{T_R}{2}+RR_3\cos\beta_{h3}) - F_{zu4}(\frac{T_R}{2} - RR_4\cos\beta_{h4})$$
$$- F_{yu3}(-\frac{T_R}{2}\phi_R+RR_3\cos\gamma_{h3}) - F_{yu4}(-\frac{T_R}{2}\phi_R+RR_4\cos\gamma_{h4})$$
$$+ (S_3-S_4)\frac{T_{SR}}{2} + M_{x3} + M_{x4} - O_1[(F_{zu3}+F_{zu4})\rho_R\phi_R$$
$$+ (F_{yu3} + F_{yu4})\rho_R] \quad (2.162S)$$

Note: If the pitch and roll angles θ and ϕ are assumed to be small,

$$\Sigma N_{\phi u} = (S_2-S_1)T_F/2 + (S_4-S_3)T_{SR}/2 - (F_{yu3}+F_{yu4})z_R$$
$$- F_{yu1}(z_F+RR_1-h_{FC}) - F_{yu2}(z_F+RR_2-h_{FC})$$
$$- O_4[F_{yu1}\delta_1+F_{yu2}\delta_2+(F_{yu3}+F_{yu4})\delta_R]$$
$$+ M_{x1} + M_{x2} \quad (2.163S)$$

$$\Sigma N_{\theta u} = (S_1+S_2)a - (S_3+S_4)b + 2(F_{SWF}{}^2-F_{SWR}b)$$
$$+ F_{xu1}(z_F+RR_1) + F_{xu2}(z_F+RR_2) + F_{xu3}(z_R+RR_3$$
$$+ T_R\phi_R/2 + F_{xu4}(z_R+RR_4-T_R\phi_R/2) + O_1[\rho_R(F_{xu3}$$
$$+ F_{xu4})] + O_4(F_{xu1}\delta_1+F_{xu2}\delta_2+F_{xu3}\delta_R+F_{xu4}\delta_R)$$
$$+ O_7[(RR_1F_{zu1}+RR_2F_{zu2}+RR_3F_{zu3}+RR_4F_{zu4})\theta$$
$$- I_{WF}I\dot{\omega}_1+\dot{\omega}_2)-I_{WR}(\dot{\omega}_3+\dot{\omega}_4)] \qquad (2.164S)$$

$$\Sigma N_{\psi u} = (F_{yu1}+F_{yu2})a - (F_{yu3}+F_{yu4})b + (F_{xu2}-F_{xu1})T_F/2$$
$$+ (F_{xu4}-F_{xu3})T_R/2 + M_{z1} + M_{z2} + M_{z3} + M_{z4}$$
$$+ O_1[\rho_R(F_{xu3}+F_{xu4})\phi_R] \qquad (2.165)$$

$$\Sigma N_{\phi R} = (S_3-S_4)T_{SR}/2 - F_{yu3}(RR_3+T_R\phi_R/2)$$
$$- F_{yu4}(RR_4-T_R\phi_R/2)+F_{zu3}(T_R/2-RR_3\phi_R)$$
$$- F_{zu4}(T_R/2+RR_4\phi_R) + M_{x3} + M_{x4}$$
$$- O_1\{\rho_R[(F_{yu3}+F_{yu4})+(F_{zu3}+F_{zu4})\phi_R]\} \qquad (2.166S)$$

---

where

$$\cos \gamma_{Ri} = \frac{\cos^2 \alpha_{ywi} + \cos^2 \beta_{ywi}}{\sqrt{\cos^2 \alpha_{ywi} + \cos^2 \beta_{ywi}}} \tag{2.167}$$

$$\cos \alpha_{Ri} = \frac{-\cos \gamma_{ywi} \cos \alpha_{ywi}}{\sqrt{\cos^2 \alpha_{ywi} + \cos^2 \beta_{ywi}}} \tag{2.168}$$

$$\cos \beta_{Ri} = \frac{-\cos \gamma_{ywi} \cos \beta_{ywi}}{\sqrt{\cos^2 \alpha_{ywi} + \cos^2 \beta_{ywi}}} \tag{2.169}$$

$$\cos \alpha_{hi} = a_{11} \cos \alpha_{Ri} + a_{21} \cos \beta_{Ri} + a_{31} \cos \gamma_{Ri} \tag{2.170}$$

$$\cos \beta_{hi} = a_{12} \cos \alpha_{Ri} + a_{22} \cos \beta_{Ri} + a_{32} \cos \gamma_{Ri} \tag{2.171}$$

$$\cos \gamma_{hi} = a_{13} \cos \alpha_{Ri} + a_{23} \cos \beta_{Ri} + a_{33} \cos \gamma_{Ri} \tag{2.172}$$

$$\Sigma N_{\phi u} = (S_2 - S_1)\frac{T_F}{2} + (S_4 - S_3)\frac{T_R}{2}$$

$$-F_{yu1}\left[z_F + h_1 \cos \gamma_{h1} - h_{FC} + 0_4(\delta_1)\right]$$

$$-F_{yu2}\left[z_F + h_2 \cos \gamma_{h2} - h_{FC} + 0_4(\delta_2)\right]$$

$$-F_{yu3}\left[z_R + h_3 \cos \gamma_{h3} - h_{RC} + 0_4(\delta_3)\right]$$

$$-F_{yu4}\left[z_R + h_4 \cos \gamma_{h4} - h_{RC} + 0_4(\delta_4)\right]$$

$$+M_{x1} + M_{x2} + M_{x3} + M_{x4} \tag{2.159I}$$

$$\Sigma N_{\theta u} = 2F_{SWF}a - 2F_{SWR}b + (S_1+S_2)a - (S_3+S_4)b$$
$$+F_{xu1}[z_F+h_1\cos\gamma_{h1}+O_4(\delta_1)]$$
$$+F_{xu2}[z_F+h_2\cos\gamma_{h2}+O_4(\delta_2)]$$
$$+F_{xu3}[z_R+h_3\cos\gamma_{h2}+O_4(\delta_3)]$$
$$+F_{xu2}[z_F+RR_2\cos\gamma_{h2}+O_4(\delta_2)]$$
$$+F_{xu3}[z_R+RR_3\cos\gamma_{h3}+O_4(\delta_3)]$$
$$+F_{xu4}[z_R+RR_4\cos\gamma_{h4}+O_4(\delta 4)]$$
$$+O_7[(RR_1F_{zu1}+RR_2F_{zu2}$$
$$+RR_3F_{zu3}+RR_4F_{zu4})\sin\theta]-I_{WF}(\dot{\omega}_1+\dot{\omega}_2)$$
$$-I_{WR}(\dot{\omega}_3+\dot{\omega}_4)] \qquad (2.160I)$$

NOTE: If the pitch and roll angles θ and ϕ are assumed small, then,

$$\Sigma N_{\phi u} = (S_2-S_1)T_F/2 + (S_4-S_3)T_R/2$$
$$-F_{yu1}[z_F + RR_1 + O_4(\delta_1) - h_{FC}]$$
$$-F_{yu2}[z_F + RR_2 + O_4(\delta_2) - h_{FC}]$$
$$-F_{yu3}[z_R + RR_3 + O_4(\delta_3) - h_{RC}]$$
$$-F_{yu4}[z_R + RR_4 + O_4(\delta_4) - h_{RC}]$$
$$+M_{x1} + M_{x2} + M_{x3} + M_{x4} \qquad (2.163I)$$

$$\Sigma N_{\phi J} = 2F_{SWF}a - 2F_{SWR}b + (S_1+S_2)a$$
$$- (S_3+S_4)b + F_{xu1}[z_F + RR_1 + O_4(\delta_1)]$$
$$+ F_{xu2}[z_F + RR_2 + O_4(\delta_2)]$$
$$+ F_{xu3}[z_R + RR_3 + O_4(\delta_3)]$$
$$+ F_{xu4}[z_R + RR_4 + O_4(\delta_4)]$$
$$+ O_7[(RR_1F_{zu1}+RR_2F_{zu2}+RR_3F_{zu3}+RR_4F_{xu4})\sin\theta]$$
$$- I_{WF}(\dot{\omega}_1 + \dot{\omega}_2) - I_{WR}(\dot{\omega}_3 + \dot{\omega}_4)$$

(2.164I)

The jacking forces are given by:

$$F_{J1} = -F_{yu1}\tan^{-1}(2h_{FC}/T_F) \qquad (2.173)$$

$$F_{J2} = F_{yu2}\tan^{-1}(2h_{FC}/T_F) \qquad (2.174)$$

$$F_{J3} = -F_{yu3}\tan^{-1}(2h_{RC}/T_R) \qquad (2.175I)$$

$$F_{J4} = F_{yu4}\tan^{-1}(2h_{RC}/T_R) \qquad (2.176I)$$

§2.3.6. Steering Equations

The steering equations are given by:

$$\begin{aligned} M_{Ti} &= -(y_{SAi} - RR_l \phi_{SAOi}) [(F_{xui} - F_{zui}\theta_{Si})\cos \psi_i' \\ &+ (F_{yui} + F_{zui}\phi_{SAi})\sin \psi_i'] \\ &- \overline{PT}_i \cos \psi_i' [(F_{yui} + F_{zui}\phi_{SAi})\cos \psi_i' \\ &- (F_{xui} - F_{zui}\theta_{Si})\sin \psi_i'] \end{aligned} \tag{2.177}$$

$$\begin{aligned} y_{CR} &= a_p S_w / N_G + a_p^2 [(M_{Tl} + M_{zl} - I_{FW}\dot{r})/A_{Ll} \\ &+ (M_{T2} + M_{z2} - I_{FW}\dot{r})/A_{L2}]/K_{SC}N_G^2) \end{aligned} \tag{2.178}$$

$$\delta_{FWi} = y_{CR}/A_{Li} + (M_{Ti} + M_{zi} - I_{FW}\dot{r})/K_{SLi}, \quad i=1,2$$

$$M_{SSi} = K_{SLi} (\delta_{Fwi} - y_{CR}/A_{Li}), \quad i=1,2 \tag{2.179}$$

§2.3.7. Tire Rolling Radii

The rolling radii of the tires are calculated by, for i = 1...4:

$$\begin{aligned} RR_i &= \Delta_i, \text{ for } R_{RIMi} \leq \Delta_i \leq R_{wi} \\ &= R_{RIMi} \text{ for } R_{RIMi} \geq \Delta_i \\ &= R_{wi} \text{ for } R_{wi} < \Delta_i \end{aligned} \tag{2.180}$$

$$z_1 = z + a_{31}a + a_{32}\, T_F/2 + a_{33}z_F + a_{33}\, O_4(\delta_1) \tag{2.181}$$

$$z_2 = z + a_{31}a - a_{32}\, T_F/2 + a_{33}\, z_F + a_{33}\, O_4(\delta_2) \tag{2.182}$$

$$\begin{aligned} z_3 = {} & z - a_{31}b + a_{32}\, T_R/2 + a_{33}(z_R + T_R\phi_R/2) \\ & + a_{33}\, O_4(\delta_R) - O_1(a_{32}\rho_R\phi_R - a_{33}\rho_R) \end{aligned} \tag{2.183S}$$

$$\begin{aligned} z_4 = {} & z - a_{31}b - a_{32}\, T_R/2 + a_{33}(z_R - T_R\phi_R/2) \\ & + a_{33}\, O_4(\delta_R) - O_1(a_{32}\rho_R\phi_R - a_{33}\rho_R) \end{aligned} \tag{2.184S}$$

$$\Delta_i = \frac{z_{Si} - z_i}{\cos\gamma_{Ri}} \tag{2.185}$$

$$z_3 = z - a_{31}b + a_{32}T_R/2 + a_{33}z_R + a_{33}O_4(\delta_R) \qquad (2.183I)$$

$$z_4 = z - a_{31}b - a_{32}T_R/2 + a_{33}z_R + a_{33}O_4(\delta_R) \qquad (2.184I)$$

NOTE: If the pitch and roll angles θ and ϕ are assumed to be small,

$$RR_i = -z_i + z_{Si}, \quad i=1...4$$

If

$$RR_i < R_{RIMi}, \; RR_i = R_{RIMi}, \quad i=1...4$$

If

$$RR_i > R_{wi}, \; RR_i = R_{wi}, \; i=1...4 \qquad (2.186)$$

$$z_1 = z - a\theta + T_F\phi/2 + z_F + O_4(\delta_1) \qquad (2.187)$$

$$z_2 = z - a\theta - T_F\phi/2 + z_F + O_4(\delta_2) \qquad (2.188)$$

$$z_3 = z + b\theta + z_R + (\phi+\phi_R)T_R/2 + O_4(\delta_R) + O_1[\rho_R(1-\phi\phi_R)] \qquad (2.189S)$$

$$z_4 = z + b\theta + z_R - (\phi+\phi_R)T_R/2 + O_4(\delta_R) + O_1[\rho_R(1-\phi\phi_R)] \qquad (2.190S)$$

$$z_3 = z + b\theta + z_R + T_R/2 + O_4(\delta_R) \qquad (2.189I)$$

$$z_4 = z + b\theta + z_R - T_R/2 + O_4(\delta_R) \qquad (2.190I)$$

The ground elevation z_{Si} which appears in the above equation is calculated in the program by the equations

$$X_{Ci} = X + a\, a_{11} - (-1)^i T_F a_{12}/2 + Z\, a_{13},\ i = 1,2 \quad (2.191)$$

$$Y_{Ci} = Y + a\, a_{21} - (-1)^i\, T_F\, a_{22}/2 + Z\, a_{23},\ i = 1,2 \quad (2.192)$$

$$X_{Ci} = X - b\, a_{11} - (-1)^i\, T_R\, a_{12}/2 + Z\, a_{13},\ i = 3,4 \quad (2.193)$$

$$Y_{Ci} = Y - b\, a_{21} - (-1)^i\, T_R\, a_{22}/2 + Z\, a_{23},\ i = 3,4 \quad (2.194)$$

$$z_{Si} = h_t \sin[(X_{Ci}-X_o)/X_{wv}] \sin[(Y_{Ci}-Y_o)/Y_{wv}],\ i = 1\ldots4 \quad (2.195)$$

§2.3.8. Tire Slip Angles and Contact Patch Velocities.

The velocities along the vehicle axis of the tire contact patches are determined by:

$$u_i = u + (-1)^i T_F r/2 + z_F q + O_4(\delta_i q), \quad i=1...2 \tag{2.196}$$

$$v_i = v + ar - (z_F+RR_i)p + O_3[RR_i(1-\cos\gamma_{hi})p] + O_4(-\delta_i p), \quad i=1...2. \tag{2.197}$$

$$w_i = w - aq - (-1)^i T_F p/2 + \dot{\delta}_i + O_3(RR_i \cos\beta_{hi} p) \quad i = 1,2 \tag{2.198}$$

$$u_i = u + (-1)^i T_R r/2 + z_R q + (-1)^i T_R q\phi_R/2 + O_1(\rho_R\phi_R r) + O_5(q\delta_R), \quad i = 3, 4 \tag{2.199S}$$

$$v_i = v - br - (z_R+RR_i)p - RR_i\dot{\phi}_R + (-1)^i T_R p\phi_R/2 + O_1[-\rho_R(p+\dot{\phi}_R)] + O_3[RR_i(1-\cos\gamma_{hi})(p+\dot{\phi}_R)] + O_5(-p\delta_R) + O_6[(-1)^i T_R\dot{\phi}_R\phi_R/2], \quad i = 3, 4 \tag{2.200S}$$

$$w_i = w + bq + \dot{\delta}_R - (-1)^i(p+\dot{\phi}_R)T_R/2 + O_1(-\rho_R\phi_R p) + O_{16}(-\rho_R\dot{\phi}_R\phi_R) + O_3[RR_i \cos\beta_{hi}(p+\dot{\phi}_R)], \quad i = 3, 4 \tag{2.201S}$$

$$u_i = u + (-1)^i T_R r/2 + z_R q + O_5(q\delta_R), \quad i = 3, 4 \tag{2.199I}$$

$$v_i = v - br - (z_R + RR_i)p + O_3[RR_i(1-\cos\gamma_{hi})p] + O_5(-p\delta_R) \quad i = 3, 4 \tag{2.200I}$$

$$w_i = w + bq + \dot{\delta}_i - (-1)^i(p)T_R/2 + O_3[RR_i\cos\beta_{hi}(p)] \quad i = 3, 4 \tag{2.201I}$$

$$\cos\theta_{XGi} = \frac{\cos\theta\cos\phi}{\sqrt{\cos^2\phi + \sin^2\phi\sin^2\theta}} \tag{2.202}$$

$$\sin\theta_{XGi} = \frac{\sin\theta}{\sqrt{\cos^2\phi + \sin^2\phi\sin^2\theta}}$$

NOTE: If the pitch and roll angles θ and ϕ are assumed to be small then,

$$\cos\theta_{XGi} = 1 \tag{2.204}$$

$$\sin\theta_{XGi} = \theta \tag{2.205}$$

$$u_{Gi} = u_i \cos\theta_{XGi} + w_i \sin\theta_{XGi}, \quad i = 1,2,3,4 \tag{2.206}$$

$$v_{Gi} = v_i \cos\phi - w_i \sin\phi \quad i = 1,2,3,4 \tag{2.207}$$

$$C_{vi} = (u_{Gi}^2 + v_{Gi}^2)^{1/2}, \quad i=1...4 \tag{2.208}$$

$$\psi_i' = \cos^{-1}\left[\frac{a_{11}\cos\beta_{ywi} - a_{21}\cos\alpha_{ywi}}{\cos\theta\sqrt{\cos^2\alpha_{ywi} + \cos^2\beta_{ywi}}}\right], \quad i=1...4 \tag{2.209}$$

$$(Vel)_i = u_{Gi}\cos\psi_i' + v_{Gi}\sin\psi_i', \quad i=1...4 \tag{2.210}$$

$$\beta_i = \tan^{-1}\left(\frac{v_{Gi}}{|u_{Gi}|}\right) - \psi_i' \operatorname{sgn}(u_{Gi}), \quad i = 1,2,3,4 \tag{2.211}$$

NOTE: If the pitch and roll angles θ and ϕ are assumed to be small, then

$$\psi_i' = \psi_i, \quad i=1...4 \tag{2.212}$$

$$(Vel)_i = u_{Gi}\cos\psi_i + v_{Gi}\sin\psi_i, \quad i=1...4 \tag{2.213}$$

$$\beta_i = \tan^{-1}\left[\frac{v_{Gi}}{|u_{Gi}|}\right] - \psi_i \operatorname{sgn} u_{Gi}, \quad i=1,2,3,4 \tag{2.214}$$

§2.3.9. Wheel Spins and Longitudinal Slips

The wheel angular velocities are given by

$$\omega_i = (1-s_i)RR_i/(Vel)_i \quad , \quad i=1...4 \tag{2.215}$$

The longitudinal slips are calculated by:

FRONT END

$$D_1 = (Vel)_1\Delta_1 \tag{2.216}$$

$$D_2 = (Vel)_2\Delta_1 \tag{2.217}$$

$$\Delta_1 = \bar{I}_F^2 - \bar{I}_{FC}^2 \tag{2.218}$$

$$\bar{I}_F = I_{WF} + \tfrac{1}{4}I_{DF}(\overline{AR}_F)^2 \tag{2.218a}$$

$$\bar{I}_{FC} = \tfrac{1}{4}I_{DF}(\overline{AR}_F)^2 \tag{2.218b}$$

$$F_{Ci} = \eta_i + \zeta_i s_i \tag{2.218c}$$

$$\eta_i = [s_i^0\frac{\partial\mu_i'}{\partial s_i}(s_i^0)-\mu_i'(s_i^0)]F_{Ri}' \tag{2.218d}$$

$$\zeta_i = -F_{Ri}'\frac{\partial\mu_i'}{\partial s_i}(s_i^0) \tag{2.218e}$$

$$Q_1 = (\dot{Vel})_1/(Vel)_1 - (RR_1)^2\bar{I}_F\zeta_1/D_1 \tag{2.219}$$

$$Q_2 = (\dot{Vel})_2/(Vel)_2 - (RR_2)^2\bar{I}_F\zeta_2/D_2 \tag{2.220}$$

$$E_1 = (RR_1)(RR_2)\bar{I}_{FC}\zeta_2/D_1 \tag{2.221}$$

$$E_2 = (RR_1)(RR_2)\bar{I}_{FC}\zeta_1/D_2 \tag{2.222}$$

$$\tau_i = (1-\lambda_D)(\overline{AR}_F/2)\overline{TQ}_D + \overline{TQ}_{Bi} \quad , \quad i=1,2... \tag{2.223}$$

$$R_1 = (\dot{Vel})_1/(Vel)_1 + [(RR_1)^2\bar{I}_F\eta_1-(RR_1)(RR_2)\bar{I}_{FC}\eta_2 - (RR_1)(\bar{I}_F\tau_1-\bar{I}_{FC}\tau_2)]/D_1 \quad (2.224)$$

$$R_2 = (\dot{Vel})_2/(Vel)_2 + [(RR_2)^2\,\bar{I}_F\eta_2 - (RR_1)(RR_2)\bar{I}_{FC}\eta_1 - (RR_2)(\bar{I}_F\tau_2-\bar{I}_{FC}\tau_1)]/D_2 \quad (2.225)$$

$$\Gamma_1 = \frac{R_1}{Q_1} + \frac{E_1E_2R_1 - E_1R_2Q_1}{Q_1(Q_1Q_2 - E_1E_2)} \quad (2.226)$$

$$\Gamma_2 = \frac{R_2}{Q_2} + \frac{E_1E_2R_2 - E_2R_1Q_2}{Q_2(Q_1Q_2 - E_1E_2)} \quad (2.227)$$

$$\lambda_1 = -\frac{Q_1 + Q_2}{2} + \tfrac{1}{2}[(Q_1+Q_2)^2 - 4(Q_1Q_2 - E_1E_2)]^{\frac{1}{2}} \quad (2.228)$$

$$\lambda_2 = -\frac{Q_1 + Q_2}{2} - \tfrac{1}{2}[(Q_1+Q_2)^2 - 4(Q_1Q_2 - E_1E_2)]^{\frac{1}{2}} \quad (2.229)$$

$$\Theta_1 = [(s_1^o-\Gamma_1)(\lambda_2+Q_1)-E_1(\Gamma_2-s_2^o)]/(\lambda_2-\lambda_1) \quad (2.230)$$

$$\Theta_2 = [E_1(\Gamma_2-s_2^o)-(s_1^o-\Gamma_1)(\lambda_1+Q_1)]/(\lambda_2-\lambda_1) \quad (2.231)$$

$$s_1 = \Gamma_1 + \Theta_1 e^{\lambda_1(t-t_o)} + \Theta_2 e^{\lambda_2(t-t_o)} \quad (2.232)$$

$$s_2 = \Gamma_2 - (\frac{\lambda_1+Q_1}{E_1})\Theta_1 e^{\lambda_1(t-t_o)} - (\frac{\lambda_2+Q_1}{E_1})\Theta_2 e^{\lambda_2(t-t_o)} \quad (2.233)$$

Special Case: If $E_1 = 0$

$$s_1 = \Gamma_1 + (s_1^o - \Gamma_1)e^{-Q_1(t-t_o)} \tag{2.234}$$

$$s_2 = \Gamma_2 - (\Gamma_2 - s_2^o)e^{-Q_2(t-t_o)} \tag{2.235}$$

Note that for both cases if

$$s_i > 1 \quad , \quad s_i \equiv 1 \quad , \quad i = 1,2 \tag{2.236}$$

$$\dot{s}_1 = R_1 - Q_1 s_1 - E_1 s_2 \tag{2.237}$$

$$\dot{s}_2 = R_2 - Q_2 s_2 - E_2 s_1 \tag{2.238}$$

$$\dot{\omega}_1 = \frac{1}{RR_2}[(\dot{Vel})_1(1-s_1) - \dot{s}_1(Vel)_1] \tag{2.239}$$

$$\dot{\omega}_2 = \frac{1}{RR_2}[(\dot{Vel})_2(1-s_2) - \dot{s}_2(Vel)_2] \tag{2.240}$$

REAR END

$$D_3 = (Vel)_3 \Delta_2 \tag{2.241}$$

$$D_4 = (Vel)_4 \Delta_2 \tag{2.242}$$

$$\Delta_2 = \bar{I}_R^2 - I_{RC}^2 \tag{2.243}$$

$$\bar{I}_R = I_{WR} + \tfrac{1}{4} I_{DR}(\overline{AR}_R)^2 \tag{2.243a}$$

$$\bar{I}_{RC} = \tfrac{1}{4} I_{DR}(\overline{AR}_R)^2 \tag{2.243b}$$

$$Q_3 = (\dot{Vel})_3/(Vel)_3 - (RR_3)^2 \bar{I}_R \zeta_3 / D_3 \tag{2.244}$$

$$Q_4 = (\dot{Vel})_4/(Vel)_4 - (RR_4)^2 \bar{I}_R \zeta_4 / D_4 \tag{2.245}$$

$$E_3 = (RR_3)(RR_4)\bar{I}_{RC}\zeta_4/D_3 \tag{2.246}$$

$$E_4 = (RR_3)(RR_4)\bar{I}_{RC}\zeta_3/D_4 \tag{2.247}$$

$$\tau_i = \lambda_D(\overline{AR}_R/2)\overline{TQ}_D + \overline{TQ}_{Bi} \quad , \quad i = 3,4 \tag{2.248}$$

$$R_3 = (\dot{Vel})_3/(Vel)_3 + [(RR_3)^2\bar{I}_R\eta_3 - (RR_3)(RR_4)\bar{I}_{RC}\eta_4 - (RR_3)(\bar{I}_R\tau_3-\bar{I}_{FC}\tau_4)]/D_3 \tag{2.249}$$

$$R_4 = (\dot{Vel})_4/(Vel)_4 + [(RR_4)^2\bar{I}_R\eta_4 - (RR_3)(RR_4)\bar{I}_{RC}\eta_3 - (RR_4)(\bar{I}_R\tau_4-\bar{I}_{RC}\tau_3)]/D_4 \tag{2.250}$$

$$\Gamma_3 = \frac{R_3}{Q_3} + \frac{E_3E_4R_3 - E_3R_4Q_3}{Q_3(Q_3Q_4-E_3E_4)} \tag{2.251}$$

$$\Gamma_4 = \frac{R_4}{Q_4} + \frac{E_3E_4R_4 - E_4R_3Q_4}{Q_4(Q_3Q_4-E_3E_4)} \tag{2.252}$$

$$\lambda_3 = -\frac{Q_3+Q_4}{2} + \tfrac{1}{2}[(Q_3+Q_4)^2 - 4(Q_3Q_4-E_3E_4)]^{\frac{1}{2}} \tag{2.253}$$

$$\lambda_4 = -\frac{Q_3+Q_4}{2} + \tfrac{1}{2}[(Q_3+Q_4)^2 - 4(Q_3Q_4-E_3E_4)]^{\frac{1}{2}} \tag{2.254}$$

$$\Theta_3 = [(s_3^o-\Gamma_3)(\lambda_4+Q_3)-E_3(\Gamma_4-s_4^o)]/(\lambda_4-\lambda_3) \tag{2.255}$$

$$\Theta_4 = [E_3(\Gamma_4-s_4^o)-(s_3^o-\Gamma_3)(\lambda_3+Q_3)]/(\lambda_4-\lambda_3) \tag{2.256}$$

$$s_3 = \Gamma_3 + \Theta_3 e^{\lambda_3(t-t_o)} + \Theta_4 e^{\lambda_4(t-t_o)} \tag{2.257}$$

$$s_4 = \Gamma_4 - (\frac{\lambda_3+Q_3}{E_3})\Theta_3 e^{\lambda_3(t-t_o)} - (\frac{\lambda_4+Q_3}{E_3})\Theta_4 e^{\lambda_4(t-t_o)} \tag{2.258}$$

Special case: If $E_3 = 0$

$$s_3 = \Gamma_3 + (s_3^o-\Gamma_3)e^{-Q_3(t-t_o)} \tag{2.259}$$

$$s_4 = \Gamma_4 - (\Gamma_4-s_4^o)e^{-Q_4(t-t_o)} \tag{2.260}$$

Note that for both cases, if

$$s_i > 1 \quad , \; s_i \equiv 1 \quad , \quad i = 3,4 \tag{2.261}$$

$$\dot{s}_3 = R_3 - Q_3 s_3 - E_3 s_4 \tag{2.262}$$

$$\dot{s}_4 = R_4 - Q_4 s_4 - E_4 s_3 \tag{2.263}$$

$$\dot{\omega}_3 = \frac{1}{RR_3}[(\dot{Vel})_3(1-s_3) - \dot{s}_3(Vel)_3] \tag{2.264}$$

$$\dot{\omega}_4 = \frac{1}{RR_4}[(\dot{Vel})_4(1-s_4) - \dot{s}_4(Vel)_4] \tag{2.265}$$

§2.3.10. Tire Camber Angles

The tire camber angles are calculated by

$$\phi_{CGi} = \sin^{-1}(\cos \gamma_{ywi}) + K_{CF} F_{Si} \quad i = 1,2 \qquad (2.266)$$

$$\phi_{CGi} = \sin^{-1}(\cos \gamma_{ywi}) + K_{CR} F_{Si} \quad i = 3,4 \qquad (2.267)$$

NOTE: If the pitch and roll angles θ and ϕ are assumed to be small, then

$$\phi_{CGi} = \theta \sin \psi_i + \phi \cos \psi_i + \phi_i + K_{CF} F_{Si} \quad i = 1,2 \qquad (2.268)$$

$$\phi_{CGi} = \theta \sin \psi_i + \phi \cos \psi_i + \phi_i + K_{CR} F_{Si} \quad i = 3,4 \qquad (2.269)$$

§2.3.11. Tire Forces and Moments

The tire radial forces are calculated by, for i = 1...4:

$$F_{Ri} = K_{Ti}(R_{wi}-RR_i) \tag{2.270}$$

$$F'_{Ri} = \frac{F_{Ri}-F_{Si}\sin\phi_{CGi}}{\cos\phi_{CGi}} \tag{2.271}$$

Note: If the pitch and roll angles θ and ϕ are assumed to be small then

$$F'_{Ri} = F_{Ri} \tag{2.272}$$

Camber causes the slip angles to be modified by β'_i, where:

For $F'_{Ri} \leq A_{T1i}$

$$\text{(a)} \quad \beta'_i = \frac{A_{T3i}(A_{4i}-F'_{Ri})F'_{Ri}\phi_{CGi}}{A_{4i}[A_{1i}(F'_{Ri}-A_{2i})F'_{Ri}-A_{T2i}]} \tag{2.273}$$

For $F'_{Ri} \quad A_{T1i}$

$$\text{(b)} \quad \beta'_i = \frac{A_{T5i}\phi_{CGi}}{A_{4i}A_{T4i}} \tag{2.274}$$

where

$$A_{T1i} = A_{2i}A\Omega_{Ti} \quad , \quad i=1...4 \tag{2.274a}$$

$$A_{T2i} = A_{0i}A_{2i} \quad , \quad i=1...4 \tag{2.274b}$$

$$A_{T3i} = A_{2i}A_{3i} \quad , \quad i=1...4 \tag{2.274c}$$

$$A_{T4i} = A_{1i}A_{T1i}(A\Omega_{Ti}-1) - A_{0i} \quad , \quad i=1...4 \tag{2.274d}$$

$$A_{T5i} = A_{T1i}A_{3i}(A_{4i}-A_{T1i}) \quad , \quad i=1...4 \tag{2.274e}$$

The circumferential tire forces are calculated by:

$$\mu_{Pi} = P_{B1i} + P_{B2i}F'_{Ri} + P_{B3i}F'^{2}_{Ri} \quad (2.275)$$

$$\mu_{Si} = S_{0i} + S_{1i}F'_{Ri} + S_{2i}F'^{2}_{Ri} \quad (2.276)$$

$$SI_i = -R_{0i} - R_{1i}F'_{Ri} \quad (2.277)$$

$$\mu_{1i} = \mu_{Si}|\cos(\beta_i)|SN_i \quad (2.278)$$

$$m_{1i} = \frac{\mu_{Pi}}{SI_i}(1.0-57.3B_{ci}|\beta_i+\bar{\beta}_i|)SN_i \quad (2.279)$$

$$m_{2i} = \frac{\mu_{1i} - \mu_{Pi}(1.0-57.3B_{ci}|\beta_i+\bar{\beta}_i|)SN_i}{(1.0-SI_i)} \quad (2.280)$$

$$\text{If } m_{1i} < \frac{\mu_{1i}}{SI_i}, \; m_{1i} = \frac{\mu_{1i}}{SI_i} \text{ and } m_{2i} = 0.0 \quad (2.281)$$

$$\mu_{0i} = \mu_{1i} - m_{2i} \quad (2.282)$$

$$\text{If } s_i > SI_i, \; \mu'_i = m_{2i}s_i + \mu_{0i} \quad (2.283)$$

$$\eta_i = -\mu_{0i}F'_{Ri}, \; \zeta_i = -m_{2i}F'_{Ri} \quad (2.284)$$

$$\text{If } s_i \leq SI_i, \; \mu'_i = m_{1i}s_i \quad (2.285)$$

$$\eta_i = 0, \; \zeta_i = -m_{1i}F'_{Ri} \quad (2.286)$$

$$F_{Ci} = -\mu'_i F'_{Ri} \quad (2.287)$$

The tire side forces are given by, using the CALSPAN - APL method:

$$\mu_{yi} = (B_{1i}F'_{Ri} + (BC)_i + B_{4i}F'^{2}_{Ri})SN_i \quad (2.288)$$

$$(BC)_i = B_{3i} + B_{2i}\,C_{vi} \quad (2.289)$$

For $F'_{Ri} \leq A_{T1i}$

$$(a)\quad \bar{\beta}_i = \frac{A_{1i}F'_{Ri}(F'_{Ri} - A_{2i}) - A_{T2i}}{A_{2i}F'_{Ri}\mu_{yi}} (\beta_i + \beta'_i) \tag{2.290}$$

For $F'_{Ri} > A_{T1i}$

$$(b)\quad \bar{\beta}_i = \frac{A_{T4i}}{\mu_{yi}F'_{Ri}} (\beta_i + \beta'_i) \tag{2.291}$$

If $|\bar{\beta}_i| < 3$

$$(a)\quad g(\bar{\beta}_i) = \bar{\beta}_i - \frac{1}{3}\bar{\beta}_i |\bar{\beta}_i| + \frac{1}{27}\bar{\beta}_i^3 \tag{2.292}$$

otherwise

$$(b)\quad g(\bar{\beta}_i) = \bar{\beta}_i / |\bar{\beta}_i| \tag{2.293}$$

$$F'_{Si} = F'_{Ri}\mu_{yi}g(\bar{\beta}_i) \tag{2.294}$$

If the partial Data Deck model is used, the tire side forces are calculated from:

$$T_1 = \frac{|\beta_i|}{SP1_i} + 1 \tag{2.295}$$

$$T_2 = \frac{F'_{Ri} - F_{RMini}}{SP2_i} \tag{2.296}$$

$$\text{If } \beta_i \geq 0,\ T_3 = \frac{\phi_{CGi} - \phi_{Mini}}{SP3_i} + 1 \tag{2.297}$$

$$\text{If } \beta_i < 0,\ T_3 = \frac{\phi_{Maxi} - \phi_{CGi}}{SP3_i} + 1 \tag{2.298}$$

$$J_1 = [T_1],\ \xi_1 = T_1 - J_1 \tag{2.299}$$

$$J_2 = [T_2],\ \xi_2 = T_2 - J_2 \tag{2.300}$$

$$J_3 = [T_3],\ \xi_3 = T_3 - J_3 \tag{2.301}$$

where [ ] means to truncate to the closest smaller integer,

$$F'_{Si} = T_i(J_1,J_2,J_3)+\xi_1[T_i(J_1+1,J_2,J_3)-T_i(J_1,J_2,J_3)]+$$
$$\xi_2[T_i(J_1,J_2+1,J_3)-T_i(J_1,J_2,J_3)]+\xi_3[T_i(J_1,J_2,J_3+1)-$$
$$T_i(J_1,J_2,J_3)]+\xi_1\xi_2[T_i(J_1+1,J_2+1,J_3)-T_i(J_1+1,J_2,J_3)-$$
$$T_i(J_1,J_2+1,J_3)+T_i(J_1,J_2,J_3)]+\xi_1\xi_3[T_i(J_1+1,J_2,J_3+1)-$$
$$T_i(J_1+1,J_2,J_3)-T_i(J_1,J_2,J_3+1)+T_i(J_1,J_2,J_3)]+\xi_2\xi_3 \times$$
$$[T_i(J_1,J_2+1,J_3+1)-T_i(J_1,J_2+1,J_3)-T_i(J_1,J_2,J_3+1)+$$
$$T_i(J_1,J_2,J_3)]+\xi_1\xi_2\xi_3[T_i(J_1+1,J_2+1,J_3+1)-T_i(J_1+1,J_2+1,J_3)$$
$$T_i(J_1+1,J_2,J_3+1)-T_i(J_1,J_2+1,J_3+1)+T_i(J_1+1,J_2,J_3)+$$
$$T_i(J_1,J_2+1,J_3)+T_i(J_1,J_2,J_3+1)-T_i(J_1,J_2,J_3)] \quad \frac{\beta_i}{|\beta_i|} SN_i \tag{2.302}$$

In both methods of calculating the side forces, the effects of longitudinal slip are accounted for by a friction roll-off table. The amount that the side force is reduced is F_i, where

For j such that $F_{Si(j-1)1} \leq |s_i| < F_{Sij1}$, then

$$F_i = F_{Si(j-1)2} + \frac{(|s_i|-F_{Si(j-1)1})}{(F_{Sij1}-F_{Si(j-1)1})}(F_{Sij2}-F_{Si(j-1)2}) \tag{2.303}$$

$$F_{Si} = F'_{Si}(1-F_i) + F'_{Ri}\mu_{Si}|\sin(\beta_i)|F_i\frac{F'_{Si}}{|F'_{Si}|}SN_i \tag{2.304}$$

The tire aligning and overturning moments are given by

$$M_{xi} = O_{0i} + (O_{1i}+O_{2i}|\phi_{CGi}|)F_{Si}F'_{Ri} + O_{3i}\phi_{CGi}F_{Ri} \tag{2.305}$$

$$M_{zi} = (K_{1i}F'_{Ri}+K_{2i}|F_{Si}|)F_{Si} + K_{3i}F'_{Ri}\sqrt{\phi_{CGi}} \quad (2.306)$$

The skid number ratios are given by

$$SN_i = (SN)_{SOi}/(SN)_{Ti} \quad , \quad i=1...4 \quad (2.306a)$$

§2.3.12. Brake and Drive Torques

The drive torque can be specified explicitly as a function of time through the Driver Module. If this is not done, it is given by:

$$\text{If} \qquad u > V_c \ , \quad \overline{TQ}_D = 0. \tag{2.307}$$

$$\text{Otherwise} \qquad \overline{TQ}_D = K_{TQ}(V_c - u) \tag{2.308}$$

$$\text{If} \qquad TQ_D > TQ_{DMAX} \ , \quad TQ_D = TQ_{DMAX} \ . \tag{2.309}$$

When the antilock system is absent, the brake torques are found from:

For j such that $B_{F1(j-1)} < P_{FL} \leq B_{F1j}$, then:

$$\overline{TQ}_{B1} = \lambda_{B1}[B_{F2(j-1)} + (P_{FL} - B_{F1(j-1)})(B_{F2j} - B_{F2(j-1)})/(F_{F1j} - B_{F1(j-1)})] \tag{2.310}$$

$$\overline{TQ}_{B2} = \lambda_{B2}[B_{F3(j-1)} + (P_{FL} - B_{F1(j-1)})(B_{F3j} - B_{F3(j-1)})/(B_{F1j} - B_{F1(j-1)})] \tag{2.311}$$

For j such that $B_{R1(j-1)} < P_{FL} \leq B_{R1j}$, then:

$$\overline{TQ}_{B3} = \lambda_{B3}[B_{R2(j-1)} + (P_{FL} - B_{R1(j-1)})(B_{R2j} - B_{R2(j-1)})/(B_{R1j} - B_{R1(j-1)})] \tag{2.312}$$

$$\overline{TQ}_{B4} = \lambda_{B4}[B_{R3(j-1)}+(P_{FL}-B_{R1(j-1)})(B_{R3j} - B_{R3(j-1)})/(B_{R1j}-B_{R1(j-1)})] \quad (2.313)$$

The antilock systems in the simulation are described in detail in Ref. [2.1]. If activated, then the inputs are

$$P_F = \frac{1}{2}(\lambda_{B1}+\lambda_{B2})P_{FL} \quad (2.314)$$

$$P_R = \frac{1}{2}(\lambda_{B3}+\lambda_{B4})P_{FL} \quad (2.315)$$

and the output is the brakeline pressures B_{P1}, B_{P2}, which are used to calculate brake torques via:

For j such that $B_{F1(j-1)} \leq B_{P1} < B_{F1j}$, then

$$\overline{TQ}_{B1} = B_{F2(j-1)} + (B_{P1}-B_{F1(j-1)})(B_{F2j} - B_{F2(j-1)})/(B_{F1j}-B_{F1(j-1)}) \quad (2.316)$$

$$\overline{TQ}_{B2} = B_{F3(j-1)} + (B_{PL}-B_{FL(j-1)})(B_{F3j} - B_{F3(j-1)})/(B_{FLj}-B_{FL(j-1)}) \quad (2.317)$$

For j such that $B_{R1(j-1)} \leq B_{P2} < B_{R1j}$, then

$$\overline{TQ}_{B3} = B_{R2(j-1)} + (B_{P2}-B_{R1(j-1)})(B_{R2j} - B_{R2(j-1)})/(B_{R1j}-B_{R1(j-1)}) \quad (2.318)$$

$$\overline{TQ}_{B4} = B_{R3(j-1)} + (B_{P2}-B_{R1(j-1)})(B_{R3j} - B_{R3(j-1)})/(B_{R1j}-B_{R1(j-1)}) \quad (2.319)$$

The antilock system is organized as follows:

MODULE = 1 : $P_{BP1} = P_F$, $P_{BP2} = P_R$ (2.320)

MODULE = 2 : $P_{BP1} = P_{BP2} = P_F$, $P_{BP3} = P_R$ (2.321)

MODULE = 3 : $P_{BP1} = P_{BP2} = P_F$, $P_{BP3} = P_{BP4} = P_R$ (2.322)

LOGIC TO DETERMINE IF ANTILOCK IS CURRENTLY ON OR OFF.

ANTILOCK NEVER ON:

$$BLPi = B_{LPi} + \cancel{R_i}^{0} \Delta t \quad (2.323)$$

NOTE: $B_{LPi} = P_{BPi}$ (2.324)

ANTILOCK ON AT SOME TIME:

NOT CURRENTLY ON:

$$B_{LPi} = B_{LPi} + R_i \Delta t \quad (2.325)$$

ANTILOCK CURRENTLY ON:

$$B_{LPi} = B_{LPi} + R_i \Delta t \quad (2.326)$$

NOTE:

$$R_i = -B_{LPi}/\tau_1 \quad (2.327)$$

NOTE: $B_{LPi} \leq P_{Bi}$ = INPUT PRESSURE

MODULE = 1 $B_{P1} = B_{P2} = B_{LP1}$, $B_{P3} = B_{P4} = B_{LP2}$ (2.328)

MODULE = 2 $B_{P1} = B_{LP1}$, $B_{P2} = B_{LP2}$, $B_{P3} = B_{P4} = B_{LP3}$ (2.329)

MODULE = 3 $B_{P1} = B_{LP1}$, $B_{P2} = B_{LP2}$ (2.330)

$B_{P3} = B_{LP3}$, $B_{P4} = B_{LP4}$ (2.331)

$$\omega_{D1i} = \omega_{D1i} - 1.5\, g\Delta t/\overline{RR}_i \tag{2.332}$$

$$\omega_{D2i} = \omega_{D2i} - 4\, g\Delta t/\overline{RR}_i \tag{2.333}$$

$$R_i = \sqrt{|P_{BPi} - B_{LPi}|}\ /\tau_2 \tag{2.334}$$

$$V_{OLi} = -K_2 \sqrt{|P_{BPi} - B_{LPi}|} \tag{2.335}$$

$$V_{OLi} = V_{OLi} + \dot{V}_{OLi}\, \Delta t \tag{2.336}$$

$$R_i = -B_{LPi}/\tau_1 \tag{2.337}$$

$$\dot{V}_{OLi} = K_1\, B_{LPi} \tag{2.338}$$

$$V_{OLi} = V_{OLi} + \dot{V}_{OLi}\, \Delta t \tag{2.339}$$

The output quantities are B_{P1}, B_{P2}, B_{P3}, B_{P4}.

§2.3.13. Center of Mass Accelerations

The accelerations of the center of mass are given by

$$A_X = \dot{u} - vr + wq \tag{2.340}$$

$$A_Y = \dot{v} + ur - wp \tag{2.341}$$

§2.4. Nomenclature

Symbol	Definition
a	x-distance between the center of gravity of the sprung mass and the centerline of the front wheels.
a_{ij}	Elements of the (3x3) matrix relating the orientation of the vehicle fixed axis system to the inertial frame.
A_{Li}, i=1,2	Length of steering linkage arm at front wheel i.
a_p	Length of Pitman arm.
$\overline{AR}_F$, $\overline{AR}_R$	Ratio of propeller shaft speed to wheel speed for front and rear respectively.
$A_{T1i}, A_{T2i}, A_{T3i}, A_{T4i}, A_{T5i}$	Temporary variables defined in §2.3.11.
A_X, A_Y	Accelerations of the center of mass in the X and Y directions, respectively.
$A\Omega_{Ti}$	Proportionality factors giving limits of small-angle cornering and camber stiffness variation with tire loadings.
A_{0i}, A_{1i}, A_{2i}, A_{3i}	Coefficients of curves fitted to small angle cornering stiffness at wheel i.
A_{4i}, i=1...4	Coefficients of curves fitted to small angle camber stiffness at wheel i.

Symbol	Definition
b	y-distance between the center of gravity of the sprung mass and the centerline of the rear wheels.
B_{ci}	Tire parameters which give the influence of slip angle and camber angle on the circumferential tire force (not measured by Calspan).
B_{Fij}, B_{F2j}, B_{F3j}	Coefficients in look-up table for brake line pressure versus torque for front wheels.
B_{LPi}	Brake line pressure outputs from antilock pressure modulator.
B_{1i}, B_{2i}, B_{3i}, B_{4i}	Coefficients of curves fitted to the lateral friction coefficient at wheel i.
$(BPT)_i$	Coulomb friction breakpoints.
B_{R1j}, B_{R2j}, B_{R3j}	Coefficients in look-up table for brake line pressure versus torque for rear wheels.
C'_{Fi}, C'_{Ri}	Coulomb damping coefficients for the suspensions, front and rear, respectively.
C_L, C_M, C_N	Aerodynamic moment coefficients.
C'_L, C'_M, C'_N	Temporary variables used in §2.3.4.
C_{ℓ_p}, C_{ℓ_r}, C_{m_α}, C_{m_q}, C_{n_p}, C_{n_r}, C_{y_p}, C_{y_r}, C_{z_α}, C_{z_q}	Aerodynamic stability derivatives.
$C_{\tau ik}$	Arrav containing C_L, C_M, C_N, C_X, C_Y and C_Z as tabular functions of the aerodynamic angle of sideslip τ for zero aerodynamic angle of attack.

Symbol	Definition
C_{vi}	Resultant velocity of the contact point of wheel i in the ground plane.
C_X, C_Y, C_Z	Aerodynamic force coefficients. For zero angle of attack they are given as tabular functions of the aerodynamic angle of sideslip τ.
C_{1j}, C_{2j}, C_{3j}, C_{4j}	Coefficients of the fifth degree polynomials fitted to wheel camber angles versus suspension deflections.
d_{CG}	Horizontal distance between the aerodynamic center and the sprung mass center of gravity.
dC_{xik}	Array containing the aerodynamic increments in the axial force coefficients as a tabular function of the aerodynamic angle of attack.
D_1, D_2, D_3, D_4	Temporary variables used in §2.3.9.
D_{1j}, D_{2j}, D_{3j}, D_{4j}	Coefficients of fifth degree polynomials fitted to wheel toe angle versus suspension deflections.
E_1, E_2, E_3, E_4	Temporary variables used in §2.3.9.
E_{1j}, E_{2j}	Coefficients of fifth degree polynomials fitted to front wheel caster angles versus suspension deflections.

Symbol	Definition
F_{APi}	Antipitch forces in suspensions.
F_{ARi}	Antiroll forces in suspensions.
F_{BSi}	Differences between linear and piecewise linear modeling of spring forces.
F_{Ci}	Circumferential tire force at wheel i.
F_i	Percentage reduction in side force at wheel i due to longitudinal slip.
f(RAC)	Temporary variable used in §2.3.4.
F_{J1}, F_{J2}, F_{J3}, F_{J4}	Jacking forces.
F_{Ri}	Radial tire force at wheel i.
F'_{Ri}	Tire normal force to ground at wheel i.
F_{RMini}	Smallest value of the normal force at wheel i for which data is available.
F_{SHij}	Shock absorber forces at the discrete values $\dot{\chi}_{ij}$.
F_{Si}	Tire side force at wheel i.
F'_{Si}	Variable connected with the tire side force calculation used in §2.3.11.
F_{Spij}	Spring forces at the discrete points χ_{ij}.

Symbol	Definition
F_{SWF}, F_{SWR}	Front and rear static components of the sprung mass weight.
F_{Sijk}	Nondimensional tire side force shaping function versus slip at wheel i. Defined at points, linear interpolation in between (friction roll-off curve).
F_{xINi}	Initial values of the tire side forces in the x-direction when the vehicle is in the static equilibrium position.
F_{xui}	Components of the tire side force in the x-direction.
F_{yINi}	Initial values of the tire side forces in the y-direction when the vehicle is in the static equilibrium position.
F_{yui}	Components of the tire side force in the y-direction.
F_{zui}	Components of the tire side force in the z-direction.
F_{z1}, F_{z2}, F_{z3}, F_{z4}	Components of the tire forces in the z-direction.
F(1), F(2), F(3), F(4), F(5), F(6), F(7), F(8), F(9), F(10)	Elements of the "force and moment" column vector in the equations of motion.
F_{1i}	Coulomb damping forces in suspensions.
F_{2i}	Suspension forces produced by deflection of springs and bump stops.

Symbol	Definition
F_{3i}	Viscous damping forces in suspensions.
F_{4i}	Suspension forces produced by auxiliary roll stiffnesses.
g	Acceleration due to gravity.
h_{FC}	Distance between the ground and the static roll center of the independent front and rear suspension, respectively.
$\bar{I}_F$, $\bar{I}_{FC}$	Variables used in §2.3.9.
I_{FW}	Moment of inertia of individual front wheels about the kingpin axis.
I_R	Moment of inertia of solid rear axle about a line through its center of gravity and parallel to the x-axis.
$\bar{I}_R$, $\bar{I}_{RC}$	Variables used in §2.3.9.
I_{WF}, I_{WR}	Moment of inertia of individual front and rear wheels about their spin axis.
I_x, I_y, I_z	Moment of inertia of the sprung mass about the x,y,z-axes, respectively.
I_{xz}	Product of inertia of the sprung mass with respect to the x,z-axes.
I'_{xz}	Variable defined in §2.3.1.
I'_y	Variable defined in §2.3.1.

Symbol	Definition
J_1, J_2, J_3	Indices of a point in the tire data array. J_1 gives the value of the slip angle, J_2 gives the value of the radial force and J_3 gives the camber angle.
K_{CF}	Lateral force compliance camber coefficient front wheels.
K_{CR}	Lateral force compliance camber coefficient, rear wheels.
K_{Fi}	Variables used in §2.3.3.
K_{OT1}, K_{OT2}	Front overturning moment compliance cambers.
K_{OT3}, K_{OT4}	Rear overturning moment compliance cambers.
K_{RS}	Roll steer coefficient of the solid rear axle (positive for roll understeer).
K_{SC}	Flexibility in steering column and the steering gear box.
K_{SLi}	Flexibility in steering linkage at front wheel i.
K_{SR}	Aligning torque compliance steer coefficient at the rear wheels.
K_{Ti}	Tire load deflection rate in the quasi-linear range for a single tire at wheel i.
K_{TQ}	Gain in the drive torque.
K_{1i}, K_{2i}, K_{3i}	Coefficients of curves fitted to the tire aligning torque at wheel i.
K_{LR}	Rear lateral force compliance steer.

Symbol	Definition
l	Length of the vehicle (ℓ= a+b)
l_v	Characteristic vehicle length upon which the aerodynamic moment coefficients are referenced.
M(i,j)	Matrix multiplying the column vector of accelerations.
Module	Variable specifying the type of antilock system present. MODULE can take on the values 1, 2, or 3. MODULE=1: Two modules, one sensing the average of the two front wheel spin rates and controlling the front brakes, and the other similarly senses and controls the rear. MODULE=2: Three modules, one sensing the average of the two rear wheel spin rates and controlling the rear brakes, and the other two independently sense and control the two front wheels. MODULE=3: Four modules, each sensing one wheel spin rate and controlling the corresponding brake.
M_S	Total sprung mass.
M_{SSi}	Torque applied to front wheel i by the steering system connecting rod.
M_{Ti}	Moment acting at front wheel i about the kingpin axis due to tire-road contact forces.
M_{uF}, M_{uR}	Total front and rear unsprung mass, respectively.

Symbol	Definition
$M_{x1}, M_{x2}, M_{x3}, M_{x4}$	Tire overturning moments.
$M_{z1}, M_{z2}, M_{z3}, M_{z4}$	Tire aligning moments.
m_{1i}, m_{2i}	Slopes of straight line segments approximating the circumferential friction coefficient at wheel i.
N_G	Gear ratio of the steering gear box.
$O_{ijk...}$	$O_{ijk...}$ is defined by: $O_{ijk...}$ = 0 IF ASSUMPTION i OR ASSUMPTION j OR ASSUMPTION k...IS BEING MADE. OTHERWISE $O_{ijk...}$ = 1.

Assumptions are:

1. The distance between the rear axle center of gravity and the roll center is taken to be zero, i.e.,

$$\rho_R = 0.$$

2. The angular velocities are taken to be small so that their products and squares can be neglected, i.e.,

$$pq, pr, qr, p^2, q^2, r^2 \simeq 0.$$

3. The roll angle ϕ and pitch angle θ of the sprung mass are taken to be small so that

$$\sin\phi \simeq \phi, \quad \sin\theta \simeq \theta$$

$$\cos\phi \simeq 1, \quad \cos\theta \simeq 1$$

4. The suspension deflections δ_1, δ_2, and δ_R are taken to be much smaller than the distances z_F and z_R, i.e.,

$$\delta_1, \delta_2, \delta_R << z_F, z_R$$

Symbol	Definition
	5. The suspension deflections δ_1, δ_2, δ_R and their derivatives $\dot{\delta}_1$, $\dot{\delta}_2$, $\dot{\delta}_R$ are taken to be so small that the following products can be neglected: $\dot{\delta}_j p, \dot{\delta}_j q, \delta_j \dot{q}, \delta_j \dot{r}, \dot{\delta}_j^2 \simeq 0$, $j=1,2,R$.
	6. The roll angle ϕ_R is taken to be so small that the following products can be neglected: $\dot{\phi}_R\dot{\phi}_R, \phi_R\dot{\phi}_R^2, \phi_R^2, \phi_R^2\dot{\phi}_R, \dot{\phi}_R^2, \phi_R\ddot{\phi}_R \simeq 0$
	7. Terms not present in the APL model.
$O_{0i}, O_{1i}, O_{2i}, O_{3i}$	Coefficients of functions fitted to tire overturning moments at wheel i.
P_{BP1}, P_{BP2}, P_{BP3}, P_{BP4}	Proportional brake pressure input to brake pressure modulator.
P_F, P_R	Proportional brake pressure input to brake pressure modulator, front and rear, respectively.
P_{FL}	Brake line pressure.
P_{i1}, P_{i2}, P_{i3}	Coefficients of curves fitted to antipitch forces.
p	Angular velocity of the sprung mass about the x-axis.
$\bar{p}$	Dimensionless x-component of the angular velocity of the sprung mass relative to the wind.
$\overline{PT_i}$	Front wheel caster offset.

Symbol	Definition
q	Angular velocity of the sprung mass about the y-axis.
q_a	Dynamic pressure.
$\overline{q}$	Dimensionless y-component of the angular velocity of the sprung mass relative to the wind.
Q_1, Q_2, Q_3, Q_4	Variables used in §2.3.9.
R_i	Variable used in §2.3.12.
R_{i1}, R_{i2}, R_{i3}	Coefficients of curves fitted to antiroll coefficients.
R_F	Auxiliary roll stiffness at front suspension.
R_R	Auxiliary roll stiffness at rear suspension.
RR_i	Rolling radius of wheel i.
$\overline{RR_i}$	Average value of the rolling radius of wheel i.
R_{RIMi}	Rim radius of wheel i.
R_{wi}	Undeflected radius of tire i.
R_{0i}, R_{1i}	Coefficients fitted to curves giving the value of the longitudiral slip at which the peak circumferential tire force at wheel i occurs.
R_1, R_2, R_3, R_4	Variables used in §2.3.9.
r	Angular velocity of the sprung mass about the z-axis.
$\overline{r}$	Dimensionless z-component of the angular velocity of the sprung mass relative to the wind.

Symbol	Definition
S_f	Projected frontal area of the vehicle.
SI_i	Value of the longitudinal slip for wheel i at which the peak circumferential tire force occurs.
s_i	Longitudinal slip at wheel i.
s_i^o	Value of the longitudinal slip at wheel i at a previous time.
SN_i	Skid number ratio at wheel i.
$(SN)_{SOi}$	Skid number of simulated surface at wheel i.
$(SN)_{Ti}$	Skid number at wheel i of surface on which the tire data were obtained.
$SP1_i$	Change in the slip angle between tire data points at wheel i.
$SP2_i$	Change in the normal force between tire data points at wheel i.
$SP3_i$	Change in the camber angle between tire data points at wheel i.
$(ST)_1$, $(ST)_2$	Variables used in §2.3.3.
S_{0i}, S_{1i}, S_{2i}	Coefficients of curves fitted to the slide braking coefficient at wheel i.
S_1, S_2, S_3, S_4	Suspension forces.
$\overline{S_1}$, $\overline{S_2}$, $\overline{S_3}$, $\overline{S_4}$	First average of suspension forces.
$\overline{\overline{S_1}}$, $\overline{\overline{S_2}}$, $\overline{\overline{S_3}}$, $\overline{\overline{S_4}}$	Second average of suspension forces.

Symbol	Definition
T_F, T_R	Wheel tread width at the front and rear, respectively.
$\overline{TQ}_{Bi}$	Brake torque at wheel i.
$\overline{T_{QD}}$	Drive torque at wheel i.
TQ_{Dmax}	Maximum value of the drive torque.
T_{SR}	y-distance between the spring centers for the solid rear axle.
T_1, T_2, T_3	Variables used in §2.3.11.
t	Time.
t_o	Time prior to the current time increment.
u	Velocity component of the sprung mass in the x-direction.
u_{Gi}	Forward velocity of the contact points of the front wheels in the ground plane.
u_i	Velocity component of the contact point of wheel i in the x-direction.
u_r	x-component of the sprung mass velocity relative to the wind.
v	Velocity component of the sprung mass in the y-direction.
V_{CW}	Magnitude of the vehicle velocity relative to the wind.
V_c	Desired vehicle velocity.
$(Vel)_i$	Velocity in the direction of the wheel plane of the tire contact point of wheel i in the ground plane.

Symbol	Definition
v_{Gi}	Lateral velocity of the contact point of wheel i.
v_i	Velocity component of the contact point of wheel i in the y-direction.
V_{OLi}	Fluid volume in expansion chambers of pressure modulator.
v_r	y-component of the sprung mass velocity relative to the wind.
V_{yw}	Velocity of the cross wind with respect to the inertial axes, measured at the sprung mass center of gravity.
w	Velocity component of the sprung mass in the z-direction.
wd_{tjk}	Array giving the cross wind velocity as a function of the position X.
w_i	Velocity component of the contact point of wheel i in the z-direction.
w_r	z-component of the sprung mass velocity relative to the wind.
X	Inertial coordinate
X_{Ci}	Inertial coordinate of the contact patch of wheel i.
X_o	Road elevation datum coordinate.
X_{wv}	Wavelength of the road undulation in the X-direction.

Symbol	Definition
x	Sprung mass fixed coordinate.
Y	Inertial coordinate.
y	Sprung mass fixed coordinate.
Y_{Ci}	Inertial coordinate of the contact patch of wheel i.
y_{CR}	Displacement of the steering system connecting rod.
Y_o	Road elevation datum coordinate.
Y_{SAi}	Distance between the kingpin axis and wheel center-line, measured along the wheel spin axis at front wheel i.
Y_{wv}	Wavelength of the road undulation in the Y-direction.
Z	Inertial coordinate.
z	Sprung mass fixed coordinate.
z_F, z_R	z-distance between the center of gravity of the sprung mass and the centers of gravity of the front and rear unsprung masses, respectively.
z_i	Coordinate of wheel i center above the road surface.
z_{Si}	Road elevation under wheel i.
$Z_{(0)}$	Value of Z at time equal to zero.

Symbol	Definition
α	Aerodynamic angle of attack.
α_{ci}	Angles the lines of intersection of the wheel planes with the ground plane make with the X-axis.
α_{h1}, α_{h2}, α_{h3}, α_{h4}	Angles the tire radial forces make with the x-axis.
α_{R1}, α_{R2}, α_{R3}, α_{R4}	Angles the tire radial forces make with the X-axis.
α_{yw1}, α_{yw2}, α_{yw3}, α_{yw4}	Angles the lines perpendicular to the tires make with the X-axis.
β_{ci}	Angles the lines of intersection of the wheel planes with the ground plane make with the Y-axis.
β_{h1}, β_{h2}, β_{h3}, β_{h4}	Angles the tire radial forces make with the y-axis.
β_i	Slip angle at wheel i.
β_i'	Equivalent slip angle at wheel i produced by camber.
$\bar{\beta}_i$	Nondimensional slip angle at wheel i.
β_{R1}, β_{R2}, β_{R3}, β_{R4}	Angles the tire radial forces make with the Y-axis.
β_{yw1}, β_{yw2}, β_{yw3}, β_{yw4}	Angles the lines perpendicular to the tires make with the Y-axis.
Γ_1, Γ_2	Variables used in §2.3.9.
γ_{h1}, γ_{h2}, γ_{h3}, γ_{h4}	Angles the tire radial forces make with the z-axis.
γ_{R1}, γ_{R2}, γ_{R3}, γ_{R4}	Angles the tire radial forces make with the Z-axis.

Symbol	Definition
γ_{yw1}, γ_{yw2}, γ_{yw3}, γ_{yw4}	Angles the lines perpendicular to the tires make with the Z-axis.
γ_1, γ_2' γ_5'	Variables used in §2.3.1.
Δ_1, Δ_2	Variables used in §2.3.9.
$\Delta\psi_i$	Static toe angle bias at wheel i.
$\Delta\theta_1$, $\Delta\theta_2$	Static caster angle at wheel i.
δ_{Fwi}	Angular displacement of front wheel i produced by the steering system.
δ_{INi}	Static deflection of wheel i due to the vehicle load.
δ_R	Suspension deflection relative to the vehicle from the position of static equilibrium measured from the center of the solid rear axle.
δ_{Si}	Dynamic suspension deflection relative to the vehicle measured at the center of wheel i, or at the spring location for the solid rear axle, from the no load position.
δ_{Sw}	Steering wheel angular displacement.
δ_1, δ_2, δ_3, δ_4	Suspension deflections relative to the vehicle from the position of static equilibrium measured from the centers of wheels 1, 2, 3 and 4, respectively.
ζ_i	Variables used in §2.3.9. and §2.3.11.
η_i	Variables used in §2.3.9. and §2.3.11.

Symbol	Definition
$\Theta_1, \Theta_2, \Theta_3, \Theta_4$	Variables used in §2.3.9.
θ	Pitch angle.
θ_{S1}, θ_{S2}	Caster angles relative to the vehicle fixed coordinate system (positive for rearward inclination of the steering axis in the upward direction).
θ_{XGi}	Angle between the x-axis and the ground plane at wheel i.
$\lambda_{B1}, \lambda_{B2}, \lambda_{B3}, \lambda_{B4}$	Brake torque multipliers.
λ_D	Drive torque distribution factor.
$\lambda_1, \lambda_2, \lambda_3, \lambda_4$	Variables used in §2.3.9.
μ_i'	Variable used in §2.3.11.
μ_{Pi}	Peak braking coefficient at wheel i.
μ_{Si}	Coefficient of sliding friction at wheel i.
μ_{yi}	Lateral friction coefficient at wheel i.
μ_{0i}, μ_{1i}	Circumferential friction coefficients at wheel i for slip equal 0 and 1, respectively.
ξ_1, ξ_2, ξ_3	Variables used in §2.3.10.
ρ_a	Air density
ρ_R	Distance between rear axle center of gravity and roll center, positive for roll center above the c.g.

Symbol	Definition
ΣF_{xu}, ΣF_{yu}	x and y-components, respectively, of the resultant forces on the unsprung mass.
ΣM	Sum of all the masses.
$\Sigma N_{\theta s}$	y-component of the resultant aerodynamic moment on the sprung mass.
$\Sigma N_{\theta u}$	y-component of the resultant moment due to the forces acting on the unsprung mass.
$\Sigma N_{\phi R}$	Rolling moment acting on the solid rear axle.
$\Sigma N_{\phi s}$	x-component of the resultant aerodynamic moment on the sprung mass.
$\Sigma N_{\phi u}$	x-component of the resultant moment due to the forces acting on the unsprung masses.
$\Sigma N_{\psi s}$	z-component of the resultant aerodynamic moment on the sprung mass.
$\Sigma N_{\psi u}$	z-component of the resultant moment due to the forces acting on the unsprung mass.
τ	Aerodynamic angle of sideslip.
τ_1, τ_2, τ_3, τ_4	Variables used in §2.3.9.
ϕ_{CGi}	Camber angle of wheel i relative to the ground plane.
ϕ_{maxi}	Largest value of the camber angle at wheel i for which data is available.

Symbol	Definition
ϕ_{mini}	Smallest value of the camber angle at wheel i for which data is available.
ϕ_{SAi}	Right and left kingpin inclination angle at equilibrium suspension position.
ϕ_{SA01}, ϕ_{SA02}	Front wheel kingpin inclinations at the equilibrium position.
ϕ	Roll angle.
$\phi_1, \phi_2, \phi_3, \phi_4$	Camber angles of the wheels relative to the vehicle fixed coordinate system. (Positive when clockwise viewed from the rear).
ϕ_R	Angular displacement of the solid rear axle about a line parallel to the x-axis through the rear axle center of gravity (positive when clockwise viewed from the rear).
χ_i	Suspension deflection relative to the vehicle from the position of static equilibrium measured at the spring location i.
χ'_i	Deflection of wheel i (for a solid rear axle) relative to the vehicle from the position of static equilibrium.
χ_{ij}	Coefficients for piecewise linear springs.
ψ	Yaw angle.
ψ'_i	Steer angle of wheel i in the ground plane.
$\psi_1, \psi_2, \psi_3, \psi_4$	ψ_i is the steer angle of wheel i relative to the vehicle-fixed coordinate axis system, positive for clockwise steer as viewed from above the vehicle.

Symbol	Definition
ω_{D1i}, ω_{D2i}	Threshold levels of the angular deceleration of the wheels.
ω_{xw}, ω_{yw}	Angular velocity components of the wind with respect to the inertial axes.
ω_1, ω_2, ω_3, ω_4	ω_i is the angular velocity of wheel i.

§2.5 DIFFERENCES BETWEEN THE CURRENT SIMULATION AND THE APL HYBRID SIMULATION

Introduction. The current simulation differs from the APL simulation with respect to the following items: (i) The numerical treatment of the wheel slip equations. (ii) The numerical treatment of the steering system. (iii) The availability of tire modelling via a partial Data Deck Model. (iv) The capability of separate braking at each wheel. (v) The calculation of the static suspension forces. (vi) The calculation of the pitch equations. (vii) The introduction of suspension averaging. (viii) The availability of an antilock system.

These differences will now be discussed individually.

§2.5.1. Algebraic Form of the Wheel Spin Equations.

In deriving the wheel spin equations, the inertial coupling of the wheels through the differential gears and the effects of drive-line inertia cannot be neglected in general. This model is reflected in Fig. 2.3 below, which shows the front wheels.

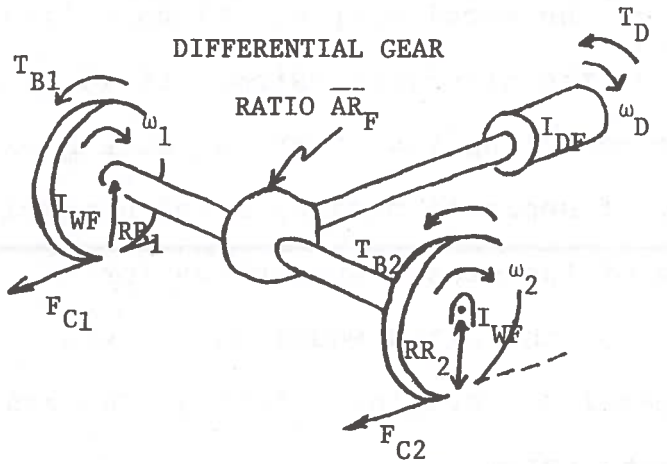

Fig 2.3

The kinetic energy of the system shown in the figure is

$$T = \tfrac{1}{2}I_{WF}\omega_1^2 + \tfrac{1}{2}I_{WF}\omega_2^2 + \tfrac{1}{2}I_{DF}\omega_D^2 \qquad (2.342)$$

where

$$\omega_D = \tfrac{1}{2}(\overline{AR}_F)(\omega_1 + \omega_2) \qquad (2.343)$$

It is assumed that elastic deformations are negligible, so that the potential energy may be taken to be zero. Then Lagrange's give, on calculating the work done,

$$\bar{I}_F\dot{\omega}_1 + I_{FC}\dot{\omega}_2 = -F_{C1}RR_1 + \tau_1 \qquad (2.344)$$

$$I_{FC}\dot{\omega}_1 + \bar{I}_F\dot{\omega}_2 = -F_{C2}RR_2 + \tau_2 \qquad (2.345)$$

where

$$\bar{I}_F = I_{WF} + I_{FC} \tag{2.346}$$

$$I_{FC} = \tfrac{1}{4} I_{DF} (\overline{AR}_F)^2 \tag{2.347}$$

$$\tau_i = (1-\lambda_D)(\overline{AR}_F/2)\overline{TQ}_D + \overline{TQ}_{Bi}, i=1,2 \tag{2.348}$$

Solving eqs. (2.344) and (2.345) for $\dot{\omega}_1$ and $\dot{\omega}_2$ gives

$$\dot{\omega}_1 = [\bar{I}_F(-RR_1 F_{C1}+\tau_1)-I_{FC}(-RR_2 F_{C2}+\tau_2)]/(\bar{I}_F^2 - I_{FC}^2) \tag{2.349}$$

$$\dot{\omega}_2 = [I_F(-RR_2 F_{C2}+\tau_2)-I_{FC}(-RR_1 F_{C1}+\tau_1)]/(I_F^2 - I_{FC}^2) \tag{2.350}$$

The wheel spin kinematic equations are

$$s_i = 1 - \omega_i (RR_i)/(Vel)_i, \quad i=1,2 \tag{2.351}$$

$$(Vel)_i = u_{Gi}\cos\psi_i' + v_{Gi}\sin\psi_i' \tag{2.352}$$

Eqs. (2.349) and (2.350) are stiff differential equations and are very expensive to integrate digitally. Considerable cost saving is achieved on converting them to algebraic equations. The idea to achieve this, set forth by Bernard [2.2], will now be followed. Consider a time interval $t_o<t<t+\Delta t_o$ in which Δt_o is small enough that RR_i may be considered as constants. Then differentiating (2.351)

$$\dot{s}_i = [\omega_i RR_i(\dot{Vel})_i - \dot{\omega}_i RR_i (Vel)_i]/(Vel)_i^2, \quad i=1,2 \tag{2.353}$$

Substituting for ω_i and $\dot{\omega}_i$ from eqs. (2.349), (2.350), (2.353) and (2.351) yields.

$$\dot{s}_i = (\dot{Vel})_1(1-s_1)/(Vel)_1 - RR_1[\bar{I}_F(\tau_1 - RR_1F_{C1}) - I_{FC}(\tau_2 - RR_2F_{C2})]/(Vel)_1[(\bar{I}_F)^2 - I_{FC}^2] \quad (2.354)$$

$$\dot{s}_2 = (\dot{Vel})_2(1-s_2)/(Vel)_2 - RR_2[\bar{I}_F(\tau_2 - RR_2F_{C2}) - I_{FC}(\tau_1 - RR_1F_{C1})]/(Vel)_2[(\bar{I}_F)^2 - I_{FC}^2] \quad (2.355)$$

Consider now the circumferential force-normal force relationship

$$F_{Ci} = -\mu_i' F_{Ri}' \ , \ i=1,2 \quad (2.356)$$

Let s_i^0 be the value of the slips s_i at time t_0. Then expanding μ_i' in a two-term Taylor series gives, on substituting into eq. (2.356),

$$F_{Ci} = \eta_i + \zeta_i s_i \ , \ i=1,2 \quad (2.357)$$

where

$$\eta_i = [s_i^0 \frac{\partial \mu_i'}{\partial s_i}(s_i^0) - \mu_i'(s_i^0)]F_{Ri}' \ , \ i=1,2 \quad (2.358)$$

$$\zeta_i = -F_{Ri}' \frac{\partial \mu_i'}{\partial s_i}(s_i^0) \ , \ i=1,2 \quad (2.359)$$

Substituting eq. (2.357) into eqs. (2.354) and (2.355) gives, after some rearranging,

$$\dot{s}_1 + Q_1 s_1 + E_1 s_2 = R_1 \quad (2.360)$$

$$\dot{s}_2 + Q_2 s_2 + E_2 s_1 = R_2 \quad (2.361)$$

where

$$Q_1 = (\dot{Vel})_1/(Vel)_1 - (RR_1)^2\bar{I}_F\zeta_1/D_1 \tag{2.362}$$

$$Q_2 = (\dot{Vel})_2/(Vel)_2 - (RR_2)^2\bar{I}_F\zeta_2/D_2 \tag{2.363}$$

$$E_1 = (RR_1)(RR_2)I_{FC}\zeta_2/D_1 \tag{2.364}$$

$$E_2 = (RR_1)(RR_2)I_{FC}\zeta_1/D_2 \tag{2.365}$$

$$R_1 = (\dot{Vel})_1/(Vel)_1+[(RR_1)^2\bar{I}_F\eta_1-(RR_1)(RR_2)I_{FC}\eta_2 \tag{2.366}$$

$$-(RR_1)(\bar{I}_F\tau_1-I_{FC}\tau_2)]/D_1 \tag{2.367}$$

$$R_2 = (\dot{Vel})_2/(Vel)_2+[(RR_2)^2\bar{I}_F\eta_2-(RR_1)(RR_2)I_{FC}\eta_1 \tag{2.368}$$

$$-(RR_2)(\bar{I}_F\tau_2-I_{FC}\tau_1)]/D_2 \tag{2.369}$$

$$D_1 = (Vel)_1\Delta_1 \tag{2.370}$$

$$D_2 = (Vel)_2\Delta_1 \tag{2.371}$$

$$\Delta_1 = \bar{I}_F^2 - I_{FC}^2 \tag{2.372}$$

The coefficients in eqs. (2.360) and (2.361) are regarded as constants in the time interval in question. With this assumption, the solutions are

$$s_1 = \Gamma_1 + \Theta_1 e^{\lambda_1(t-t_o)} + \Theta_2 e^{\lambda_2(t-t_o)} \tag{2.373}$$

$$s_2 = \Gamma_2 - (\frac{\lambda_1+Q_1}{E_1})\Theta_1 e^{\lambda_1(t-t_o)} - (\frac{\lambda_2+Q_1}{E_1})\Theta_2 e^{\lambda_2(t-t_o)} \tag{2.374}$$

Special Case: If $E_1 = 0$

$$s_1 = \Gamma_1 + (s_1^o-\Gamma_1)e^{-Q_1(t-t_o)} \tag{2.375}$$

$$s_2 = \Gamma_2 - (\Gamma_2-s_2^o)e^{-Q_2(t-t_o)} \tag{2.376}$$

---

where:

$$\Gamma_1 = \frac{R_1}{Q_1} + \frac{E_1E_2R_1 - E_1R_2Q_1}{Q_1(Q_1Q_2-E_1E_2)} \tag{2.377}$$

$$\Gamma_2 = \frac{R_2}{Q_2} + \frac{E_1E_2R_2 - E_2R_1Q_2}{Q_2(Q_1Q_2-E_1E_2)} \tag{2.378}$$

$$\lambda_1 = -\frac{Q_1+Q_2}{2} + \tfrac{1}{2}[(Q_1+Q_2)^2-4(Q_1Q_2-E_1E_2)]^{\frac{1}{2}} \tag{2.379}$$

$$\lambda_2 = -\frac{Q_1+Q_2}{2} - \tfrac{1}{2}[(Q_1+Q_2)^2-4(Q_1Q_2-E_1E_2)]^{\frac{1}{2}} \tag{2.380}$$

$$\theta_1 = [(s_1^o-\Gamma_1)(\lambda_2+Q_1)-E_2(\Gamma_2-s_2^o)]/(\lambda_2-\lambda_1) \tag{2.381}$$

$$\theta_2 = [(E_1(\Gamma_2-s_2^o)-(s_1^o-\Gamma_1)(\lambda_1+Q_1)]/(\lambda_2-\lambda_1) \tag{2.382}$$

The rear wheels are treated similarly.

§2.5.2. Static Treatment of the Steering System.

The steering equations as given in Bohn et al [1.6] are

$$(\ddot{r}+\ddot{\delta}_{Fwi})I_{FW} = -H_i\dot{\delta}_{Fwi}+M_{Ti}-M_{SSi}+M_{zi} \quad , \; i=1,2 \tag{2.383}$$

$$M_{CR}\ddot{y}_{CR} = -C_{FCR}(\dot{y}_{CR})-C_{CR}\dot{y}_{CR}+(T_p)/(a_p)$$
$$+(M_{SS1})/(A_{L1})+(M_{SS2})/(A_{L2}) \tag{2.384}$$

$$T_p = N_G\{K_{SC}[(\delta_{Sw}-N_G\frac{y_{CR}}{a_p})-\frac{\varepsilon_{sp}}{2}sgn(\delta_{Sw}-N_G\frac{y_{CR}}{a_p})]\} \tag{2.385}$$

$$M_{SSi} = K_{SLi}[\delta_{Fwi}-\frac{y_{CR}}{A_{Li}}-\frac{\varepsilon_{sp}}{2}sgn(\delta_{Fwi}-\frac{y_{CR}}{A_{Li}})] \tag{2.386}$$

where $\ddot{r}$ is the angular acceleration about the z-axis, δ_{Fwi} are the angular displacements of the front wheels produced by the steering system, I_{FW} is the moment of inertia of the individual front wheels about the kingpin axis, H_i is a viscous damping coefficient at the front wheel i, M_{Ti} is the moment acting at the front wheel i about the kingpin axis due to tire forces, M_{SSi} is the moment applied to the front wheel i by the steering system connecting rod, M_{zi} is the tire aligning moment at wheel i, M_{CR} is the effective mass of the steering system connecting rod, y_{CR} is the displacement of the steering system connecting rod, $C_{FCR}(\dot{y}_{CR})$ is the Coulomb friction in the steering gear (effective at the connecting rod), C_{CR} is the viscous damping in the steering gear (effective at the connecting rod), a_p is the length of the Pitman arm, A_{Li} is the length of the steering linkage at the front wheel i, N_G is the gear ratio of the steering gear, K_{SC} is the flexibility in the steering column and

the steering gear box, δ_{Sw} is the angular displacement of the steering wheel, ε_{sp} is the free play in steering gear box. K_{SLi} is the flexibility in the steering linkage at the front wheel i, and ε_{pi} is the free play in steer of front wheel i.

The quantities I_{FW} and M_{CR} are quite small, so that the differential equations (2.383) and (2.384) are "stiff" in the sense that the frequencies involved are much greater than those associated with the sprung mass degrees of freedom. One approach to such stiff equations is to use "multiple book-keeping", i.e., use a much finer mesh for them than is used for the sprung mass differential equations. However this can be a costly approach. It is felt that for severe maneuvers the high frequencies involved have little overall effect on the vehicle dynamics and so the dynamics terms, which are underscored by a solid line, in eqs. (2.383) and (2.384) are ignored. In addition, free-play effects, which are underscored by a dashed line, are felt to be negligible in severe maneuvers and these are ignored in eqs. (2.385) and (2.386).

The tire-road reaction moments acting about the kingpins are computed by the following equations:

$$
\begin{aligned}
M_{Ti} = &- (y_{SAi} - RR_i \phi_{SAOi})[(F_{xui} - F_{zui}\theta_{Si})\cos\psi_i \\
&+ (F_{yui} + F_{zui}\phi_{SAi})\sin\psi_i] \\
&- \overline{PT}_i \cos\psi_i \,[(F_{yui} + F_{zui}\phi_{SAi})\cos\psi_i \\
&- (F_{xui} - F_{zui}\theta_{Si})\sin\psi_i]
\end{aligned}
$$

where y_{SAi} is the distance between the kingpin axis and wheel centerline, measured along the wheel spin axis at the front wheel i, RR_i are rolling radii, ϕ_{SAOi} are the front wheel kingpin inclinations at the equilibrium suspension position, F_{xui}, F_{yui} and F_{zui} are the components of the tire side force in the x,y and z-directions, respectively, θ_{Si} are the front wheel caster angles relative to the x,y,z-axes, ψ_i is the steer angle of wheel i relative to the x,y,z-axes, ϕ_{SAi} are the front wheel kingpin inclinations, and $\overline{PT}_i$ is the front wheel caster offset.

§2.5.3. PARTIAL-DATA-DECK TIRE MODEL

In this section, the partial data deck model for calculating the lateral tire force that is available in the simulation will be discussed. Recall that the main features of the CALSPAN-APL model are:

(i) The dependence of the small-angle cornering stiffness on the radial force F_R' is approximated by a 2nd order polynomial, the coefficients of which are determined by a least squares fit to the experimental data.

(ii) The dependence of the maximum side force on the radial force F_R' is approximated by a 2nd order polynomial, the coefficients of which are determined by a least squares fit to the experimental data.

(iii) Camber effects are taken into account through an equivalent slip angle.

(iv) The dependence of the side force on the slip angle is approximated by a 3rd order polynomial (Fiala's approximation).

So that the potential user is not locked in to the above assumptions, the PARTIAL-DATA-DECK TIRE MODEL uses look-up tables and interpolation. In this model the user must supply the measured values of the side force F_S' as functions of slip angle β, camber angle ϕ_{CG}, and radial force F_R'. The relevant equations are:

$$T_1 = \frac{|\beta_i|}{SP1_i} + 1 \qquad (2.387)$$

$$T_2 = \frac{F'_{Ri} - F_{RMini}}{SP2_i} + 1 \tag{2.388}$$

$$\text{If } \beta_i \geq 0 \quad , \quad T_3 = \frac{\phi_{CGi} - \phi_{Mini}}{SP3_i} + 1 \tag{2.389}$$

$$\text{If } \beta_i < 0 \quad , \quad T_3 = \frac{\phi_{Maxi} - \phi_{CGi}}{SP3_i} + 1 \tag{2.390}$$

$$J_1 = [T_1] \quad , \quad \xi_1 = T_1 - J_1 \tag{2.391}$$

$$J_2 = [T_2] \quad , \quad \xi_2 = T_2 - J_2 \tag{2.392}$$

$$J_3 = [T_3] \quad , \quad \xi_3 = T_3 - J_3 \tag{2.393}$$

where [ ] means to truncate to the closest smaller integer.

$$\begin{aligned} F'_{Si} = {} & \{T_i(J_1,J_2,J_3)+\xi_1[T_i(J_1+1,J_2,J_3)-T_i(J_1,J_2,J_3)]+ \\ & \xi_2[T_i(J_1,J_2+1,J_3)-T_i(J_1,J_2,J_3)]+\xi_3[T_i(J_1,J_2,J_3+1)- \\ & T_i(J_1,J_2,J_3)]+\xi_1\xi_2[T_i(J_1+1,J_2+1,J_3)-T_i(J_1+1,J_2,J_3)- \\ & T_i(J_1,J_2+1,J_3)+T_i(J_1,J_2,J_3)]+\xi_1\xi_3[T_i(J_1+1,J_2,J_3+1)- \\ & T_i(J_1+1,J_2,J_3)-T_i(J_1,J_2,J_3+1)+T_i(J_1,J_2,J_3)]+\xi_2\xi_3 \\ & [T_i(J_1,J_2+1,J_3+1)-T_i(J_1,J_2+1,J_3)-T_i(J_1,J_2,J_3+1)+ \\ & T_i(J_1,J_2,J_3)]+\xi_1\xi_2\xi_3[T_i(J_1+1,J_2+1,J_3+1)-T_i(J_1+1,J_2+1,J_3)- \\ & T_i(J_1+1,J_2,J_3+1)-T_i(J_1,J_2+1,J_3+1)+T_i(J_1+1,J_2,J_3)+ \\ & T_i(J_1,J_2+1,J_3)+T_i(J_1,J_2,J_3+1)-T_i(J_1,J_2,J_3)]\}\frac{\beta_i}{|\beta_i|}SN_i \end{aligned}$$

Though this scheme has the advantage that the measured values can be used directly, the simulation user should be cautioned that considerable memory storage is involved in its utilization. Differences between the two models will be discussed further in Chapter 4.

2.5.4 Four Wheel Braking

To simulate many realistic cases the program allow a different brake torque at each wheel for a given brake line pressure.

This is effected through modification of the two-dimensional arrays B_{Fij} and B_{Rij} in eqs. (2.310) through (2.313) and (2.316) through (2.319). These arrays give data points in "look-up" tables. For i = 1, the arrays specify values for the brake line pressure. For i = 2,3 the table contains the corresponding broke line torques for the right and left wheels, respectively. To return to the APL simulation, in which the right and left wheels receive the same braking, the case i = 3 is deleted.

§2.5.5. Derivation of the Static Suspension Forces

Fig. 2.4 is a sketch of the vehicle at rest. All of the state variables are taken to be zero except for the pitch angle, θ, and the center of gravity height, Z.

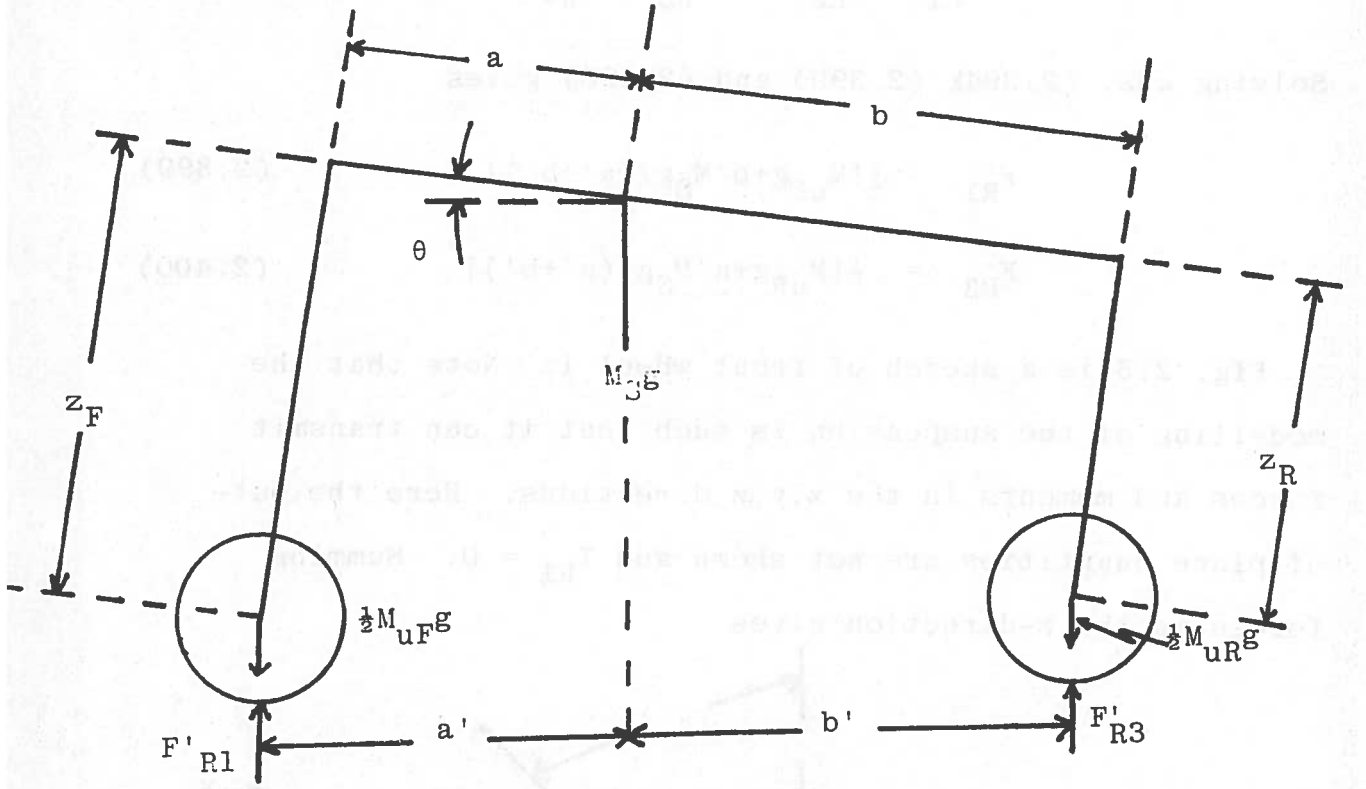

Fig 2.4. Free body diagram of the vehicle at rest.

Summing forces in the vertical direction gives

$$F'_{R1} + F'_{R2} + F'_{R3} + F'_{R4} = (\Sigma M)g \qquad (2.394)$$

Taking moments about the y-axis gives

$$(F'_{R1}+F'_{R2}-M_{uF}g)a' = (F'_{R3}+F'_{R4}-M_{uR}g)b' \qquad (2.395)$$

where

$$a' = a\cos\theta + z_F\sin\theta \tag{2.396}$$

$$b' = b\cos\theta - z_R\sin\theta \tag{2.397}$$

For a symmetric vehicle,

$$F'_{R1} = F'_{R2} \quad , \quad F'_{R3} = F'_{R4} \tag{2.398}$$

Solving eqs. (2.394), (2.395) and (2.396) gives

$$F'_{R1} = \tfrac{1}{2}[M_{uF}g + b'M_S g/(a'+b')] \tag{2.399}$$

$$F'_{R3} = \tfrac{1}{2}[M_{uR}g + a'M_S g/(a'+b')] \tag{2.400}$$

Fig. 2.5 is a sketch of front wheel 1. Note that the modelling of the suspension is such that it can transmit forces and moments in the x,y,z directions. Here the out-of-plane quantities are not shown and $T_{R1} = 0$. Summing forces in the z-direction gives

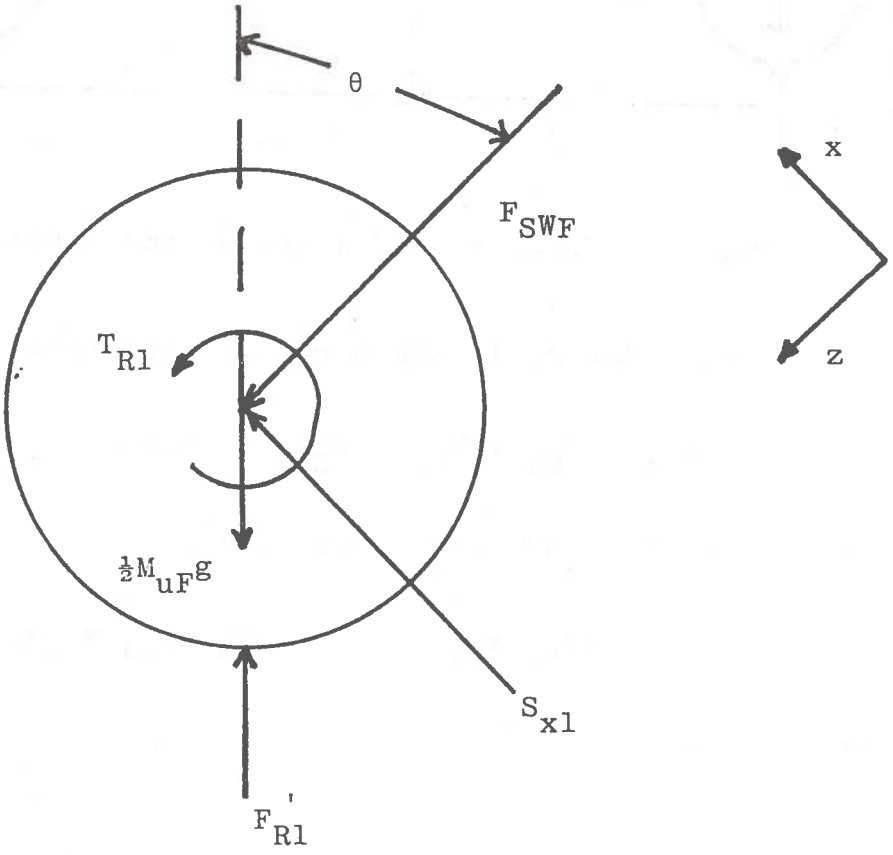

Fig 2.5. Free body diagram of front wheel 1.

$$F_{SWF} = (b'M_S g\cos\theta)/(a'+b') \qquad (2.401)$$

Similarly

$$F_{SWR} = (a'M_S g\cos\theta)/(a'+b') \qquad (2.402)$$

§ 2.5.6. Derivation of the Pitch Equation

The current simulation contains certain terms involving wheel inertias and tire forces which are not in the APL simulation. The occurrence of such terms will be demonstrated for the simple case of no wheel steer or camber and no roll. Shown in Fig. 2.6 is a free body diagram of the sprung mass. Since the out-of-plane quantities do not arise in the subsequent calculations, they are not shown on the sketch. Taking moments about the y-axis gives

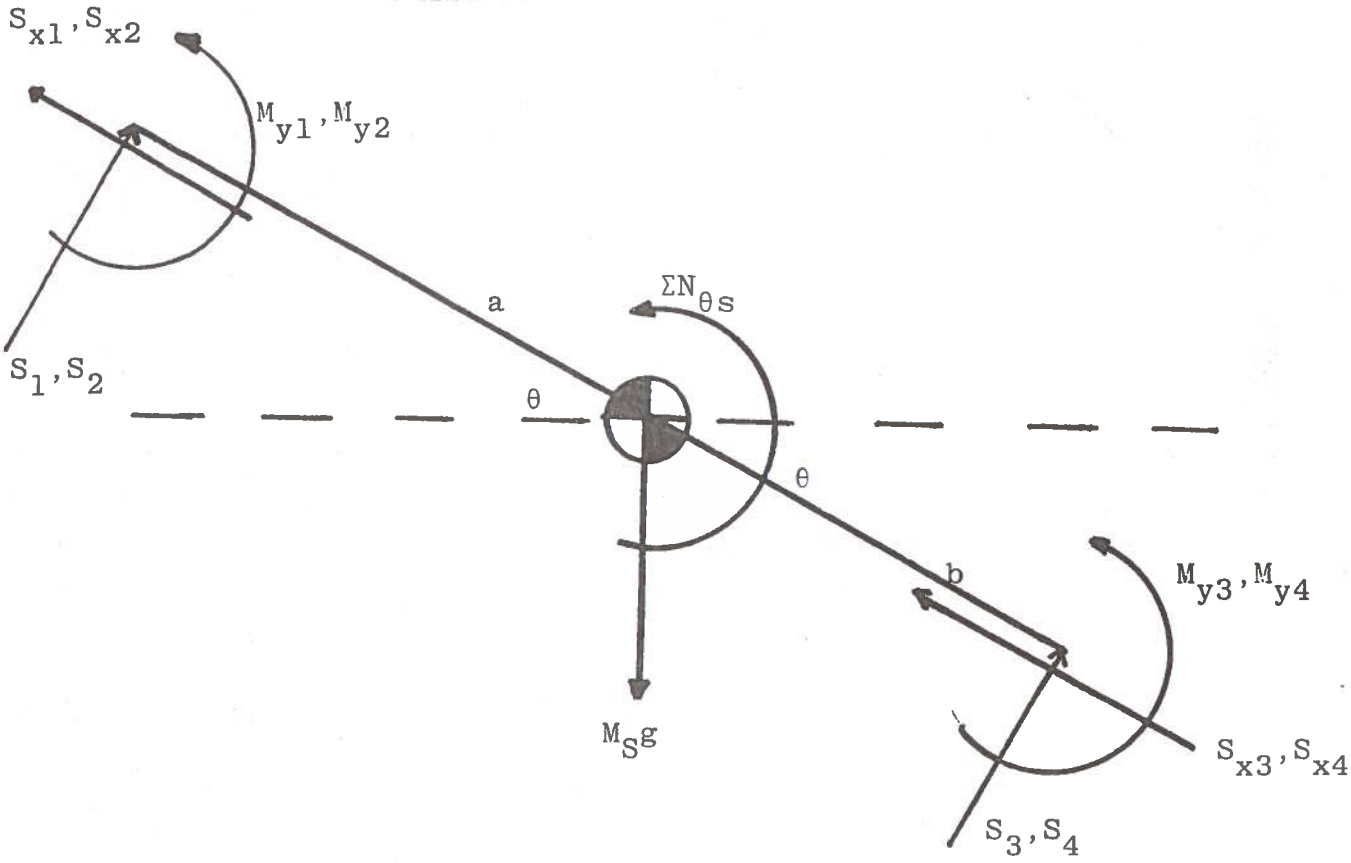

Fig. 2.6. Free body diagram of the sprung mass.

$$I_y \dot{q} - r^2 I_{xz} = a(S_1+S_2) - b(S_3+S_4) - \sum_{i=1}^{4} M_{yi} - \Sigma N_{\theta S} \qquad (2.403)$$

where the M_{yi} are suspension moments.

Fig. 2.7 is a sketch of the suspension for wheel 1.

Taking moments about the y-axis through the point P gives,

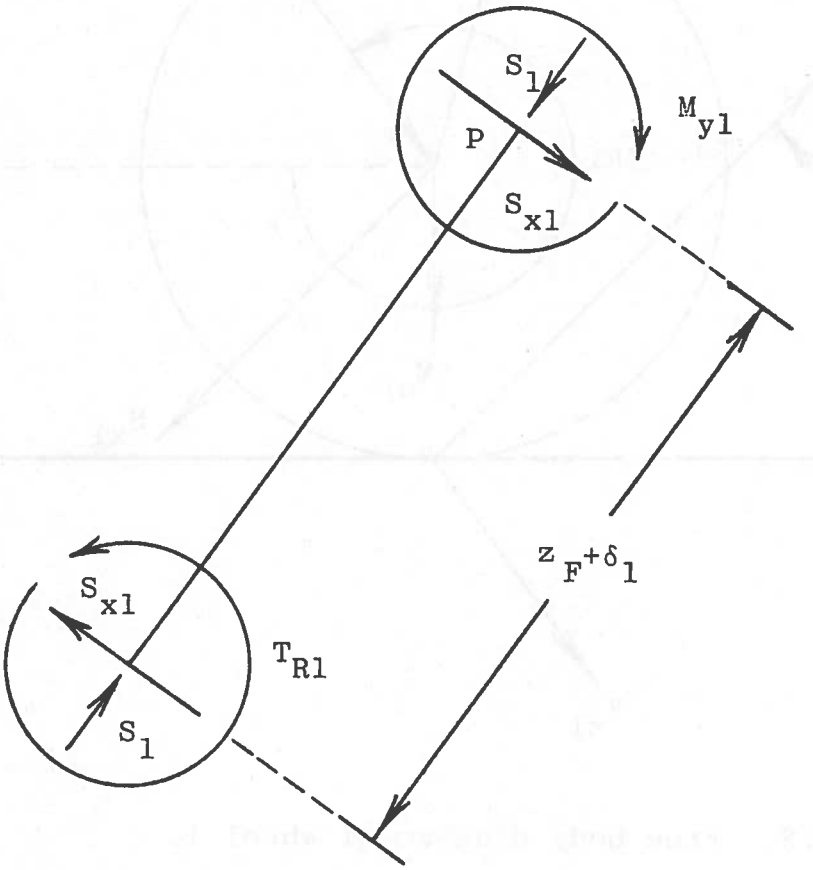

Figure 2.7. Suspension at wheel 1.

on assuming an inertialess suspension,

$$M_{y1} + S_{x1}(z_F+\delta_1) - T_{R1} = 0 \qquad (2.404)$$

A free body diagram of wheel 1 is given in Fig. 2.8. Taking moments about the y-axis through the wheel center gives

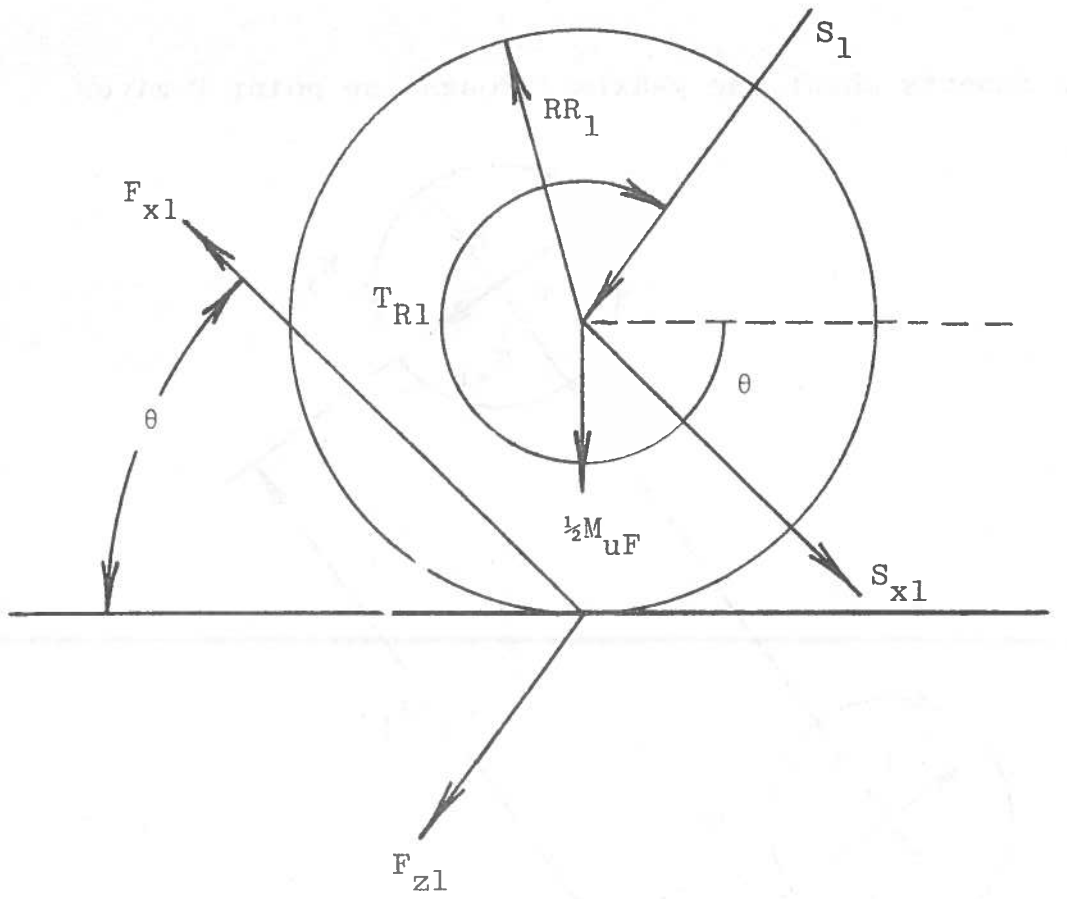

Figure 2.8. Free body diagram of wheel 1.

$$T_{R1} = I_{WF}\dot{\omega}_1 + RR_1(F_{x1}\cos\theta + F_{z1}\sin\theta) \qquad (2.405)$$

Summing forces in the x-direction yields

$$F_{x1} - S_{x1} - \frac{1}{2} M_{uF} g \sin\theta = \frac{1}{2} M_{uF} a_{x1} \qquad (2.406)$$

where a_{x1} is the acceleration of the center of gravity of wheel 1 in the x-direction.

Substituting eqs. (2.405)and (2.406) into eq. (2.404) gives

$$M_{y1} = I_{WF}\dot{\omega}_1+RR_1(F_{x1}\cos\theta+ F_{z1}\sin\theta) - (z_F+\delta_1)[F_{x1}- \tfrac{1}{2} M_{uF}(g\sin\theta+a_{x1})] \quad (2.407)$$

Similarly for wheel 2,

$$M_{y2} = I_{WF}\dot{\omega}_2+RR_2(F_{x2}\cos\theta+F_{z2}\sin\theta) - (z_F+\delta_2) [F_{x2}- \tfrac{1}{2} M_{uF}(g\sin\theta+a_{x2})] \quad (2.408)$$

The accelerations a_{x1} and a_{x2} are given by

$$a_{x1} = \dot{u}-vr+wq+2q\dot{\delta}_1-a(q^2+r^2)- \frac{T_F}{2} \dot{r}+(z_F+\delta_1)\dot{q} \quad (2.409)$$

$$a_{x2} = u-vr+wq+2q\dot{\delta}_2-a(q^2+r^2) - \frac{T_F}{2} \dot{r}+(z_F+\delta_2)\dot{q} \ . \quad (2.410)$$

In the case of an independent suspension we similarly get

$$M_{y3} = I_{WF}\dot{\omega}_3+RR_3(F_{x3}\cos\theta+F_{z3}\sin\theta) - (z_R+\delta_3)[F_{x3}- \tfrac{1}{2} M_{uR}(g\sin\theta+a_{x3})] \quad (2.411)$$

$$M_{y4} = I_{WF}\dot{\omega}_4+RR_4(F_{x4}\cos\theta+F_{z4}\sin\theta) - (z_R+\delta_4)[F_{x4}- \tfrac{1}{2} M_{uR}(g\sin\theta+a_{x4})] \quad (2.412)$$

$$a_{x3} = \dot{u}-vr+wq+2q\dot{\delta}_3-b(q^2+r^2)-\frac{T_R}{2}\dot{r}+(z_R+\dot{\delta}_3)\dot{q} \quad (2.413)$$

$$a_{x4} = \dot{u}-vr+wq+2q\dot{\delta}_4-b(q^2+r^2)- \frac{T_R}{2}\dot{r}+(z_R+\delta_4)\dot{q} \quad (2.414)$$

Substituting eqs. (2.407) through (2.414) into eq. (2.403) gives

$$I_y\dot{q} - r^2 I_{xz} = a(S_1+S_2)-b(S_3-S_4)-\Sigma N_{\theta s} - I_{WF}\dot{\omega}_1-RR_1(F_{x1}\cos\theta+F_{z1}\sin\theta)+(z_F+\delta_1)F_{x1}$$

(continued)

$$
\begin{aligned}
&- \tfrac{1}{2} M_{uF}(z_F+\delta_1)g\sin\theta - \tfrac{1}{2} M_{uF}[\dot{u}-vr+wq+2q\dot{\delta}_1 \\
&- a(q^2+r^2) - \frac{T_F}{2}\dot{r}+(z_F+\delta_1)\dot{q}] - I_{WF}\dot{\omega}_2 \\
&- RR_2(F_{x2}\cos\theta+F_{z2}\sin\theta)+(z_F+\delta_2)F_{x2} - \tfrac{1}{2} M_{uF}(z_F+\delta_2)\sin\theta \\
&- \tfrac{1}{2} M_{uF}(z_F+\delta_2)[\dot{u}-vr+wq+2q\dot{\delta}_2-a(q^2+r^2) \\
&- \frac{T_F}{2}\dot{r} + (z_F+\delta_2)\dot{q}] \\
&- I_{WF}\dot{\omega}_3-RR_3(F_{x3}\cos\theta+F_{z3}\sin\theta)+(z_R+\delta_3)F_{x3} - \tfrac{1}{2} M_{uR}(z_R+\delta_3)g\sin\theta \\
&- \tfrac{1}{2} M_{uR}(z_R+\delta_3)[\dot{u}-vr+wq+2q\dot{\delta}_3-b(q^2+r^2) \\
&- \frac{T_R}{2}\dot{r}+(z_R+\delta_3)\dot{q}] - I_{WF}\dot{\delta}_4+RR_4(F_{x4}\cos\theta+F_{z4}\sin\theta) \\
&+ (z_R+\delta_4)F_{x4} - \tfrac{1}{2} M_{uR}(z_R+\delta_4)g\sin\theta \\
&- \tfrac{1}{2} M_{uR}(z_R+\delta_4)[\dot{u}-vr+wq+2q\dot{\delta}_4-b(q^2+r^2) - \frac{T_R}{2}\dot{r} \\
&+ (z_R+\delta_4)\dot{q}\ ] \qquad (2.415)
\end{aligned}
$$

Such analyses lead to slightly different results than the APL mathematical model. The terms that are different are indicated in §2.3.1 by the "assumption O_7."

2.5.7. Suspension Averaging

To improve the accuracy of numerical integration, and to allow the use of a larger integration time step, the suspension forces are averaged over the two preceding time steps. Taking the average removes the higher frequencies present in the suspensions.

The equations used for averaging are:

First Averaging

$$\bar{S}_i(t) = \frac{1}{2}(S_i(t)+S_i(t-\Delta t)) \qquad (2.416)$$

Second Averaging

$$\bar{\bar{S}}_i(t) = \frac{1}{2}(\bar{S}_i(t)+\bar{S}_i(t-\Delta t)\ )$$

$$= \frac{1}{4}[S_i(t)+2S_i(t-\Delta t)+S_i(t-2\Delta t)\ ) \qquad (2.417)$$

§2.5.8. Antilock System.

Antilock systems as described in Ref. [2.1] are available, at the users' choice, in the current simulation. They are described in detail in §2.3.12.

References for Chapter Two

2.1. R. D. Ervin, J. D. Campbell, M. Sayers and H. Bunch," Improved Passenger Car Braking Performance," Final Technical Report, DOT-HS-6-01368, March 1978.

2.2. J. E. Bernard, "Some Time Saving Methods for the Digital Simulation of Highway Vehicles," Simulation, December 1973.

CHAPTER THREE
MATHEMATICAL MODEL OF THE DRIVER

§3.1 Introduction. This chapter presents the mathematical model of the driver that is implemented in the digital program: IDSFC Driver Module. Several different models of the driver have been implemented in the Driver Module. Section 3.2 gives a summary of the equations programmed and Section 3.3 the nomenclature used. Open loop control of the vehicle is discussed in Section 3.4.

In Sections 3.5 and 3.6, two basic types of driver modelling will be discussed and developed. Such models are an essential ingredient for closed-loop maneuvers, an important feature of the current simulation. The models are the preview-predictor type (see Ref. [3.1]) and the describing-function type (see McRuer et al, Ref.[3.2]).

Preview-predictor models are based on a psychological process viewpoint. Arbitrary trajectories are considered and two types of predictor are developed, namely, one using an algebraic method and another using a three-degree-of-freedom vehicle model.

The describing function models are based on a system control viewpoint and were developed for regulatory path following. In the development here, straight-line path following is treated separately from curved path following.

§ 3.2 Driver Module Equations

The Driver Module equations are subdivided as follows:

§ 3.2.1. Open Loop Command Table

§ 3.2.2 Preprogrammed Open Loop Maneuvers

§ 3.2.3 Preview - Predictor Equations

- § 3.2.3.1 Geometric Predictor
- § 3.2.3.2 Three-Degree-of-Freedom Predictor
- § 3.2.3.3 Steering and Speed Control Corrections
- § 3.2.3.4 Obstacle Avoidance
- § 3.2.3.5 Generation of Control Commands When Sampling Does Not Occur

§ 3.2.4 Describing Function Equations

§ 3.2.5 Calculating Errors

§ 3.2.6 Curvature Calculation

§ 3.2.7 Driver Module - Vehicle Model Interface

§ 3.2.1 Open Loop Command Table

$$F_{rac} = (t-t_{OLi})/(t_{OL(i+1)}-t_{OLi}) \qquad (3.1)$$

$$\delta_{Sw} = \delta_{Swi} + (F_{rac})(\delta_{Sw(i+1)}-\delta_{Swi}) \qquad (3.2)$$

$$P_{FL} = P_{FLi} + (F_{rac})(P_{FL(i+1)}-P_{FLi}) \qquad (3.3)$$

$$TQ_{D} = TQ_{Di} + (F_{rac})(TQ_{D(i+1)}-TQ_{Di}) \qquad (3.4)$$

$$VC = VC_{i} + (F_{rac})(VC_{i+1}-VC_{i}) \qquad (3.5)$$

$$d_{4} = d_{4i} + (F_{rac})(d_{4(i+1)}-d_{4i}) \qquad (3.6)$$

§3.2.2 Preprogrammed Open Loop Maneuvers

For the sinusoidal steer, the steering wheel angle is given by:

$$\delta_{Sw} = \begin{cases} 0, t \leq t_{sts} \\ a_{mp}\sin[2\pi(t-t_{sts})\tau_1], t_{sts} \leq t \leq t_{ens} \\ 0, t > t_{ens} \end{cases} \quad (3.7)$$

while for the trapezoidal steer:

$$\delta_{Sw} = \begin{cases} 0, t < t_{sts} \\ a_{mp}(t-t_{sts})/t_{rs}, t_{sts} \leq t < (t_{sts}+t_{rs}) \\ a_{mp}, (t_{sts}+t_{rs}) \leq t < (t_{ens}-t_{ds}) \\ a_{mp}(t_{ens}-t)/t_{ds}, (t_{ens}-t_{ds}) \leq t < t_{ens} \\ 0, t \leq t_{ens} \end{cases} \quad (3.8)$$

For the double trapezoidal steer:

$$\delta_{Sw} = \begin{cases} 0, t < t_{sts} \\ a_{mp}(t-t_{sts})/t_{rs}, t_{sts} \leq t < (t_{sts}+t_{rs}) \\ a_{mp}, (t_{sts}+t_{rs}) \leq t < \frac{1}{2}(t_{ens}-t_{sts})-t_{ds} \\ a_{mp}[\frac{1}{2}(t_{ens}-t_{sts})-t]/t_{ds}, [\frac{1}{2}(t_{ens}-t_{sts})-t_{ds}] \leq t < \frac{1}{2}(t_{ens}-t_{sts}) \\ -a_{mp}[t-\frac{1}{2}(t_{ens}-t_{sts})]/t_{rs}, \frac{1}{2}(t_{ens}-t_{sts}) \leq t < \frac{1}{2}(t_{ens}-t_{sts})+t_{rs} \\ -a_{mp}, [\frac{1}{2}(t_{ens}-t_{sts})+t_{rs}] \leq t < (t_{ens}-t_{ds}) \\ -a_{mp}(t_{ens}-t)/t_{ds}, (t_{ens}-t_{ds}) \leq t < t_{ens} \\ 0, t \leq t_{ens} \end{cases} \quad (3.9)$$

For the trapezoidal steer with a sinusoidal perturbation:

$$\delta_{Sw} = \begin{cases} 0, & t<t_{sts} \\ a_{mp}(t-t_{sts})/t_{rs}, & t_{sts} \leq t<(t_{sts}+t_{rs}) \\ a_{mp}+a_{mp2}\sin 2\,(t-t_{sts}-t_{rs})/\tau_2, & (t_{sts}+t_{rs}) \leq t<t_{ens} \\ a_{mp}(t_{ens}-t)/t_{ds}, & (t_{ens}-t_{ds}) \leq t<t_{ens} \\ 0, & t \geq t_{ens} \end{cases} \tag{3.10}$$

All of the above maneuvers can be performed with a trapezoidal brakeline pressure given by:

$$P_{FL} = \begin{cases} 0, & t<t_{stb} \\ p_{max}(t-t_{stb})/t_{rb}, & t_{stb} \leq t\,(t_{stb}+t_{rb}) \\ p_{max}, & (t_{stb}+t_{rb}) \leq t<(t_{enb}-t_{db}) \\ p_{max}(t_{enb}-t)/t_{db}, & (t_{enb}-t_{db}) \leq t<t_{enb} \\ 0, & t \geq t_{enb} \end{cases} \tag{3.11}$$

A sinusoidal steering sweep without braking is given by:

$$\delta_{Sw} = \begin{cases} 0 & t<t_{sts} \\ a_{mp}\sin\omega_{sl}(t-t_{sts})^2, & t_{sts} \leq t<\frac{1}{2}(t_{ens}+t_{sts}) \\ -a_{mp}\sin\omega_{sl}(t_{ens}-t)^2, & \frac{1}{2}(t_{ens}+t_{sts})<t<t_{ens} \\ 0, & t>t_{ens} \end{cases} \tag{3.12}$$

§3.2.3. Preview - Predictor Equations

§3.2.3.1 Geometric Predictor

When a geometric predictor is employed, the predicted positions and velocities are obtained by repeated use of:

$$\Delta X_i = [uP_{i-1} \cos(\psi P_{i-1}) - vP_{i-1} \sin(\psi P_{i-1})] \Delta t \quad (3.13)$$

$$\Delta Y_i = [uP_{i-1} \sin(\psi P_{i-1}) + vP_{i-1} \cos(\psi P_{i-1})] \Delta t \quad (3.14)$$

$$SP_i = SP_{i-1} + \sqrt{\Delta X_i^2 + \Delta Y_i^2} \quad (3.15)$$

$$XP_i = XP_{i-1} + \Delta X_i \quad (3.16)$$

$$YP_i = YP_{i-1} + \Delta Y_i \quad (3.17)$$

$$\psi P_i = \psi P_{i-1} + rP_{i-1} \Delta t \quad (3.18)$$

$$uP_i = uP_{i-1} + \dot{u}_{per} \Delta t \quad (3.19)$$

$$vP_i = vP_{i-1} + \dot{v}_{per} \Delta t \quad (3.20)$$

$$rP_i = rP_{i-1} + \dot{r}_{per} \Delta t \quad (3.21)$$

§3.2.3.2. Three-Degree-of-Freedom Predictor

When the three-degree-of-freedom predictor is employed, the predicted positions and velocities are obtained by integrating the differential equations:

$$\dot{X}_{pr} = u_{pr} \cos(\psi_{pr}) - v_{pr} \sin(\psi_{pr}) \quad (3.22)$$

$$\dot{Y}_{pr} = u_{pr} \sin(\psi_{pr}) + v_{pr} \cos(\psi_{pr}) \quad (3.23)$$

$$\dot{\psi}_{pr} = r_{pr} \quad (3.24)$$

$$\dot{u}_{pr} = a_{cc} - [FS_1 \sin(\delta+\delta_{toe1}) + FS_2 \sin(\delta+\delta_{toe2})] / M_{TOT} + v_{pr} r_{pr} \quad (3.25)$$

$$\dot{v}_{pr} = (FS_1 \cos(\delta+\delta_{toe1})+FS_2 \cos(\delta+\delta_{toe1}) +FS_3+FS_4)/M_{TOT} - u_{pr}\, r_{pr} \quad (3.26)$$

$$\dot{r}_{pr} = \{FS_1 [x_1 \cos(\delta+\delta_{toe1})+y_1 \sin(\delta+\delta_{toe1})]+FS_2 [x_2 \cos(\delta+\delta_{toe2})+y_2 \sin(\delta+\delta_{toe2})]+x_3 \times (FS_3+FS_4) / I_{zz} \quad (3.27)$$

$$\dot{S}_{pr} = [(\dot{X}_{pr})^2+(\dot{Y}_{pr})^2]^{1/2} \quad (3.28)$$

$$u_i = u_{pr} - y_i . r_{pr} \quad (3.29)$$

$$v_i = v_{pr} + x_i . r_{pr} \quad (3.30)$$

$$\theta_i = \tan^{-1}(v_i/u_i) \quad (3.31)$$

$$a_x = \dot{u}_{pr} - v_{pr}\, r_{pr} \quad (3.32)$$

$$a_y = \dot{v}_{pr} + u_{pr}\, r_{pr} \quad (3.33)$$

$$\alpha_i = \theta_i - \delta - \delta_{toei} \quad , \quad i=1,2 \quad (3.34)$$

$$\alpha_1 = \theta_i \quad i=3,4 \quad (3.35)$$

$$FN_i = \frac{1}{2}[-g\, x_{i+2}-a_x . c+(x_{i+2}\, c\, a_y)/y_i]M_{TOT}/(a+b), i+1,2 \quad (3.36)$$

$$FN_i = \frac{1}{2}[g\, x_{i-2}+a_x\, c-(x_{i-2}\, c\, a_y)/y_i]M_{TOT}/(a+b) \quad (3.37)$$

$$i=3,4 \quad (3.38)$$

$$\delta = \delta_{Swh} GR$$

For i such that $BT_1(i-1) < P_{FLh} \leq BT_{1i}$

$$TQ_B = BT_{2i} - (BT_{1i} - P_{FLh})\,(BT_{2i} - BT_{2(i-1)})/ (BT_{1i} - BT_{1(i-1)}) \quad (3.39)$$

$$a_{cc} = TQ_B/BK_{con} + TQ_D/DV_{con} \quad (3.40)$$

The tire side forces FS_i are given by:

If $FN_i \leq A2_i$:

$$C_{\alpha i} = AO_i + (A1_i)(FN_i) - (A1_i/A2_i)(FN_i)^2 \quad (3.41)$$

If $FN_i > A2_i$:

$$C_{\alpha i} = AO_i \quad (3.42)$$

$$F_{maxi} = (B3_i)(FN_i) + (B1_i)(FN_i)^2 + (B4_i)(FN_i)^3 \quad (3.43)$$

$$\bar{\alpha}_i = -(C_{\alpha i})(\alpha_i)/F_{maxi} \quad (3.44)$$

If $|\alpha_i| < 3$:

$$FS_i = F_{maxi}[\bar{\alpha}_i - \bar{\alpha}_i|\bar{\alpha}_i|/3) + (\bar{\alpha}_1{}^3/27)] \quad (3.45)$$

If $|\bar{\alpha}_i| > 3$:

$$FS_i = F_{maxi} \mathrm{sgn}\bar{\alpha}_i \quad (3.46)$$

§ 3.2.3.3. Steering and Speed Control Corrections

A weighted average of the errors is calculated by:

$$ERR_{acc} = \frac{1}{N_{pred}} \sum_{i=1}^{N_{pred}} \frac{WT_{aci} ERR_{u2i}}{2SP_i} \tag{3.47}$$

$$ERR_{st} = \sum_{i=1}^{N_{pred}} (WT_{sti} D_{pi} KP_i) \tag{3.48}$$

$$KP_i = \frac{2(a+b)[1+KD(uP_i^2 + vP_i^2)]}{N_{pred}(SP_i)^2} \tag{3.49}$$

Note. SP_1 is taken equal to SP_2

Using these errors, control commands are generated by:

$$\delta_{des} = \delta - G_{st} ERR_{st} \quad , \quad |\delta_{des}| \leq \delta_{max} \tag{3.50}$$

$$a_{ccdes} = a_{cc} - G_{ac} ERR_{acc} \quad , \quad a_{ccmin} \leq a_{ccdes} \leq a_{ccmax} \tag{3.51}$$

$$a_{ccdes} \leq \frac{1}{2}[(u_{maxj})^2 - (uP_j)^2]/SP_j$$

$$j = 1 \ldots N_{pred}$$

$$u_{maxi} = \{(ala_{max})(ACC_{Lmax})/\kappa_{1i}\}^{1/2}, \quad i = 1...(N_{pred}-1)$$

$$u_{maxi} = u_{max(i-1)}, \quad i = N_{pred} \tag{3.52}$$

The commands are then stored in a command table generated by:

$$i = [100(t - t_1 - 0.1)]^* \tag{3.53}$$

If $t_1 < t_{1n}$, $t_1 = t_{1n}$ where

$$t_{1n} = 0.01[100(t - 0.1)]^* \tag{3.54}$$

$$i_T = [100(t + \tau_{1pp} - t_1) + 1]^* \tag{3.55}$$

For $j = 1, 2, ... i_T$ do equations (3.55) and (3.56)

$$\delta_j = \delta_{(1+j)} \tag{3.56}$$

$$a_{ccj} = a_{cc(i+j)} \tag{3.57}$$

$$k = 0 \tag{3.58}$$

For $j = i_T + 1, i_T + 2, ..., 300$ do equations (3.58) through (3.66)

$$e_F = 1 - \exp\{(t + \tau_1 - 0.01(j-1)/\tau_m\} \tag{3.59}$$

$$\delta_j = \delta_{iT} + (\delta_{des} - \delta_{iT})\, e_F \tag{3.60}$$

If $(\delta_j - \delta_{(j-1)}) > 0.01\dot{\delta}_{max}$

$$\delta_j = \delta_{(j-1)} + 0.01\dot{\delta}_{max} \tag{3.61}$$

If $(\delta_{(j-1)} - \delta_j) > 0.01\dot{\delta}_{max}$

$$\delta_j = \delta_{(j-1)} - 0.01\dot{\delta}_{max} \tag{3.62}$$

$$a_{cc(j+k)} = a_{cci_T} + (a_{ccdes} - a_{cci_T})e_F \tag{3.63}$$

If $(a_{cc(j+k)} - a_{ccsw})(a_{cc(j+k-1)} - a_{ccsw}) \leq 0$

*Where [ ] means truncate to the nearest smallest integer.

then do equations (3.63)-(3.66); otherwise return to eqn. (3.58).

$$\ell = [100\tau_{ab}] \tag{3.64}$$

$$k = k + \ell \tag{3.65}$$

$$a_{cc(j+k)} = a_{cc(j+k-\ell)} \tag{3.66}$$

$$a_{cc}(j+k-\ell-1+m) = a_{ccsw},\ m = 1,2,\ldots\ell \tag{3.67}$$

§ 3.2.3.4. Obstacle Avoidance

The distance to the obstacle from the point of first sighting is determined by:

$$D_{view} = \{(X_{per} - X_{RPi})^2 + (Y_{per} - Y_{RPi})^2\}^{1/2}$$

$$\text{for } i = I_{OP} \tag{3.68}$$

The time increment between predicted points becomes

$$t_{ppt} = \frac{u_{per}}{D_{view} \cdot (N_{pred} - 1)} \tag{3.69}$$

The desired path is moved to the right or left by a distance C_{ob}.

§ 3.2.3.5. Generation of Control Commands when Sampling Does Not Occur.

The command table previously generated is used together with the following equations to generate control commands:

$$i = [100(t-t_1)] + 1 \tag{3.70}$$

$$\xi = 100(t-t_1) + 1 - i \tag{3.71}$$

$$\delta = COMD_{1i} + \xi\,(COMD_{1(i+1)} - COMD_{1i}) \tag{3.72}$$

$$a_{cc} = COMD_{2i} + \xi\,(COMD_{2(i+1)} - COMD_{2i}) \tag{3.73}$$

§ 3.2.4. Describing Function Equations

For the straight line cross-over model, the control commands are calculated by

$$e_Y = -Y \tag{3.74}$$

$$e_{\dot{Y}} = -u\sin\Psi - v\cos\Psi \tag{3.75}$$

$$e_\Psi = -\Psi \tag{3.76}$$

$$e_{\dot{\Psi}} = -r \tag{3.77}$$

$$e_u = V_{des} - u \tag{3.78}$$

$$\delta_{Swnew} = G_Y e_Y + G_{\dot{Y}} e_{\dot{Y}} + G_\Psi e_\Psi + G_{\dot{\Psi}} e_{\dot{\Psi}} \tag{3.79}$$

$$a_{ccnew} = G_u e_u \tag{3.80}$$

For the general cross-over model, the control commands are calculated by

$$\delta_{Swnew} = (a+b)[1+(KD)u^2](e_{\dot{\Psi}}+r)/u(GR)+G_Y e_Y+G_{\dot{Y}} e_{\dot{Y}}+G_\Psi e_\Psi+G_{\dot{\Psi}} e_{\dot{\Psi}} \tag{3.81}$$

$$a_{ccnew} = G_u e_u \tag{3.82}$$

The control commands given above are delayed by the driver's neuromuscular response time τ_L.

§ 3.2.5. Error Calculation

The differences between the predicted and desired paths, i.e., the errors, are calculated in the preview predictor model by

$$D_{pj} = [(XP_j - X_{int})^2 + (YP_j - Y_{int})^2]^{\frac{1}{2}} \quad (3.83)$$

$$d_{12}^2 = (X_1 - X_2)^2 + (Y_1 - Y_2)^2 \quad (3.84)$$

$$X_{int} = [(Y_{PERP} - Y_1)(Y_1 - Y_2)(X_1 - X_2) + X_1(Y_1 - Y_2)^2 + X_{PERP}(X_1 - X_2)^2]/d_{12}^2 \quad (3.85)$$

$$Y_{int} = [(X_{PERP} - X_1)(X_1 - X_2)(Y_1 - Y_2) + Y_1(X_1 - X_2)^2 + Y_{PERP}(Y_1 - Y_2)^2]/d_{12}^2 \quad (3.86)$$

$$\Omega = \mathrm{sgn}(Y_{int} - YP_j)\cos^{-1}[(X_{int} - XP_j)/D_{pj}] \quad (3.87)$$

where sgn stand for "sign of."

$$\text{If } \Omega > \psi P_j, \quad D_{pj} = -D_{pj} \quad (3.88)$$

$$u_{des} = U_{RPI_{PT}} + (X_{int} - X_1)(U_{RPI_2} - U_{RPI_{PT}})/(X_2 - X_1) \quad (3.89)$$

$$ERR_{u2j} = (up_j)^2 + (vP_j)^2 - (u_{des})^2 \quad (3.90)$$

For the general cross-over model the errors are given by:

$$e_Y = -D_{p1} \tag{3.91}$$

$$\psi_{des} = \tan^{-1}(Y_{RPj}-Y_{RPi})/(X_{RPj}-X_{RPi}) \tag{3.92}$$

$$\dot{e_Y} = -u\sin(\psi-\psi_{des}) - v\cos(\psi-\psi_{des}) \tag{3.93}$$

$$e_\psi = \psi_{des}-\psi \tag{3.94}$$

$$\dot{e_\psi} = |\vec{V}|\kappa - r \tag{3.95}$$

$$e_u = u_{des} - |\vec{V}| \tag{3.96}$$

$$|\vec{V}| = \sqrt{(uP_j)^2 + (vP_j)^2} \tag{3.97}$$

$$\kappa = \kappa_1 + (\kappa_2-\kappa_1)[(X_{int}-X_{RPI_{PT}})^2 + (Y_{int}-Y_{RPI_{PT}})^2]^{\frac{1}{2}}/[(X_{RPI_2}- X_{RPI_{PT}})^2 + (Y_{RPI_2}-Y_{RPI_{PT}})^2]^{\frac{1}{2}} \tag{3.98}$$

§ 3.2.6. Curvature Calculation

Curvature κ of a circle passing through the specified points (X_1Y_1), (X_2Y_2), (X_3Y_3) is given by:

$$d_1 = X_1 - X_2 \tag{3.99}$$

$$d_2 = X_1 - X_3 \tag{3.100}$$

$$d_3 = Y_1 - Y_2 \tag{3.101}$$

$$d_4 = Y_1 - Y_3 \tag{3.102}$$

$$d_5 = X_1^2 - X_2^2 + Y_1^2 - Y_2^2 \tag{3.103}$$

$$d_6 = X_1^2 - X_3^2 + Y_1^2 - Y_3^2 \tag{3.104}$$

$$\Delta = 2(d_1d_4 - d_2d_3) \tag{3.105}$$

$$d_7 = (d_5d_4 - d_6d_3)/\Delta \tag{3.106}$$

$$d_8 = (d_5d_2 - d_6d_1)/\Delta \tag{3.107}$$

$$\kappa = [(X_2-d_7)^2 + (Y_2-d_8)^2]^{-\frac{1}{2}} \tag{3.108}$$

§ 3.2.7. Driver Module - Vehicle Model Interface

Quantities needed by the preview - predictor methods are given by:

$$M_{TOT} = M_S + M_{uR} + M_{uF} \tag{3.109}$$

$$FR_{S1} = \frac{g}{2}\,[M_{uF}+M_S b/(a+b)] \tag{3.110}$$

$$FR_{S2} = \frac{g}{2}[M_{uR}+M_S a/(a+b)] \tag{3.111}$$

$$RR_i = R_{wi} - (FR_{S1})/(K_{Ti}),\ i=1,2 \tag{3.112}$$

$$RR_i = R_{wi} - (FR_{S2})/(K_{Ti}),\ i=3,4 \tag{3.113}$$

$$\text{If } RR_i < R_{RIMi},\ RR_i = R_{RIMi},\ i=1\ldots4 \tag{3.114}$$

$$\text{If } RR_i > R_{wi},\ RR_i = R_{wi},\ i=1\ldots4 \tag{3.115}$$

$$BK_{con} = -\,[(M_{TOT}) \sum_{i=1}^{4} RR_i]/(4 \sum_{i=1}^{4} \lambda_{Bi}) \tag{3.116}$$

$$DV_{con} = M_{TOT}\{(1-\lambda_D)\,[(1/RR_1)+(1/RR_2)]+\lambda_D[(1/RR_3)+(1/RR_4)]\} \tag{3.117}$$

$$GR = (a_p/2N_G)[(1/A_{L1}) + (1/A_{L2})] \tag{3.118}$$

$$BT_{ij} = \frac{1}{2}(B_{Fij} + B_{Rij}),\ i=1\ldots2,\ j=1\ldots11 \tag{3.119}$$

$$a_{ccmax} = (alo_{max})(TQ_{Dmax})\{(1-\lambda_D)](1/RR_1)+(1/RR_2)] + \lambda_D[(1/RR_3)+(1/RR_4)]\}/M_{TOT} \quad (3.120)$$

$$a_{ccmin} = -(alo_{min})\{\sum_{i=1}^{2}(P_{B1i})(FR_{S1})+(P_{B2i})(FR_{S1})^2 + (P_{B3i})(FR_{S1})^3]SN_i + \sum_{i=3}^{4}[(P_{B1i})(FR_{S2}) + (P_{B2i})(FR_{S2})^2+(P_{B3i})(FR_{S2})^3]SN_i\}/M_{TOT} \quad (3.121)$$

$$ACC_{Lmax} = \{\sum_{i=1}^{2}[(B_{3i})(FR_{S1})+(B_{1i})(FR_{S1})^2+(B_{4i})(FR_{S1})^3]SN_i + \sum_{i=3}^{4}[(B_{3i})(FR_{S2})+(B_{1i})(FR_{S2})^2+(B_{4i})(FR_{S2})^3]SN_i\}/M_{TOT} \quad (3.122)$$

The three-degree-of-freedom predictor also requires:

$$I_{zz} = I_z+[a^2+(T_F)^2/4]M_{uF}+b^2M_{uR} \quad (3.123)$$

$$c = \{-z_{(0)}M_S+\tfrac{1}{2}[M_{uF}(RR_1+RR_2)+M_{uR}(RR_3+RR_4)]\}/M_{TOT} \quad (3.124)$$

$$\delta_{toe1} = \frac{\pi}{180}\sum_{j=0}^{5} D_{jF}\delta_{S1}^{j} + \delta_{stat1} \quad (3.125)$$

$$\delta_{toe2} = \frac{\pi}{180}\sum_{j=0}^{5} D_{jF}\delta_{S2}^{j} + \delta_{stat2} \quad (3.126)$$

The initial acceleration is calculated from:

$$\text{If } P_{FLO} \leq 1, \quad a_{cc0} = (TQ_{DO})/(DV_{con}) \tag{3.127}$$

Otherwise, for j such that $BT_{1(j-1)} < P_{FLO} \leq BT_{1j}$,

$$TQ_B = BT_{2(j-1)} + (P_{FLO} - BT_{1(j-1)})(BT_{2j} - BT_{2(j-1)})/(BT_{1h} - BT_{1(j-1)}) \tag{3.128}$$

$$a_{cc0} = (TQ_B)/(BK_{con}) \tag{3.129}$$

The steering angle command outputed by the preview predictor models are converted to steering wheel angles by:

$$A_1 = (M_{T1} + M_{z1} - \dot{r}I_{FW})/K_{SL1} \tag{3.130}$$

$$A_2 = (M_{T2} + M_{z2} - \dot{r}I_{FW})/K_{SL2} \tag{3.131}$$

$$\delta_{Sw} = \delta/GR - \frac{N_G(A_1+A_2)}{a_p(\frac{1}{A_{L1}} \quad \frac{1}{A_{L2}})} - \frac{a_p}{N_G K_{SC}} \left(\frac{K_{SL1}A_1}{A_{L1}} + \frac{K_{SL2}A_2}{A_{L2}}\right) \tag{3.132}$$

For all of the closed-loop driver models, acceleration commands are converted to brakeline pressure and drive torque commands by:

If $a_{cc} < 0$,

$$TQ_B = a_{cc}\, BK_{con} \tag{3.133}$$

For i such that $BT_{2(i-1)} \leq TQ_B < BT_{2i}$,

$$P_{FL} = BT_{1i} - (BT_{2i} - TQ_B)(BT_{1i} - BT_{1(i-1)})/(BT_{2i} - BT_{2(i-1)}) \tag{3.134}$$

$$TQ_D = 0 \tag{3.135}$$

If $a_{cc} > 0$

$$P_{FL} = 0 \tag{3.136}$$

$$TQ_D = a_{cc}\, DV_{con} \tag{3.137}$$

§ 3.3 Driver Module Nomenclature

Some of the symbols used in the driver module equations have already been defined in the vehicle model nomenclature, § 2.4. Additional symbols used in the driver module are:

Symbol	Definitions
ACC_{Lmax}	Maximum possible lateral acceleration of the vehicle.
$AO_i, A1_i, A2_i$	Coefficients in a quadratic approximation to the cornering stiffness versus normal tire force relationship.
A_1, A_2	Variables used in §3.2.7.
a_{cc}	Current value of acceleration command.
a_{ccdes}	Desired value of the acceleration command.
a_{ccj}	Acceleration command for time t_j.
a_{ccmin}, a_{ccmax}	Minimum and maximum acceleration, respectively, driver will utilize.
a_{ccnew}	Value of the acceleration command for $t+\tau_L$, where τ_L is the driver response time lag.
a_{cco}	Initial value of acceleration.
a_{ccsw}	Acceleration level at which acceleration/braking switch-over occurs
ala_{max}	Maximum lateral acceleration driver will utilize.
alo_{max}	Fraction of vehicle acceleration capability which the driver will use.
alo_{min}	Fraction of vehicle decceleration capability which the driver will use.
a_{mp}	Maximum steering wheel angular displacement.
a_{mp2}	Amplitude of sinusoidal steering perturbation.
a_x, a_y	Vehicle acceleration components in the x and y directions, respectively.

Symbol	Definition
B_{Fij}, B_{Rij}	Coefficients in "look-up" tables for brakeline pressures versus torques for front and rear wheels, respectively.
BK_{con}	Conversion factor between brake torque and vehicle decceleration.
BT_{ij}	Array giving brakeline pressures versus torques.
$B1_i, B3_i, B4_i$	Coefficients in a cubic approximation to the relationship between the maximum tire side force and the tire normal force.
$C_{\alpha i}$	Cornering stiffness.
C_{ob}	Distance by which desired path must be shifted to avoid an obstacle.
$COMD_{1i}, COMD_{2i}$	Array containing the desired steering and acceleration commands at 0.01 second intervals.
c	Height of the center of mass of the entire vehicle above the ground level.
D_{jF}	Coefficients in a fifth degree polynomial fitted to wheel toe angles versus suspension deflections.
D_p	Perpendicular distance from predicted point to the nearest point on the road path.
D_{pi}	Distance from a predicted point to the desired path.
D_{view}	Distance from an obstacle to its point of first sighting.
DV_{con}	Drive torque - acceleration conversion factor.
$d_1, d_2, d_3, d_4, d_5, d_6, d_7, d_8$	Variables used in §3.2.6.
d_4, d_{4i}	Variables in §3.2.1.
d_{12}	The distance between the points (X_1, Y_1) and (X_2, Y_2).

Symbol	Definition
ERR_{acc}	Normalized acceleration error.
ERR_{st}	Normalized position error for steering correction.
ERR_{u2i}	Difference between squares of actual and desired forward velocities.
e_F	Variable used in §3.2.3.3.
e_ψ	Heading angle error.
e_u	Forward velocity error.
e_Y	Lateral position error.
FN_i	Normal force acting on tire i (F_{Ri} in the vehicle model)
F_{rac}	Variable used in §3.2.1.
FR_{S1}, FR_{S2}	Static radial tire force for the front and rear wheels, respectively.
FS_i	Tire side force at wheel i (F_{Si} in the vehicle model).
G_{ac}	Multiplying factor for velocity errors.
G_ψ	Heading angle gain.
$G_{\dot\psi}$	Heading rate gain.
G_{st}	Multiplying factor for position errors.
G_u	Forward velocity gain.
GR	Overall effective steering ratio ($GR = \delta/\delta_{Sw}$).
G_Y	Lateral position gain.
$G_{\dot Y}$	Lateral velocity gain.
I_{OP}	Index of road point at which obstacle is located.
I_{PT}	Index of road map point closest to a predicted point.
I_2	Index of road map point which locates other end of road segment on which lies the point closest to the vehicle.

Symbol	Definition
I_{zz}	Moment of inertia of the entire vehicle about the z-axis.
i_T	An index giving upper limit of elements of COMD table to be discarded.
KD	Understeer/oversteer coefficient.
KPi	Steering error normalizing factor.
M_{tot}	Total mass of the vehicle (ΣM in the vehicle model).
N_{pred}	Number of predicted points.
$P_{B1i}, P_{B2i}, P_{B3i}$	Coefficients of curves fitted to the peak braking friction coefficient at wheel i.
P_{FLi}	Value of the brakeline pressure at the time of the command "i", t_{OLi}.
P_{FLo}	Initial value of the brakeline pressure.
p_{max}	Maximum value of the brakeline pressure.
r_{per}	Perceived yaw rate.
rP_i	Predicted yaw rate at point i.
r_{pr}	Predicted yaw rate in the three-degree-of-freedom predictor.
S_{pr}	Distance from current position along predicted path.
SP_i	Distance from present position to predicted point i.
TQ_B	Effective brake torque.
TQ_D	Drive torque.
TQ_{Di}	Value of the drive torque at the time of the command "i", t_{OLi}.
t_{db}	Drop-off time for trapezoidal braking.
t_{ds}	Drop-off time for trapezoidal steer.
t_{enb}	Time at which braking input is terminated.
t_{ens}	Time at which steering inputs are terminated.

Symbol	Definition
t_{pps}	Sampling time interval.
t_{ppt}	Predicted point time interval.
t_{rb}	Rise time for trapezoidal braking.
t_{rs}	Rise time for trapezoidal steer.
t_{stb}	Time at which braking input is initiated.
t_{sts}	Time at which steering inputs are initiated.
t_{OL1}, t_{OL2}	Starting and ending times, respectively, of an open-loop control period.
t_1	Time corresponding to the first entry in the command table COMD.
t_{1n}	New value of t_1, the time corresponding to the first entry in the command table COMD.
U_{RPj}	Desired forward velocity at point j.
UP_i	Predicted forward velocity at the point i.
u_{des}	Desired forward velocity.
u_{maxj}	Vector of maximum allowable velocities at the predicted path points.
u_{per}	Perceived forward velocity.
u_{pr}	Predicted forward velocity in the three-degree-of-freedom predictor.
$\lvert\vec{V}\rvert$	Total vehicle speed.
V_{des}	Desired forward velocity in the straight line describing function model.
VC	Commanded velocity.
VC_i	Commanded velocity at the time of command "i", t_{OLi}.
vP_i	Predicted lateral velocity at the point i.
v_{per}	Perceived lateral velocity.

Symbol	Definition
v_{pr}	Predicted lateral velocity in the three-degree-of-freedom predictor.
WT_{aci}	Weighting factors for velocity errors.
WT_{sti}	Weighting factors for position errors.
X_{PERP}	X-coordinate of the point through which the perpendicular is drawn.
X_{RPi}	X-coordinate of the road point i.
XP_i	Predicted value of X at the point i.
X_{int}	X coordinate of the closest point on the road path.
X_{per}	Perceived value of X.
X_{pr}	Predicted value of X in the three-degree-of-freedom predictor.
X_1, X_2	X-coordinates of end points of a road segment which is being checked for perpendicular intersection point.
$(X_1,Y_1),(X_2,Y_2),$ (X_3,Y_3)	Coordinates of three specified points through which a circle must be passed.
x_i	x-coordinates of wheel locations in vehicle axis system.
Y_{PERP}	Y-coordinate of the point through which the perpendicular is drawn.
Y_{RPi}	Y-coordinate of the road point i.
YP_i	Predicted value of Y at the point i.
Y_{int}	Y coordinate of the closest point on the road path.
Y_{per}	Perceived value of Y.
Y_{pr}	Predicted value of Y in the three-degree-of-freedom predictor.
Y_1, Y_2	Y-coordinates of end points of a road segment which is being checked for perpendicular intersection point.
y_i	y-coordinates of wheel locations in vehicle axis system.

Symbol	Definition
α_i	Slip angle at wheel i.
$\bar{\alpha}_i$	Normalized slip angle at wheel i.
Δ	Variable used in §3.2.6.
δ	Average steering angle of front wheels in driver models.
δ_{des}	Desired front wheel steer angle.
δ_{max}	Maximum allowable front wheel angle.
δ_{Swi}	Value of the angular displacement of the steering wheel at the time of the command i, t_{OLi}.
δ_{Swnew}	Value of the steering wheel command for time $t + \tau_L$.
$\delta_{toe1,toe2}$	Toe-in angles of the front wheels.
κ	Desired path curvature.
κ_{1i}	Curvature of a circle passing through a predicted path point and the two neighboring points.
κ_1, κ_2	Path curvatures at the end points of the closest road-map segment.
ξ	Variable used in §3.2.3.5.
τ_{ab}	Time lag for acceleration/braking switchover.
τ_L	Time lag in describing function driver models.
τ_{Lpp}	Driver time lag in the preview-predictor model.
τ_m	Exponential rise time for driver response.
τ_1	Period of sinusoidal steer.
τ_2	Period of sinusoidal steering perturbation to the trapezoidal steer.
ψ	Heading (yaw) angle.
ψ_{des}	Tangent angle to the desired path at the closest point on the road path.

Symbol	Definition
ψP_i	Value of the heading angle at the predicted point i.
ψ_{pr}	Predicted value of the heading angle in the three-degree-of-freedom predictor.
Ω	Angle from line between predicted point and the point of perpendicular intersection to the X-axis.
ω_{s1}	Circular frequency of the sinusoidal sweep at time t = 1.0 sec.

§3.4 Open Loop Vehicle Control

The Driver Module can be used for open loop control of the vehicle. When in this mode, the user desired maneuver is input to the vehicle as either:

1. A preprogrammed maneuver
2. A table of commands
3. A user supplied subroutine

Five types of preprogrammed maneuvers have been supplied. These are:

1. Sinusoidal steer
2. Trapezoidal steer
3. Double trapezoidal steer
4. Trapezoidal steer with a sinusoidal perturbation
5. Sinusoidal sweep steer

With maneuvers one through four, a trapezoidal braking command has also been implemented. See Section 4.3. of the User's Guide (Vol. 4 in this series) for further details.

Section 3.2.2 contains the equations for each of these maneuvers. By correctly choosing the values of the parameters in these equations, a very large number of maneuvers can be simulated. Section 4.4 of the User's Guide discusses choosing these parameters to simulate the Vehicle Handling Test Procedures.

For greater flexibility, the user may specify an open loop command table. Here the user enters values of the control variables at specified times. For times other than those specified, linear interpolation between the data points is

used. Section 3.2.1 contains the relevant equations. The control variables to be specified are:

1. Steering wheel angle and one of:
2. Brake line pressure
3. Drive torque
4. Commanded vehicle velocity

Space has been left in the table for a fifth, user defined control input. Section 4.2 of the User's Guide discusses the command table in greater detail.

Finally, the user may specify the control inputs by means of a user written subroutine. See section 4.5 of the User's Guide for details and an example.

§3.5. Preview-Predictor Models.

§3.5.1. Over View:

The preview-predictor models of closed-loop human driver behavior are based, to a certain extent, on a psychological process framework. In these models it is assumed that the driver evaluates, or samples, the status of the vehicle at regular time intervals. Based on this evaluation, at each sample time he predicts what the future path and speed of the vehicle will be, and compares the predicted quantities to desired ones. The difference (≡errors) between the predicted path and velocities and the desired quantities serve as the basis for changes in control inputs to the vehicle.

This process of sampling, predicting, comparing and correcting at discrete intervals has been implemented by two related algorithms, which differ mainly in the techniques used to predict. Two control commands are involved, namely the average front-wheel steering angle δ and the forward acceleration a_{cc} (which may be positive or negative). These variables were chosen instead of the actual simulation control variables, namely, the steering wheel angle, the drive torque and the brakeline pressure, since (i) it was felt that the human driver's response is more related to these quantities, i.e., a driver is interested in the rate the vehicle is slowing down and not in the brakeline pressure and (ii) the DRIVER MODULE would depend less on the specific vehicle model used.

§3.5.2. Driver Model Flow.

When using the preview-predictor driver model, the Driver Module has two distinct modes of operation. These are the driver sampling mode and the command matrix mode. In the driver sampling mode, the driver scans his environment and uses this information to generate a series of steering and braking commands which are stored at regular time intervals in the command matrix. In the command matrix mode, steering and braking commands for the current time are generated, using linear interpolation, if necessary. During the majority of the calls to the Driver Module the command matrix mode is used. However, the driver sampling mode will be used if a time greater than the sampling interval t_{pps} has elapsed since the driver sampling mode was last used.

§3.5.2.1. Driver Sampling Mode.

When the driver sampling mode is used the current values of X, Y, ψ, u, v, r and their time derivatives, which give the overall motion of the vehicle, are passed from the vehicle simulation to the Driver Module. The simulation allows them to be modified, (if desired by the user) by normally distributed random errors to simulate human perception errors. The perceived quantities (as opposed to actual values) are denoted by X_{per}, etc.. Based on these perceived quantities and a hypothetical set of future steering and acceleration commands, a prediction is made of the vehicle trajectory and velocity for a period of time, t_{pred}, into the future, where

$$t_{pred} = (N_{pred}-1)t_{ppt} \qquad (3.138)$$

A choice has to be made for the value of the interval between predicted points t_{ppt}. In his work, Kroll used a prediction distance but it is felt that the distance a driver predicts ahead will vary with vehicle speed and so prediction times have been used here instead. The values chosen for the parameters in the sample runs were $N_{pred} = 8$ and $t_{ppt} = 0.2727$ secs. At a velocity of 50 mph. this yields Kroll's prediction distance of 240 inches. These values can be changed by the user.

The predicted path shown in Fig. 3.1 is calculated by one of two methods. These methods are quite different, one involving a simple algebraic technique and the other being a three degree of freedom vehicle model involving the integration of differential equations.

Control commands are generated by comparing this predicted path with a desired path -- the ideal (but usually unrealizable) path along which the driver would like to guide the vehicle. This desired path is represented in the Driver Module as a series of line segments. These segments are specified in a user-supplied "road map table" consisting of a sequence of points at the segment endpoints and the desired velocities at these points. The desired path and velocity are then defined by linear interpolation between the values of these points. For obstacle avoidance maneuvers, its desired path may be modified. See §3.5.7.

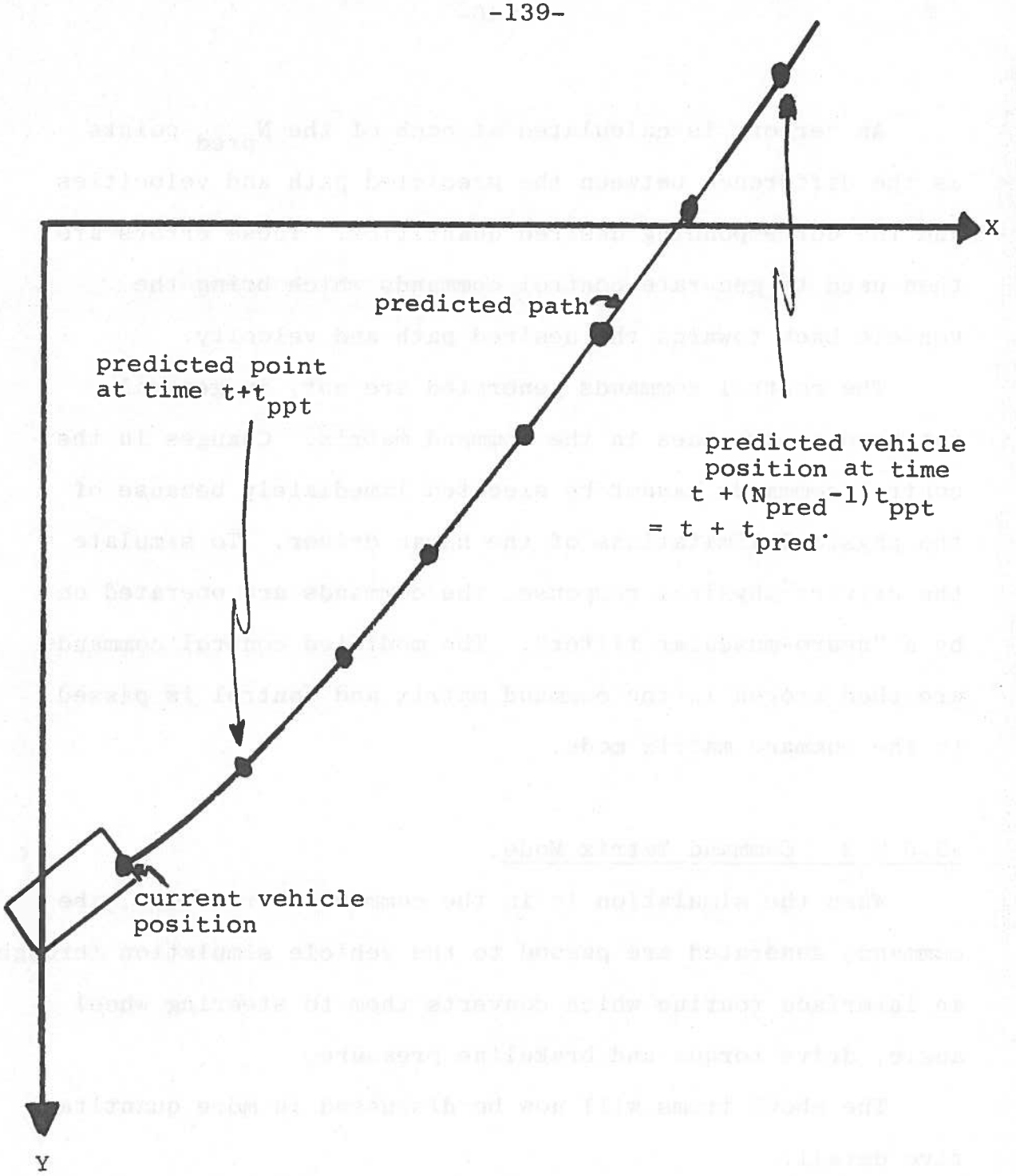

Fig 3.1. The predicted path of the vehicle

An "error" is calculated at each of the N_{pred} points as the difference between the predicted path and velocities and the corresponding desired quantities. These errors are then used to generate control commands which bring the vehicle back towards the desired path and velocity.

The control commands generated are not, in general, the same as the ones in the command matrix. Changes in the control commands cannot be executed immediately because of the physical limitations of the human driver. To simulate the drivers physical response, the commands are operated on by a "neuro-muscular filter". The modified control commands are then stored in the command matrix and control is passed to the command matrix mode.

§3.5.2.2. Command Matrix Mode.

When the simulation is in the command matrix mode, the commands generated are passed to the vehicle simulation through an interface routine which converts them to steering wheel angle, drive torque and brakeline pressure.

The above items will now be discussed in more quantitative detail.

§3.5.3. Path and Velocity Prediction.

Two different methods for predicting the path and velocity of the vehicle are available in the Driver Module They are an algebraic or geometric predictor and a 3 d.o.f. vehicle model, which involves integration of a set of differential equations. The algebraic predictor operates only

on the perceived vehicle kinematics at the time the sampling occurs, whereas the 3 d.o.f. predictor takes into account the drivers intended control inputs during the upcoming prediction period t_{pred}. The algebraic predictor is considerably less complex, and therefore less expensive to run. The path and velocity predicted by the 3 d.o.f. predictor is more accurate, especially during periods of rapid change of control inputs.

It should be noted that Kroll, in his work with this sort of model, used an even simpler predictor which constructed a quadratic path with constant lateral acceleration given by

$$a_y = \delta |\vec{V}|^2 / [(a+b)(1+KD|\vec{V}|^2)]$$

where δ is the average front wheel steer angle, $|\vec{V}|$ is the vehicle speed, a and b are distances from the c.g. to the front and rear of the vehicle, respectively, and KD is the understeer/oversteer coefficient. This allowed him to use a very efficient method for computing desired changes in control commands. However the method was found here to become inaccurate for maneuvers involving large lateral accelerations.

The predicted quantities of interest to the driver are position (XP, YP) and forward velocity uP. The predicted quantities during the prediction period t_{pred} are given by, in principle,

$$XP(t+\Delta t) = X_{per}(t) + \int_{t}^{t+\Delta t} \frac{dXP}{dt}\, dt \qquad (3.139)$$

$$YP(t+\Delta t) = Y_{per}(t) + \int_{t}^{t+\Delta t} \frac{dYP}{dt}\, dt \qquad (3.140)$$

$$uP(t+\ t) = u_{per}(t) + \int_{t}^{t+\Delta t} \frac{duP}{dt}\, dt \qquad (3.141)$$

where "per" stands for perceived and $0 \leq \Delta t \leq t_{pred}$. Two methods of calculation will now be discussed.

Algebraic Predictor.

In this model, predictions are based solely on the perceived quantities at the beginning of the sampling interval. A simple step-wise integration technique is used, the step size being $\Delta t = t_{ppt}$ so that the only values generated are at the N_{pred} points on the predicted path (these values are then stored for use later in computations of the "errors"). In the process, the following assumptions are made:

1) During the entire integration interval, the derivatives $\dot{\psi}$, $\dot{u}P$, $\dot{v}P$, $\dot{r}P$, remain constant at their initially perceived values, so that $\dot{u}P \equiv \dot{u}_{per}$, etc.

2) Since roll and pitch angles are not among the perceived quantities in this model, it is assumed that $\dot{\psi}P = rP$, $\ddot{\psi}P = \dot{r}P$.

With these assumptions, predicted state increments are calculated from:

$$\Delta X \equiv XP(t+t_{ppt}) - X_{per}(t) = \dot{X}P(t)t_{ppt} \quad (3.142)$$

$$\Delta Y \equiv YP(t+t_{ppt}) - Y_{per}(t) = \dot{Y}P(t)t_{ppt} \quad (3.143)$$

$$\Delta\psi \equiv \psi P(t+t_{ppt}) - \psi_{per}(t) = \dot{r}_{per}(t)t_{ppt} \quad (3.144)$$

$$\Delta u \equiv uP(t+t_{ppt}) - u_{per}(t) = \dot{u}_{per}(t)t_{ppt} \quad (3.145)$$

$$\Delta v \equiv vP(t+t_{ppt}) - v_{per}(t) = \dot{v}_{per}(t)t_{ppt} \quad (3.146)$$

$$\Delta r \equiv r(t+t_{ppt}) - r(t) = \dot{r}_{per}(t)t_{ppt} \quad (3.147)$$

The length SP of the line segment joining the initial point to the predicted point is given by

$$\Delta SP = \sqrt{\Delta X^2 + \Delta Y^2} \quad (3.148)$$

The inertial quantities $\dot{X}P$ and $\dot{Y}P$ are related to the components with respect to body axes, uP and vP (see Fig. 3.2) by

$$\dot{X}P = uP\cos\psi P - vP\sin\psi P = u_{per}\cos\psi_{per} - v_{per}\sin\psi_{per} \quad (3.149)$$

$$\dot{Y}P = uP\sin\psi P + vP\cos\psi P = u_{per}\sin\psi_{per} + v_{per}\cos\psi_{per} \quad (3.150)$$

Equations (3.142), (3.143), (3.144) and (3.150) are used to calculate X and Y for the first predicted point. The increments for an arbitrary increment mt_{ppt}, where the integer m ranges between 1 and $(N_{pred}-1)$, are given by

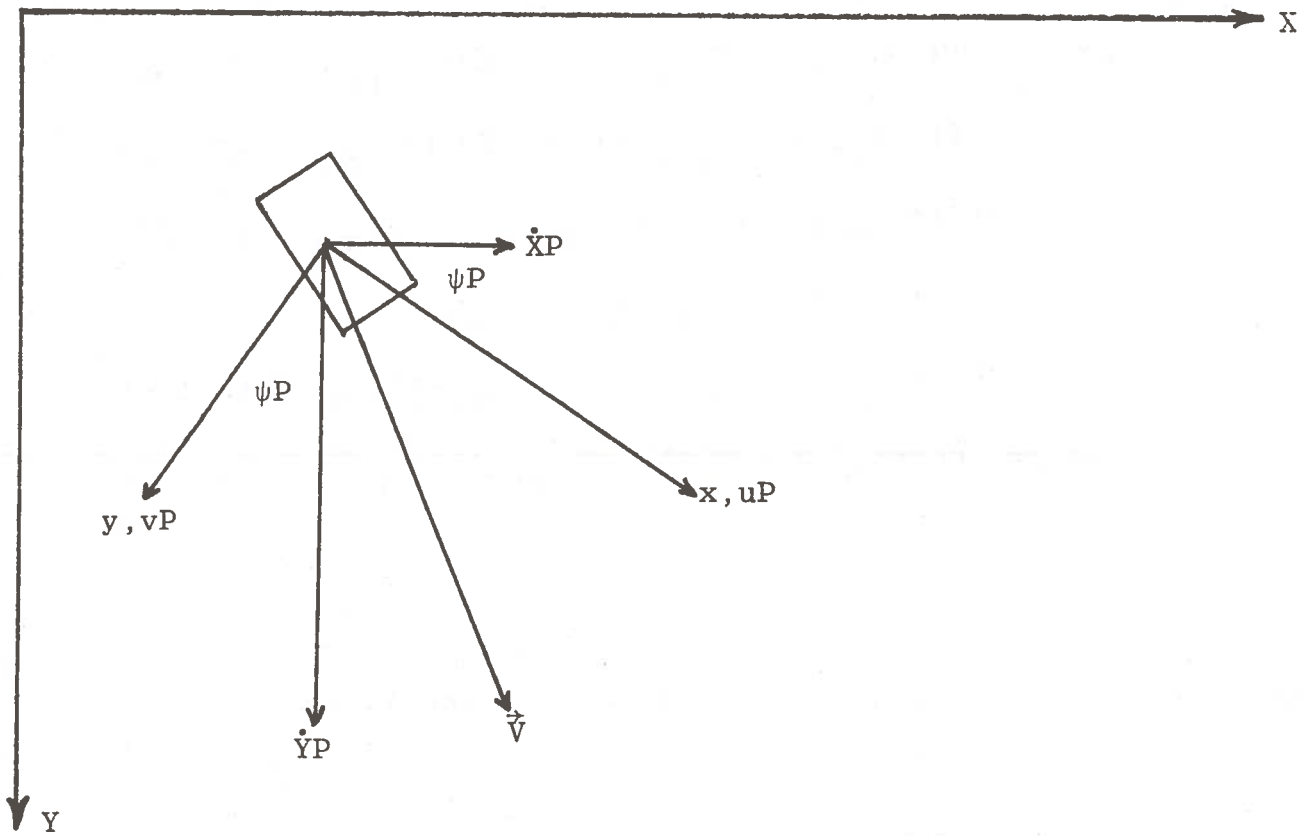

Fig 3.2 Vehicle kinematics at time $t + t_{pps}$

$$\Delta X \equiv XP(t+mt_{ppt}) - XP[t+(m-1)t_{ppt}]$$

$$= \{uP[t+(m-1)t_{ppt}] \cos\psi P[t+(m-1)t_{ppt}]$$

$$- vP[t+(m-1)t_{ppt}] \sin\psi P[t+(m-1)t_{ppt}]\}t_{ppt} \quad (3.151)$$

$$\Delta Y \equiv YP(t+mt_{ppt}) - YP[t+(m-1)t_{ppt}]$$

$$= \{uP[t+(m-1)t_{ppt}] \sin\psi P\ t+(m-1)t_{ppt}]$$

$$+ uP[t+(m-1)t_{ppt}] \cos\psi P\ t+(m-1)t_{ppt}]\}t_{ppt} \quad (3.152)$$

The increments $\Delta\psi$, Δu, Δv and Δr are given by eqs. (3.144), (3.145), (3.146) and (3.147) as before.

Three-Degree-of-Freedom Predictor.

In the 3 d.o.f. predictor, the predicted path and velocity are generated by a 3 d.o.f. vehicle model. The perceived vehicle kinematics at the sampling time are used as initial conditions for the differential equations and the control commands δ and a_{cc} which had been stored in the command matrix at the previous sampling time are used as control inputs.

The integration time step was chosen as 0.01 seconds. The predicted kinematics of the model are stored in a "predicted kinematics matrix" at intervals of t_{ppt} seconds, corresponding to the $(N_{pred}-1)$ points on the predicted path.

The main features of the model are:

(i) The degrees of freedom are motions in the X and Y directions and rotations ψ about the Z-axis.

(ii) The normal forces acting at the wheels are determined by using the equations of motion at a previous time step and the assumptions that the vehicle is symmetric about its x-axis and that side-to-side normal force differences on the front and rear axles are proportional to the static weight distribution between the two axles.

(iii) The acceleration-control command a_{cc} is interpreted as a force per unit mass applied along the vehicle x-axis. This seems a reasonable model for acceleration with rear-wheel drive and front-wheel drive and braking for small steering angles. It is less accurate for braking and front wheel drive acceleration at large steering angles.

(iv) The tire side forces are calculated by means of a simplified Calspan model in which there is only dependence on normal force and slip angle.

The equations describing the model have been given in §3.2.3.2.

§3.5.4. Error Measures and Control Commands.

Given the desired path and velocity (in the form of a "predicted kinematics matrix"), the driver must compute corrections to the control variables δ and a_{cc}. This is done as follows:

(i) The perpendicular distance D_{pi} to the desired path is computed for each predicted path point. Also, the differences ERR_{u2i} in the squares of the predicted and desired velocity at the points of perpendicular intersection are calculated (see Fig. 3.3). Further discussion will be given in §3.7.

(ii) The "desired" steering and acceleration commands to be fed to the vehicle model for future times are computed by the following equations (the "desired" commands cannot actually be realized, due to neuromuscular lags):

$$\delta_{des} = \delta_{now} - G_{st}ERR_{st} \tag{3.153}$$

$$a_{ccdes} = a_{ccnow} - G_{ac}ERR_{acc} \tag{3.154}$$

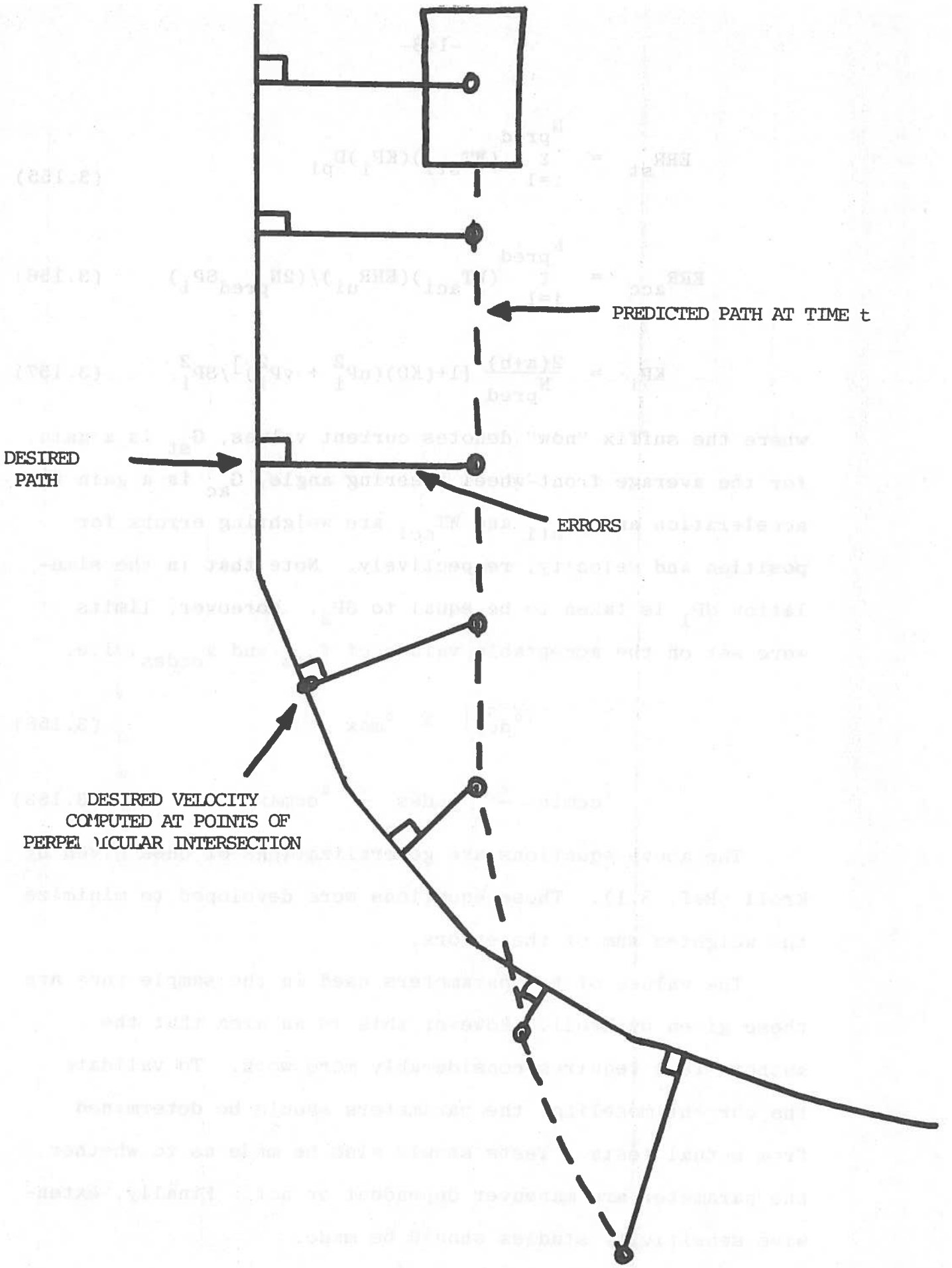

Fig. 3.3. Illustration of Preview-Predictor Concept

$$ERR_{st} = \sum_{i=1}^{N_{pred}} (WT_{sti})(KP_i)D_{pi} \qquad (3.155)$$

$$ERR_{acc} = \sum_{i=1}^{N_{pred}} (WT_{aci})(ERR_{ui})/(2N_{pred}SP_i) \qquad (3.156)$$

$$KP_i = \frac{2(a+b)}{N_{pred}} [1+(KD)(uP_i^2 + vP_i^2)]/SP_i^2 \qquad (3.157)$$

where the suffix "now" denotes current values, G_{st} is a gain, for the average front-wheel steering angle, G_{ac} is a gain for acceleration and WT_{sti} and WT_{aci} are weighting errors for position and velocity, respectively. Note that in the simulation SP_1 is taken to be equal to SP_2. Moreover, limits were set on the acceptable values of δ_{des} and a_{ccdes}, i.e.

$$|\delta_{des}| \leq \delta_{max} \qquad (3.158)$$

$$a_{ccmin} \leq a_{ccdes} \leq a_{ccmax} \qquad (3.159)$$

The above equations are generalizations of ones given by Kroll (Ref. 3.1). These equations were developed to minimize the weighted sum of the errors.

The values of the parameters used in the sample runs are these given by Kroll. However this is an area that the authors feel requires considerably more work. To validate the current modeling, the parameters should be determined from actual tests. Tests should also be made as to whether the parameter are maneuver dependent or not. Finally, extensive sensitivity studies should be made.

§3.5.5. Neuromuscular Filtering.

To simulate the effects of a human driver's physiological limitations the desired control commands are modified by a neuromuscular filter before being stored in the command matrix. The neuromuscular filter consists of muscular lags and an exponential rise time. As aids in understanding the process, the following are defined:

t_{now} ≡ The time at which the driver sampling mode was called by the vehicle model.

t_{cm} ≡ The time used in the command matrix operations, measured from t_{now}. $t_{cm} \geq t_{now}$.

$\delta(t_{cm})$, $a_{cc}(t_{cm})$ ≡ Contents of the command matrix after updating at t_{now}.

δ_{old}, a_{ccold} ≡ Contents of command matrix before updating at t_{now}.

The command matrix is set up by the following equations, considering δ first:

$\tau_m = 0$, $\tau_{Lpp} = 0$.

$$\delta(t_{cm}) = \delta_{des}, \; t_{cm} \geq 0 \tag{3.160}$$

$\tau_m = 0$, $\tau_{Lpp} \neq 0$.

$$\delta(t_{cm}) = \begin{cases} \delta_{old}(t_{cm}), & t_{cm} < \tau_{Lpp} \\ \delta_{des}, & t_{cm} \geq \tau_{Lpp} \end{cases} \tag{3.161}$$

$\tau_m \neq \tau_{Lpp} \neq 0.$

$$\delta(t_{cm}) = \begin{cases} \delta_{old}(t_{cm}), & t_{cm} < \tau_{Lpp} \\ \delta_{des} + (\delta_{old} - \delta_{des})\exp[-(t_{cm} - \tau_{Lpp})/\tau_m] \end{cases} \quad (3.162)$$

A constraint on the maximum permissible value of $\dot{\delta}$ is also imposed. If

$$|\delta(t_{cm}+\Delta t) - \delta(t_{cm})|/\Delta t > \dot{\delta}_{max} \quad (3.163)$$

then

$$\delta(t_{cm}+\Delta t) = \begin{cases} \delta(t_{cm}) + (\Delta t)\dot{\delta}_{max}, & \dot{\delta} > 0 \\ \delta(t_{cm}) - (\Delta t)\dot{\delta}_{max}, & \dot{\delta} < 0 \end{cases} \quad (3.164)$$

$\dot{\delta}_{max}$ is a user specified parameter. In the current simulation a value of the maximum steering wheel rate $\dot{\delta}_{SWmax}$ of 11 rad/sec is used, and the program then calculates from this a value of $\dot{\delta}_{max}$. The value of Δt is fixed at 0.01 sec.

For a_{cc} the equations are:

$\tau_m = 0, \quad \tau_{Lpp} = 0.$

$$a_{cc}(t_{cm}) = a_{ccdes}, \quad t_{cm} \geq 0 \quad (3.165)$$

$\tau_m = 0, \quad \tau_{Lpp} \neq 0.$

$$a_{cc}(t_{cm}) = \begin{cases} a_{ccold}(t_{cm}), & t_{cm} < \tau_{Lpp} + j\tau_{ab} \\ a_{ccdes}, & t_{cm} \geq \tau_{Lpp} + j\tau_{ab} \end{cases} \quad (3.166)$$

where j = 0 if

$$[a_{ccold}(\tau_{Lpp} - 0.01) - a_{ccsw}][a_{ccdes} - a_{ccsw}] > 0 \quad (3.167)$$

and j = 1 otherwise.

$\tau_m \neq 0, \tau_{Lpp} \neq 0.$

$$a_{cc}(t_{cm}) = \begin{cases} a_{ccold}(t_{cm}), \; t_{cm} < \tau_{Lpp} + j\tau_{ab} \\ a_{ccdes} + (a_{ccold} - a_{ccdes})\exp[-(t_{cm} - \tau_{Lpp} - \kappa\tau_{ab})/\tau_m] \\ \text{for } t_{cm} \geq \tau_{Lpp} + j\tau_{ab} \text{ and provided} \\ t_{cm} < t_{sw} \quad \text{OR} \quad t_{cm} > t_{sw} + \tau_{ab} \\ a_{ccsw}, \text{ for } t_{cm} \geq \tau_{Lpp} + j\tau_{ab} \text{ and} \\ t_{sw} \leq t_{cm} \leq t_{sw} + \tau_{ab} \end{cases} \tag{3.168}$$

where t_{sw} are times for which

$$[a_{cc}(t_{cm}) - a_{ccsw}][a_{cc}(t_{cm} - 0.01) - a_{ccsw}] \leq 0 \tag{3.169}$$

κ is incremented by 1 each time equation (3.169) occurs and j is as in (3.167). Equations (3.167) through (3.169) simulate an increase in the driver's time lag τ_{Lpp} by an amount τ_{ab} each time the acceleration a_{ccsw} is crossed. This corresponds to a foot movement between the throttle and brake pedal. Both a_{ccsw} and τ_{ab} are user specified. Zero values are used in the current simulation.

§3.5.6. Command Matrix

The command matrix contains the stored values of the steering and acceleration commands as functions of time, the storing interval consisting of 3 sec. after the most recent sampling time. The values are stored in tabular form with a 0.01 sec. time interval between entries. The matrix is updated at each sampling time so that the vehicle simulation actually only needs entries from the first t_{pps} seconds of the table. However the 3 d.o.f. predictor needs access to the intended control commands for the next t_{pred} sec. Hence the command matrix is made large enough to store this information. When the vehicle simulation requests steering and acceleration commands, these are obtained from the command matrix by linear interpolation between the stored values.

§3.5.7. Obstacle Avoidance.

The general purpose Driver Module contains an obstacle avoidance, closed-loop maneuver. Since the strategy involved is an area of current research and has not been tested as yet, the maneuver should be regarded as being in the tentative stage.

The maneuver is as follows: An obstacle is located at a user specified road point in the road map, which the driver first sees when the vehicle reaches another user specified point. To avoid the obstacle, the vehicle must shift its center laterally a user specified distance. The user has the following choice of strategies, which are determined by the values of an integer variable named IOBMOD:

IOBMOD = 1. The vehicle attempts to pass the obstacle on the right and maintain a constant speed.

IOBMOD = 2. The vehicle attempts to pass the obstacle on the left and maintain a constant speed.

IOBMOD = 3. The vehicle attempts to pass the obstacle on the right and brakes.

IOBMOD = 4. The vehicle attempts to pass the obstacle on the left and brakes.

Notes. (i) IOBMOD = 0 (which is the default value) removes the obstacle from the simulation.

(ii) The obstacle avoidance maneuver can only be exercised in this simulation by using the preview-predictor model of driving behavior (with either a geometric or 3 d.c.f. integrator as a predictor). Further, if mixed-mode control is used, the driver should operate in closed-loop control near the obstacle. The computer programs handles obstacle avoidance as follows:

When the obstacle comes within the driver view, the desired path is shifted to the left or right, depending on the user specified strategy, by the user specified obstacle width. If, in addition, the user has specified that braking is to occur, the desired velocity is reduced to zero.

To guarantee that the obstacle avoidance action is taken before the obstacle is reached, the driver views no further than the obstacle. The prediction time, t_{pred}, is reduced to accomplish this.

§3.5.8. Driver Module - Vehicle Simulation Interface.

The Driver Module was designed to be applicable to any digital vehicle model; consequently some provision must be made for putting the control commands in a form which can be used by the particular vehicle model. This is performed by an interface subroutine which must be supplied by the user for vehicle models other than the University of Michigan IDSFC simulation. The interface routine used with the IDSFC simulation will now be described.

The steering command δ must be converted to a steering wheel angle δ_{Sw}. This is done by approximating the vehicle model steering equations as follows:

$$A_1 = (M_{T1} + M_{z1} - rI_{FW})/K_{SL1} \tag{3.170}$$

$$A_2 = (M_{T2} + M_{z2} - rI_{FW})/K_{SL2} \tag{3.171}$$

$$\delta_{Sw} = \delta/GR - \frac{N_G(A_1+A_2)}{a_p(\frac{1}{A_{L1}} + \frac{1}{A_{L2}})} - \frac{a_p}{N_G K_{SC}}(\frac{K_{SL1}A_1}{A_{L2}} + \frac{K_{SL2}A_2}{A_{L2}}) \tag{3.172}$$

The acceleration/braking command a_{cc} must be converted to a drive torque or brake line pressure. This is done as follows:

Case 1. Closed loop control of throttle and brake pedal.

$a_{cc} < 0$

$$d_{OUT2} = 0 \tag{3.173}$$

$$T_{QB} = (a_{cc})(BK_{con}) \tag{3.174}$$

$$d_{OUT1} = \text{linear interpolation from the brake table, using } T_{QB}. \tag{3.175}$$

$a_{cc} > 0$

$$d_{OUT1} = 0 \tag{3.176}$$

$$d_{OUT2} = (a_{cc})(DV_{con}) \tag{3.177}$$

When mixed-mode driver control is used (§3.8), either the throttle or brake pedal may be open loop controlled. For those cases the interfacing is done as follows:

Case 2. Closed loop control of the throttle and open loop control of the brake pedal.

T_{QB} = linear interpolation from brake table, using d_{OUT1}. (3.178)

$$d_{OUT2} = (DV_{con})[a_{cc} - T_{QB}/(BK_{con})] \quad (3.179)$$

Case 3. Open loop control of the throttle and closed loop control of the brake pedal.

If $[a_{cc} - (d_{OUT2})/(DV_{con})] > 0$:

$$T_{QB} = (BK_{con})[a_{cc} - (d_{OUT2})/(DV_{con})] \quad (3.180)$$

d_{OUT1} = linear interpolation from the brake table, using T_{QB}. (3.181)

if $[a_{cc} - (d_{OUT2})/(DV_{con})] \leq 0$:

$$d_{OUT1} = 0 \quad (3.182)$$

§3.5.9. Initialization Procedure

At the commencement of a closed-loop run the steering wheel angle, drive torque and brake-line pressure must be specified. These are converted to Driver Module control commands δ and a_{cc} in an interface routine (which also must be user-supplied for use with simulation other than University of Michigan IDSFC) and stored in the command matrix prior to commencement of the run. The first Driver Module call will initiate the preview-predictor procedure, and desired changes in control commands are entered in the usual manner.

§3.6. Describing-Function Driver Modelling.

Describing-function driver models have been developed along the lines given by the Systems Technology Inc. group (see McRuer *et al* [3.2] and Donges [3.3]). Two cases are distinguished, namely, straight line maneuvers, and maneuvers involving curved paths. The model will first be developed for straight line maneuvers, with arbitrary trajectories considered later. Moreover the initial discussion will focus on steering control, with speed control taken up later.

§3.6.1. Control Strategy for Straight Line Maneuvers.

The vehicle-driver system is modelled as a multi-loop, feedback control system. As can be seen from the block diagram in Fig. 3.4, the driver is assumed to control the heading angle ψ via an inner loop and the lateral position Y via an outer loop. Following McRuer *et al* [3.2], the overall gain in each loop is assumed to satisfy a cross-over model form, i.e.,

$$\tilde{D}(s) \cdot \tilde{V}_T(s) = \omega_c e^{-s\tau}/s \qquad (3.183)$$

where

(i) $\tilde{D}(s)$ is either $\tilde{D}_\psi(s)$ or $\tilde{D}_Y(s)$ and is a driver's transfer function relating the Laplace transformed errors in the state variables (driver's input) to the transformed steering wheel displacement (driver's output).

(ii) $\tilde{V}_T(s)$ is either $\tilde{V}_{T\psi}(s)$ of $\tilde{V}_{TY}(s)$ and is vehicle transfer function relating the transformed steering wheel displacement (vehicle input) to the transformed vehicle state variables (vehicle output).

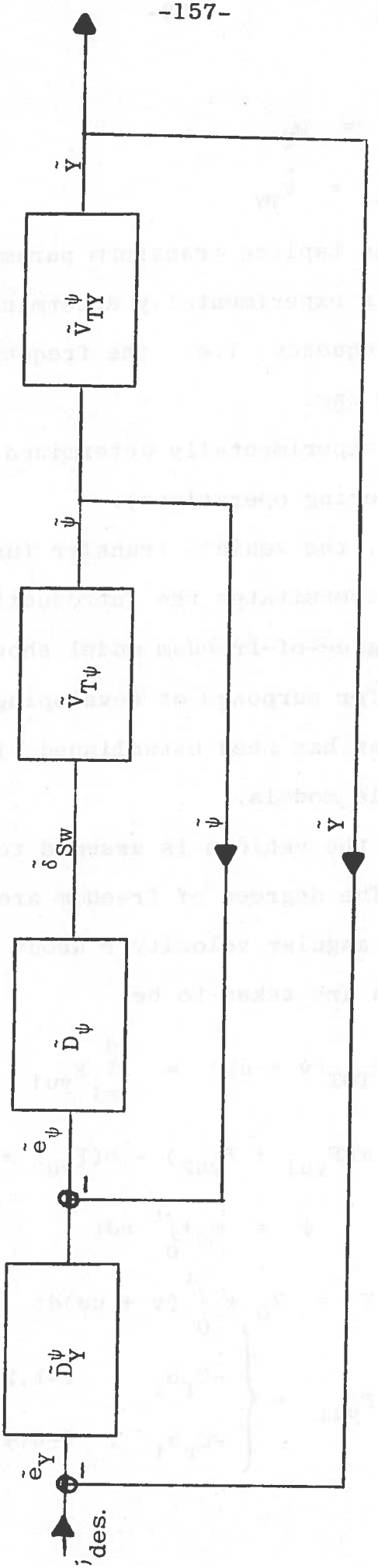

Fig 3.4. Block diagram for control strategy

(iii) $\tilde{D}_{Y}^{\psi}\ \tilde{D}_{\psi} = \tilde{D}_{Y}$ (3.184)

$\tilde{V}_{TY}^{\psi}\ \tilde{V}_{T\psi} = \tilde{V}_{TY}$ (3.185)

(iv) s is the Laplace transform parameter.

(v) ω_c is an experimentally determined driver cross-over frequency, i.e., the frequency at which the gain is one.

(vi) τ is an experimentally determined driver time lag (in steering operations).

To proceed further, the vehicle transfer function must be calculated which necessitates the introduction of a vehicle model. The two-degree-of-freedom model shown in Fig. 3.5 will be used here for purposes of developing the control law. Once the control law has been established, it can be used with more general vehicle models.

In this model the vehicle is assumed to have a constant forward speed u. The degrees of freedom are the lateral velocity v and the angular velocity r about the z-axis. The equations of motion are taken to be

$$M_{TOT}(\dot{v} + ur) = \sum_{i=1}^{4} F_{yui} \tag{3.186}$$

$$I_z\dot{r} = a(F_{yu1} + F_{yu2}) - b(F_{yu3} + F_{yu4}) \tag{3.187}$$

$$\psi = \psi_0 + \int_0^t r\,dt \tag{3.188}$$

$$Y = Y_0 + \int_0^t (v + u\psi)dt \tag{3.189}$$

$$F_{yui} = \begin{cases} -C_f\alpha_i\ , & i=1,2 \qquad (3.190) \\ -C_r\alpha_i\ , & i=3,4 \qquad (3.191) \end{cases}$$

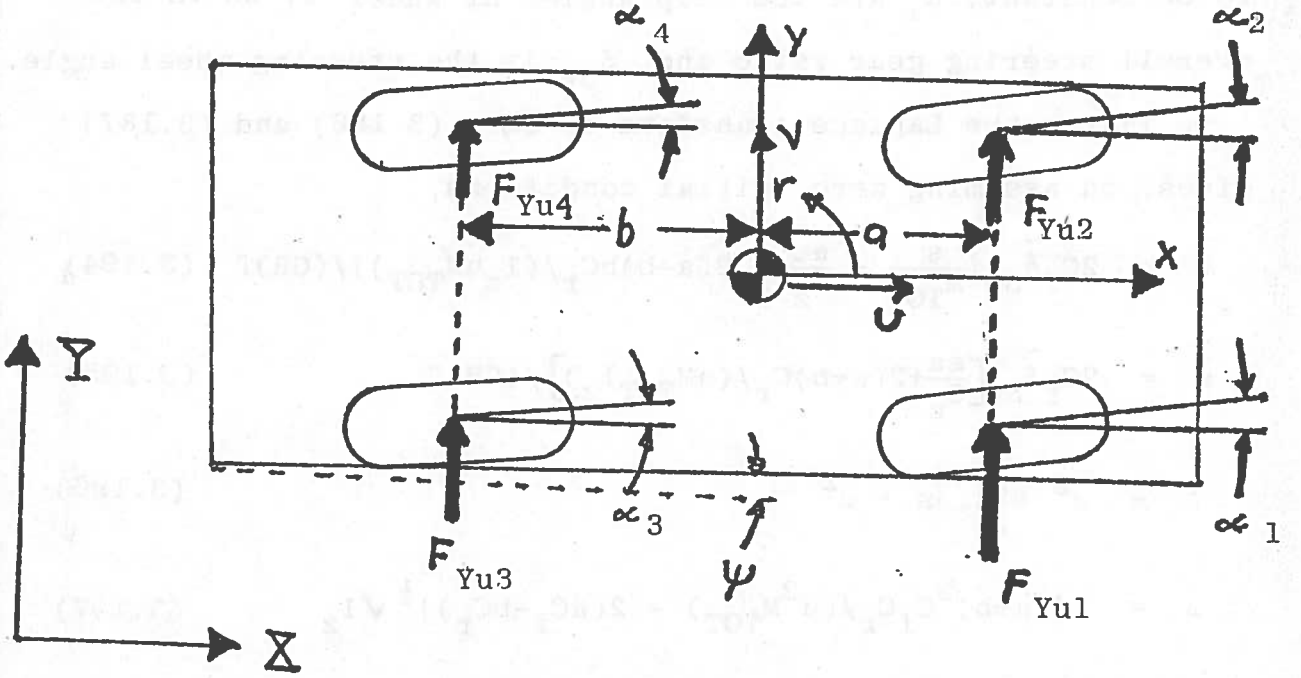

$$\alpha_i,\ \psi << 1$$

Fig. 3.5. The two-degree-of-freedom vehicle model (view from beneath the vehicle). The degrees of freedom are you rate r and the lateral velocity v.

$$\alpha_i = \begin{cases} (v + ar)/u - \delta_{Sw}/GR \quad , \; i=1,2 & (3.192) \\ (v - br)/u \quad , \quad i=3,4 & (3.193) \end{cases}$$

where M_{TOT} is the total vehicle mass, F_{yui} are the tire forces in the lateral direction, I_z is the moment of inertia of the total vehicle about the z-axis, (a+b) is the wheel base, ψ is the heading angle, C_f and C_r are cornering stiffnesses, assumed to be constant, α_i are the slip angles at wheel i, GR is the overall steering gear ratio and δ_{Sw} is the steering wheel angle.

Taking the Laplace transform of eqs. (3.186) and (3.187) gives, on assuming zero initial conditions,

$$\tilde{v} = 2C_f\tilde{\delta}_{Sw}\left[\frac{s}{M_{TOT}} - \frac{au}{I_z} - 2(a-b)bC_r/(I_z u M_{TOT})\right]/(GR)\Gamma \quad (3.194)$$

$$\tilde{r} = 2C_f\tilde{\delta}_{Sw}\left[\frac{sa}{I_z}+2(a+b)C_r/(uM_{TOT}I_z)\right]/(GR)\Gamma \quad (3.195)$$

$$\Gamma = s^2 + 2\zeta\omega s + \omega^2 \quad (3.196)$$

$$\omega = [4(a+b)^2C_fC_r/(u^2M_{TOT}) - 2(aC_f-bC_r)]^{\frac{1}{2}} \checkmark I_z \quad (3.197)$$

$$\zeta\omega = [(a^2C_f + b^2C_r)/(uI_z) + (C_f + C_r)/(uM_{TOT})] \quad (3.198)$$

Using eqs. (3.194) and (3.195), the vehicle transfer functions $\tilde{V}_{T\psi}(s)$ and $\tilde{V}_{Ty}(s)$ are given by

$$\tilde{V}_{T\psi}(s) = \frac{\tilde{\psi}(s)}{\tilde{\delta}_{Sw}} = \frac{2C_f}{(GR)s\Gamma}\left[\frac{sa}{I_z} + \frac{2(a+b)C_r}{uM_{TOT}I_z}\right] \quad (3.199)$$

$$\tilde{V}_{TY}(s) = \frac{\tilde{Y}(s)}{\tilde{\delta}_{Sw}} = \frac{2C_f}{(GR)s\Gamma}\left[\frac{s}{M_{TOT}} - \frac{2(a-b)bC_r}{uM_{TOT}I_z} + \frac{2(a+b)C_r}{sM_{TOT}I_z}\right] \quad (3.200)$$

§3.6.2. Closing the Heading Angle Loop.

In accordance with the McRuer et al [3.2] cross-over model, one takes

$$\tilde{D}_{\psi}(s)\tilde{V}_{T\psi}(s) = \omega_{c\psi}e^{-s\tau}/s \qquad (3.201)$$

where $\omega_{c\psi}$ is the cross-over frequency for the heading angle loop and

$$\tilde{D}_{\psi}(s) = \tilde{\delta}_{Sw}/\tilde{\psi}_{c}(s) \qquad (3.202)$$

where $\tilde{\psi}_{c}(s)$ is the heading angle error defined by

$$\tilde{\psi}_{c}(s) = \tilde{\psi}_{des}(s) - \tilde{\psi}(s) \qquad (3.203)$$

Note that for straight line maneuvers $\psi_{des} = 0$. It is included here for purposes of generality. Note further that the driver is assumed to have the same lag τ in both loops. Substituting eq. (3.194) into 3.201 yields

$$\tilde{D}_{\psi}(s) = \frac{(GR)\Gamma\omega_{c\psi}}{2C_{f}}\left[\frac{sa}{I_{z}} + \frac{2(a+b)C_{r}}{uM_{TOT}I_{z}}\right]^{-1} e^{-s\tau} \qquad (3.204)$$

At this point to recover the STI control law, restriction is made to a neutral steer vehicle, i.e., one for which

$$aC_{f} = bC_{r} \qquad (3.205)$$

Under these circumstances

$$\Gamma = (s + \frac{1}{T_{R}})\left[s + \frac{2(a+b)bC_{r}}{uI_{z}}\right] \qquad (3.206)$$

where

$$T_{R} = \frac{M_{TOT}ua}{2C_{r}(a+b)} \qquad (3.207)$$

Equation (3.204) can then be rewritten

$$\tilde{D}_{\psi}(s) = \frac{(GR)I_z\omega_{c\psi}}{2aC_f}\left[s + \frac{2(a+b)bC_r}{uI_z}\right]e^{-s\tau} \qquad (3.208)$$

$$= (T_L s + 1)K_{\psi}e^{-s\tau} \qquad (3.209)$$

where

$$K_{\psi} = (GR)\omega_{c\psi}(a+b)/u \qquad (3.210)$$

$$T_L = \frac{uI_z}{2a(a+b)C_f} \qquad (3.211)$$

Equation (3.209) has been advanced by the STI group on psychological grounds where T_L, K_{ψ} and τ are driver parameters to be experimentally determined. It is worthy of note that as a consequence of the model used here, namely, a 2 degree-of-freedom vehicle model, the parameters T_L and K_{ψ} depend on the forward velocity u. This point would seem worthy of further investigation.

§3.6.3. Closing the Outer(Path) Loop.

The first step in the procedure is the replacement of the inner loop by an equivalent transfer function. From Fig. 3.4

$$\tilde{\psi} = \tilde{D}_{\psi}(s)\tilde{V}_{T\psi}(s)\tilde{e}_{\psi} \qquad (3.212)$$

Substituting this into eq. (3.203) gives

$$\tilde{\psi}_{des}(s) = (\tilde{D}_{\psi}\tilde{V}_{T\psi} + 1)\tilde{e}_{\psi}$$

or, using eq. (3.201),

$$\tilde{\psi}_{des}(s) = \left(\frac{\omega_{c\psi}e^{-s\tau} + s}{s}\right)\tilde{e}_{\psi}$$

Hence, again using eq. (3.203),

$$\tilde{\psi}_{des}(s) = \left(\frac{\omega_{c\psi}e^{-s\tau}+s}{s}\right)[\tilde{\psi}_{des}(s) - \tilde{\psi}(s)]$$

which gives

$$\tilde{\psi}_{des}(s)/\tilde{\psi}(s) = \frac{\omega_{c\psi}e^{-s\tau}+s}{\omega_{c\psi}e^{-s\tau}} \qquad (3.213)$$

Now Fig. 3.4 gives, on again postulating a cross-over model,

$$\tilde{D}_Y^{\psi}\left(\frac{\omega_{c\psi}e^{-s\tau}}{\omega_{c\psi}e^{-s\tau}+s}\right)\tilde{V}_Y^{\psi} = \frac{\omega_{cy}e^{-\tau s}}{s} \qquad (3.214)$$

From eqs. (3.199) and (3.200)

$$\frac{\tilde{V}_{TY}}{\tilde{V}_{T\psi}} = \frac{\tilde{\delta}_{Sw}}{\tilde{\psi}} \cdot \frac{\tilde{Y}}{\tilde{\delta}_{Sw}} = \frac{\tilde{Y}}{\tilde{\psi}}$$

Hence

$$\tilde{V}_Y^{\psi}(s) = \frac{\left[\frac{s}{M_{TOT}} - \frac{2(a-b)bC_r}{uM_{TOT}I_z} + \frac{2(a+b)C_r}{sM_{TOT}I_z}\right]}{\left[\frac{sa}{I_z} + \frac{2(a+b)C_r}{uM_{TOT}I_z}\right]} \qquad (3.215)$$

Substituting eq. (3.215) into eq. (3.214) gives

$$\tilde{D}_Y^{\psi}\frac{\omega_{c\psi}}{\omega_{c\psi}e^{-s\tau}+s} \cdot \frac{\left[\frac{s}{M_{TOT}} - \frac{2(a-b)bC_r}{uM_{TOT}I_z} + \frac{2(a+b)C_r}{sM_{TOT}I_z}\right]}{\left[\frac{sa}{I_z} + \frac{2(a+b)C_r}{uM_{TOT}I_z}\right]} = \frac{\omega_{cY}}{s} \qquad (3.216)$$

At this juncture, the STI group makes the approximation that in the path loop only low frequencies are significant and so s maybe taken to be small. Then eq. (3.216) can be approximated by

$$\tilde{D}_Y^{\psi}\,\frac{u}{s} = \frac{\omega_{cY}}{s}$$

so that

$$\tilde{D}_Y^{\psi} = \frac{\omega_{cY}}{u} \equiv K_Y \tag{3.217}$$

§3.6.4. Calculation of the Steering Wheel Angle.

Referring to Fig. 3.4, it follows that

$$\tilde{\delta}_{Sw}(s) = (\tilde{e}_Y \tilde{D}_Y^{\psi} + \tilde{e}_{\psi})\tilde{D}_{\psi} \tag{3.218}$$

Using eqs. (3.209) and (3.217), eq. (3.218) gives

$$\tilde{\delta}_{Sw}(s) = (K_Y \tilde{e}_Y + \tilde{e}_{\psi})K_{\psi}(T_L s + 1)e^{-s\tau} \tag{3.219}$$

Inverting this laplace transform gives the control law

$$\begin{aligned}\delta_{Sw}(t) = {} & K_Y K_{\psi} e_Y(t-\tau) + K_Y K_{\psi} T_L \dot{e}_Y(t-\tau) \\ & + K_{\psi} e_{\psi}(t-\tau) + K_{\psi} T_L \dot{e}_{\psi}(t-\tau)\end{aligned} \tag{3.220}$$

which may be written

$$\begin{aligned}\delta_{Sw}(t) = {} & G_Y e_Y(t-\tau) + G_{\dot{Y}} \dot{e}_Y(t-\tau) \\ & + G_{\psi} e_{\psi}(t-\tau) + G_{\dot{\psi}} \dot{e}_{\psi}(t-\tau)\end{aligned} \tag{3.221}$$

where

$$G_Y = K_Y K_{\psi} \tag{3.222}$$

$$G_{\dot{Y}} = K_Y K_{\psi} T_L \tag{3.223}$$

$$G_{\psi} = K_{\psi} \tag{3.224}$$

$$G_{\dot{\psi}} = K_{\psi} T_L \tag{3.225}$$

Note that for the straight-line case at hand, since the desired path is $Y_{des}=0$, $\psi_{des}=0$ the errors are just the negatives of the relevant quantities, i.e.,

$$e_Y = -Y \tag{3.226}$$

$$e_{\dot{Y}} = -u\sin\psi - v\cos\psi \tag{3.227}$$

$$e_{\psi} = -\psi \tag{3.228}$$

$$e_{\dot{\psi}} = -r \tag{3.229}$$

§3.6.5. Control Strategy for General Maneuvers.

For curved path maneuvers the underlying concepts still apply, but eq. (3.221) must be modified since when the errors are zero it yields a zero value for the steering wheel angle δ_{Sw}, which in general is not true. For example, δ_{Sw} is a constant for a circular path maneuver. To overcome this difficulty a term proportional to the path curvature is added to eq. (3.227), in the spirit of McRuer et al [3.2] and Donges [3.3]. This procedure gives the control law:

$$\delta_{Sw}(t) = (a+b)[1 + (KD)u^2(t-\tau)][e_{\dot{\psi}}(t-\tau) + r(t-\tau)]/$$
$$[u(t-\tau)(GR)] + G_Y e_Y(t-\tau) + G_{\dot{Y}} e_{\dot{Y}}(t-\tau)$$
$$+ G_\psi e_\psi(t-\tau) + G_{\dot{\psi}} e_{\dot{\psi}}(t-\tau) \qquad (3.230)$$

It should be noted that the errors are now given by

$$e_Y = -D_p \qquad (3.231)$$
$$e_{\dot{Y}} = -u\sin(\psi-\psi_{des}) - v\cos(\psi-\psi_{des}) \qquad (3.232)$$
$$e_\psi = \psi_{des} - \psi \qquad (3.233)$$
$$e_{\dot{\psi}} = |\vec{v}|\kappa - r \qquad (3.234)$$

where D_p, ψ_{des} and κ are obtained from the desired path. This desired path is user specified in the form of a road map and is the same as the one in §3.5.2.

§3.6.6. Speed Control.

To the writers' knowledge there has been no quantitative treatment of speed control using describing function models. The following section should therefore be treated on a tentative basis, pending field trials.

As shown in the block diagram, Fig. 3.6, the driver-vehicle system is modelled as a single feed back loop. Postulating

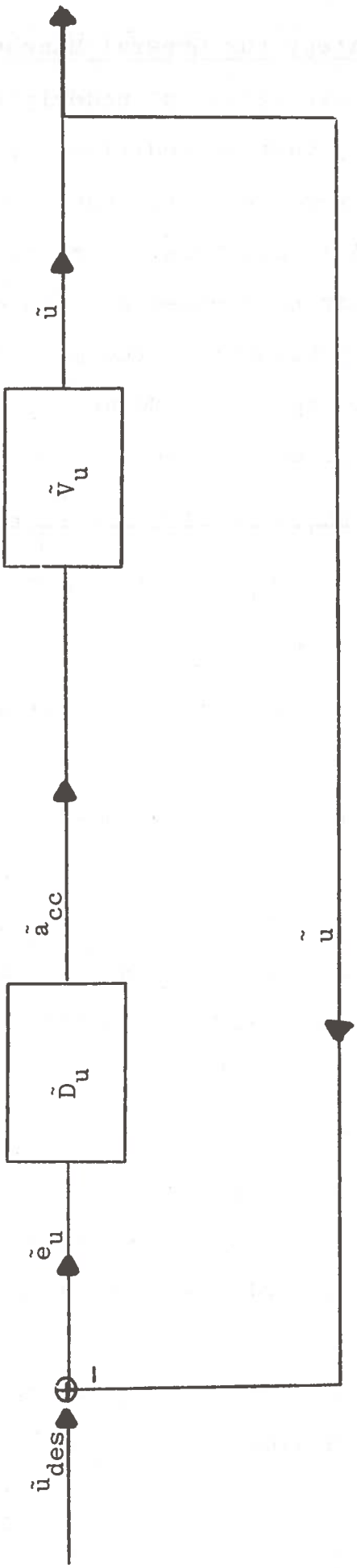

Fig. 3.6. Block diagram for speed control.

a cross-over form, it follows that

$$\tilde{D}_u(s)\tilde{V}_u(s) = \omega_{cu}e^{-s\tau}/s \qquad (3.235)$$

where ω_{cu} is the cross-over frequency for speed control. The vehicle model is taken to be:

$$\dot{u} = a_{cc} \qquad (3.236)$$

or, in the transformed plane,

$$\tilde{u} = \tilde{a}_{cc}/s \qquad (3.237)$$

which gives

$$\tilde{V}_u(s) \equiv \frac{\tilde{u}}{\tilde{a}_{cc}} = \frac{1}{s} \qquad (3.238)$$

Substituting this into eq. (3.235) gives

$$\tilde{D}_u(s) = \omega_{cu}e^{-s\tau} \qquad (3.239)$$

From Fig. 3.6, it follows that

$$\tilde{a}_{cc} = \tilde{D}_u\tilde{e}_u \qquad (3.240)$$

Substituting eq. (3.239) into eq. (3.240) and inverting gives

$$a_{cc}(t) = G_u e_u(t-\tau) \qquad (3.241)$$

where

$$G_u = \omega_{cu} \qquad (3.242)$$

and e_u is taken to be given by

$$e_u = V_{des} - |\vec{V}| \qquad (3.243)$$

---

§3.7. Error Calculation.

For both the preview-predictor driver models and the general model, the distance errors are defined as the distance between the desired path and the predicted path, for the preview-predictor models, and the desired path and the current vehicle position, for the crossover model. The distance is ideally

along a line perpendicular to the desired path and in calculated as follows: The program attempts to find the point on the desired path closest to the vehicle by a search procedure. It searches through the list of points designating the desired path until it finds a point which is farther from the vehicle than the preceding point checked. When such a point is found, the search is terminated, and it is assumed that the point found is closest to the vehicle. The starting point for the search is the point that was closest to the vehicle the last time the error was found. Such a scheme would not work, for example, if the desired were locally s-shaped. However it is felt that the sampling rate is small enough that such a contingency will not arise.

Once the closest point on the desired path has been found the computer projects a straight line through this point and the next point on the desired path (line ℓ_1). A line perpendicular to this line and its extension, and passing through the vehicle position is calculated (line ℓ_2). The point of intersection of lines ℓ_1 and ℓ_2 is then calculated. If this point lies on the road section in question, the errors now can be calculated. Otherwise, a line is calculated through the closest point and the preceeding point on the desired path (line ℓ_3). Line ℓ_2 is calculated as before and the intersection of ℓ_2 and ℓ_3 is found. If this point lies on the road section in question, the errors can now be calculated. Otherwise, the intersection of lines ℓ_1 and ℓ_3 is used to determine the errors.

The distance error is calculated as the distance between the point of intersection found above and the vehicle position. The error is negative if the vehicle is to the right of the

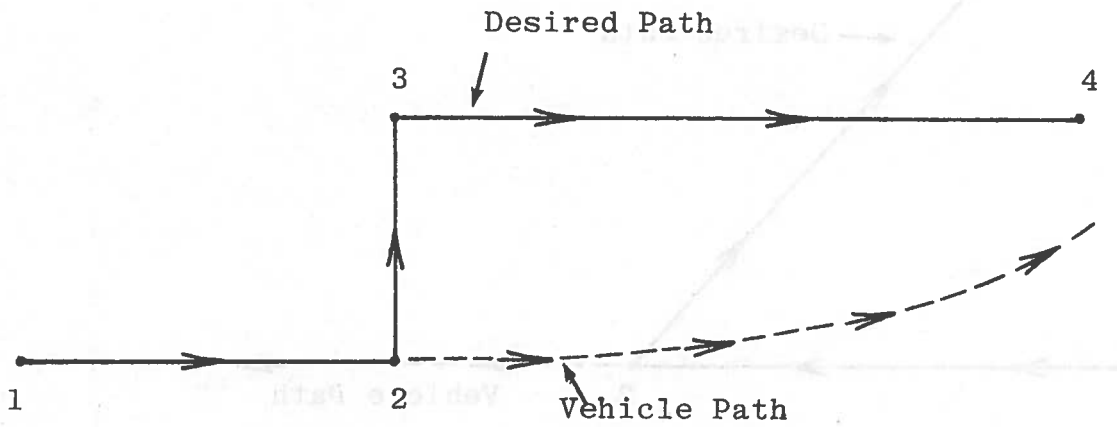

Figure 3.7. Case in which error is not found perpendicular to desired path.

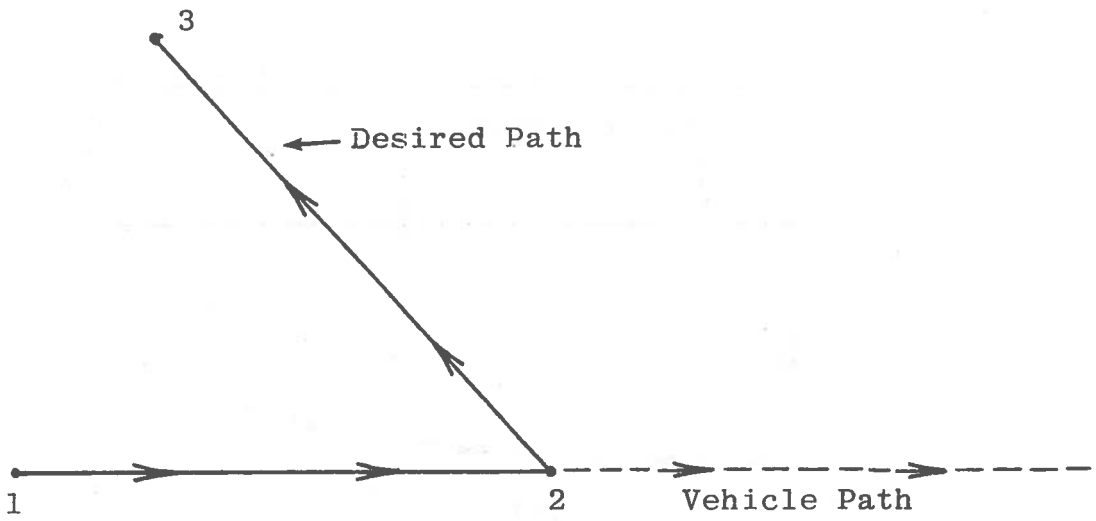

Figure 3.8. Case in which the algorithm may fail completely.

desired path as viewed from the vehicle.

This algorithim will fail locally when the vehicle is directed to go around a sharp corner of the sort shown in Fig. 3.7. If the vehicle was initially on the desired path, it will overshoot the corner. Until the vehicle is closer to point 4 than point 2, the error will be the distance from the vehicle position to point 2 instead of the distance to the line segment 3-4. As soon as point 4 becomes the closest point, the algorithm will work. For the case shown in Fig. 3.8, the algorithm could fail completely but further research is needed to clarify these issues. If the user experiences difficulties along these lines the road map supplied should be altered. The corners should be rounded and more points supplied for the region of difficulty.

§3.8. Mixed-Mode Operation

The capability exists in the Driver Module to operate in a "mixed-mode" control state during the course of one simulation run. Mixed-mode operation refers to a number of possible combinations of open-loop and closed-loop control, where closed-loop control must be provided by one of the preview-predictor models.

Two basic types of options on mixed-mode control are available to the user, namely:

(i) The driver output variables δ_{Sw}, T_{QB}, T_{QD} and VC_{OL} may be under open-loop control in the following ways:

(1) δ_{Sw} only.

(2) T_{QB} only.

(3) T_{QD} only.

(4) VC_{OL} only.

(5) T_{QB} and T_{QD} only.

(6) Dummy output variable only. This variable is currently unassigned and is included for possible future program development.

(7) All output variables.

(8) No output variables, i.e., total closed-loop control.

(ii) Different combinations of output variables under open-loop control may be specified for different time periods during one simulation run. For example, during one time interval option (7) may be specified, while in the following period option (1) may be specified.

This system flexibility allows the user to specify almost any desired open-loop inputs and then examine the resulting closed-loop driver responses. A simple but useful example might be to specify open-loop control of T_{QB} and T_{QD}, closed-loop control of δ_{Sw}, and to examine the effects of brake pulses as the driver is attempting to follow a curved path.

References for Chapter 3

3.1 C.V. Kroll et al, "A Preview-Predictor Model of Driver Behavior in Emergency Situations", Cont. No. CPR-11-3988, Federal Highway Administration 1970.

3.2 D.T. McRuer and R.H. Klein, "Automobile Controllability-Driver/Vehicle Response for Steering Control", Systems Technology Inc. , Final Rept. DOT-HS-359-3-762.

3.3 E.Donges, "A Two-Level Model of Driver Steering Behavior", Human Factors, Vol. 20, 1978, pp. 691-707.

CHAPTER 4. SIMULATION VALIDATION AND OPERATING COSTS

§4.1 Simulation Validation.

The validation of the current simulation (IDSFC), at least as regards open-loop maneuvers, was made by extensive comparisons with output from the APL hybrid simulation discussed in Ref. [1.6] , a simulation which was validated by comparisons with earlier field tests (done in connection with the work of McHenrey and DeLeys [1.2]). Further evidence was provided by Chiang [4.1], who also developed, for the Ford Motor Company, an all digital simulation for open-loop maneuvers, of what was essentially the APL mathematical model. Extensive field tests performed by the Ford Motor Company showed good agreement with the modelling.

Quite a large number of comparison runs were made with many variables involved and only a sample is given in the sequel. The first set involves a straight line braking maneuver. The vehicle parameters used were supplied by APL and correspond to a 1971 Ford Mustang. The initial speed was taken to be 50 mph and a ramp brakeline pressure was applied. The rise time was taken to be 0.1 seconds and three different values of the peak value wre used. For all of the runs the current simulation was run in the fully nonlinear, double precision mode, with the APL - CALSPAN tire model.

Figs. 4.1, 4.2 and 4.3 give results for a peak brake-line pressure of 475 psi. Fig. 4.1 gives the forward velocity u as a function of time and excellent agreement is seen, with a maximum difference of approximately 6 in/sec. (Note that

the APL simulation shuts off at a higher speed than IDSFC). Fig. 4.2 shows the lateral velocity v versus time, while Fig. 4.3 gives the vehicle trajectory, i.e., Y versus X. Since the maneuver in question is a straight ine, ideally v and Y should be zero, as in given by IDSFC. The APL results show a small deviation from these ideal values. Figs. 4.4 through 4.6 show similar output for a peak brakeline pressure of 525 psi. A maximum deviation in u of approximately 30 in/sec is now seen, as are small departures of the APL results from the ideal zero values. Results for a peak brakeline pressure of 550 psi are presented in Figs. 4.7 through 4.9. The maximum difference in the forward velocity u is now about 20 in/sec. The APL results again show minor differences in v and Y from their ideal zero values.

The second set of comparison maneuvers involved steering without braking. The vehicle is taken to be initially traveling at 50 mph along a straight line and then a trapezoidal steering pulse is applied, without braking. The rise time, dwell time and fall time of the pulse are taken to be 1 sec. and the peak value is taken to be 60°. Fig. 4.10 shows the vehicle trajectory Y versus X. Excellent agreement is seen. Figs. 4.11 and 4.12 present u and v versus time, respectively. It would seem from Fig. 4.11 that the IDSFC output is physically more reasonable in that it predicts a slowing down of the vehicle. The difference in absolute terms though are quite small. Fig. 4.12 shows that there is very good agreement for the v versus time results.

Figs. 4.13 through 4.15 are again for a trapezoidal steer with the rise time, dwell time and fall time increased to 2 seconds. The same overall trends are apparent, the agreement being on the whole very good.

§4.2. Simulation Running Costs. Though computer costs are variable even within a given installation, depending on mode and time of operation, etc., some relative comparisons can be made.

Table 4.1 is concerned with a moderate cornering and braking maneuver. On it are given costs and selected important output for four modes of running IDSFS.* Tables 4.2 and 4.3 give similar information for a severe steering maneuver without braking and a severe braking maneuver with braking.

All of the tables show that removing the nonlinear terms in the mathematical model result in a cost saving of about 20% with only minor losses in accuracy (maximum of about 5%). These results should be emphasized since one of the goals of the project was to assess the effects of nonlinearities in the severe regime. The tables also show that operating in a single precision mode cuts costs by 40% with an accuracy loss of less than 1%. Based on these observations, the authors recommend that single precision versions of the programs be used. Double precision versions were supplied for the event that the user has an exceptionally severe maneuver requiring extra accuracy in the computations.

---

*The assumption 4 mentioned is one in which the suspension deflections are regarded as negligible compared to the height of the center of gravity. In the authors experience with the simulation, this assumption is a poor one and should not be made.

Finally, it should be noted that running the simulation in a closed-loop mode will increase the costs. In particular, runs involving the three-degree-of-freedom predictor in the Driver Module will be significantly more expensive.

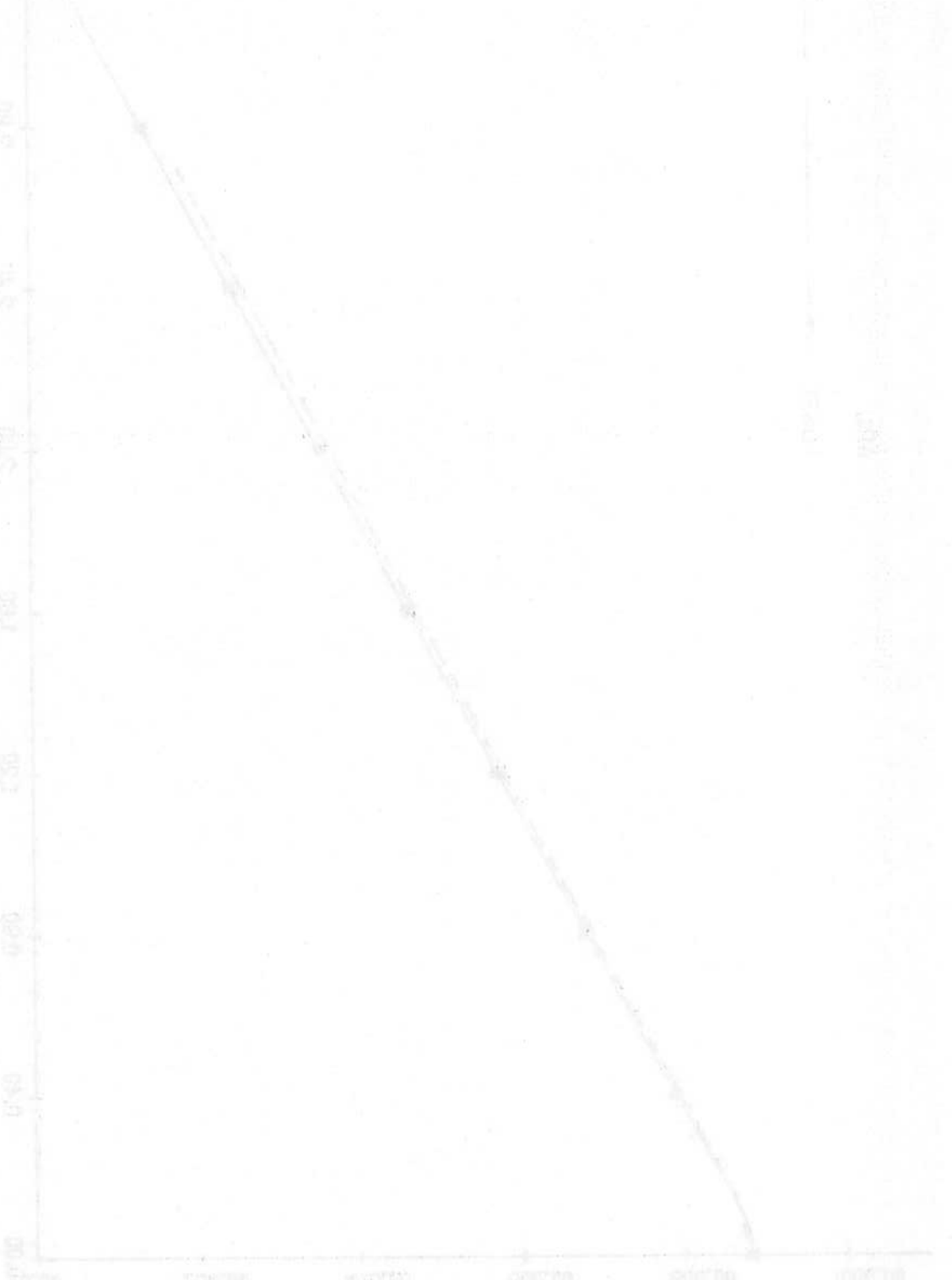

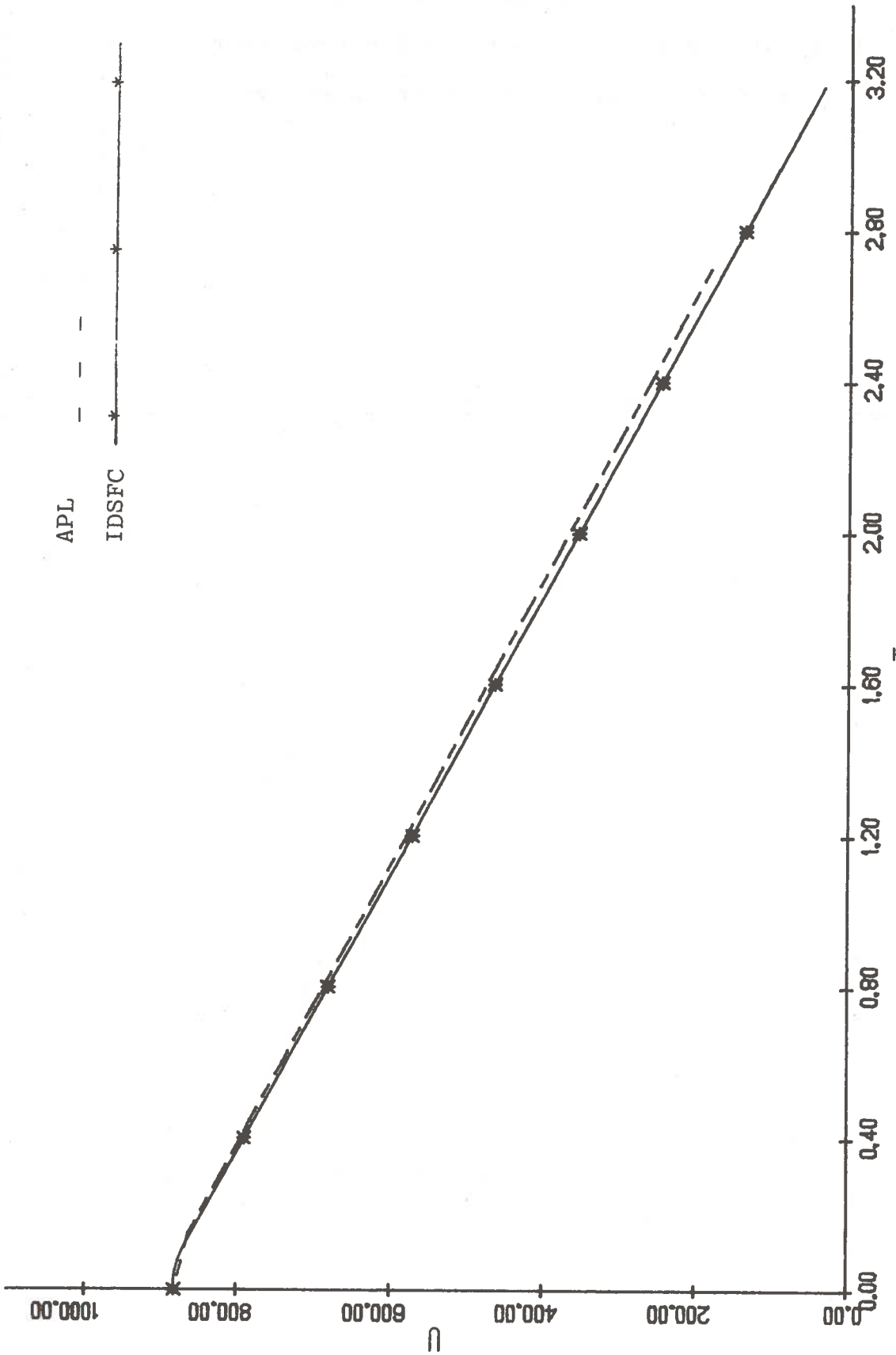

Fig. 4.1. Forward velocity u (in./sec.) as a function of time T (sec.) for a straight line braking maneuver with a peak brakeline pressure of 475 psi.

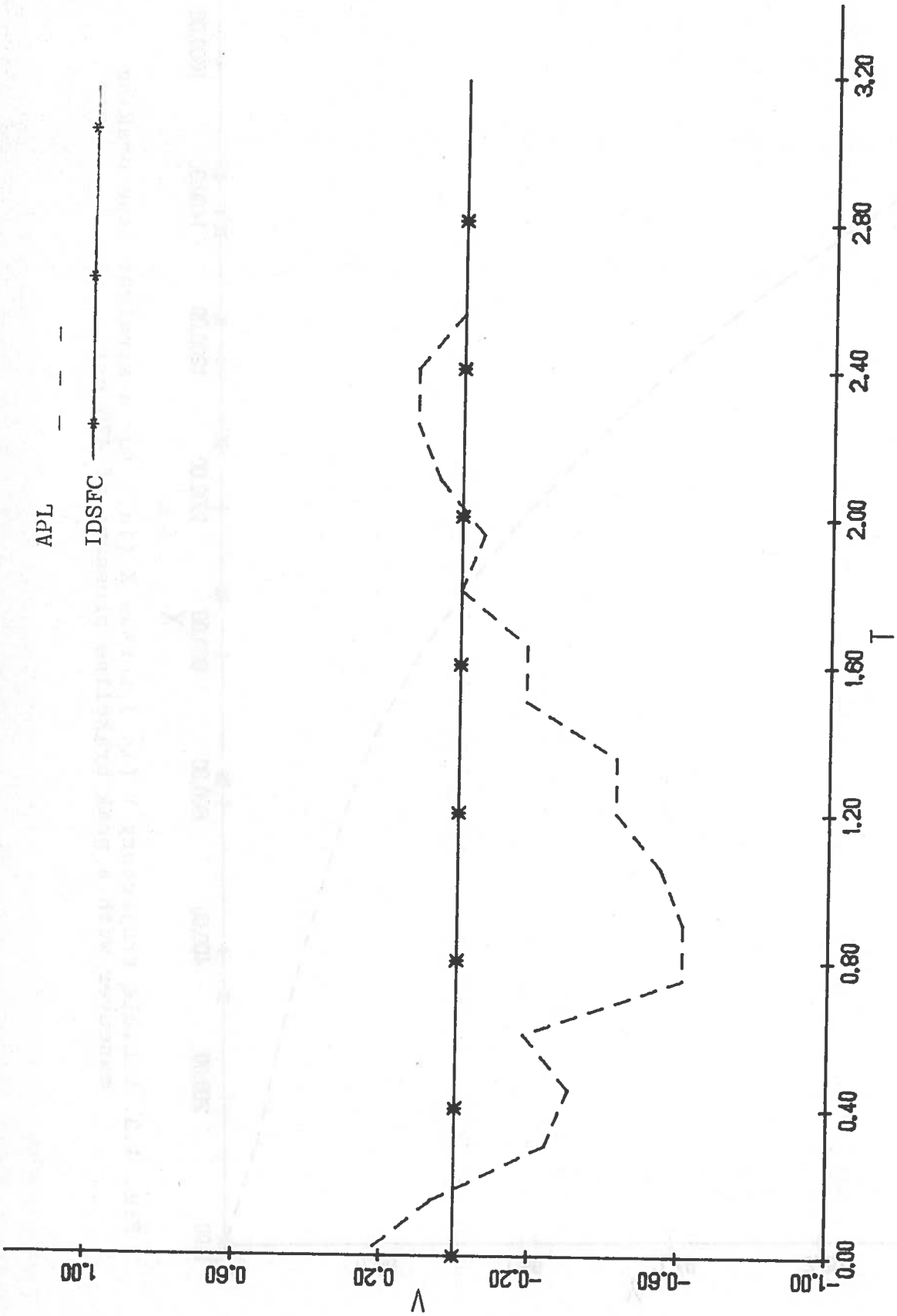

Fig. 4.2. Lateral velocity v (in./sec.) as a function of time T (sec.) for a straight line braking maneuver with a peak brakeline pressure of 475 psi.

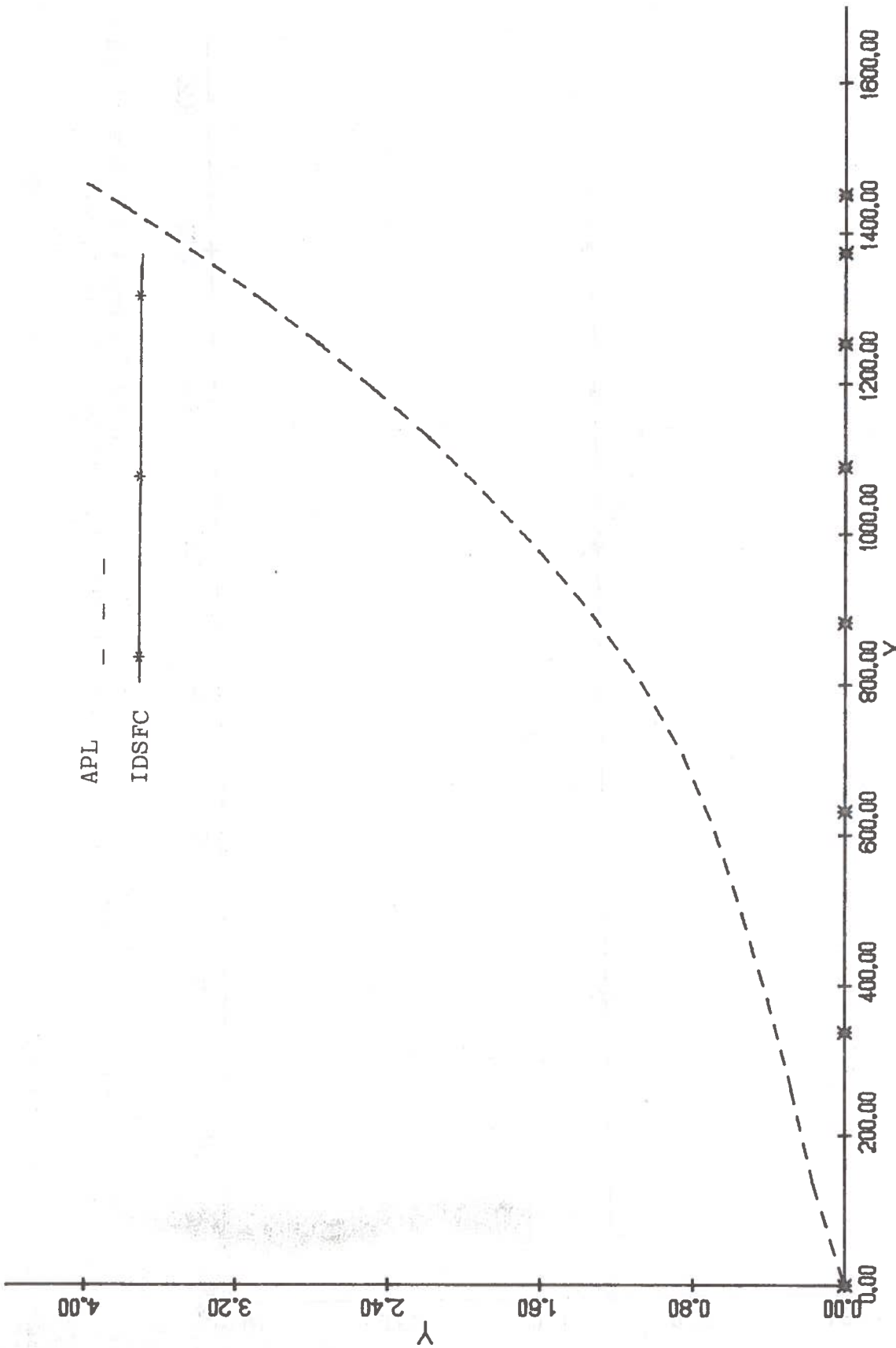

Fig. 4.3. Vehicle trajectory Y (in.) versus X (in.) for a straight line braking maneuver with a peak brakeline pressure of 475 psi.

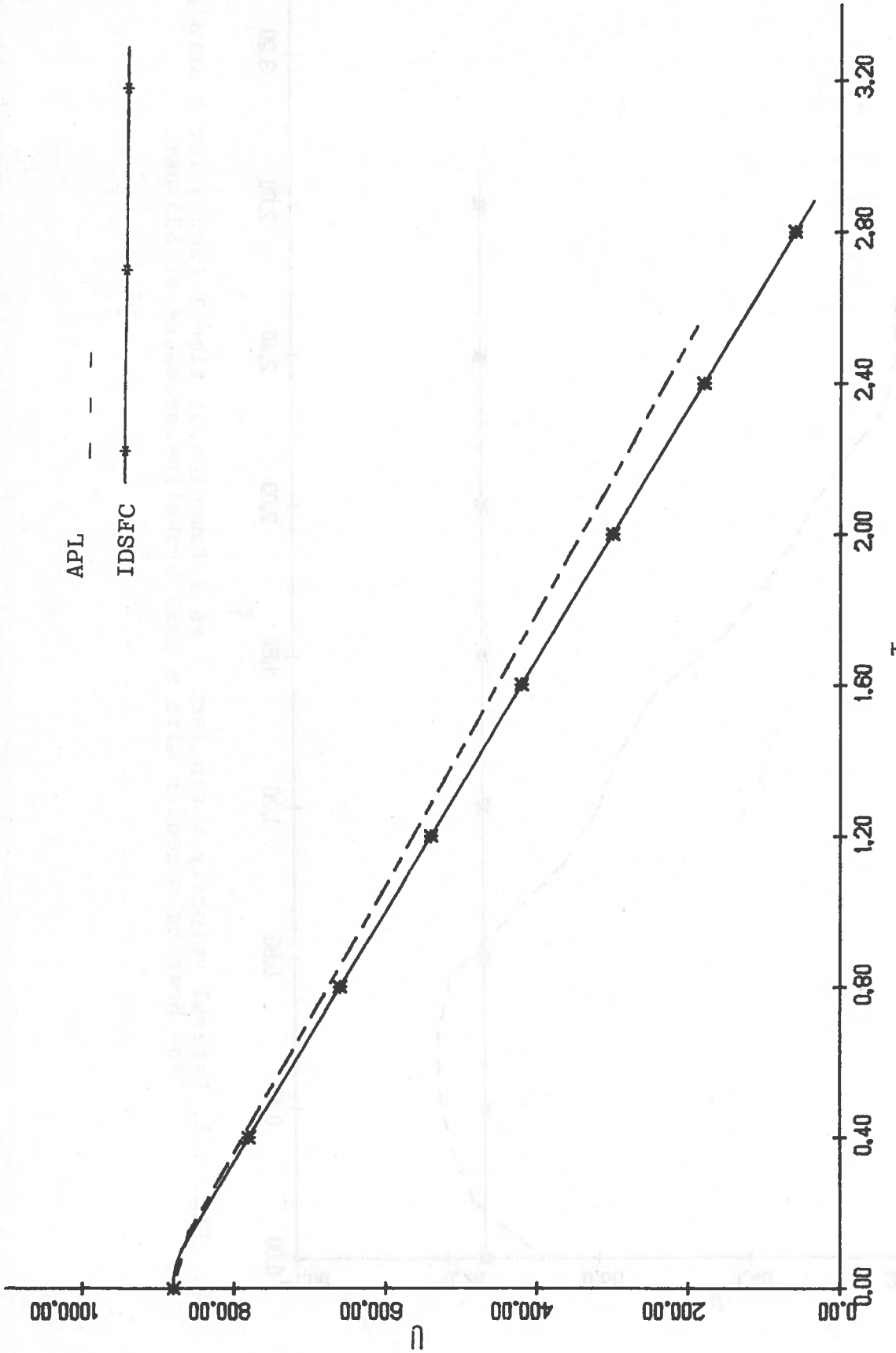

Fig. 4.4. Forward velocity u (in./sec.) as a function of time T (sec.) for a straight line braking maneuver with a peak brakeline pressure of 525 psi.

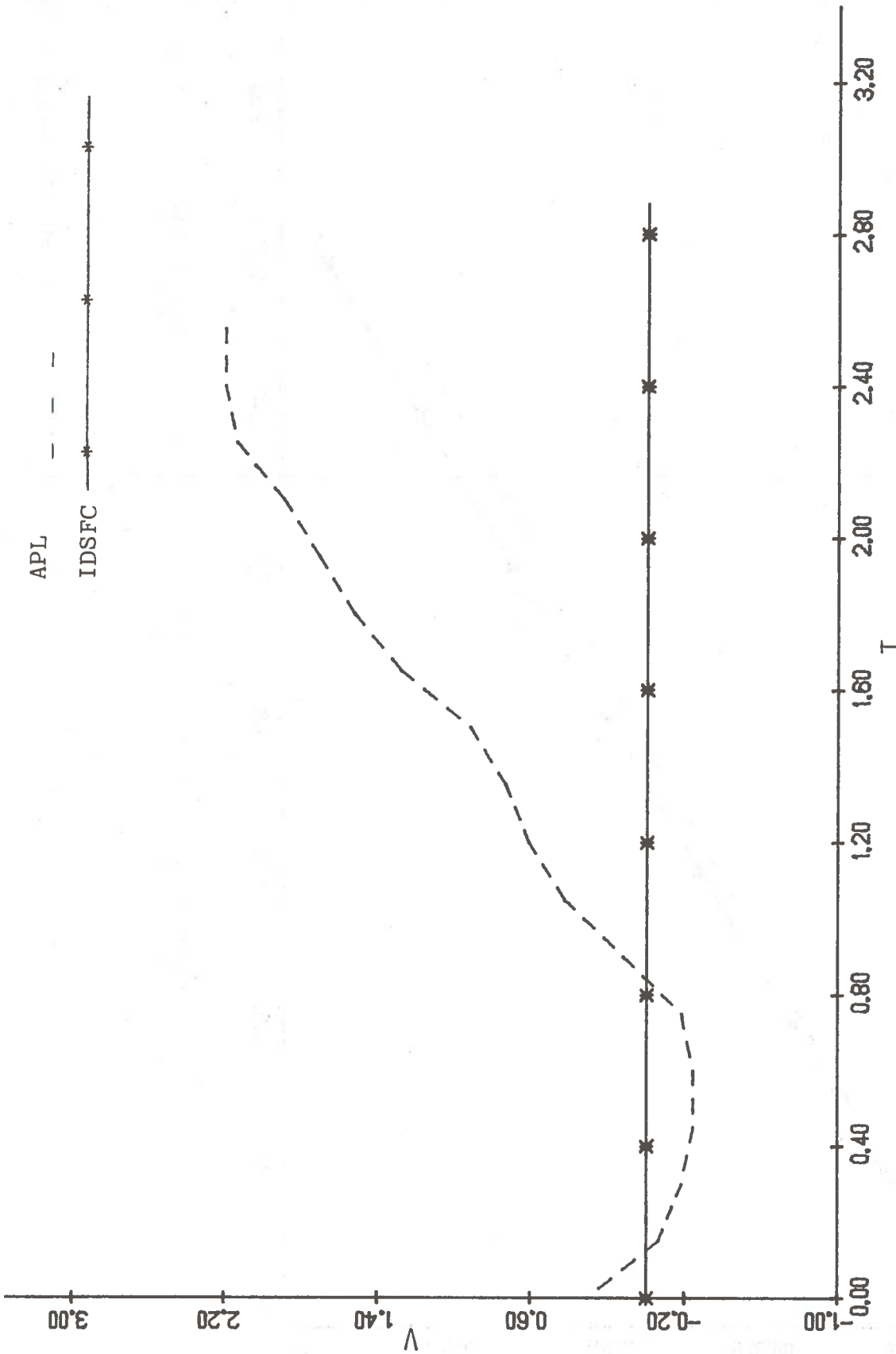

Fig. 4.5. Lateral velocity v (in./sec.) as a function of time T (sec.) for a straight line braking maneuver with a peak brakeline pressure of 525 psi.

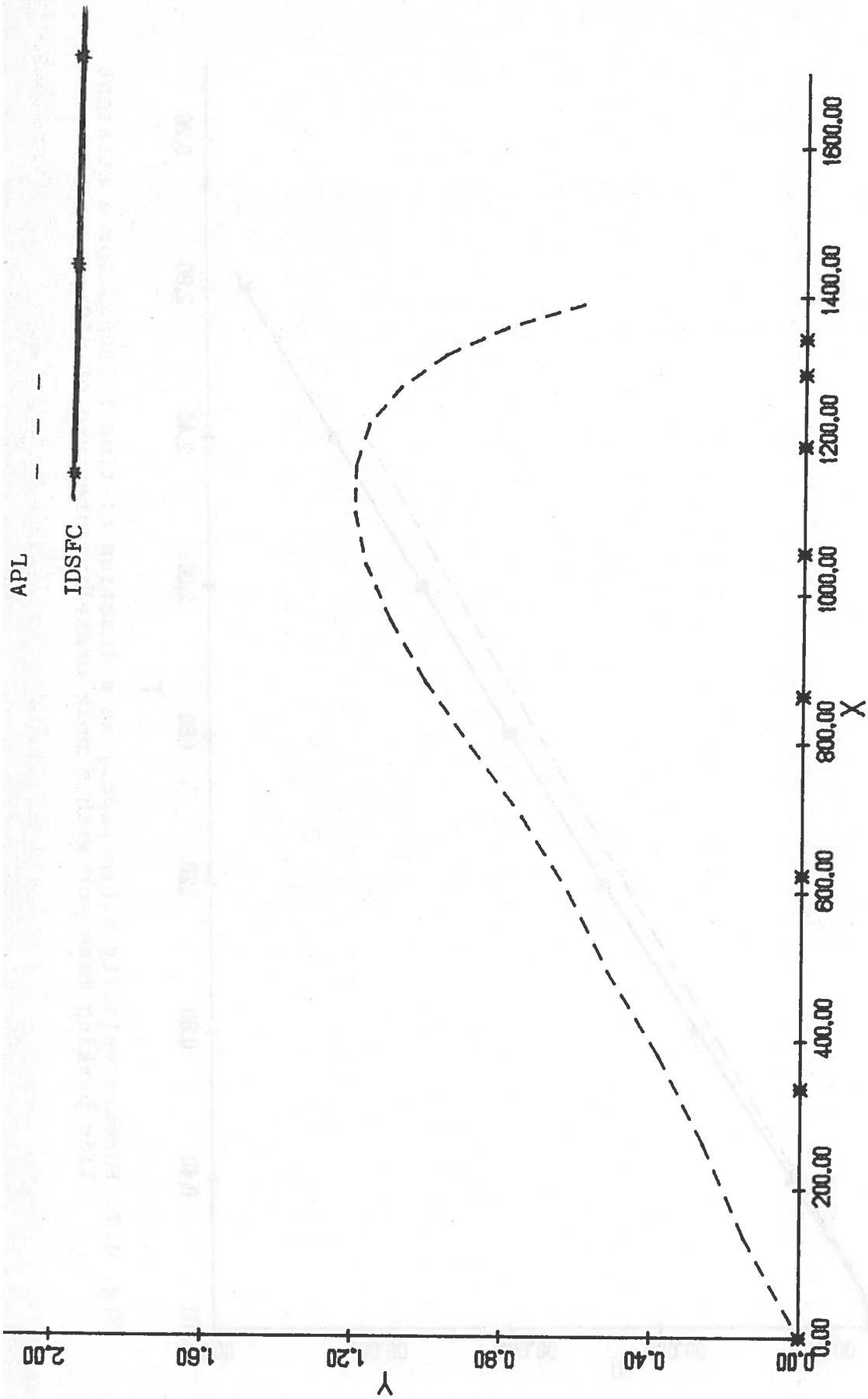

Fig. 4.6. Vehicle trajectory Y (in.) versus X (in.) for a straight line braking maneuver with a peak brakeline pressure of 525 psi.

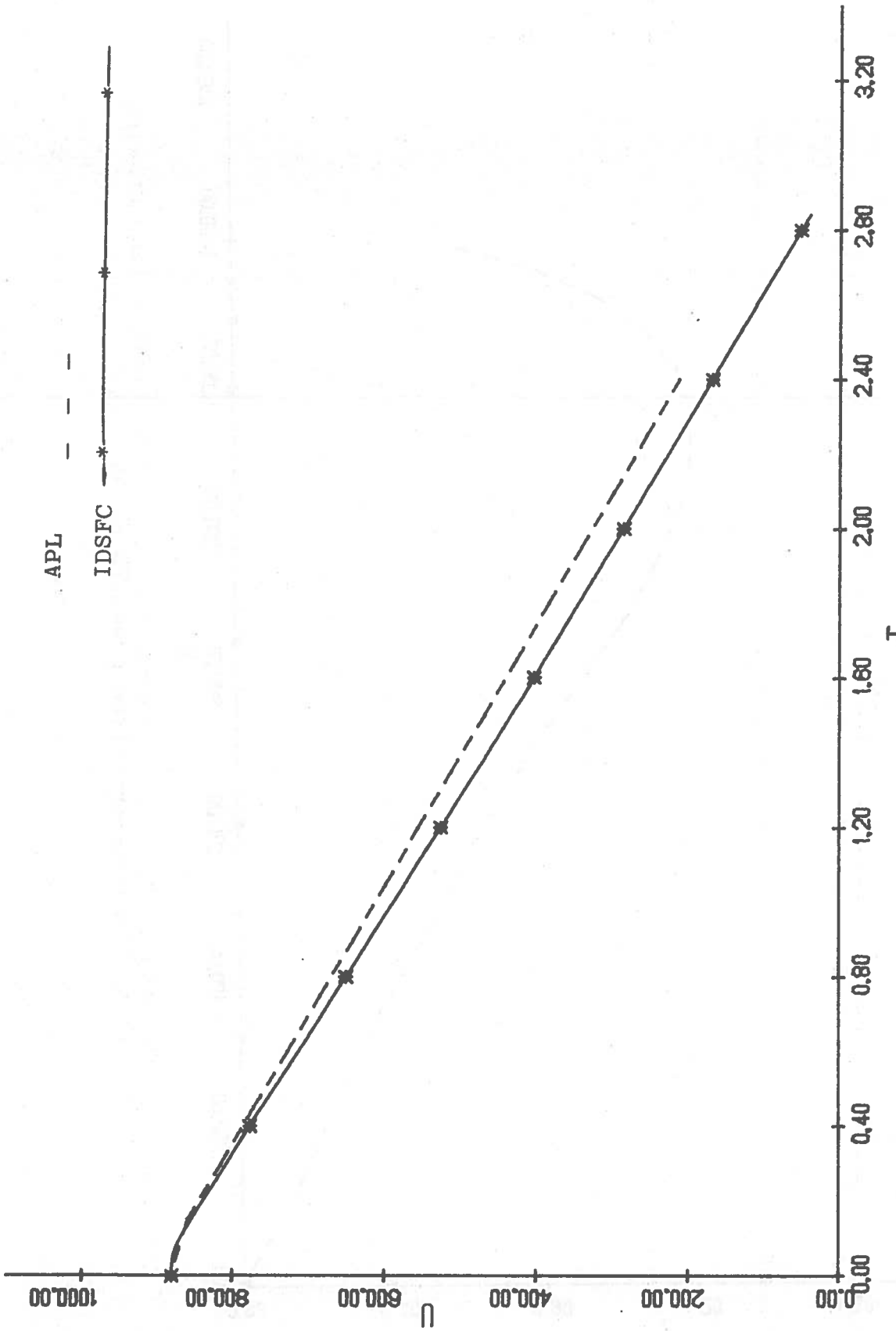

Fig. 4.7. Forward velocity u (in./sec.) as a function of time T (sec.) for a straight line braking maneuver with a peak brakeline pressure of 550 psi.

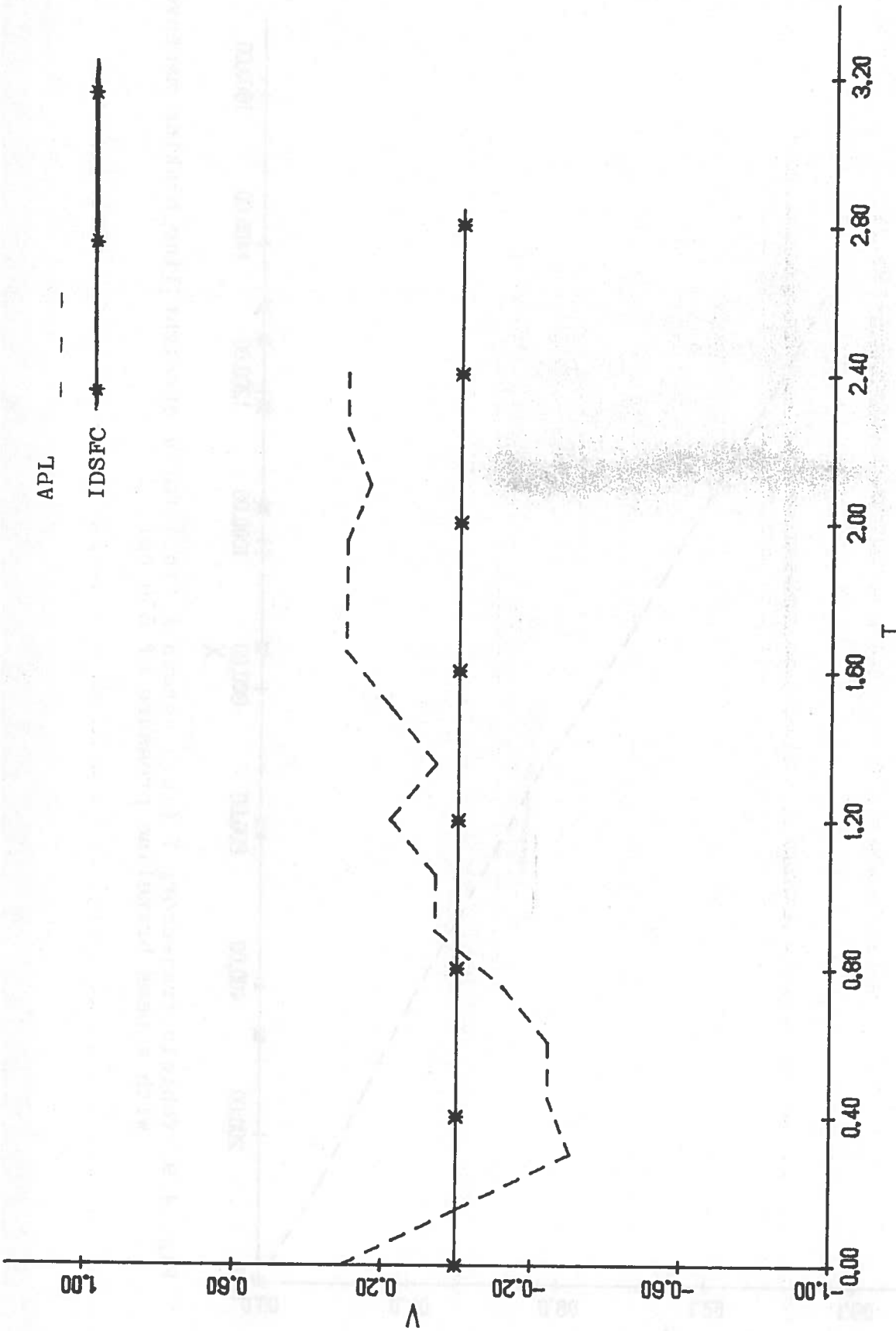

Fig. 4.8. Lateral velocity v (in./sec.) as a function of time T (sec.) for a straight line braking maneuver with a peak brakeline pressure of 550 psi.

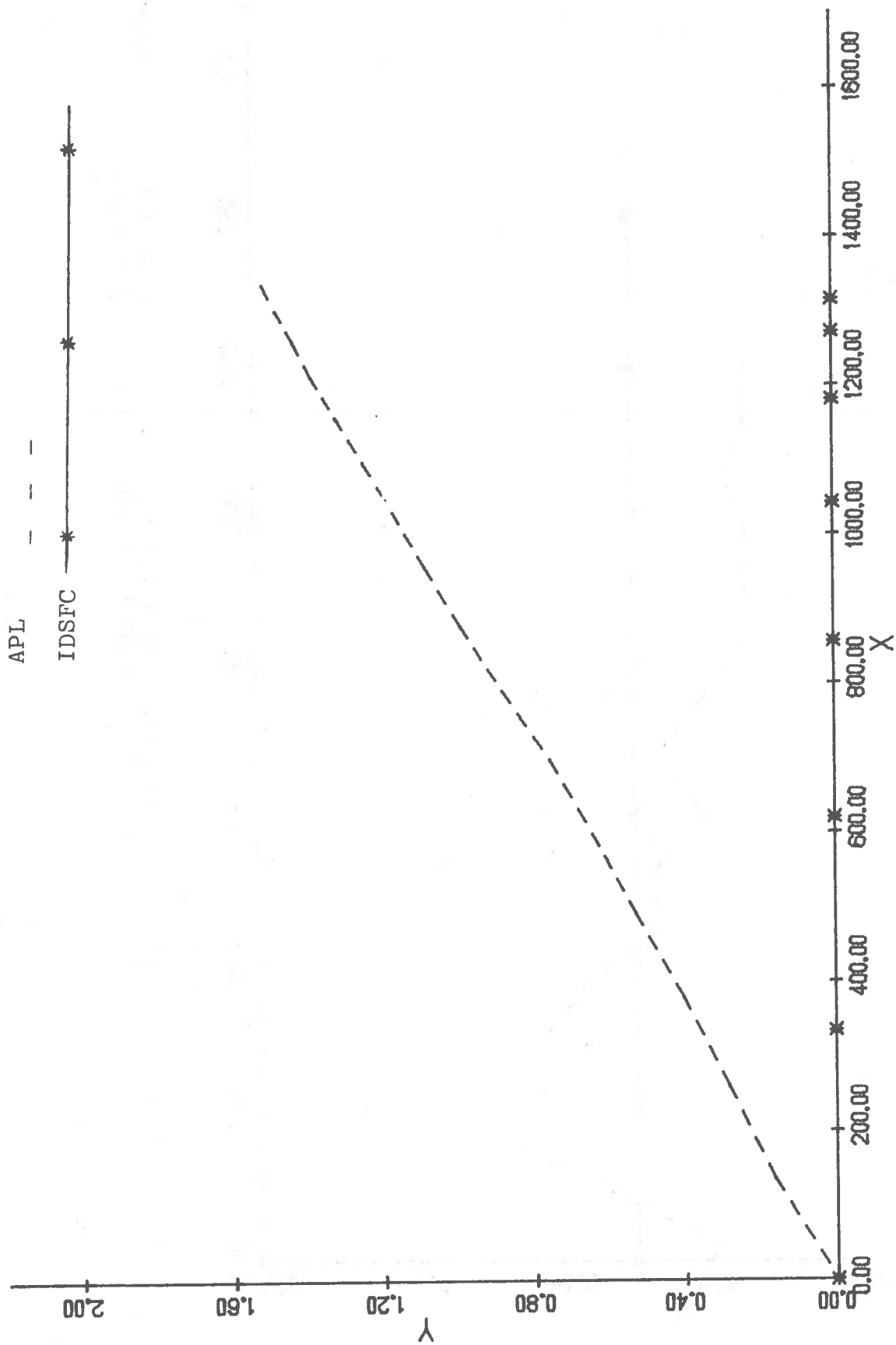

Fig. 4.9. Vehicle trajectory Y (in.) versus X (in.) for a straight line braking maneuver with a peak brakeline pressure of 550 psi.

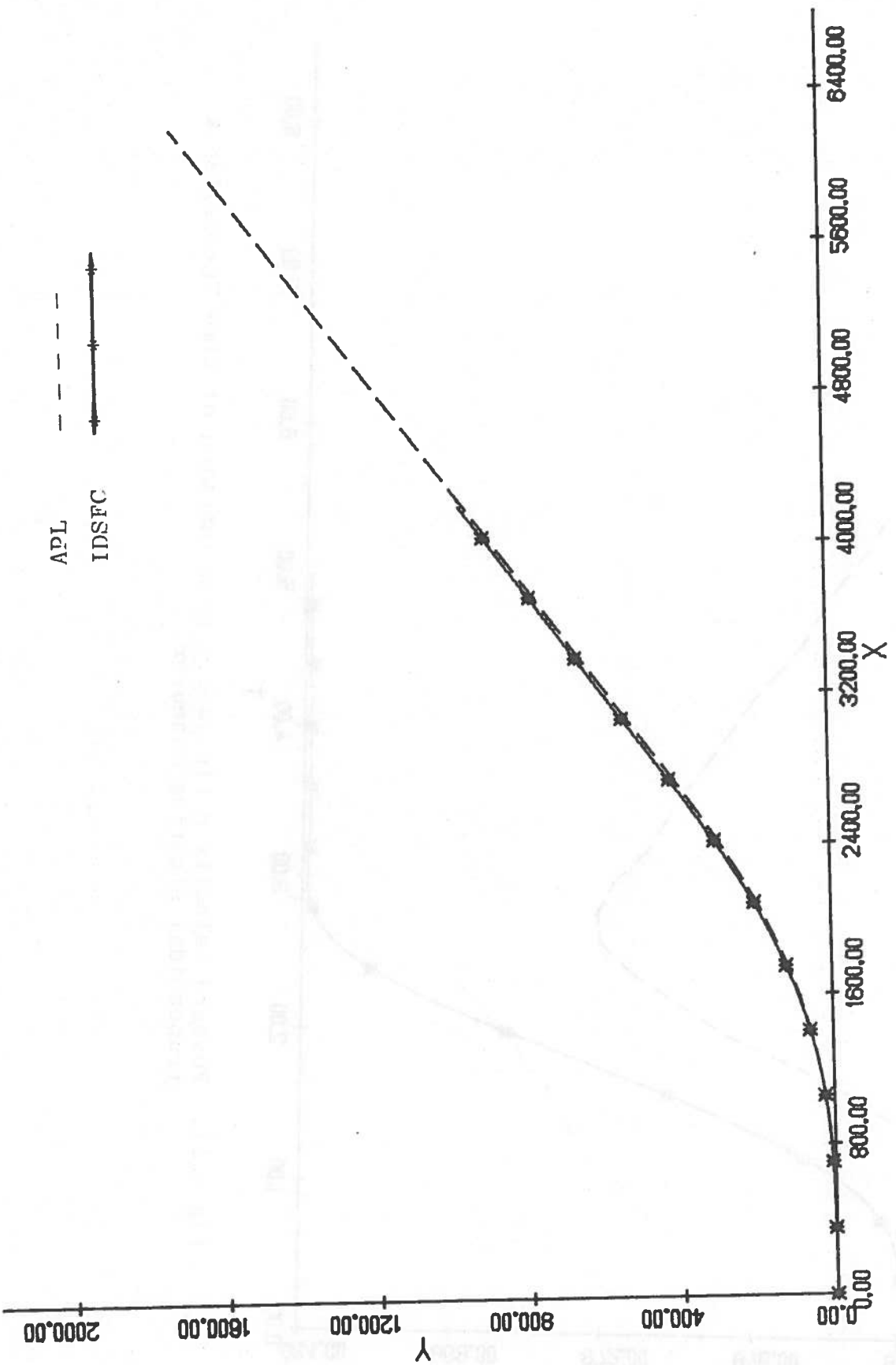

Fig. 4.10. Vehicle trajectory y (in.) versus x (in) for a trapezoidal steering maneuver.

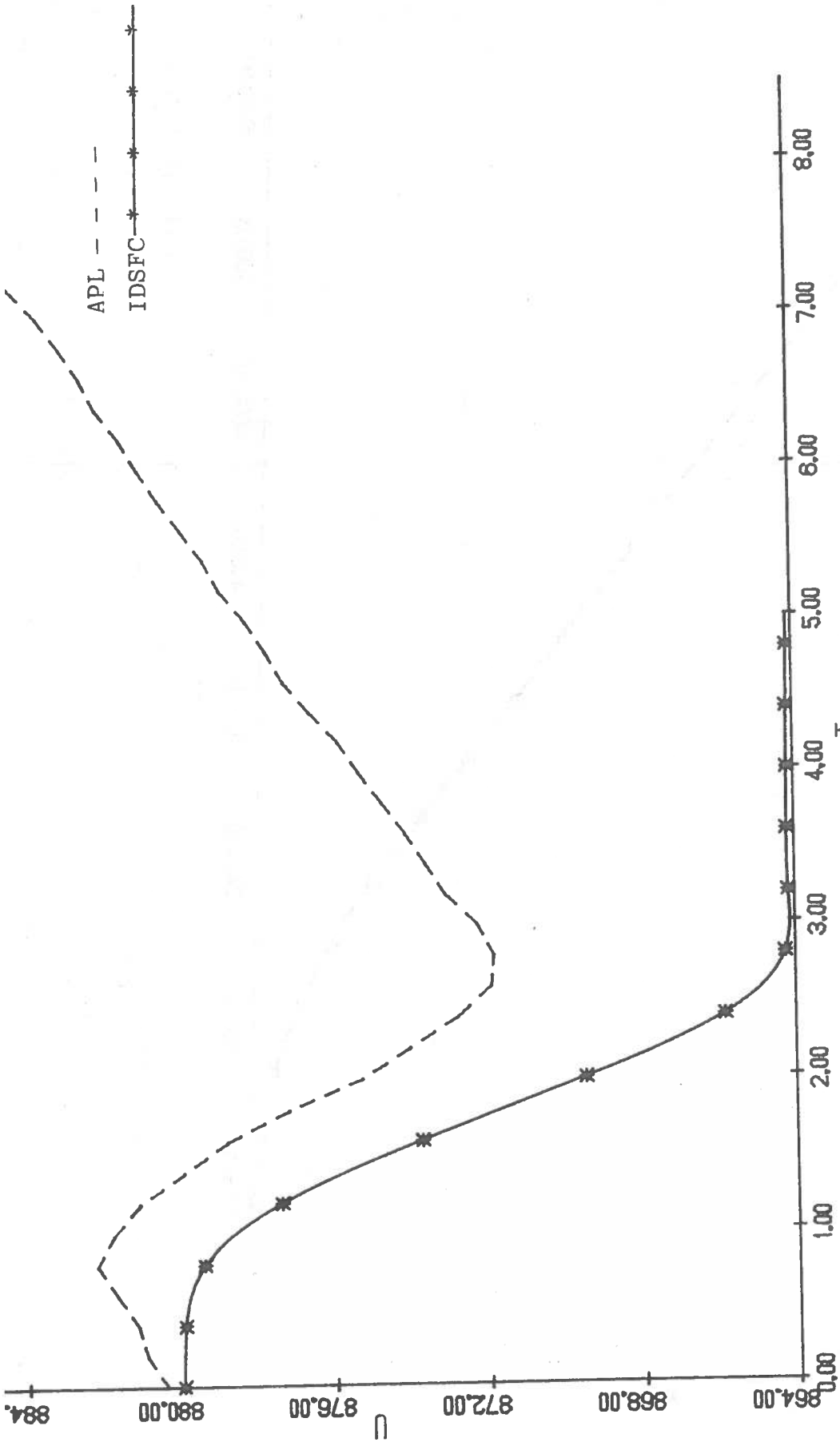

Fig 4.11. Forward velocity u (in./sec.) as a function of time T(sec.)for a trapezoidal steering maneuver.

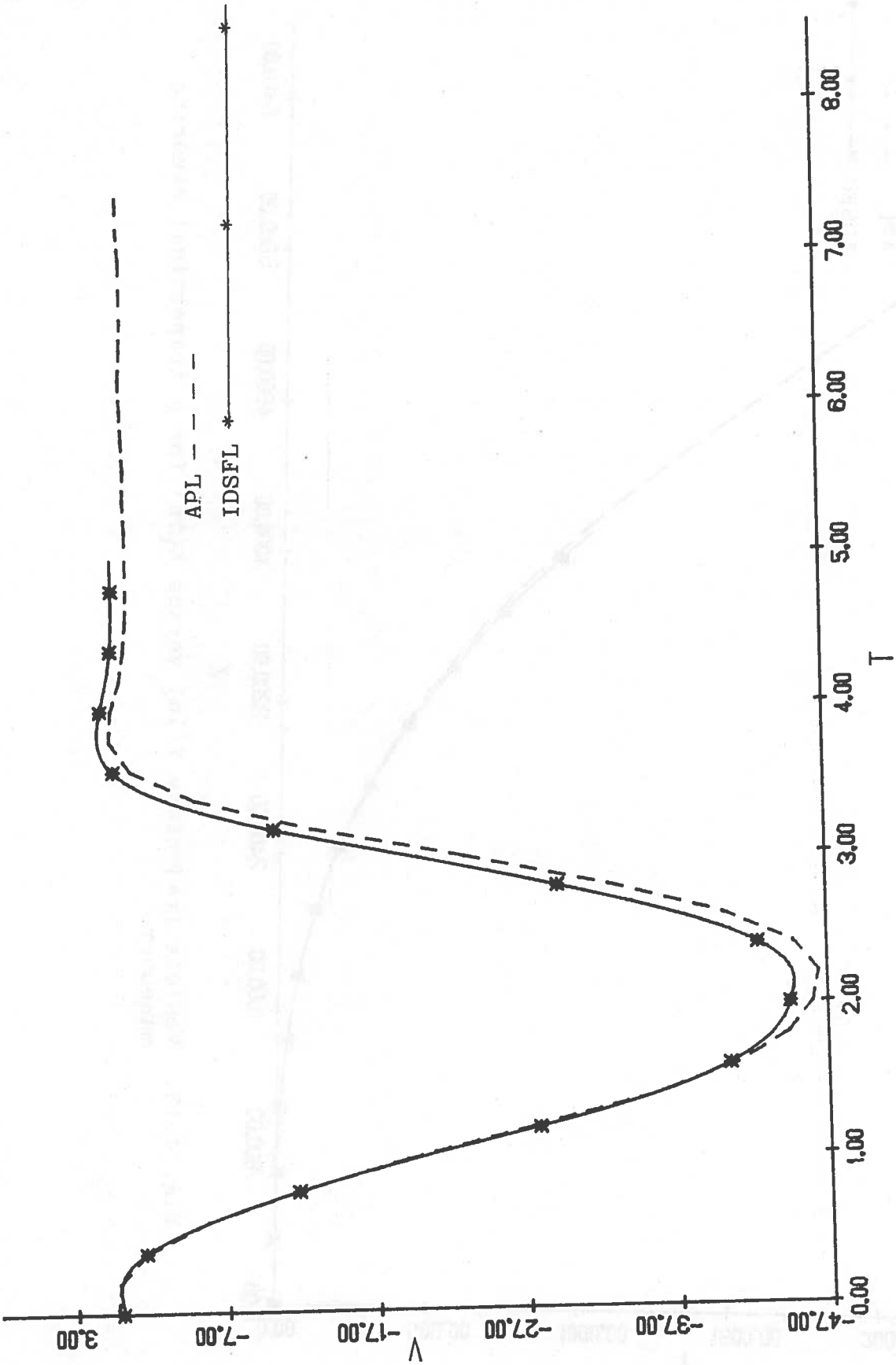

Fig. 4.12. Lateral velocity V (in./sec.) as a function of time for a trapezoidal steering maneuver.

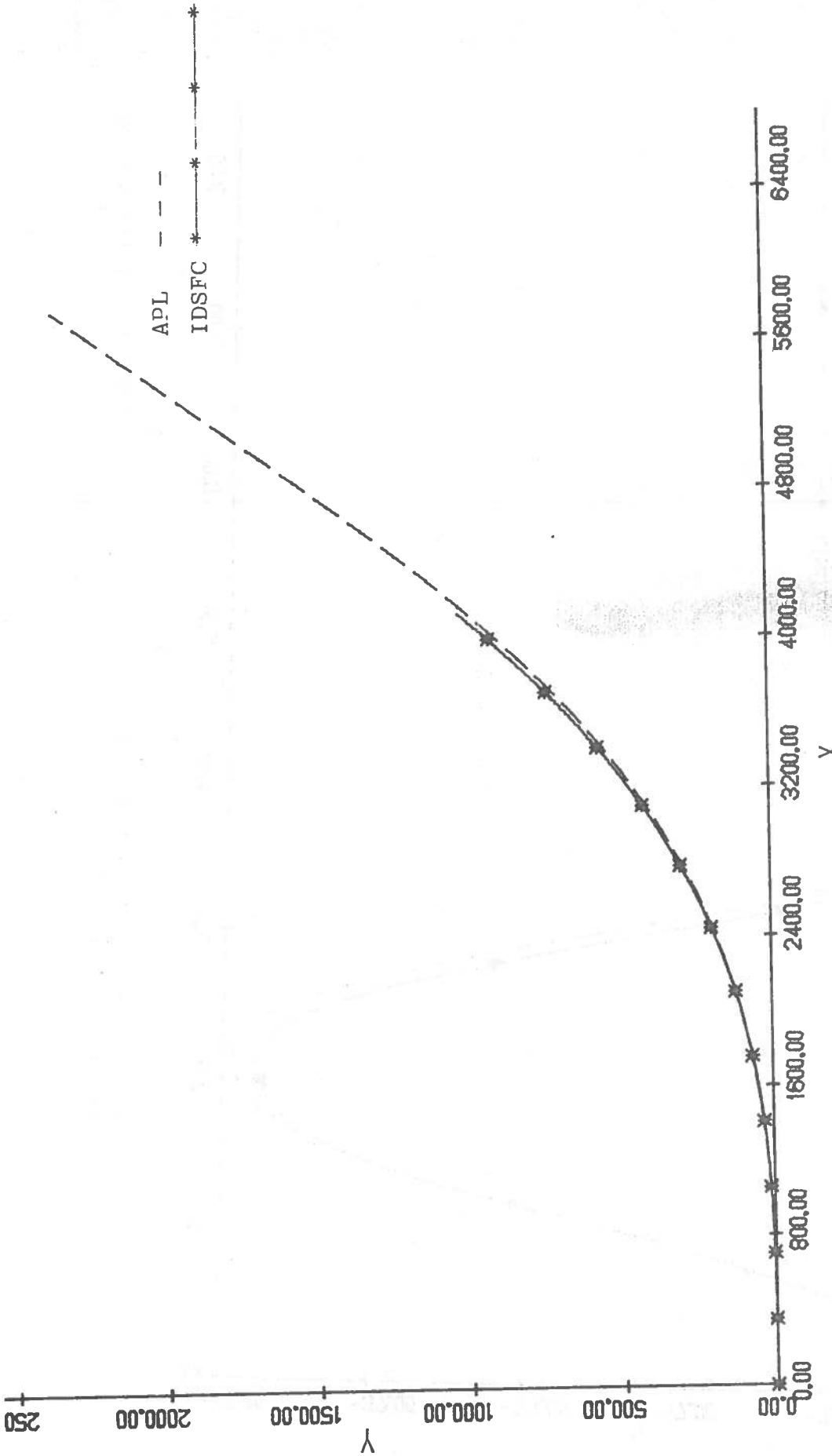

Fig. 4.13. Vehicle trajectory Y(in) versus X(in) for a trapezoidal steering maneuver.

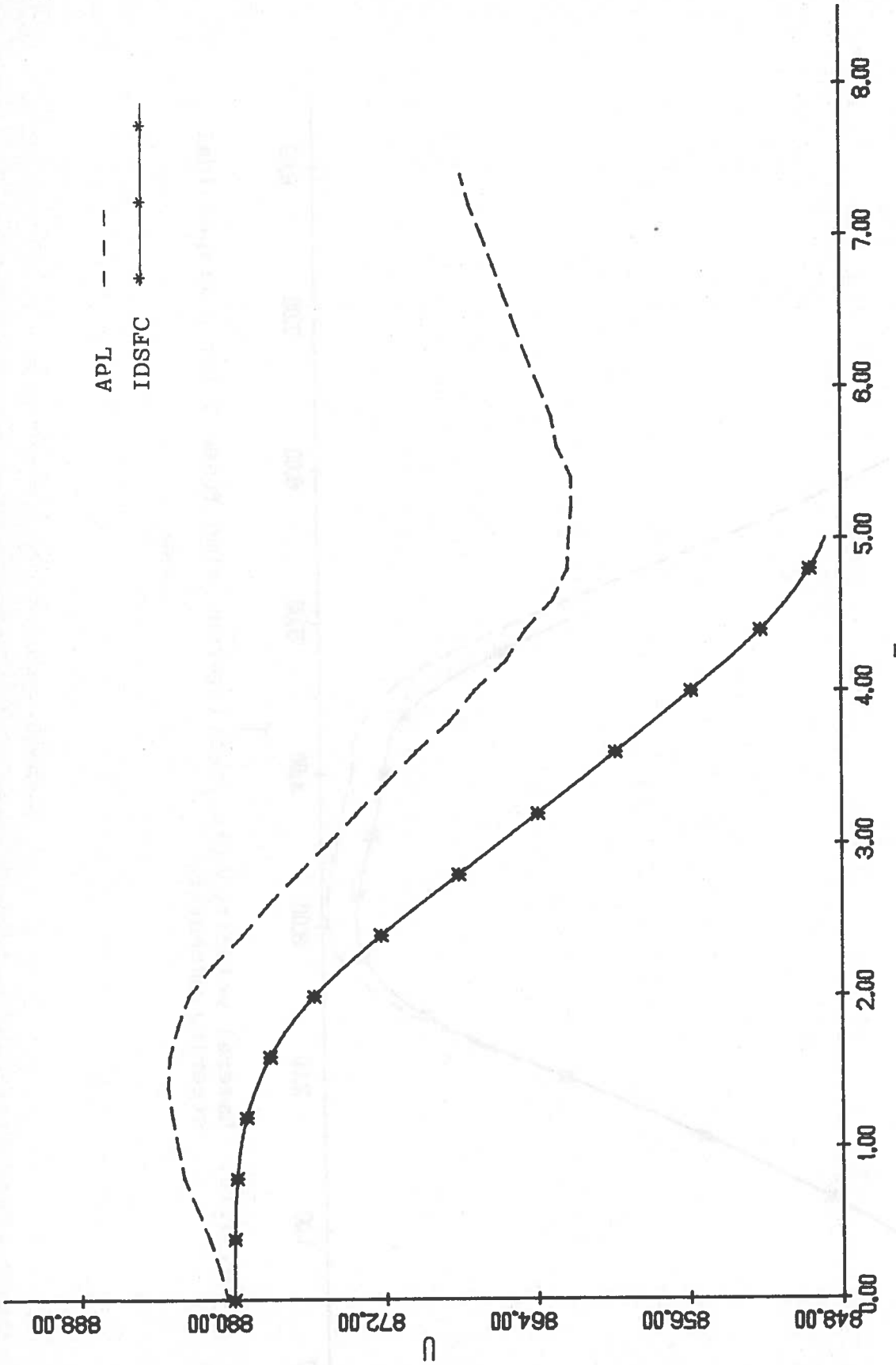

Fig. 4.14. Forward velocity u (in./sec.) as a function of time T(sec.) for a trapezoidal steering maneuver.

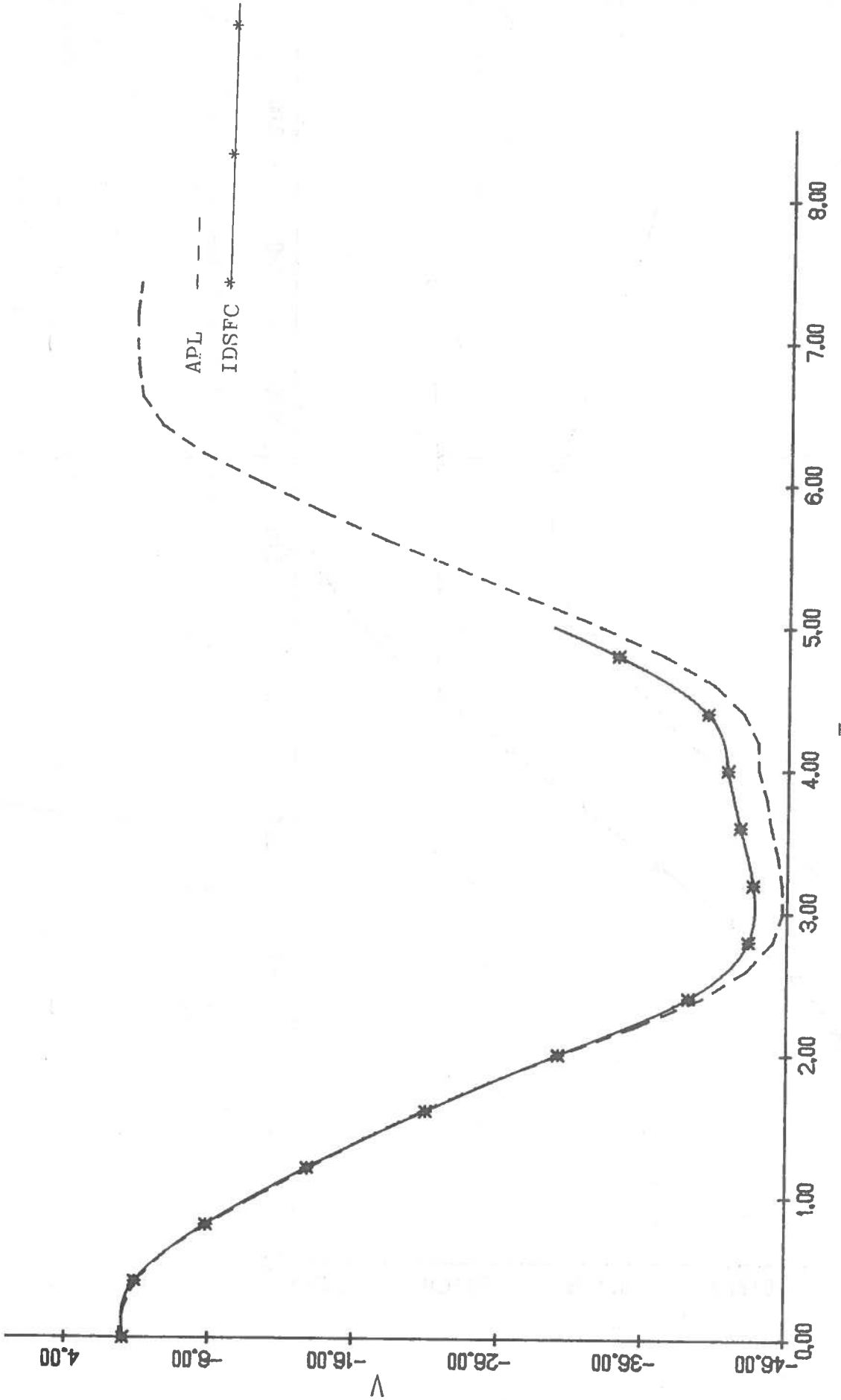

Fig. 4.15. Lateral velocity V (in./sec.) versus time T(sec.) for a trapezoidal steering maneuver.

Table 4.1

Moderate Cornering with Braking Maneuver.

Maneuver Description. (i) The initial speed of the vehicle is 50 mph.

(ii) Ramp braking is applied with a rise time of 0.1 seconds and a peak value of 400 psi.

(iii) Ramp steering is applied with a rise time of 1 second and a peak value of 43 degrees.

Quantity	Double precision. No assumptions	Double precision.All assumptions but no. 4.	Single precision. No assumptions.	Single precision.All assumptions, but no. 4
cost per vehicle second	$2.20	$1.82	$1.39	$1.12
cpu time sec.	14.208	11.856	10.606	8.744
max. x-acceleration (gees)	-0.6042	-,6058	-.6052	-0.60581
max. y-acceleration (gees)	0.1743	.1788	0.1746	0.1788
max. yaw rate deg./s.	6.4319	6.6280	6.4390	6.6268
final X-position in.	1738.11299	1739.93547	1736.74854	1738.41797
final Y-position in.	134.61056	138.37174	134.51895	138.11896
Vehicle stopping distance ft.	144.843	144.995	144.729	144.868
Vehicle stopping time sec.	3.765	3.770	3.765	3.765

Table 4.2

Severe Steering Maneuver Without Braking.

Maneuver Description. (i) The initial speed of the vehicle is 55 mph.

(ii) A sinusoidal steer with amplitude 2 rad. and period 1 sec. is applied.

(iii) There is no braking.

(iv) The running time is 5 sec.

Quantity	Double precision.No assumptions.	Double precision.All assumptions but no. 4.	Single precision.No assumptions.	Single precision.All assumptions, but no.4.
cost per vehicle second	$2.21	$1.24(low Priority)	$1.34	$1.12
cpu time sec.	19.242	15.312	13.850	11.494
max. x-acceleration (gees)	-0.0214	-0.0209	-0.0214	-0.0208
max. y-acceleration (gees)	0.6648	.6566	0.6647	0.6565
max. yaw rate deg/s.	19.0602	-19.0475	19.0611	-19.0461
final X-position in.	4280.83737	4269.83863	4282.54297	4271.56641
final Y-position in.	1488.28686	1496.42936	1488.47241	1496.71997
final velocity in/sec	873.98108	871.86272	873.09424	871.01416

Table 4.3

Severe Steering/Braking Maneuver.

Description of the Maneuver. (i) The initial vehicle speed is 55 mph.

(ii) Ramp braking is applied with a maximum brake line pressure of 480 psi and a rise time of .1 sec.

(iii) A sinusoidal steer is applied with an amplitude of 1½ rad. and a period of 1 sec.

Quantity	Double precision. No assumptions.	Double precision. All assumptions but no. 4.	Single precision. No assumptions.	Single precision. All assumptions but no. 4.
cost per vehicle second	$2.38	$1.33(on low priority)	$1.45	$1.18
cpu time sec.	14.531	11.881	10.437	8.729
max. x-acceleration (gees)	-0.7351	-0.7416	-0.7351	-0.7416
max. y-acceleration (gees)	0.2729	0.2573	0.2729	0.2573
max. yaw rate deg./s.	11.7848	11.7772	11.7779	11.7777
max. long. slip of wheel 1.	1.00000	1.00000	1.00000	1.00000
max. long. slip of wheel 2.	0.14498	0.14707	0.14498	0.14707
max. long. slip of wheel 3.	1.00000	1.00000	1.00000	1.00000
max. long. slip of wheel 4.	0.14252	0.14924	0.14255	0.14924
final X-position in.	1788.45117	1807.69776	1787.10643	1806.46582
final Y-position in.	170.19395	169.62573	169.91209	169.47066
vehicle stopping distance ft.	149.038	150.641	148.926	150.539
vehicle stopping time sec.	3.540	3.575	3.535	3.575

References for Chapter 4.

4.1 S.L. Chiang and D.S. Starr, "Using Computer Simulation to Evaluate and Improve Vehicle Handling", SAE 780009.

CHAPTER 5. ADDITIONAL OPEN-LOOP OUTPUT AND TIRE MODELLING

§5.1. Further Open-Loop Output. To lend further credibility to the simulation, maneuvers involving braking in a turn were made and the results are given in Figs. 5.1. through 5.6. Morever, important end of run quantities are given in Table 5.1. The maneuvers are severe and involve trapezoidal steering and trapezoidal braking, with peak brakeline pressures of 500, 525 and 550 psi. Inspection of the graphs and the end of run quantities reveal them to be physically reasonable, further evidence of the validity of the simulation.

§5.2. Tire Modelling.

Two methods for calculating the tire side force have been implemented for user flexibility. The first method is identical with the method used by APL. The second method uses the Calspan data points* and interpolation between them. For this method, subroutine READTD reads the Calspan measured tire data points. Using interpolation, it develops a matrix of evenly spaced points giving the tire side force as a function of slip angle, camber angle and radial force. Since there are insufficient points available from Calspan for non-zero camber angles, the Calspan empirical equations have been used to generate a modified

*A magnetic tape was obtained from Calspan which contains tire test data for the following tires:

Size	Maker	TIRE No.
ER 78-14	Goodyear	032
E 78-14	Goodyear	063
F 78-14	Goodyear	065
A 78-13	Goodyear	127

slip angle which was used to set up the matrix for non-zero camber angles. Subroutine TIRE3 then interpolates between the data points to give the side force at any desired value of slip angle, radial force and camber angle.

Table 5.2 gives values of the side force as calculated via the interpolation method versus the actual values measured by Calspan. As can be seen, the agreement is quite good. The minor discrepancies that arise are due to the fact that the Calspan data is scattered and average values are used in the interpolation scheme.

Figures 5.7, 5.8 and 5.9 show graphs of the tire side force as a function of slip angle as calculated by the two methods. Note that the side force as calculated by the APL model is less than that calculated via the interpolation method for small slip angles and greater for slip angles in the 10° to 20° range.

Figure 5.10 is a "blown up" version of 5.9 in the large slip angle range. Note that the side force, as calculated by the interpolation method, reaches a maximum at a slip angle of about 14° and then decreases with slip angle.

TABLE 5.2

Side Force for TIRF TIRE No. 032, Goodyear ER 78-14
Longitudinal Slip=0.00 in all cases

Slip Angle (deg)	Camber Angle (deg)	Radial Force (lbs)	Measured Side Force (lbs)	Calculated Side Force (lbs)
- 1.450	0.000	888.670	251.18	251.05
- 8.000	0.000	888.670	733.75	733.34
-15.740	-0.010	891.110	813.51	814.95
-19.320	0.000	896.000	781.03	786.83
- 3.830	0.000	1489.260	613.36	609.71
-13.370	-0.010	1491.700	1182.27	1182.94

In Ref [5.1] , Pacjeka points out that this fall off governs the stability in a simple, two-degree of freedom model. A similar situation may occur in the more complicated models. Hence, even though the two methods never give values of the side force that disagree by more than five percent, it may be necessary to use the interpolation method to determine the stability of the vehicle.

Experience with the simulation has been that the interpolation method costs 20 to 25% more than the APL tire model. Also, the interpolation method costs more to initialize than does the APL model. A further drawback is that, as implemented, the data deck model uses a large amount of computer memory.

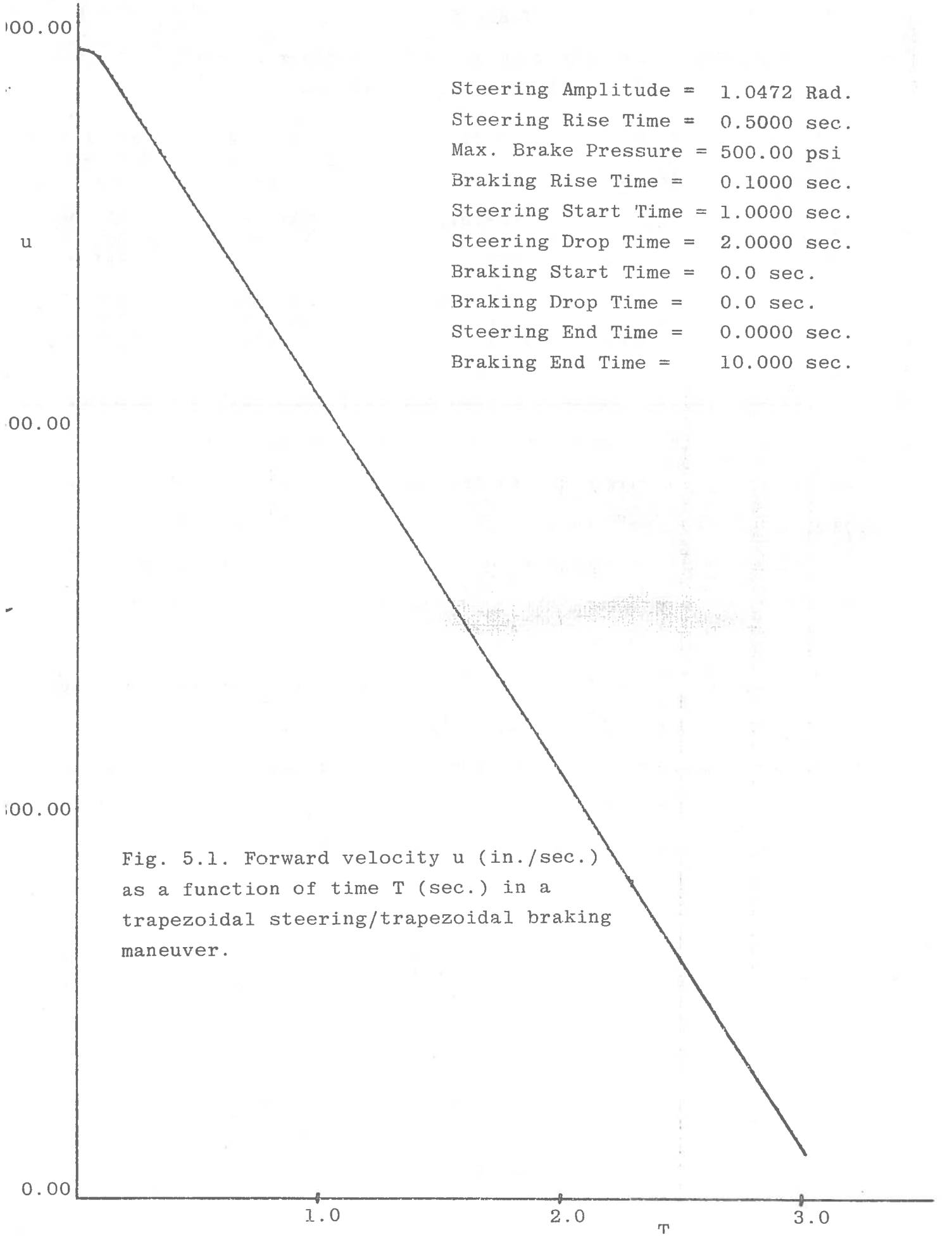

Fig. 5.1. Forward velocity u (in./sec.) as a function of time T (sec.) in a trapezoidal steering/trapezoidal braking maneuver.

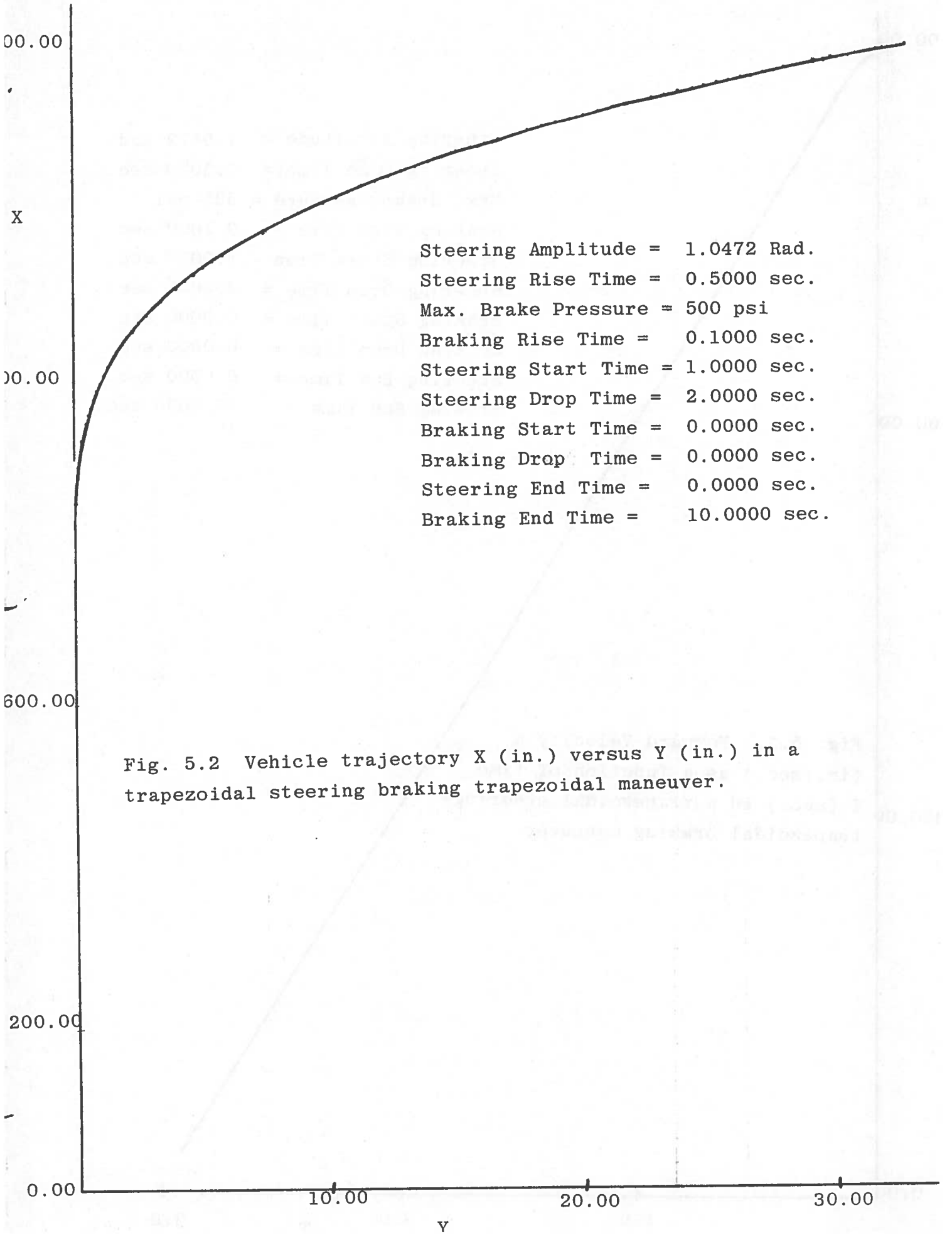

Fig. 5.2 Vehicle trajectory X (in.) versus Y (in.) in a trapezoidal steering braking trapezoidal maneuver.

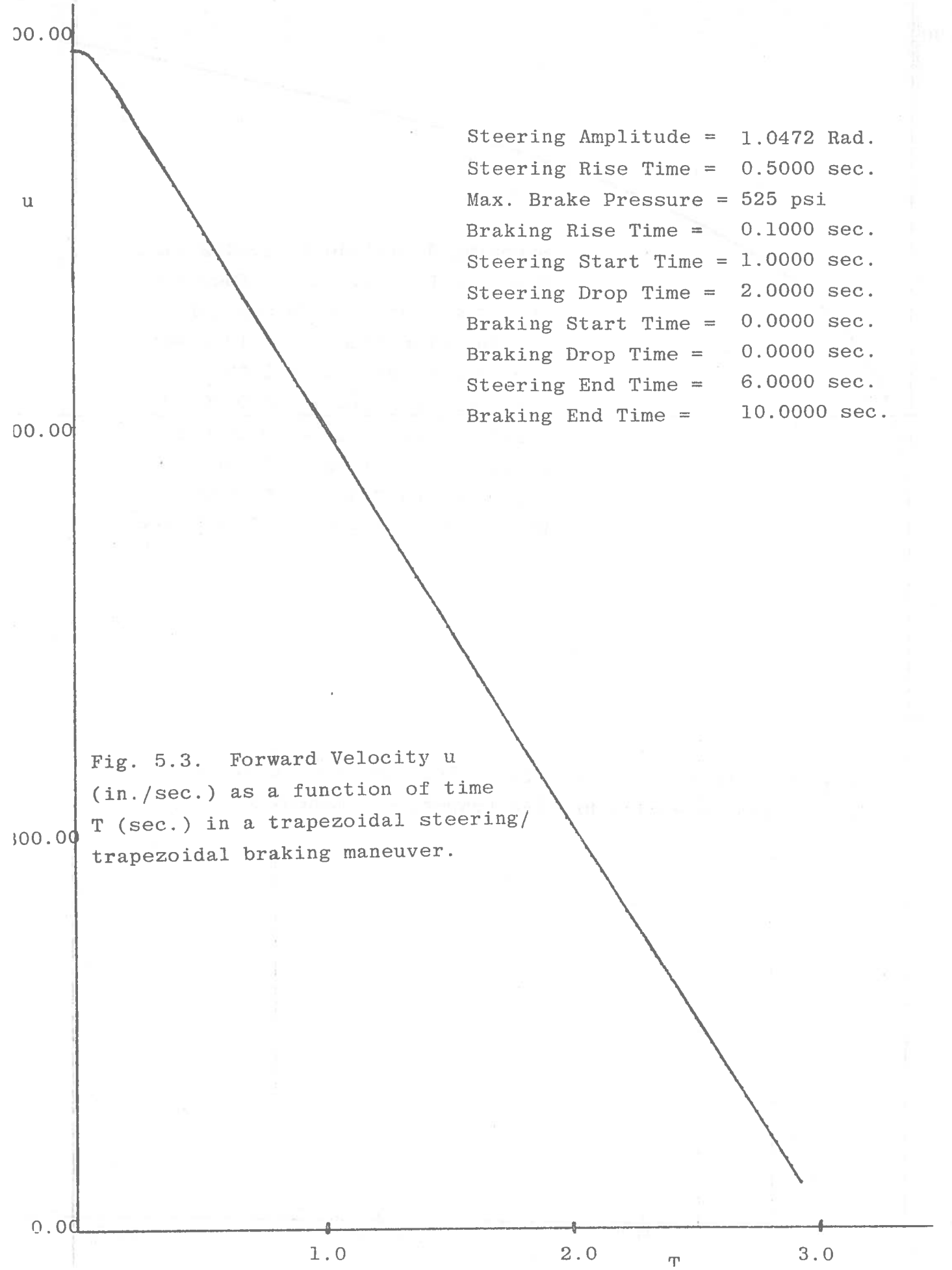

Fig. 5.3. Forward Velocity u (in./sec.) as a function of time T (sec.) in a trapezoidal steering/ trapezoidal braking maneuver.

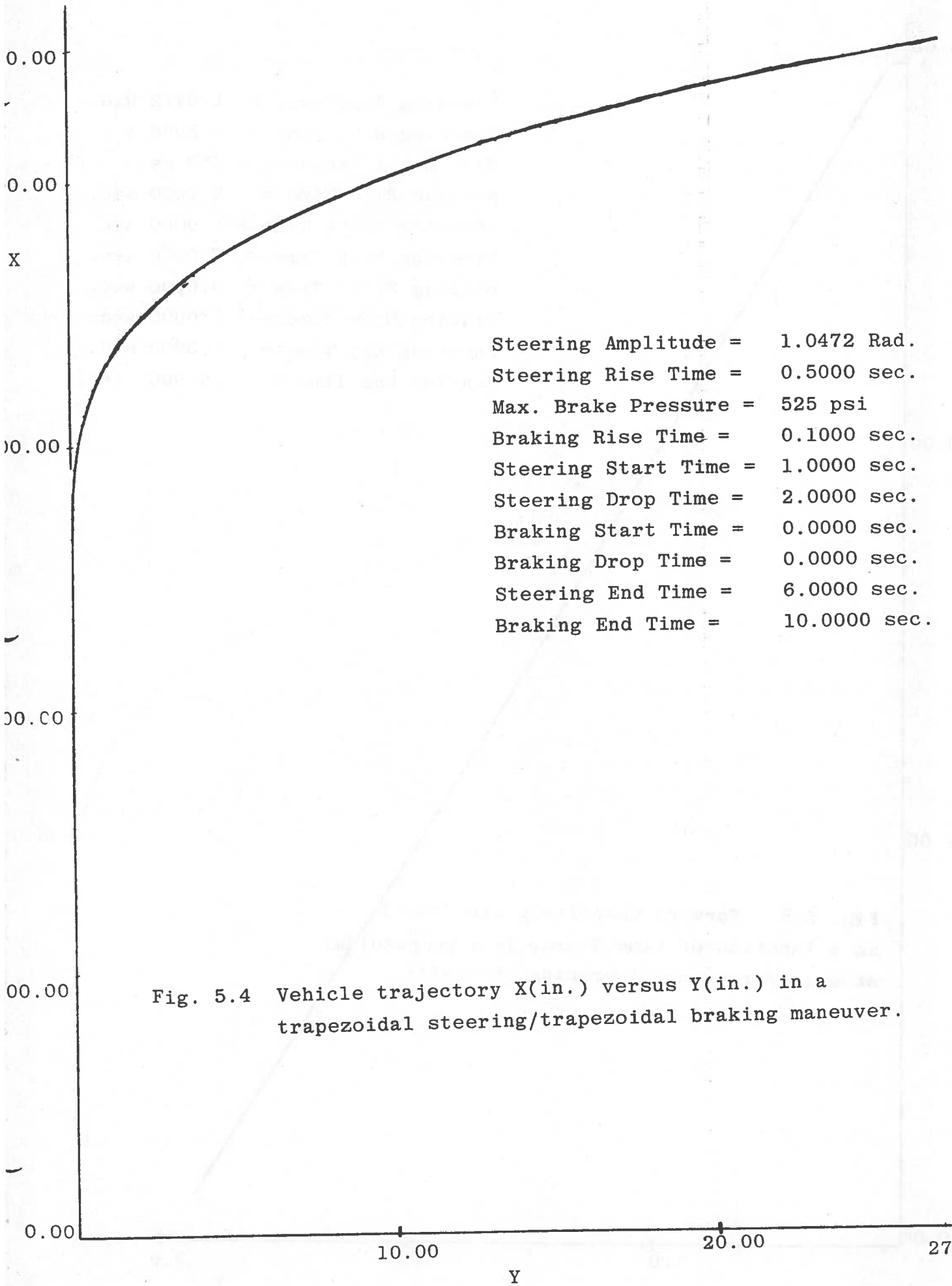

Fig. 5.4 Vehicle trajectory X(in.) versus Y(in.) in a trapezoidal steering/trapezoidal braking maneuver.

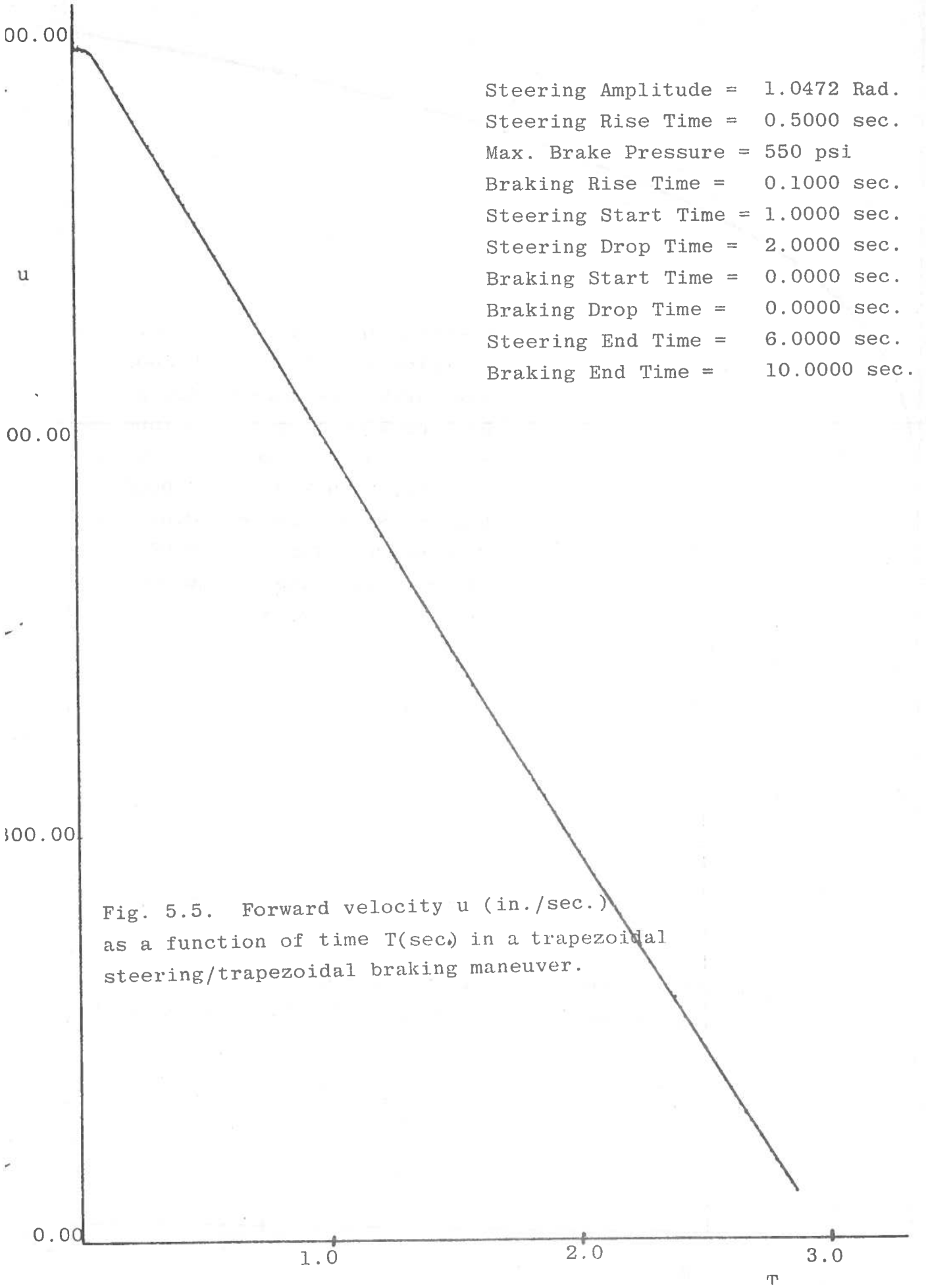

Fig. 5.5. Forward velocity u (in./sec.) as a function of time T(sec) in a trapezoidal steering/trapezoidal braking maneuver.

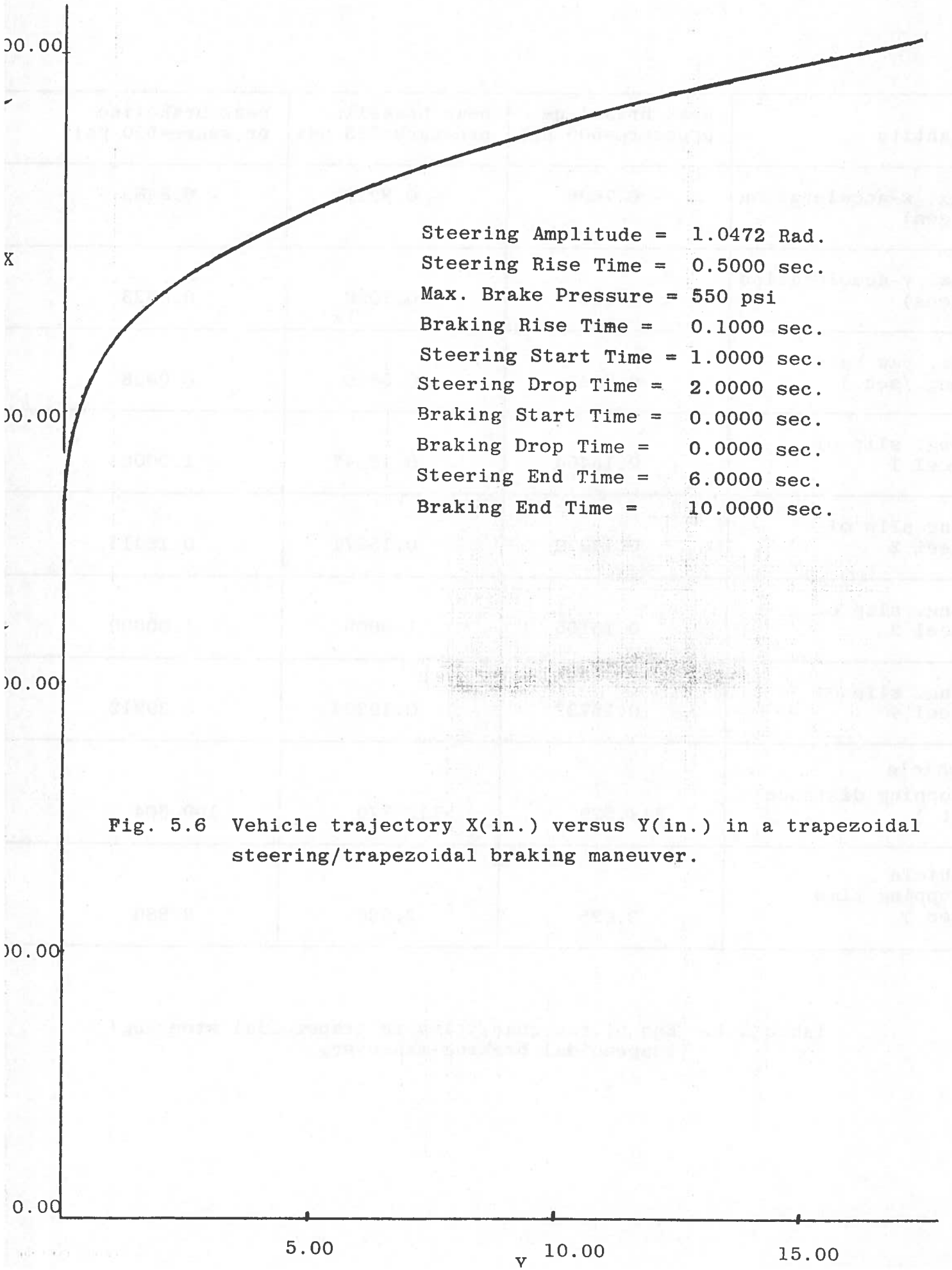

Fig. 5.6 Vehicle trajectory X(in.) versus Y(in.) in a trapezoidal steering/trapezoidal braking maneuver.

ıantity	peak brakeline pressure=500 psi	peak brakeline pressure=525 psi	peak brakeline pressure=550 psi
ıx. x-acceleration ;ees)	- 0.7668	- 0.8319	- 0.8463
ıx. y-acceleration ;ees)	0.1231	0.1096	0.0833
.x. yaw rate leg./sec.)	6.9143	6.5810	6.0908
)ng. slip of ıeel 1	0.15464	0.16147	1.00000
)ng slip of ıeel 2	0.14929	0.15671	0.16415
)ng. slip of ıeel 3	0.16105	1.0000	1.00000
)ng. slip of ıeel 4	0.15723	0.19224	0.39912
ehicle :opping distance ft.)	117.529	112.770	109.804
ehicle :opping time sec.)	3.025	2.920	2.860

Table 5.1. End of run quantities in trapezoidal steering/ trapezoidal braking maneuvers.

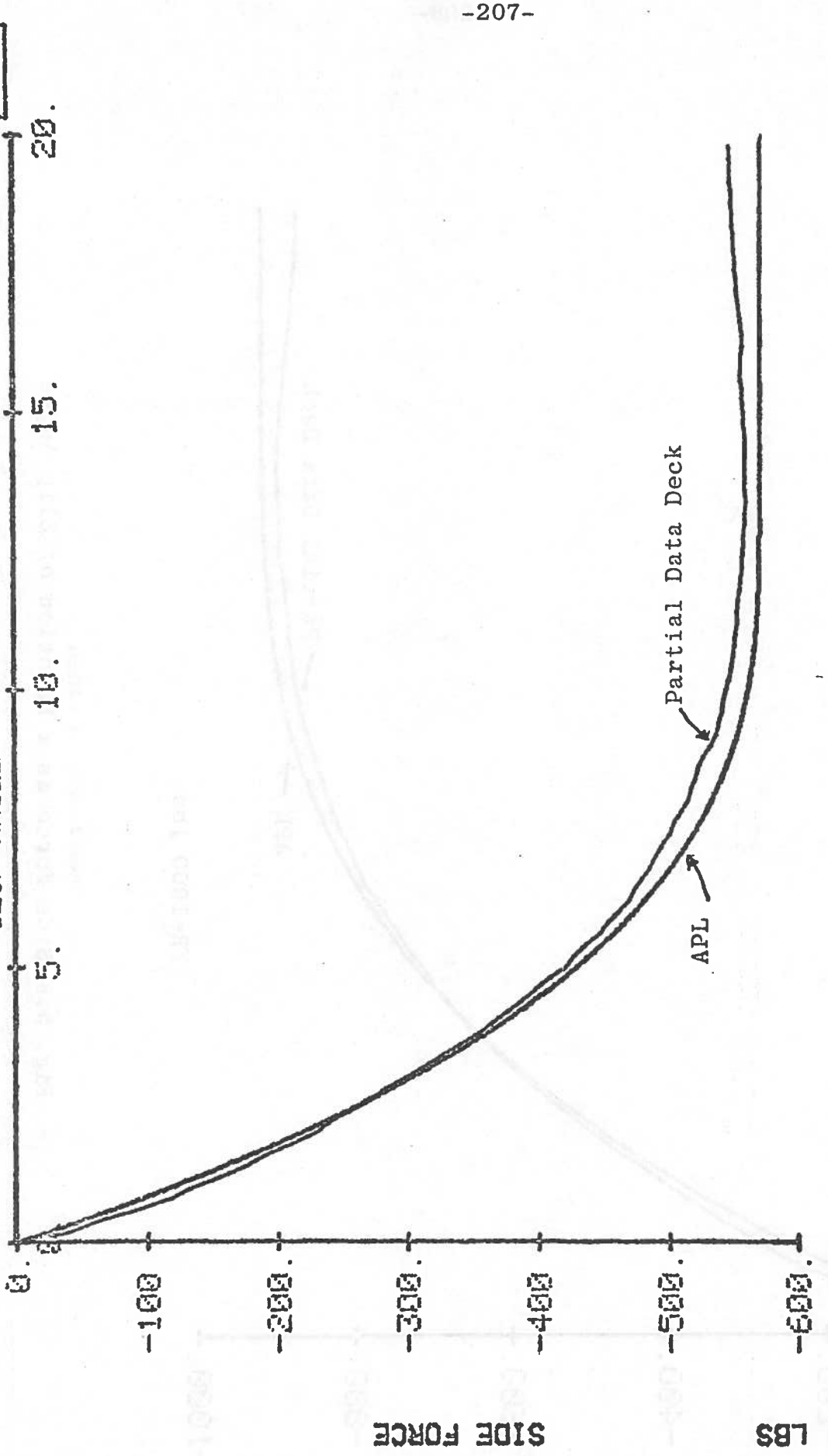

Fig. 5.7 Side Force as a Function of Slip Angle

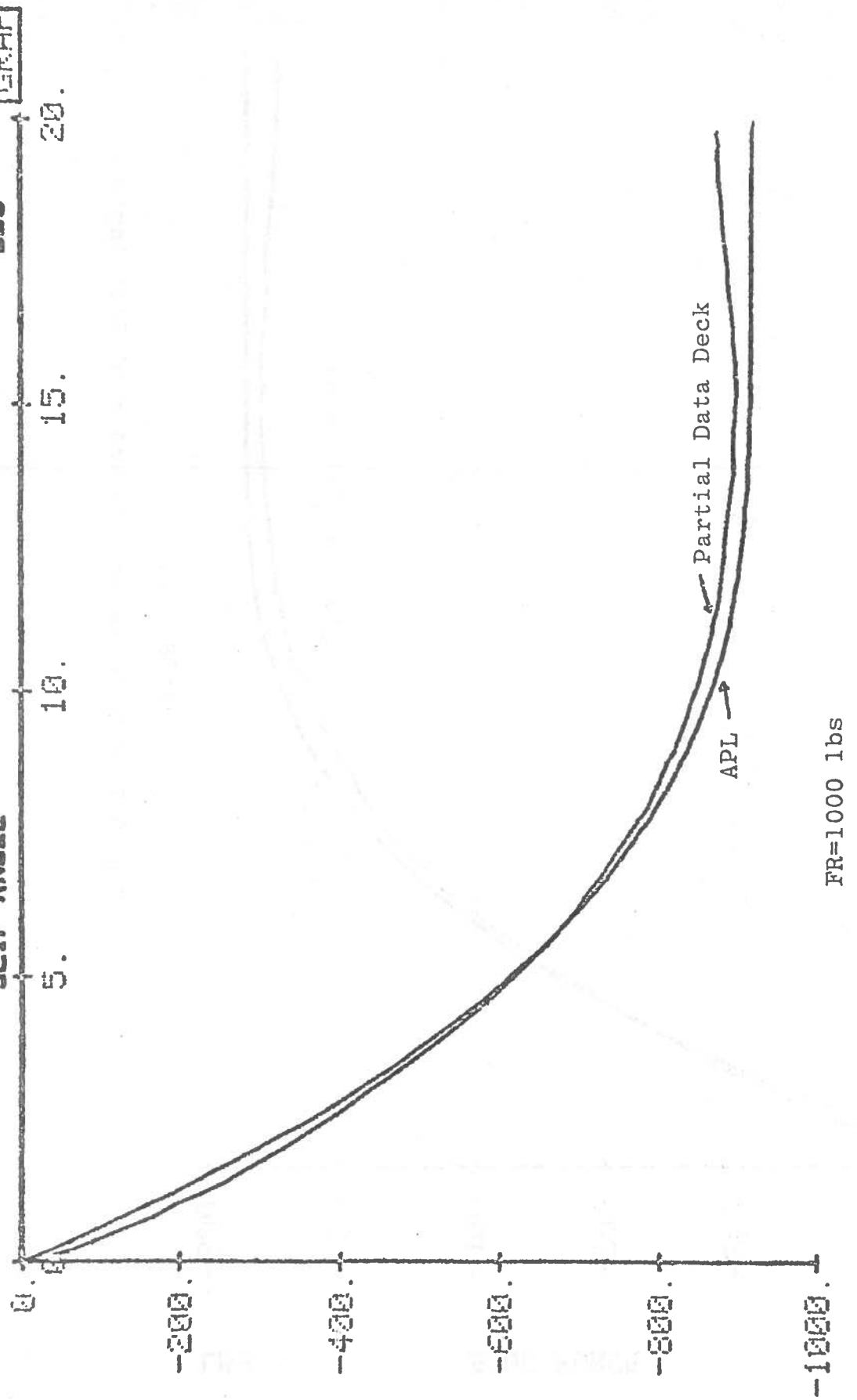

Fig. 5.8 Side Force as a Function of Slip Angle

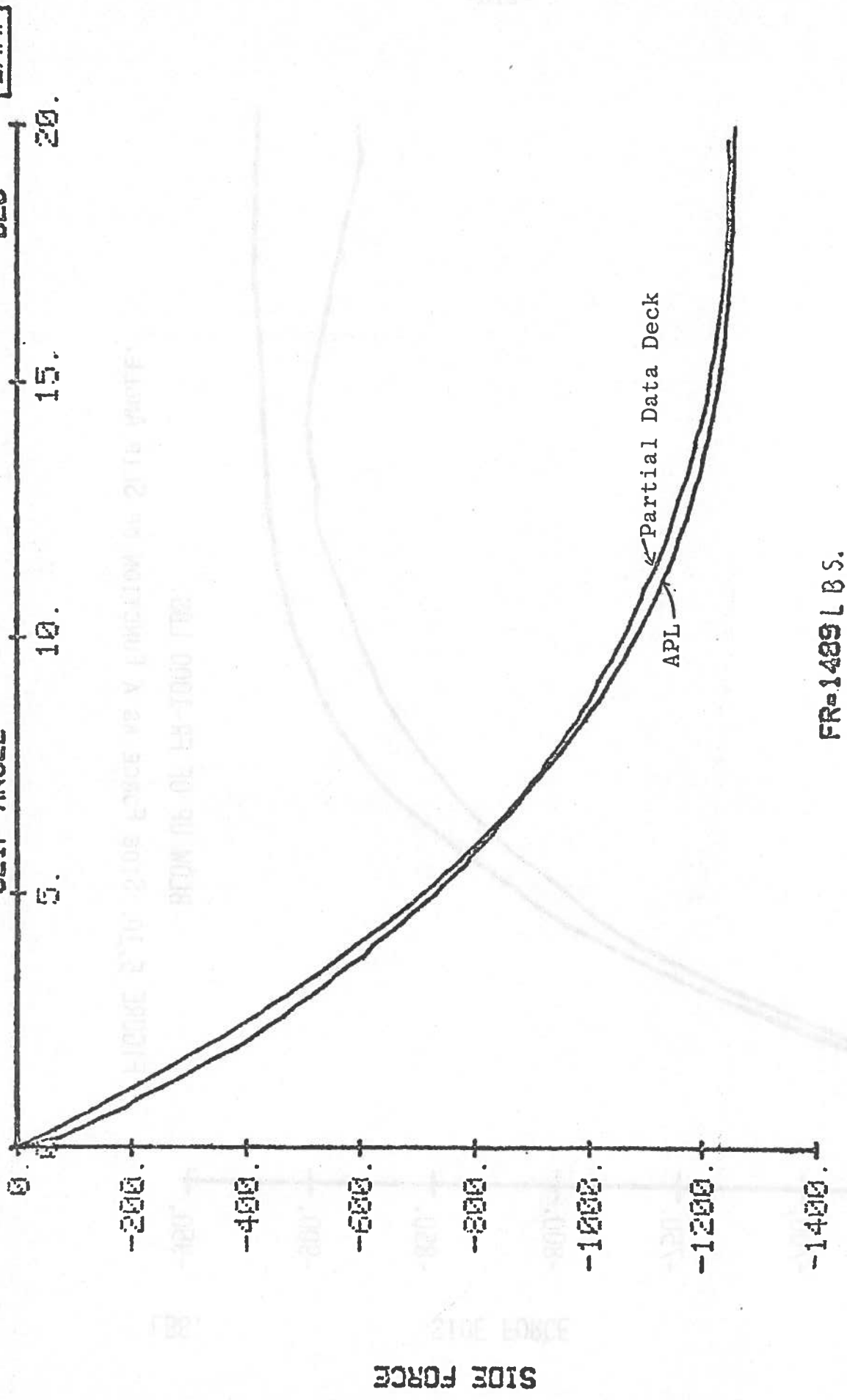

Fig. 5.9 Side Force as a Function of Slip Angle

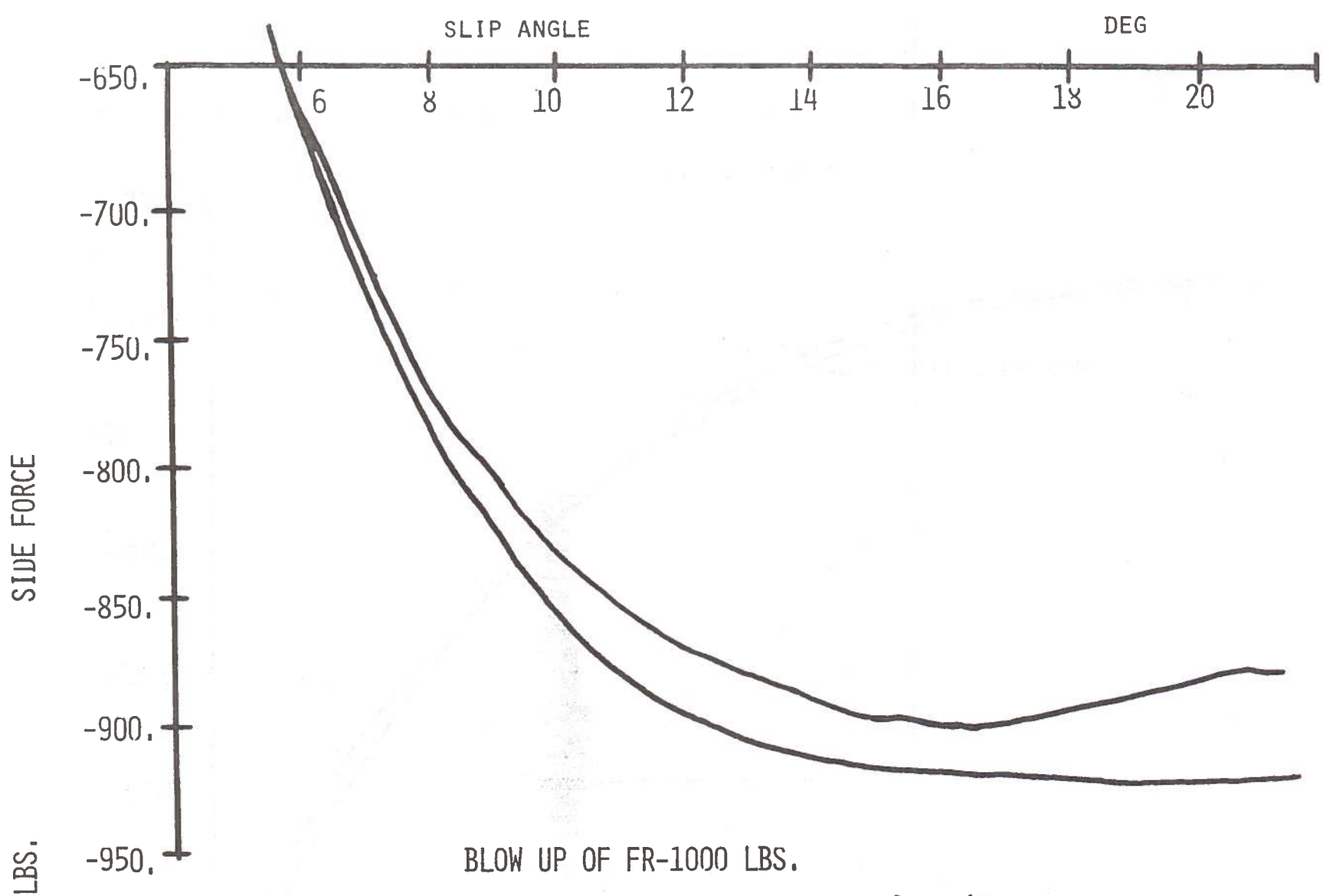

FIGURE 5.10. SIDE FORCE AS A FUNCTION OF SLIP ANGLE.

References for Chapter 5.

5.1. H.B. Pacejka, "Simplified Analysis of Steady-State Turning Behaviour of Motor Vehicles. Part 3: More Elaborate Systems, Vehicle System Dynamics, Vol. 2., 1973, pp 185-204.

CHAPTER 6. CLOSED-LOOP MANEUVERS

A major new feature of the current simulation is the capability to perform closed-loop maneuvers, a capability not present, as yet, in the APL hybrid simulation. A detailed technical discussion of the maneuvers was given in Chapter 3 and in the USER'S GUIDE. Here sample output will be presented and discussed. To the authors' knowledge, no field tests in this area have been performed and so the findings and conclusions must be regarded as tentative.

The first closed-loop maneuver treated involves a vehicle traveling at a constant-speed along a straight line (Y=0) and then subject to a wind gust. The wind gust is simulated by moving the vehicle instantaneously sideways a distance of 12 inches. The driver's task is to return the vehicle to the straight line course (Y=0) while maintaining a constant speed. The initial speed was taken to be 40 mph and, as before, the vehicle involved is a 1971 Ford Mustang.

Figs. 6.1 through 6.3 present results for the geometric preview-predictor model. The driver parameters involved are those given by Kroll [3.1]. Fig. 6.1 gives the vehicle trajectory. In the absence of field data, in all preview-predictor models the driver's neuromuscular time lag has been set to zero. An oscillatory, rapidly damped motion is seen and the system could be interpreted as stable in the sense of a rapid approach to the desired state. Figs. 6.2 and 6.3 give the steering wheel angle and the lateral velocity, respectively, as functions of time. Both show again a rapid return to the desired zero values. The rather "jerky" motion of the steering

wheel stems here, and throughout, from the nature of the command process.

Figs. 6.4 through 6.6 are results using the three-degree-of-freedeom predictor. Stability is again evident in the rapidly damped oscillations. The trajectory, δ_{sw}, and V all have less oscillations than in the geometric predictor case. The system appears to be closer to critical damping [in fact the trajectory may be overdamped]. The implication of greater stability is not too surprising in view of the more sophisticated predictor.

Figs. 6.7 through 6.9 present results for the general cross-over model. The driver parameters were obtained by requiring that the overall steering control gain have a slope of 20dB per decade at the cross-over frequencies [the authors are indebted to Mr. Calvin Matle of the Ford Motor Co. for this procedure and for the values obtained using it.]. The figures show that the maneuver in question is "stable" in the sense of the quantities rapidly going to zero. It is interesting that the vehicle trajectory and lateral velocity are very similar to those given by the geometric predictor model.

On Fig. 6.8 the effects of driver time lag and the limits set in the steering wheel velocity rate are clearly evident in the first 9.75 sec. After that time, a smoother driving process results, smoother than those in the preview-predictor models.

Results for another wind gust maneuver were also obtained and are shown in Fig. 6.10 through Fig. 6.13. In this maneuver, the driver is given the task of not only steering back to the

Y = 0 desired path, but also must slow the vehicle from 50 to 40 mph. The geometric preview-predictor driver model is the one employed. The results are very similar to those for the constant speed case. Note that the forward speed u is highly overdamped, compared to the oscillatory behavior of the trajectory, lateral velocity and steering wheel angle.

In summary of the wind gust results, it could be noted that: (i) All models executed the maneuver in an acceptable fashion. (ii) The amount of damping present should be experimentally determined and used to distinguish between driver models. (iii) Work is needed on the neuromuscular filter to improve steering response time.

The next set of closed loop maneuvers studied involved a double lane change. Fig. 6.14 shows a schematic of the desired vehicle trajectory. Figs. 6.1 , 6.16, and 6.17 give the vehicle trajectory, the steering wheel angle and the lateral velocity as given by the general cross-over model. (The ideal trapezoidal trajectory is superimposed on the actual vehicle trajectory

The maneuver on the whole is performed successfully. However considerable overshoot in the trajectory is seen, suggesting the need for further study on driver parameters. A response time lag relative to the desired path is also noted, which could indicate driver "look ahead" as suggested by Donges [3.3]. The "flat tops" in the steering wheel time history are due to the steering wheel rate limits, showing the importance of acquiring measured data in this area.

Figs. 6.18 through 6.20 present results for the same

maneuver using the three-degree-of-freedom-preview-predictor model. Overall, the maneuver is performed better than with the general cross-over model, much less overshoot occurring. It would seem however, that better parameters are required to achieve the precision that actual drivers can attain.

Figs. 6.21 through 6.23 give results for the double lane change maneuver using the geometric preview predictor model. The results, though not bad for the transient portion of the maneuver, are on the whole bad since the driver is unable to recover. For such maneuvers, more work needs to be done on the geometric-preview-predictor model if it is to be a viable option.

The main features of the double lane change results may be summarized as follows: The general cross-over model and the three-degree-of-freedom model performed acceptably, even though the maneuver was quite severe, lateral accelerations of 0.40g to 0.65g occurring, depending on the model. It should be noted that in normal driving lateral accelerations of 0.30g are rarely exceeded, so some human drivers may have trouble with the maneuver. It is also recommended that the geometric-preview-predictor model be used for maneuvers only in the linear regime.

Figs. 6.24 through 6.27 give results for a cornering maneuver. The initial vehicle speed is 20 mph. The desired vehicle path is a straight line for 100 inches and then a circular path of radius 1600 inches, while maintaining the 20 mph speed. The models used are the general cross-over model (Figs. 6.26 and 6.27) and a modified cross-over model (Figs. 6.24 and 6.24) in which, in the spirit of Donges's [3.3] work, a term propor-

tional to the curvature of the desired path is added to the steering wheel angle. Both models lead to an acceptable trajectory, with only minor differences between Figs. 6.24 and 6.26 being noted. It was hoped that addition of the path curvature term would eliminate the "spikes" in the steering time history, but as Figs. 6.25 and 6.27 show, only minor effects arise. More studies are needed in this area.

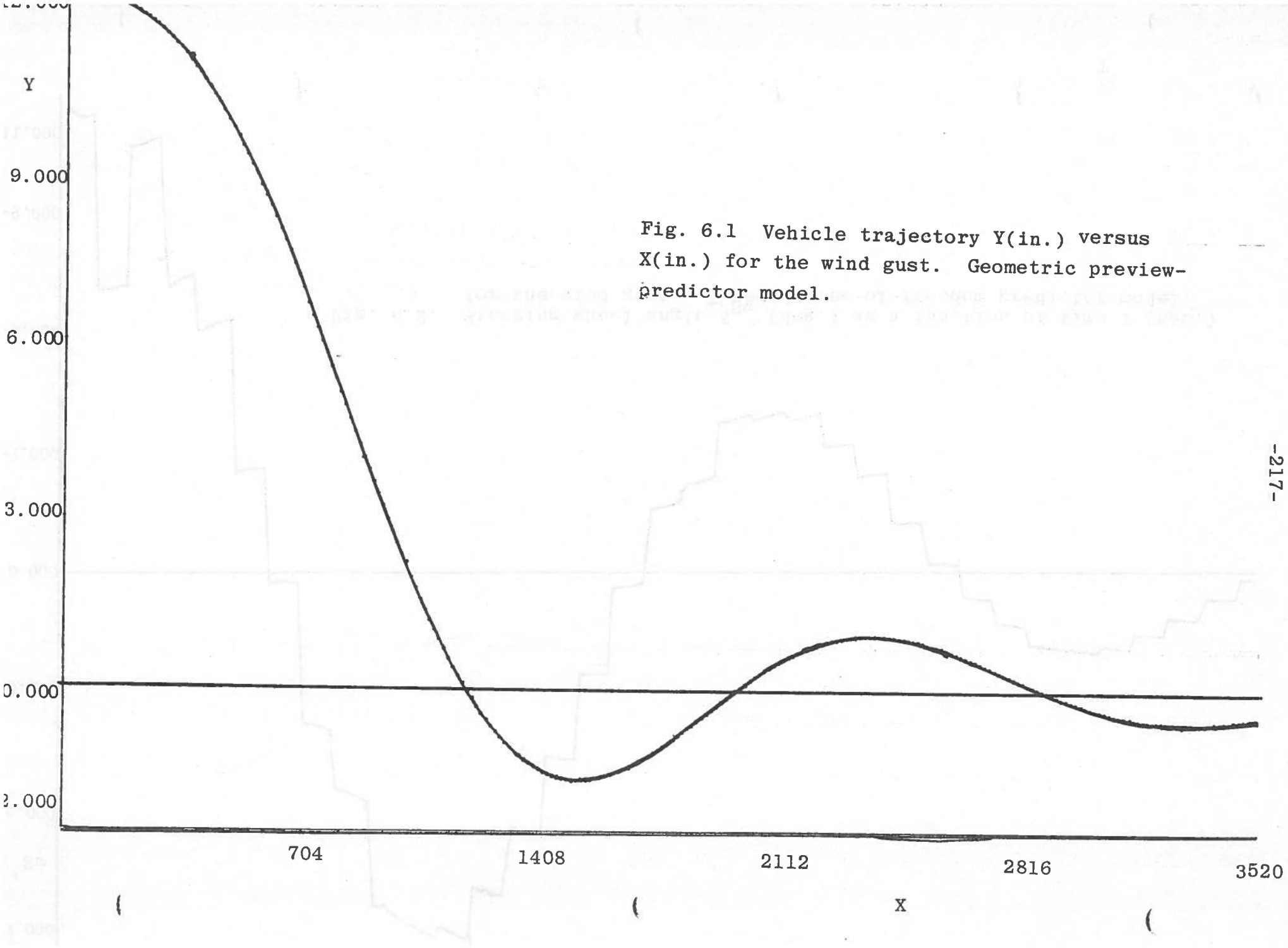

Fig. 6.1 Vehicle trajectory Y(in.) versus X(in.) for the wind gust. Geometric preview-predictor model.

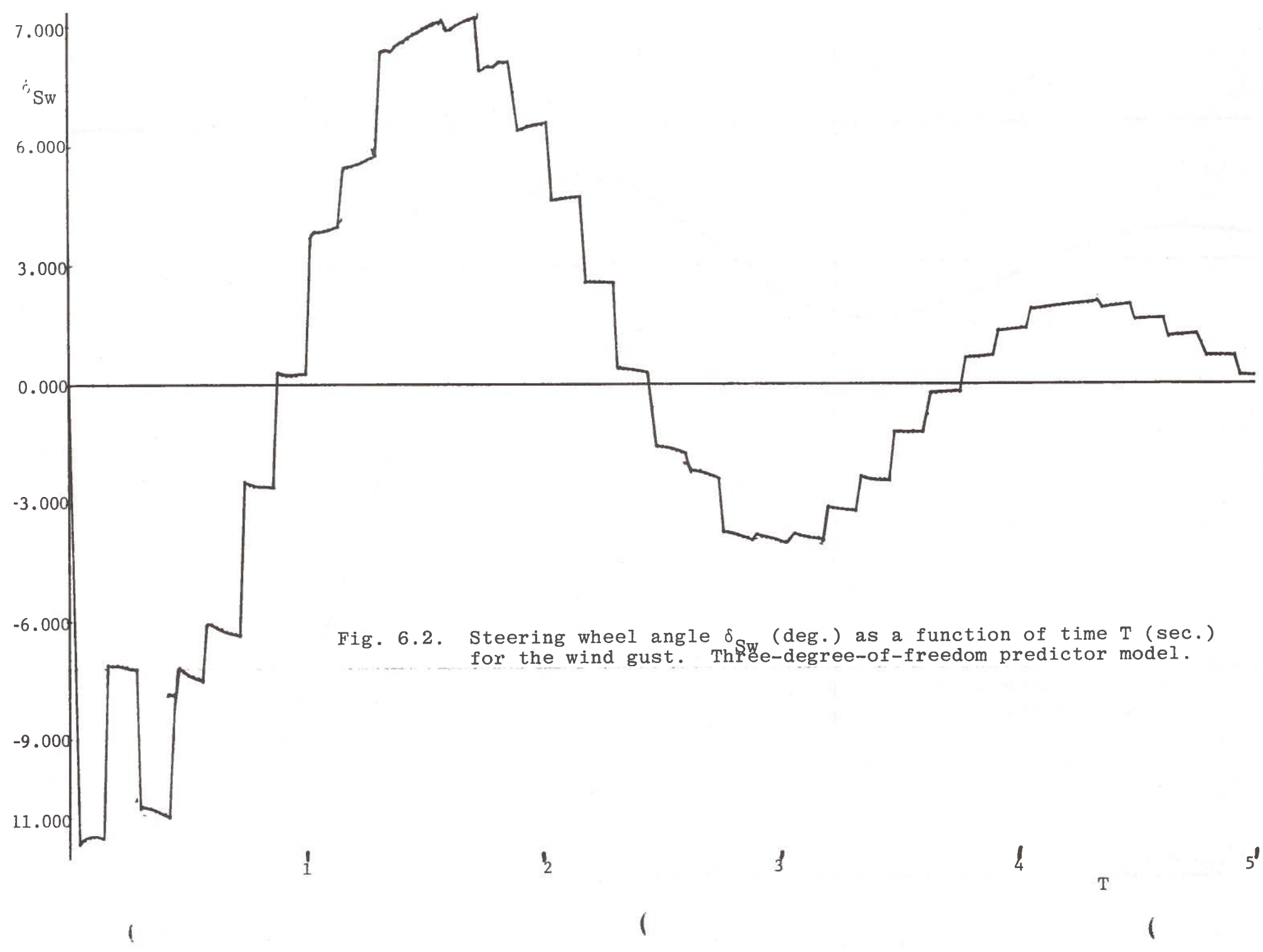

Fig. 6.2. Steering wheel angle δ_{Sw} (deg.) as a function of time T (sec.) for the wind gust. Three-degree-of-freedom predictor model.

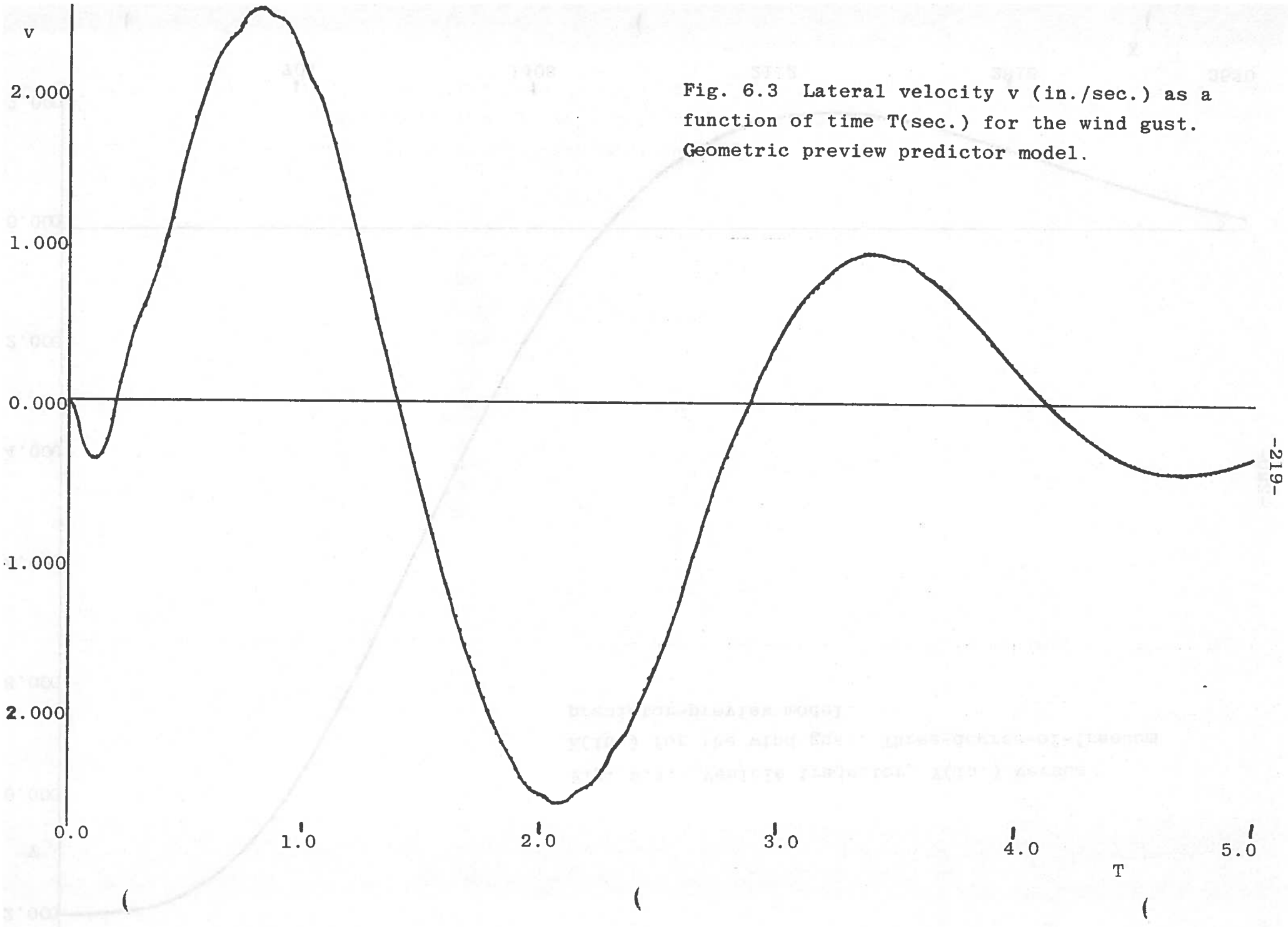

Fig. 6.3 Lateral velocity v (in./sec.) as a function of time T(sec.) for the wind gust. Geometric preview predictor model.

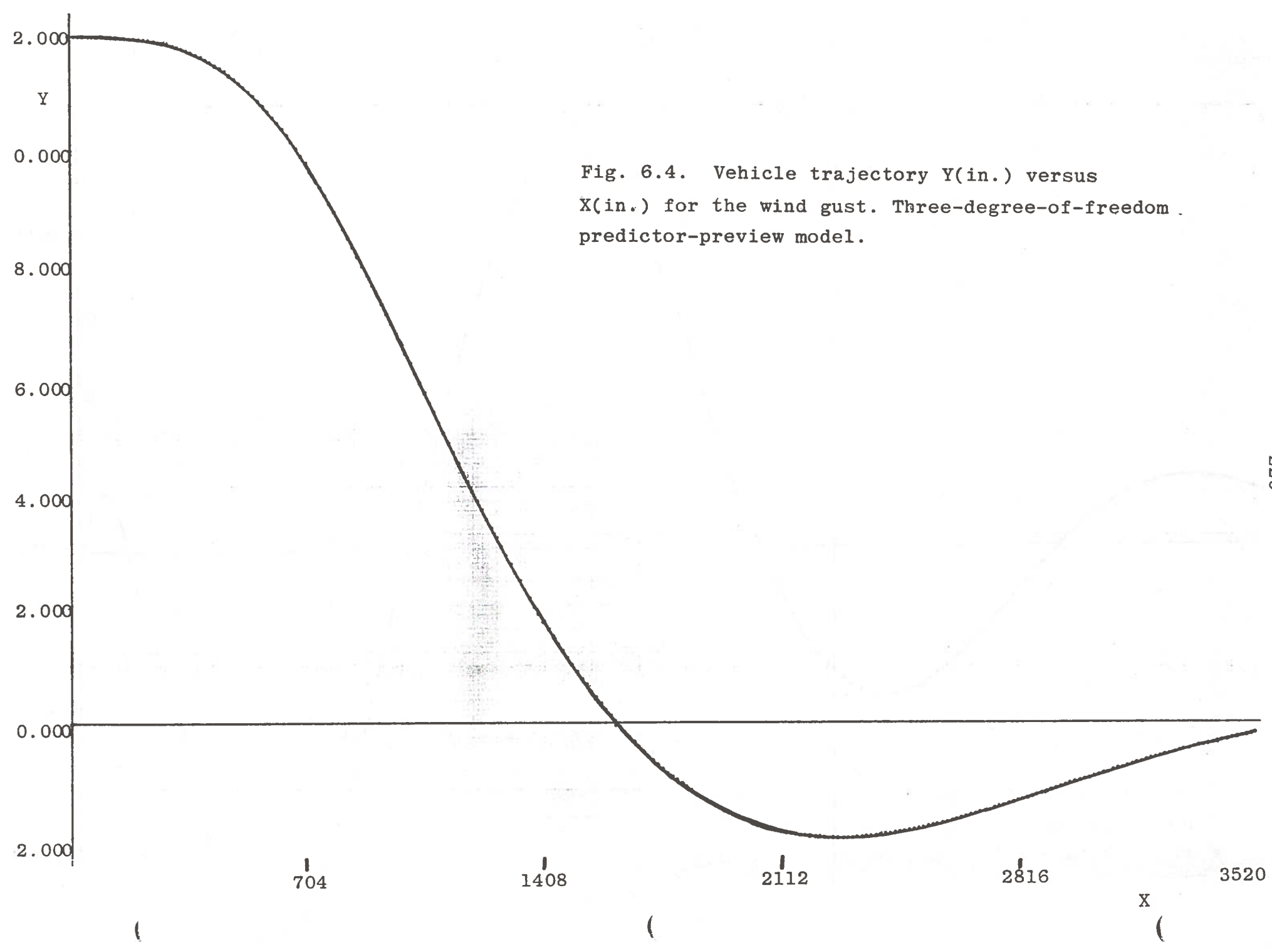

Fig. 6.4. Vehicle trajectory Y(in.) versus X(in.) for the wind gust. Three-degree-of-freedom predictor-preview model.

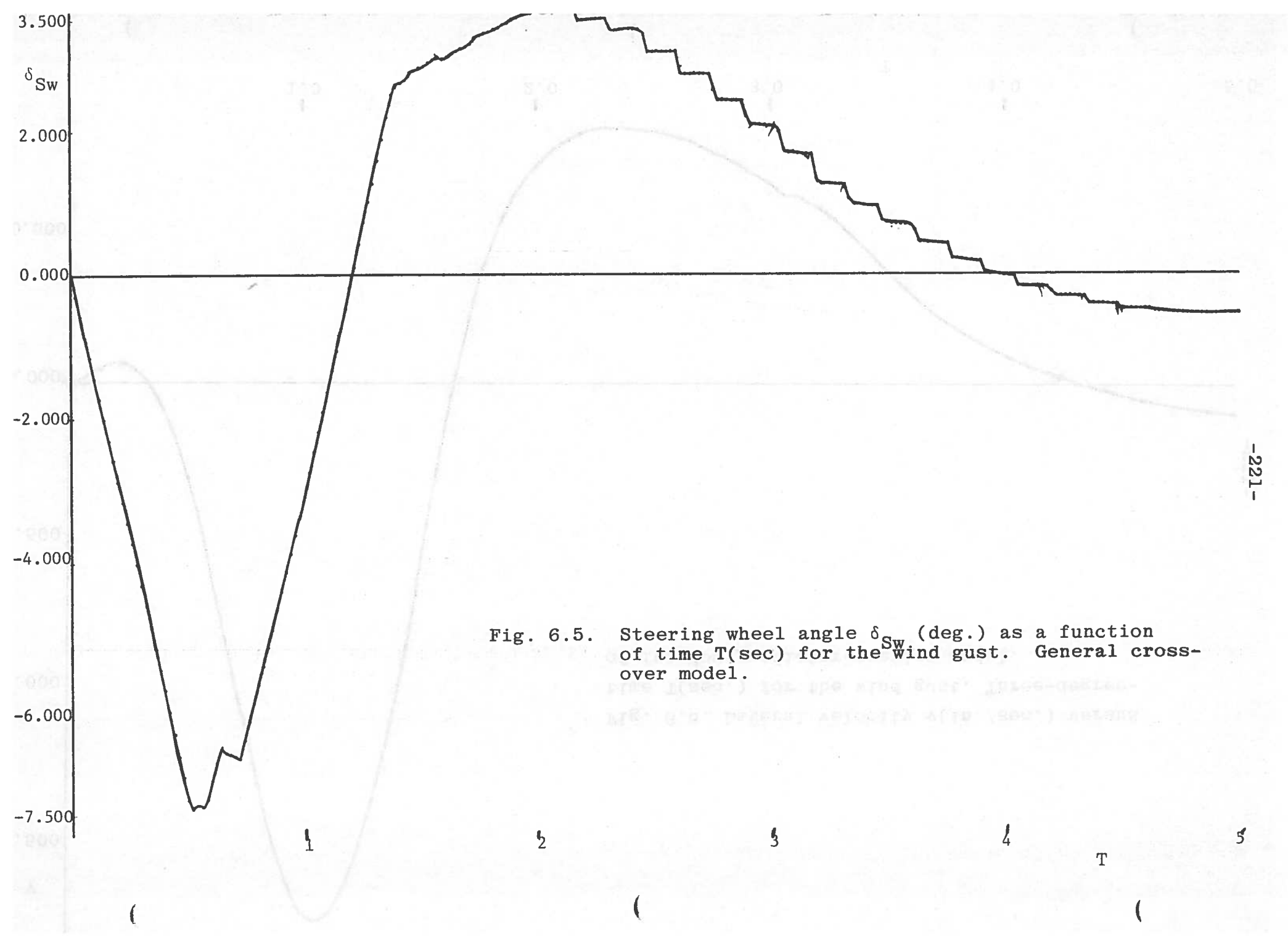

Fig. 6.5. Steering wheel angle δ_{Sw} (deg.) as a function of time T(sec) for the wind gust. General cross-over model.

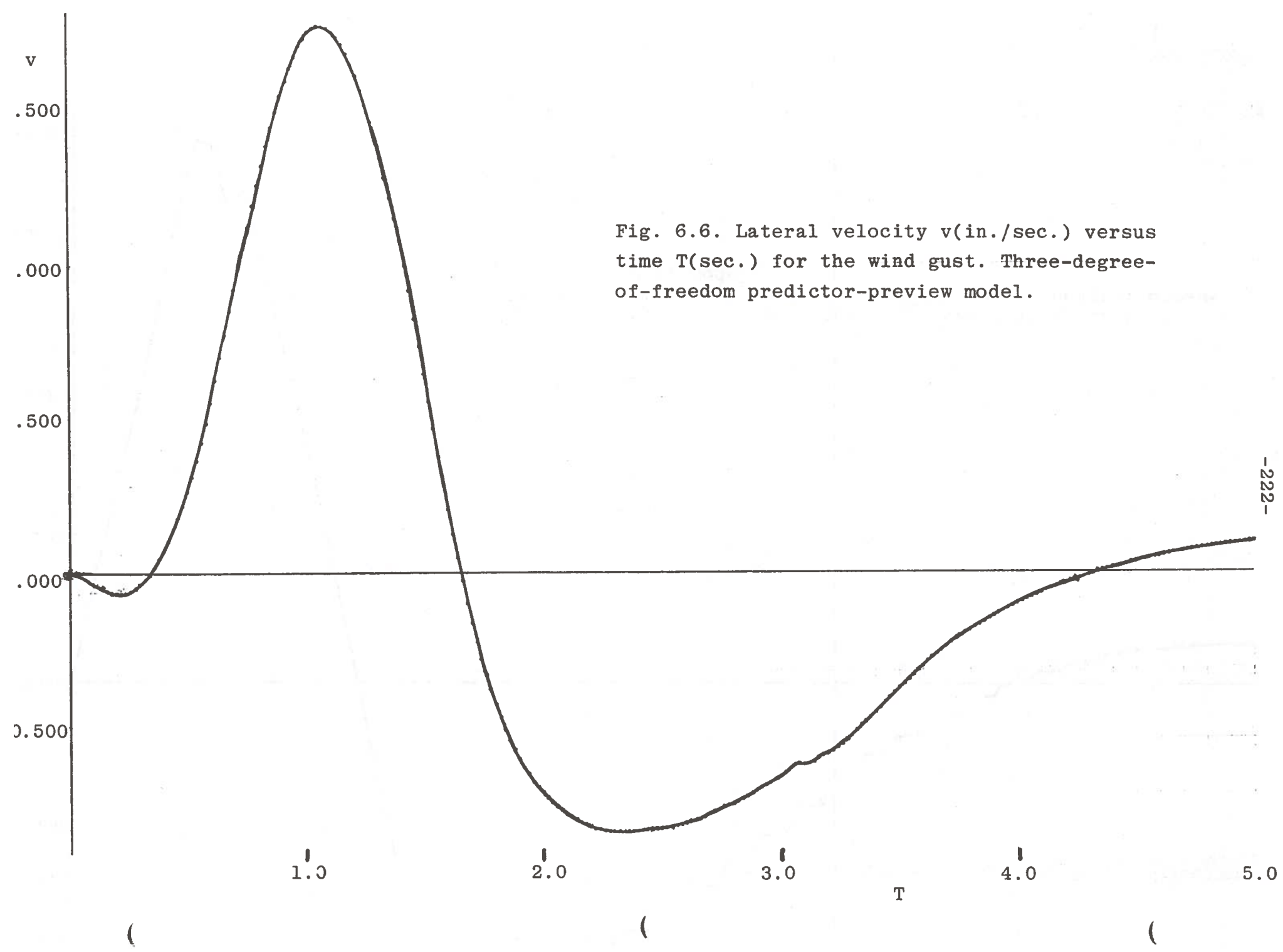

Fig. 6.6. Lateral velocity v(in./sec.) versus time T(sec.) for the wind gust. Three-degree-of-freedom predictor-preview model.

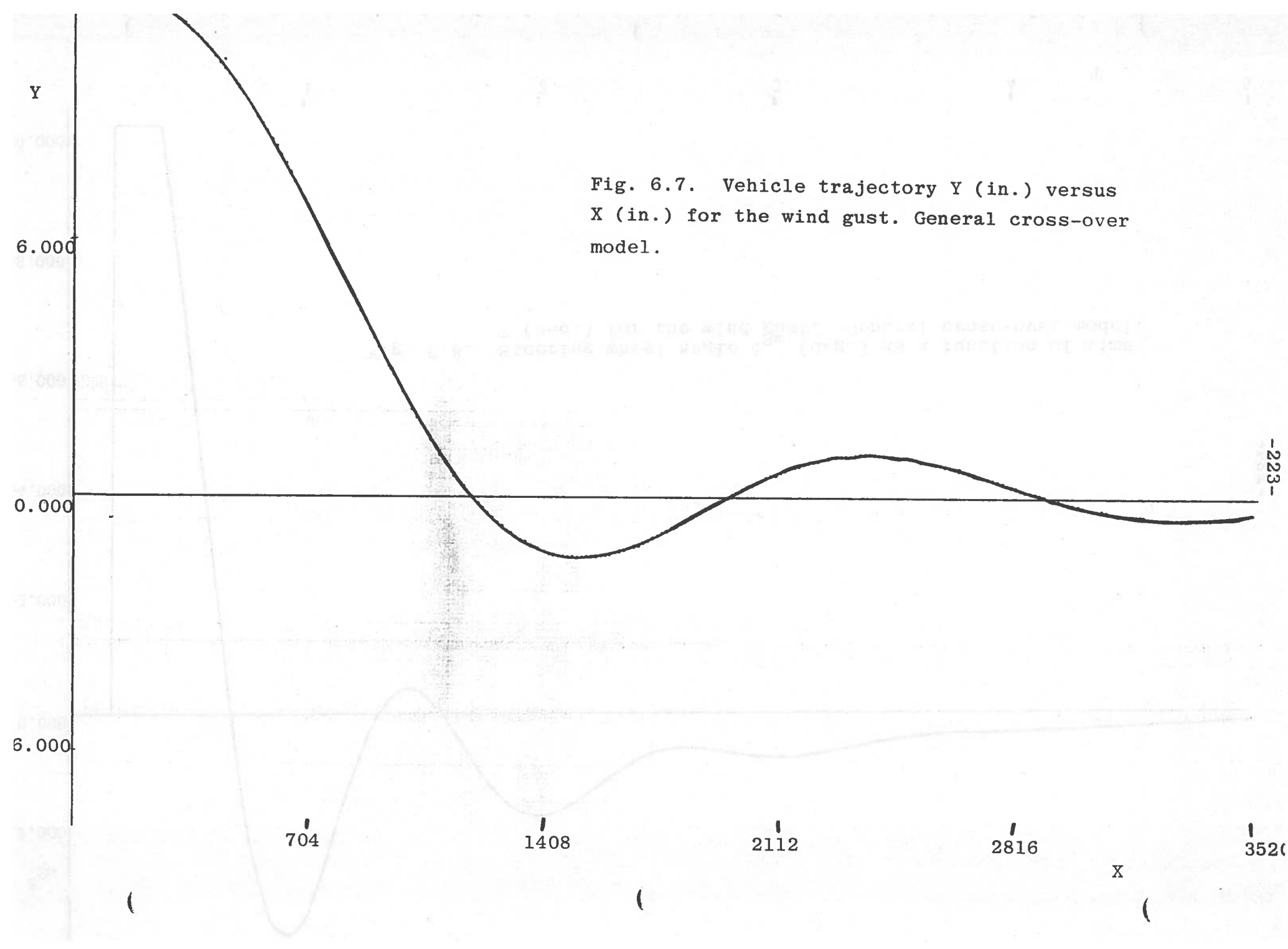

Fig. 6.7. Vehicle trajectory Y (in.) versus X (in.) for the wind gust. General cross-over model.

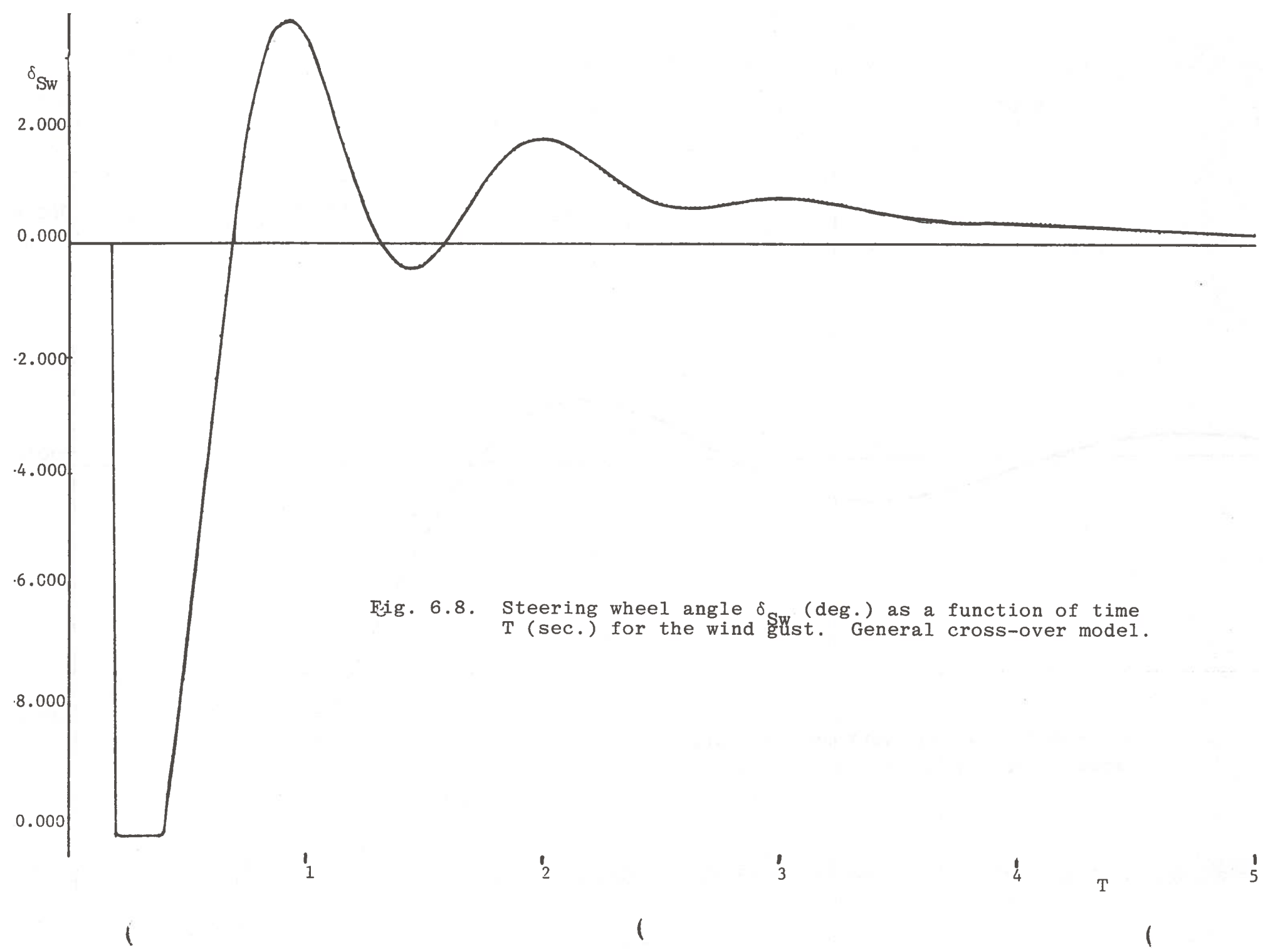

Fig. 6.8. Steering wheel angle δ_{Sw} (deg.) as a function of time T (sec.) for the wind gust. General cross-over model.

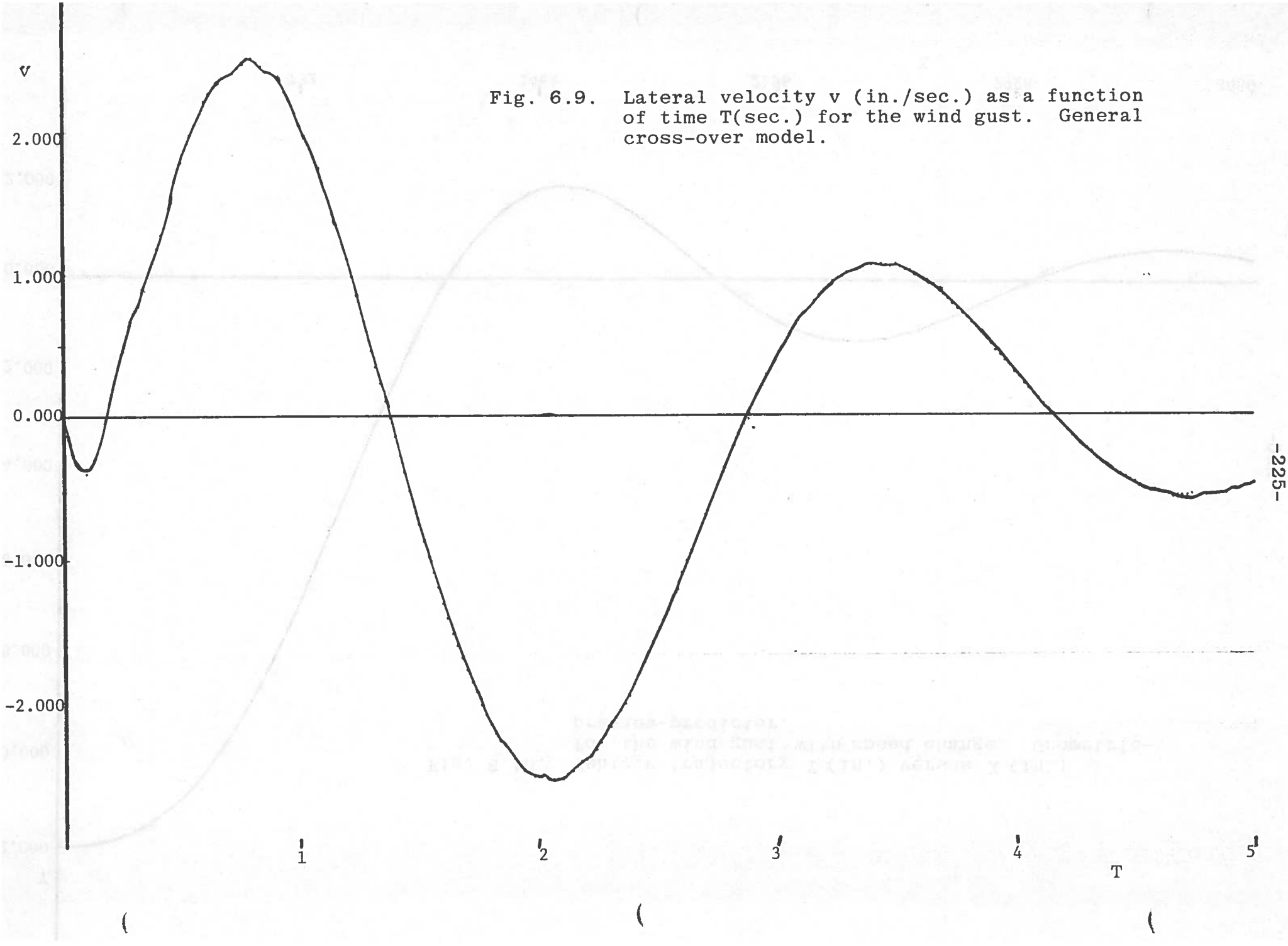

Fig. 6.9. Lateral velocity v (in./sec.) as a function of time T(sec.) for the wind gust. General cross-over model.

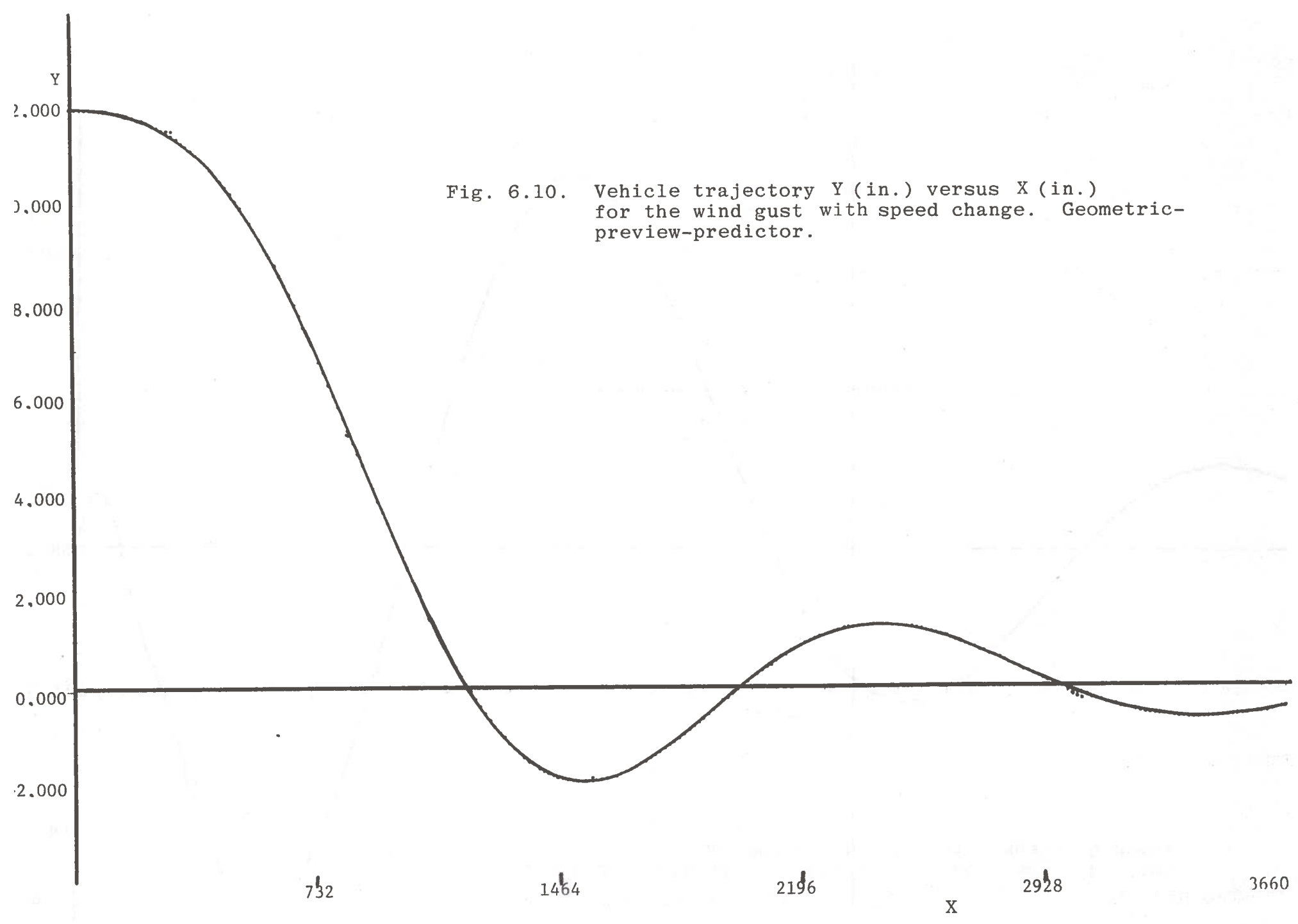

Fig. 6.10. Vehicle trajectory Y (in.) versus X (in.) for the wind gust with speed change. Geometric-preview-predictor.

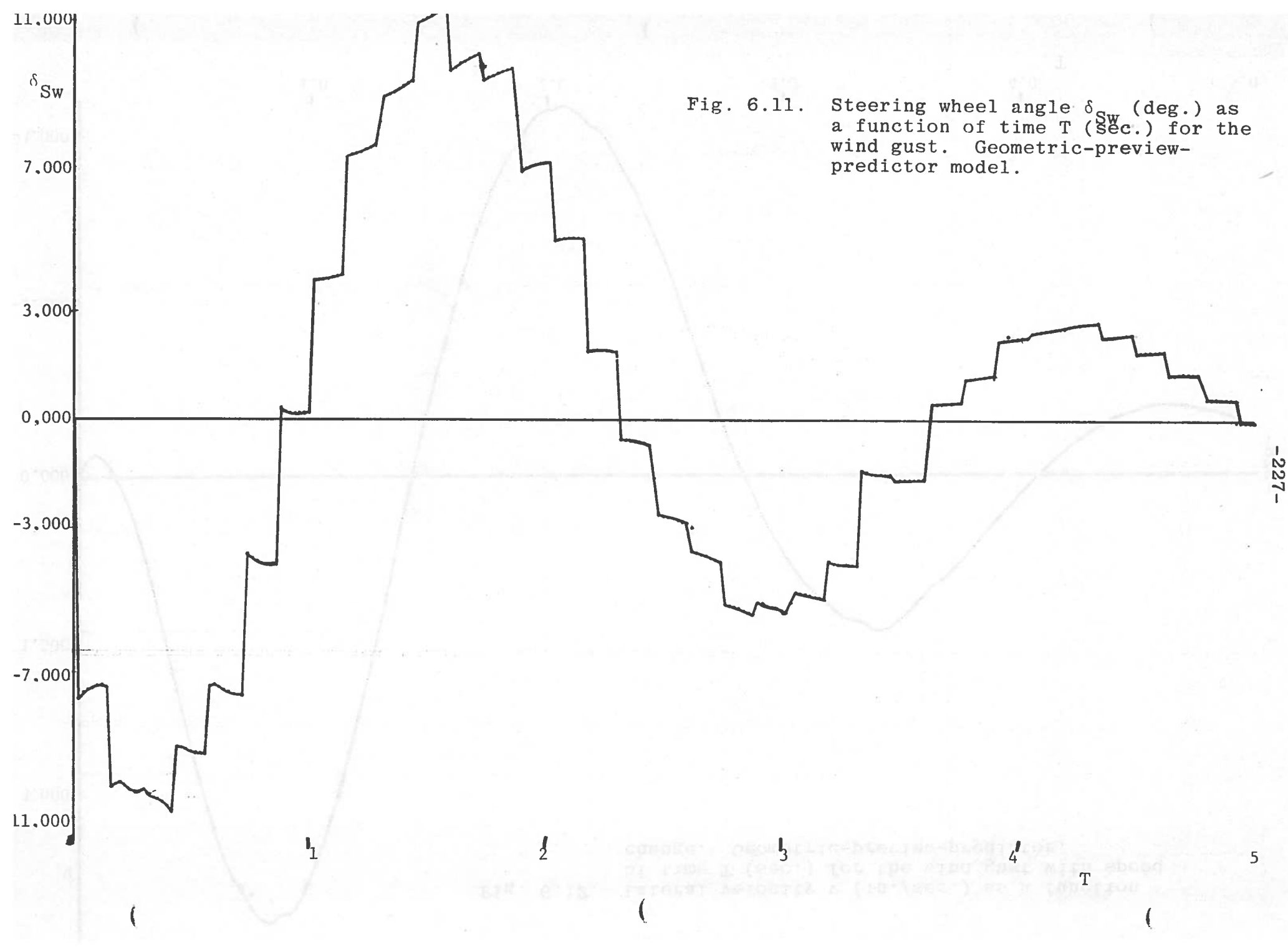

Fig. 6.11. Steering wheel angle δ_{Sw} (deg.) as a function of time T (sec.) for the wind gust. Geometric-preview-predictor model.

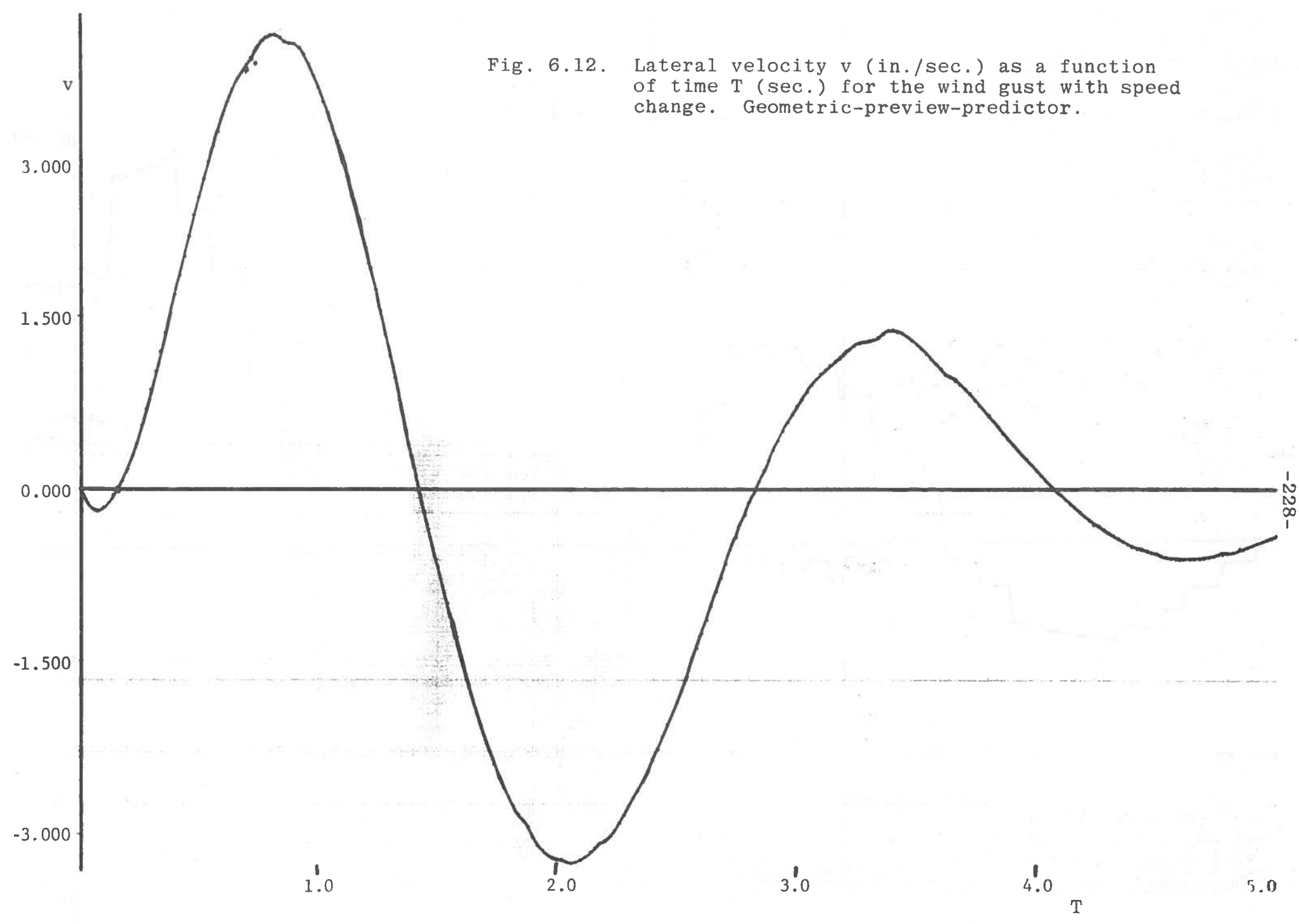

Fig. 6.12. Lateral velocity v (in./sec.) as a function of time T (sec.) for the wind gust with speed change. Geometric-preview-predictor.

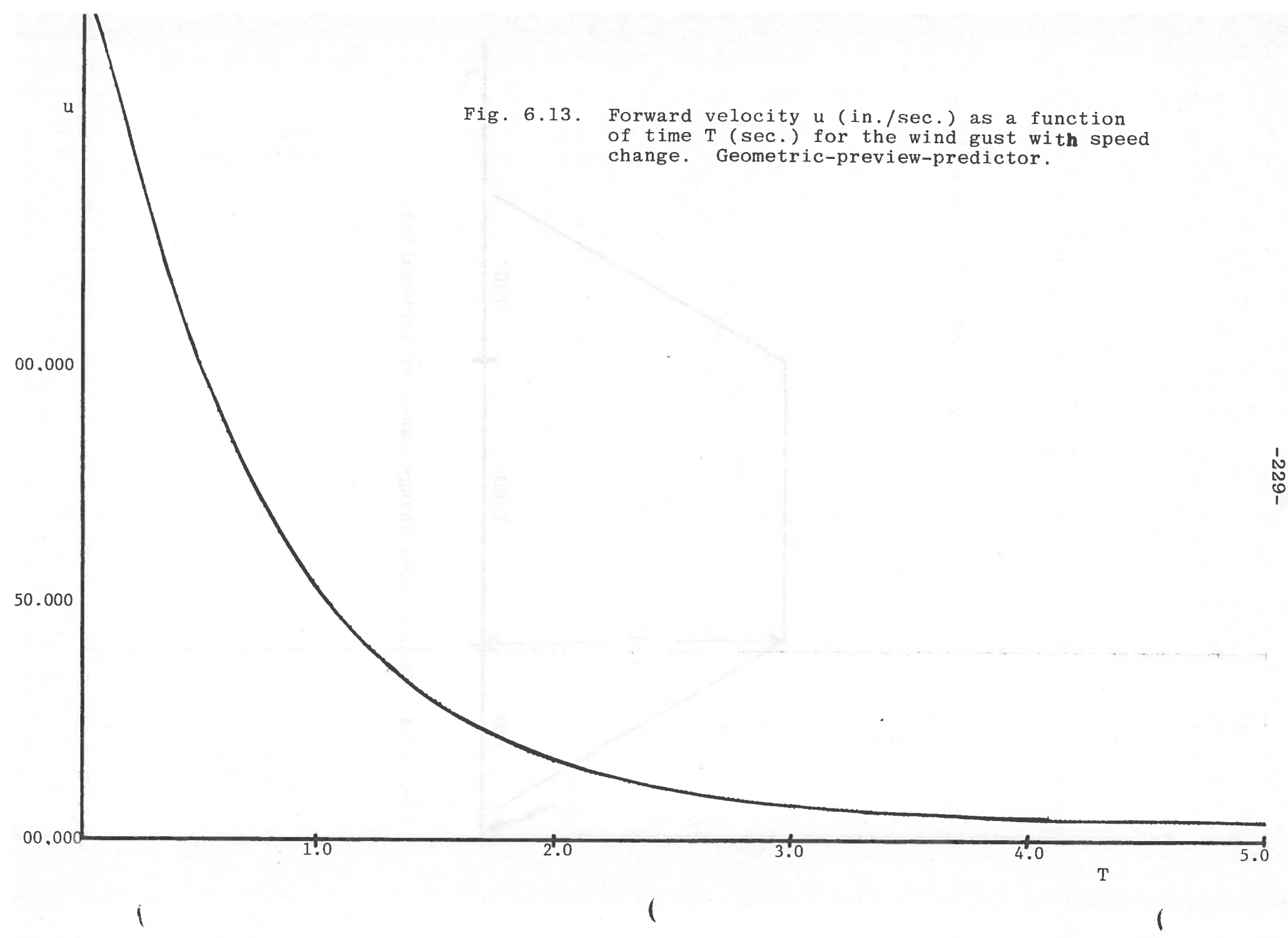

Fig. 6.13. Forward velocity u (in./sec.) as a function of time T (sec.) for the wind gust with speed change. Geometric-preview-predictor.

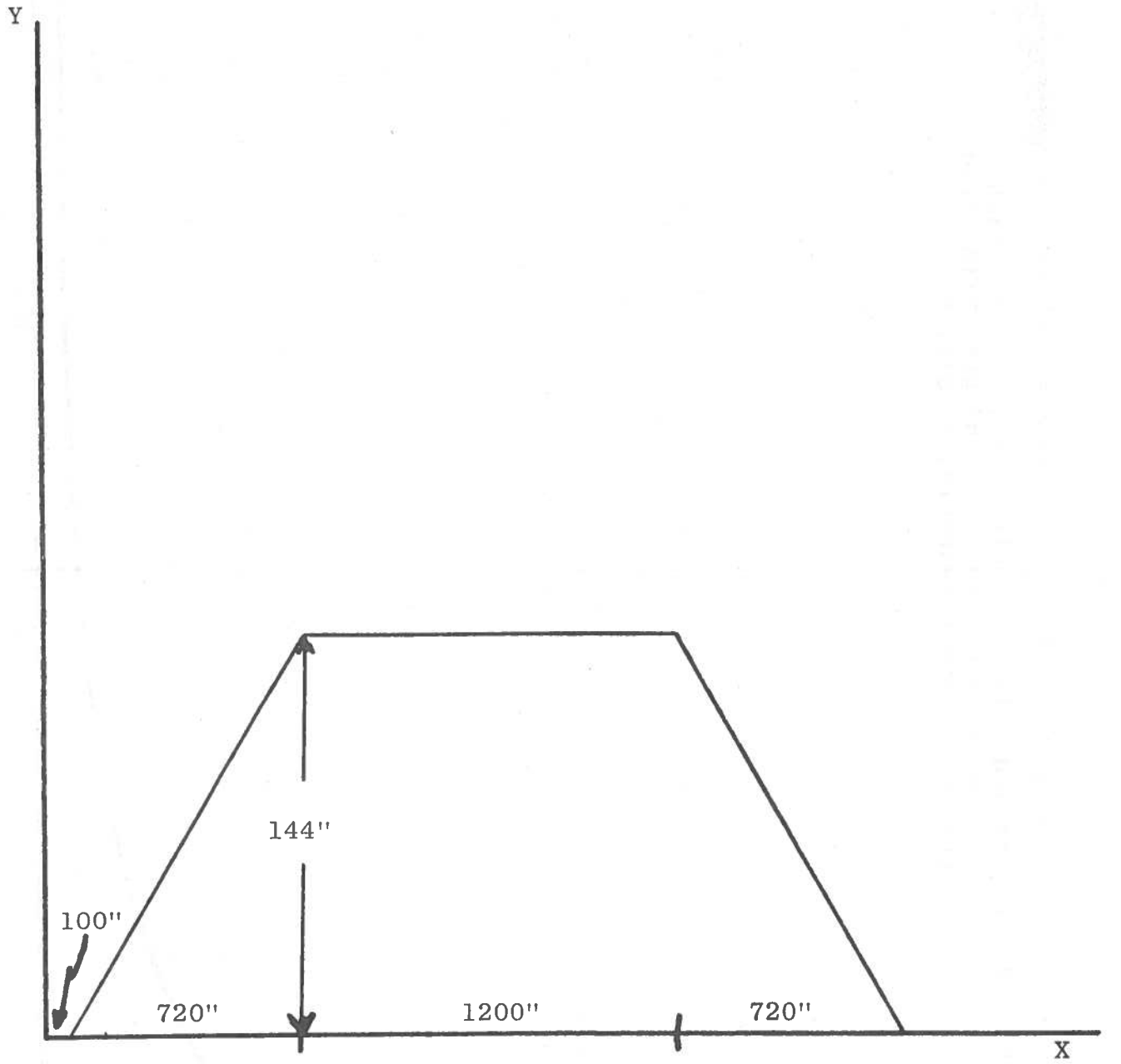

Fig. 6.14. Double lane change maneuver (schematic).

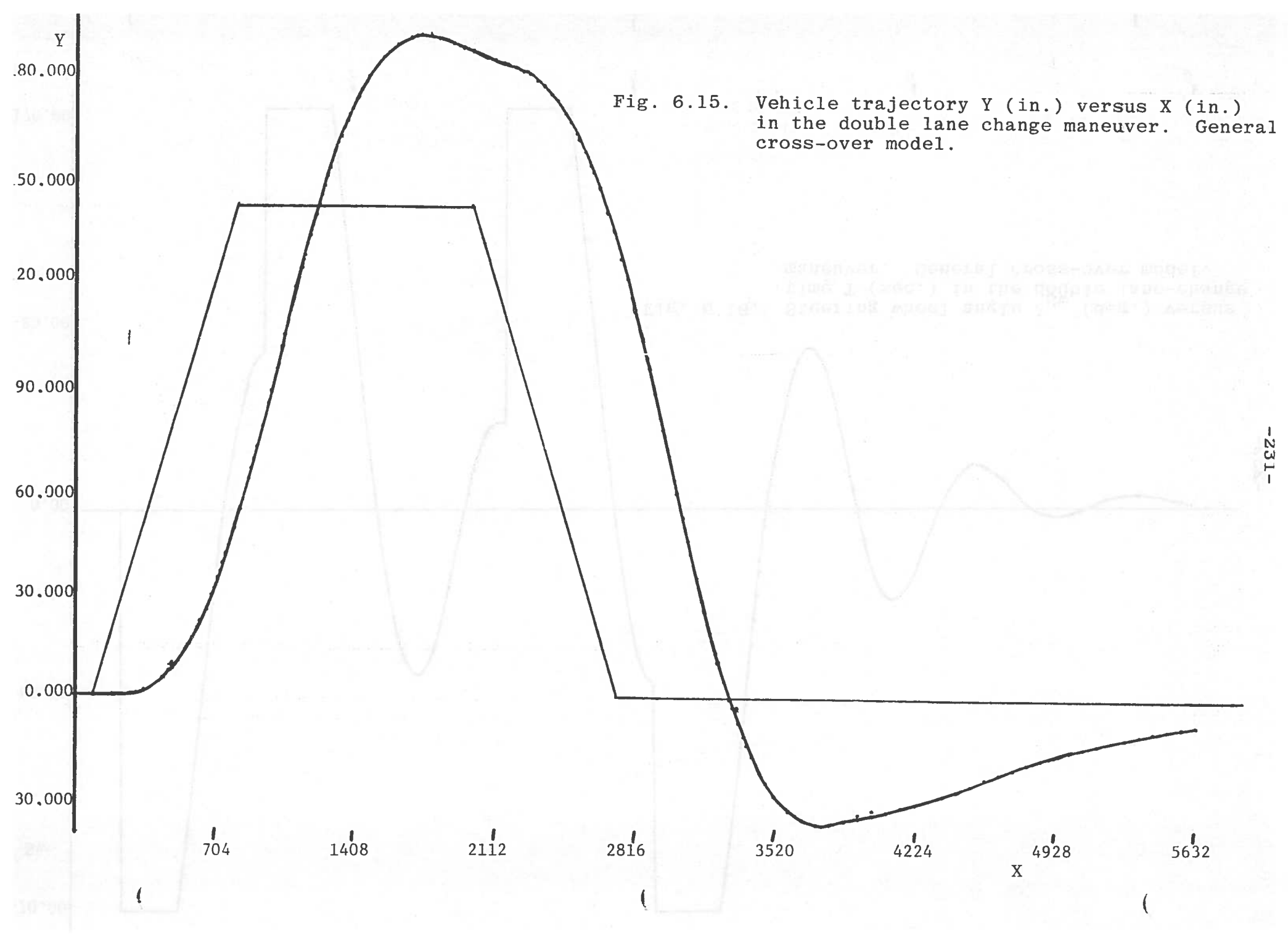

Fig. 6.15. Vehicle trajectory Y (in.) versus X (in.) in the double lane change maneuver. General cross-over model.

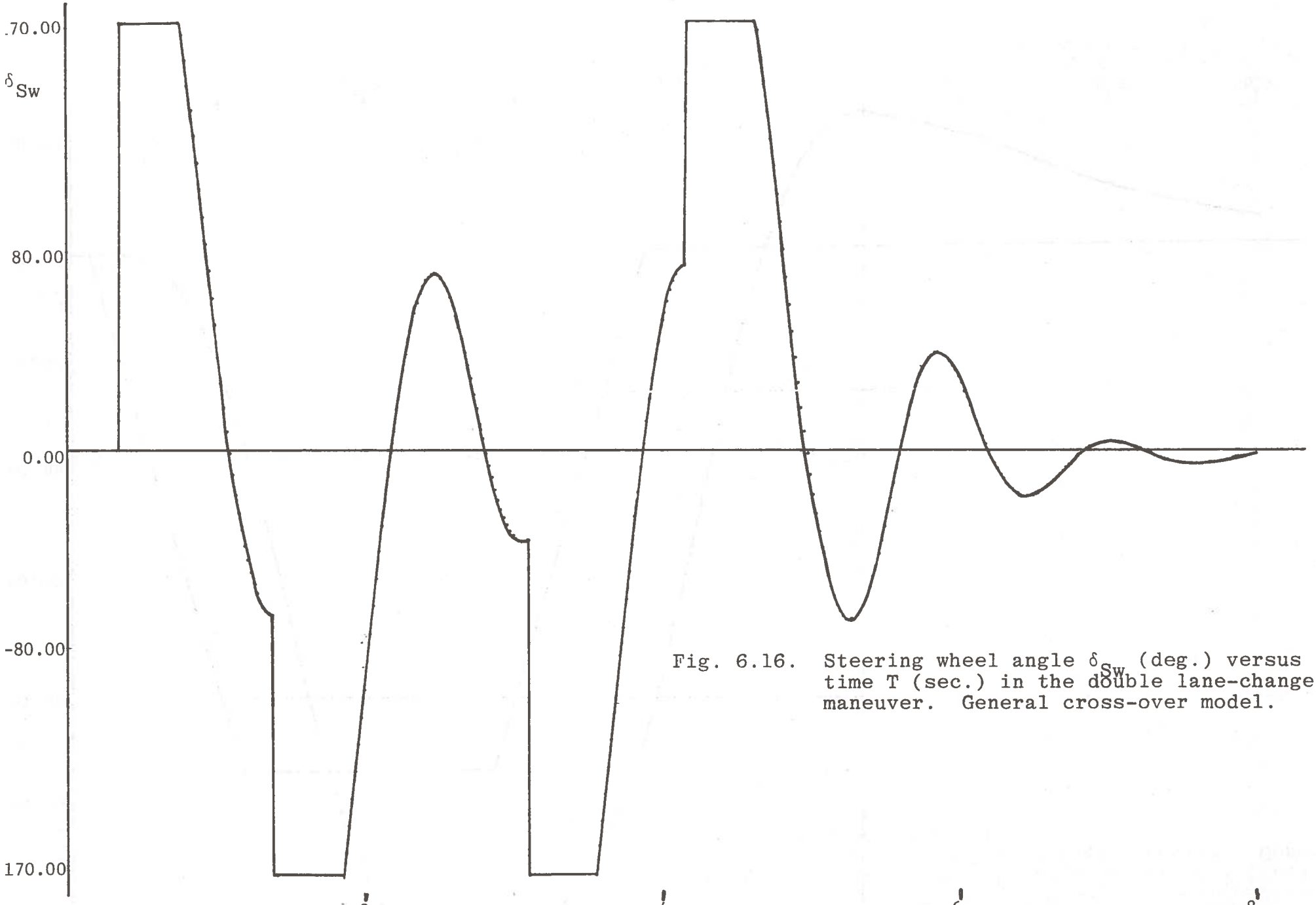

Fig. 6.16. Steering wheel angle δ_{Sw} (deg.) versus time T (sec.) in the double lane-change maneuver. General cross-over model.

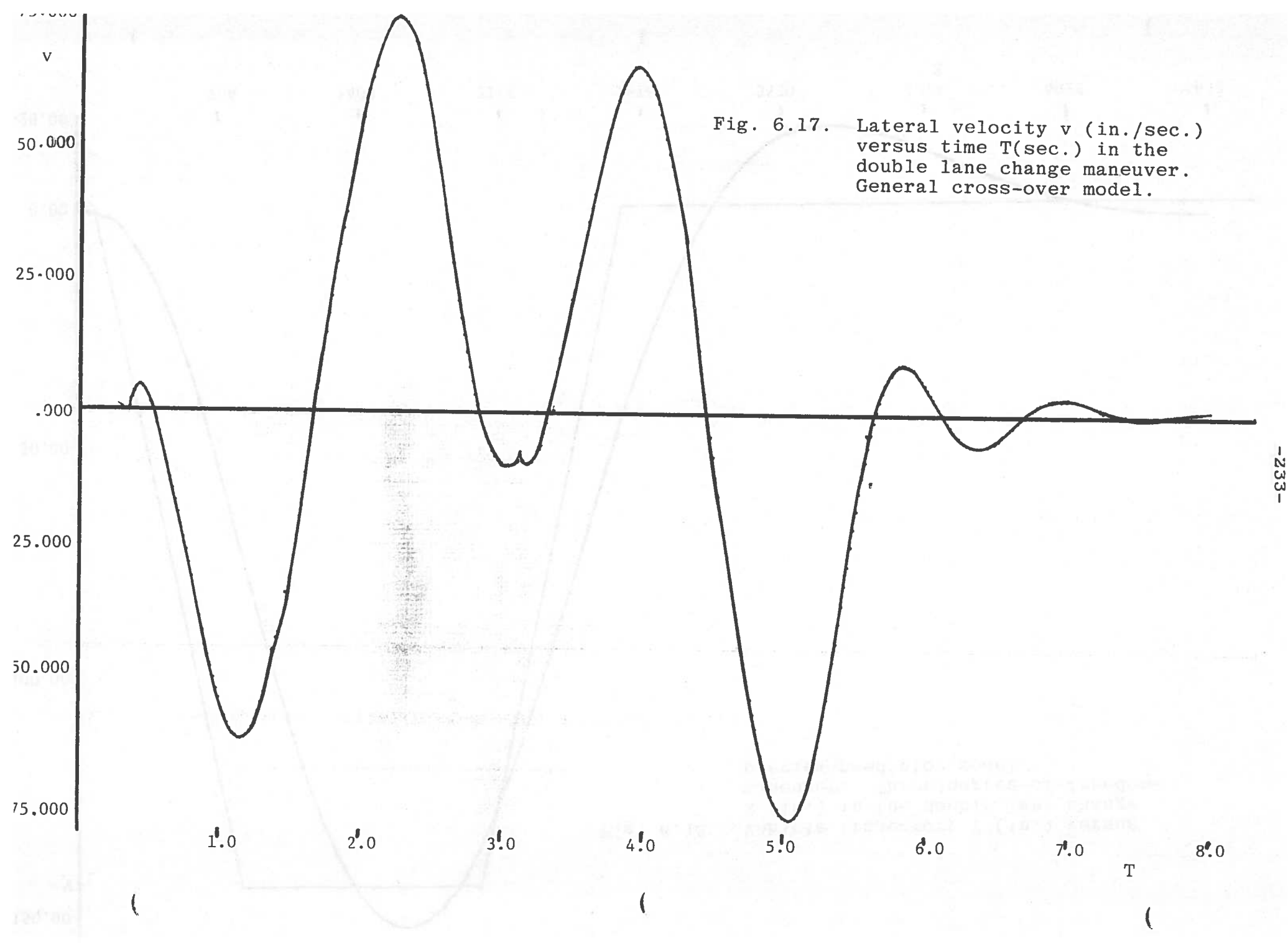

Fig. 6.17. Lateral velocity v (in./sec.) versus time T(sec.) in the double lane change maneuver. General cross-over model.

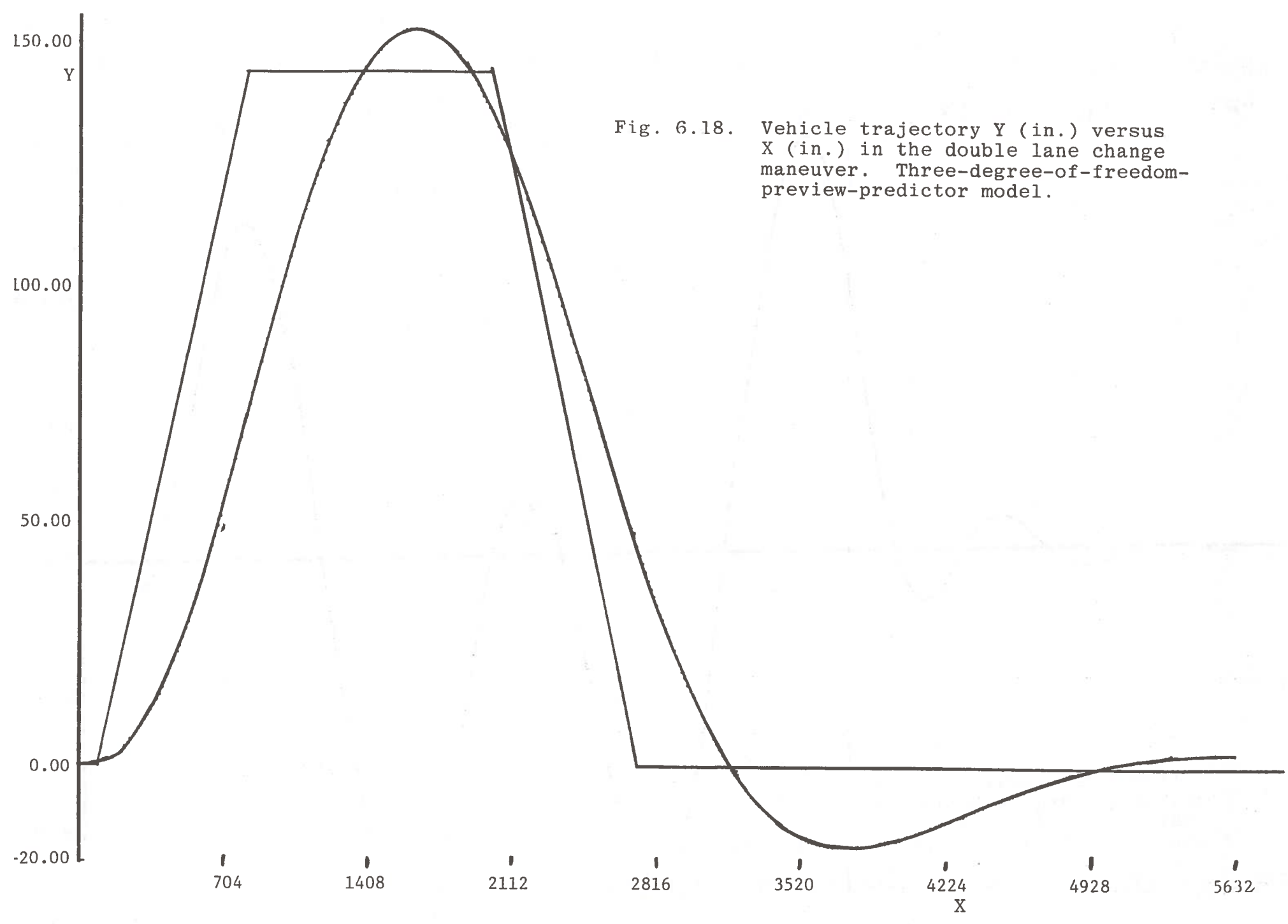

Fig. 6.18. Vehicle trajectory Y (in.) versus X (in.) in the double lane change maneuver. Three-degree-of-freedom-preview-predictor model.

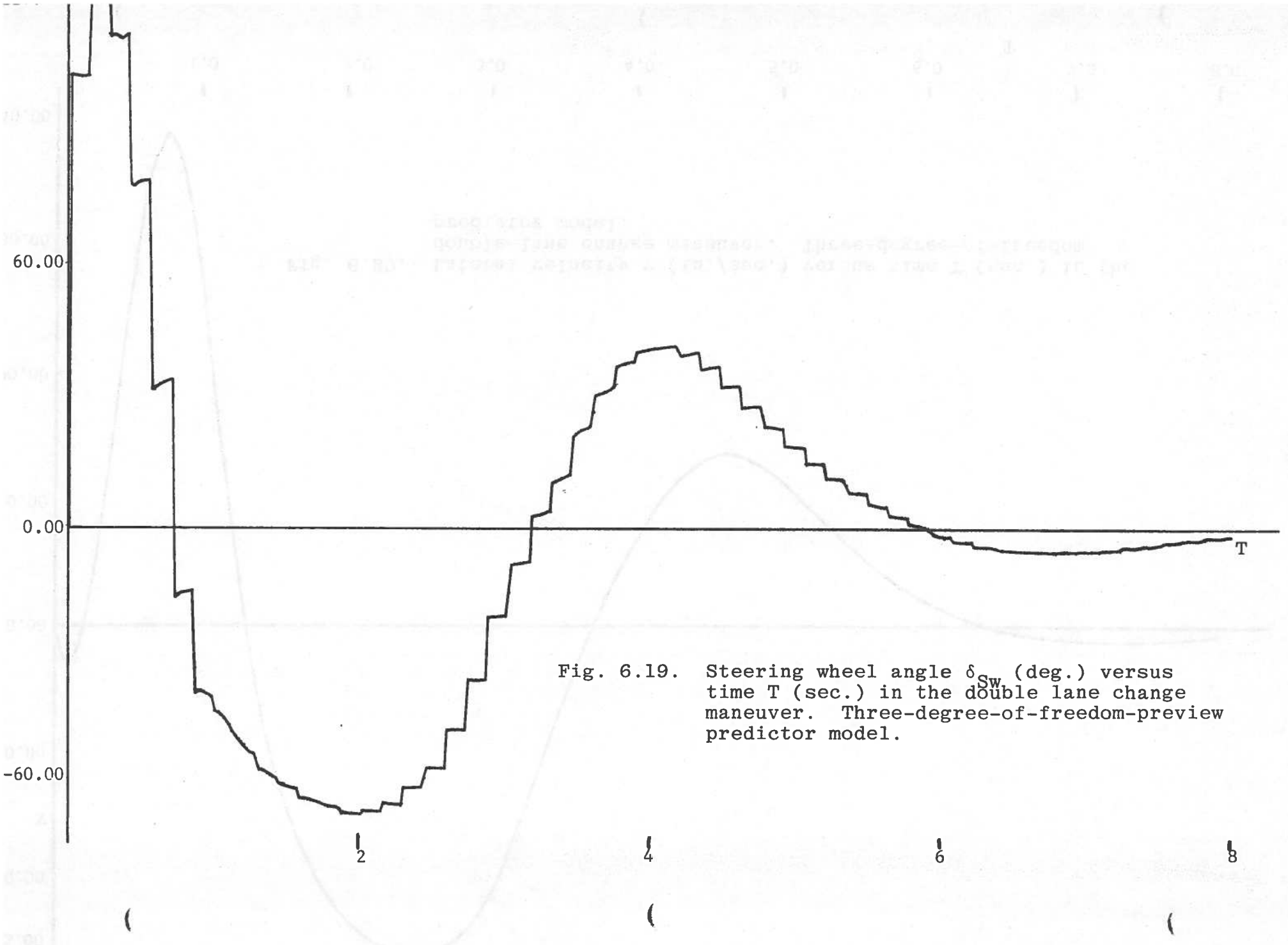

Fig. 6.19. Steering wheel angle δ_{Sw} (deg.) versus time T (sec.) in the double lane change maneuver. Three-degree-of-freedom-preview predictor model.

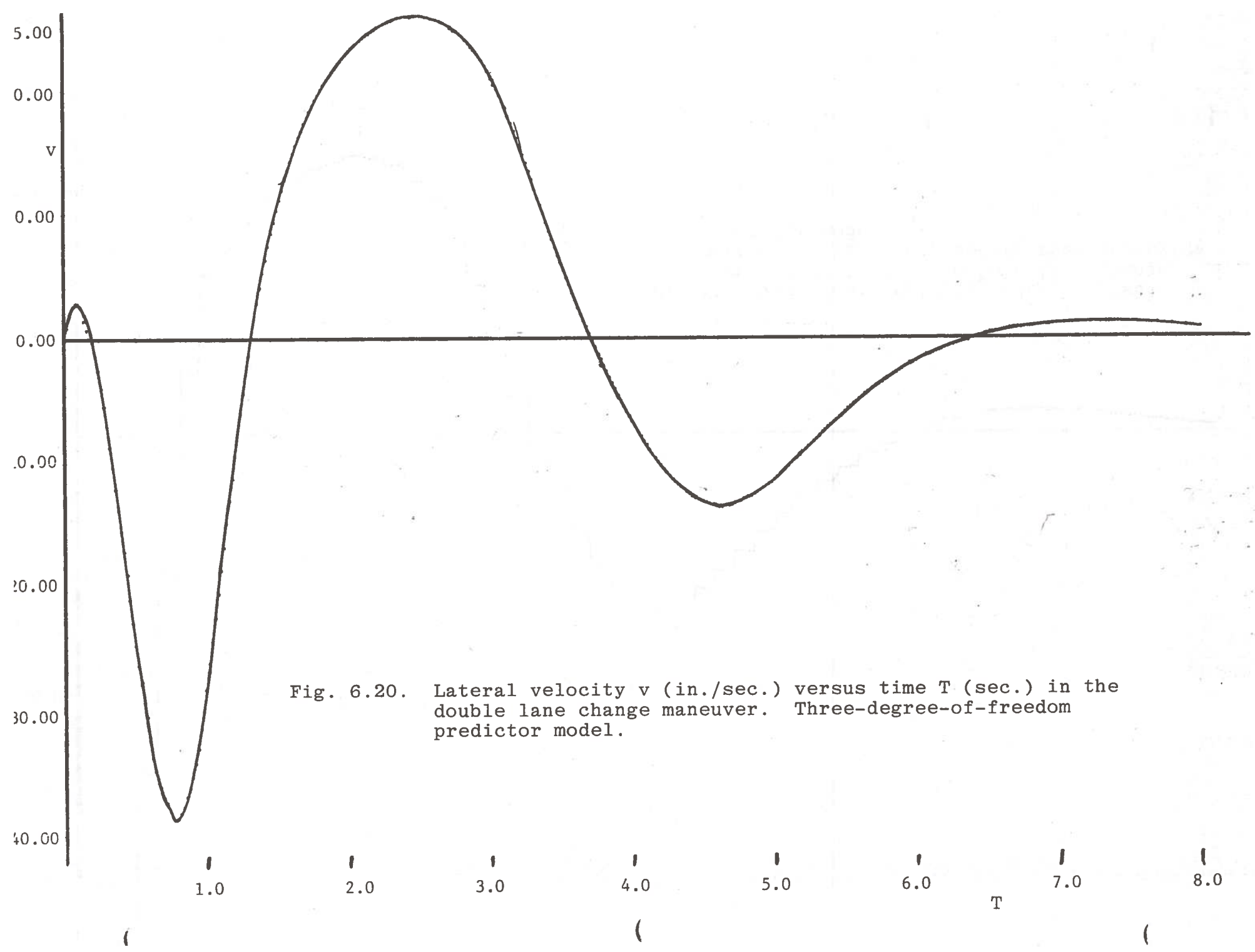

Fig. 6.20. Lateral velocity v (in./sec.) versus time T (sec.) in the double lane change maneuver. Three-degree-of-freedom predictor model.

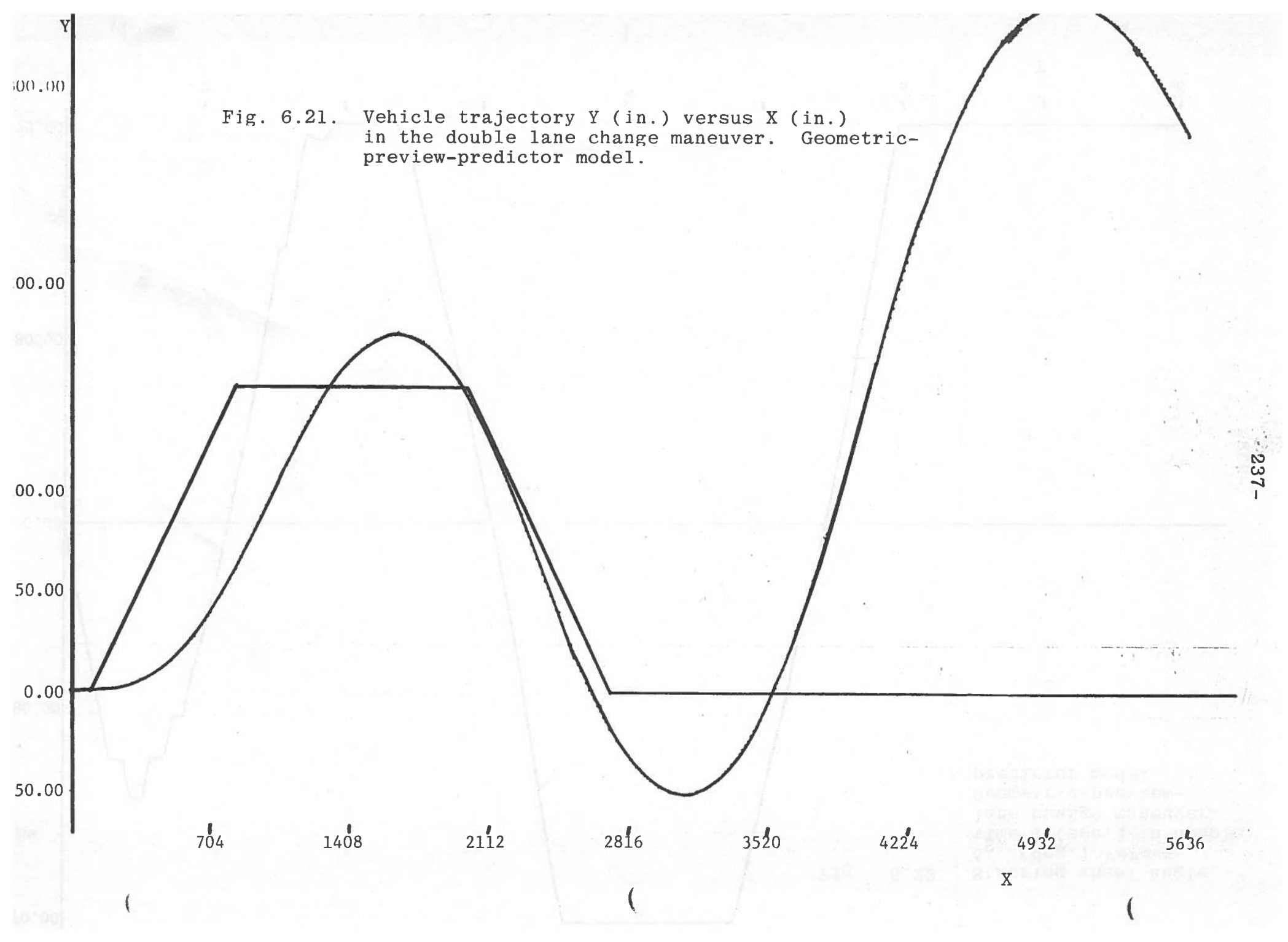

Fig. 6.21. Vehicle trajectory Y (in.) versus X (in.) in the double lane change maneuver. Geometric-preview-predictor model.

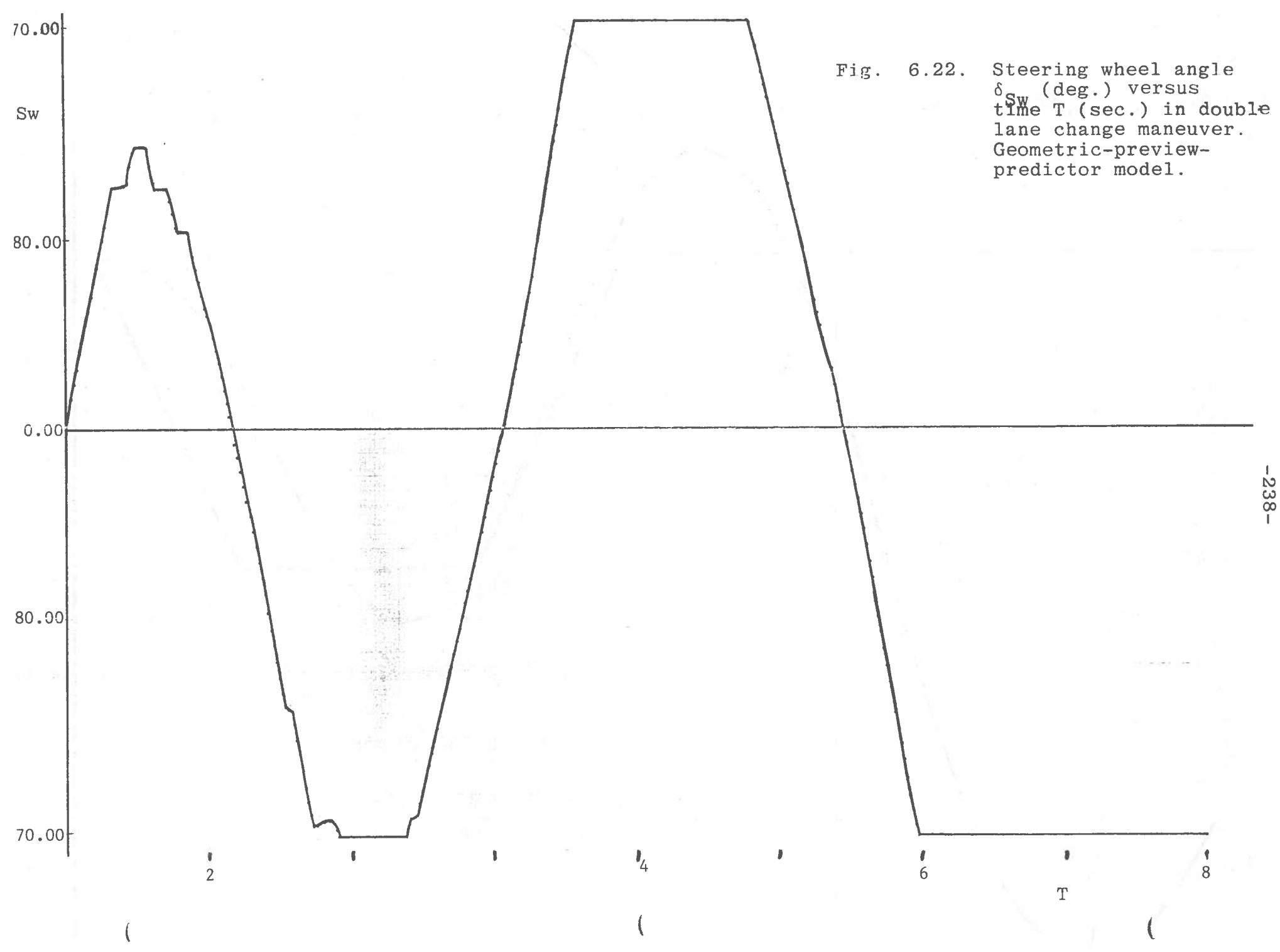

Fig. 6.22. Steering wheel angle δ_{Sw} (deg.) versus time T (sec.) in double lane change maneuver. Geometric-preview-predictor model.

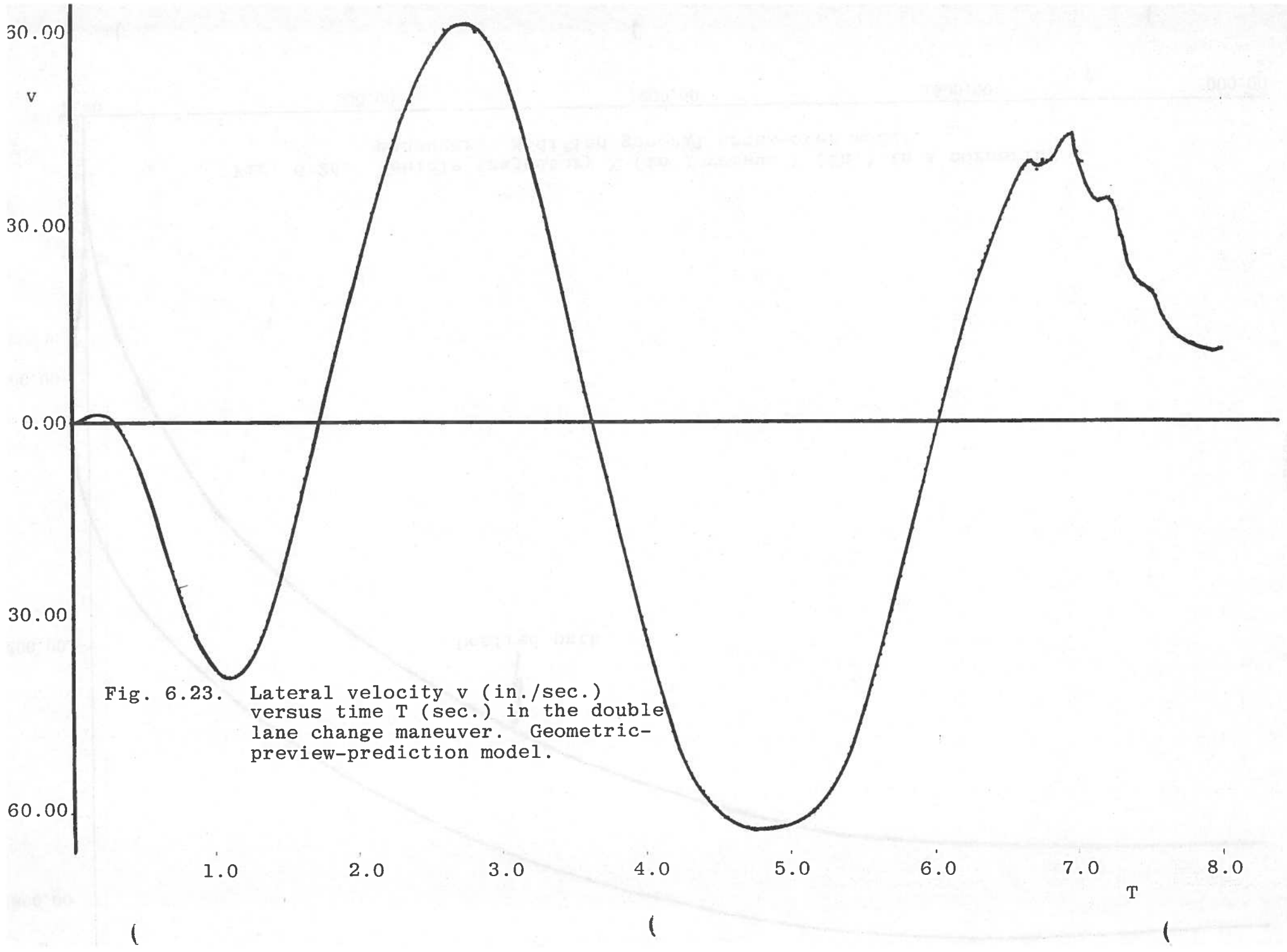

Fig. 6.23. Lateral velocity v (in./sec.) versus time T (sec.) in the double lane change maneuver. Geometric-preview-prediction model.

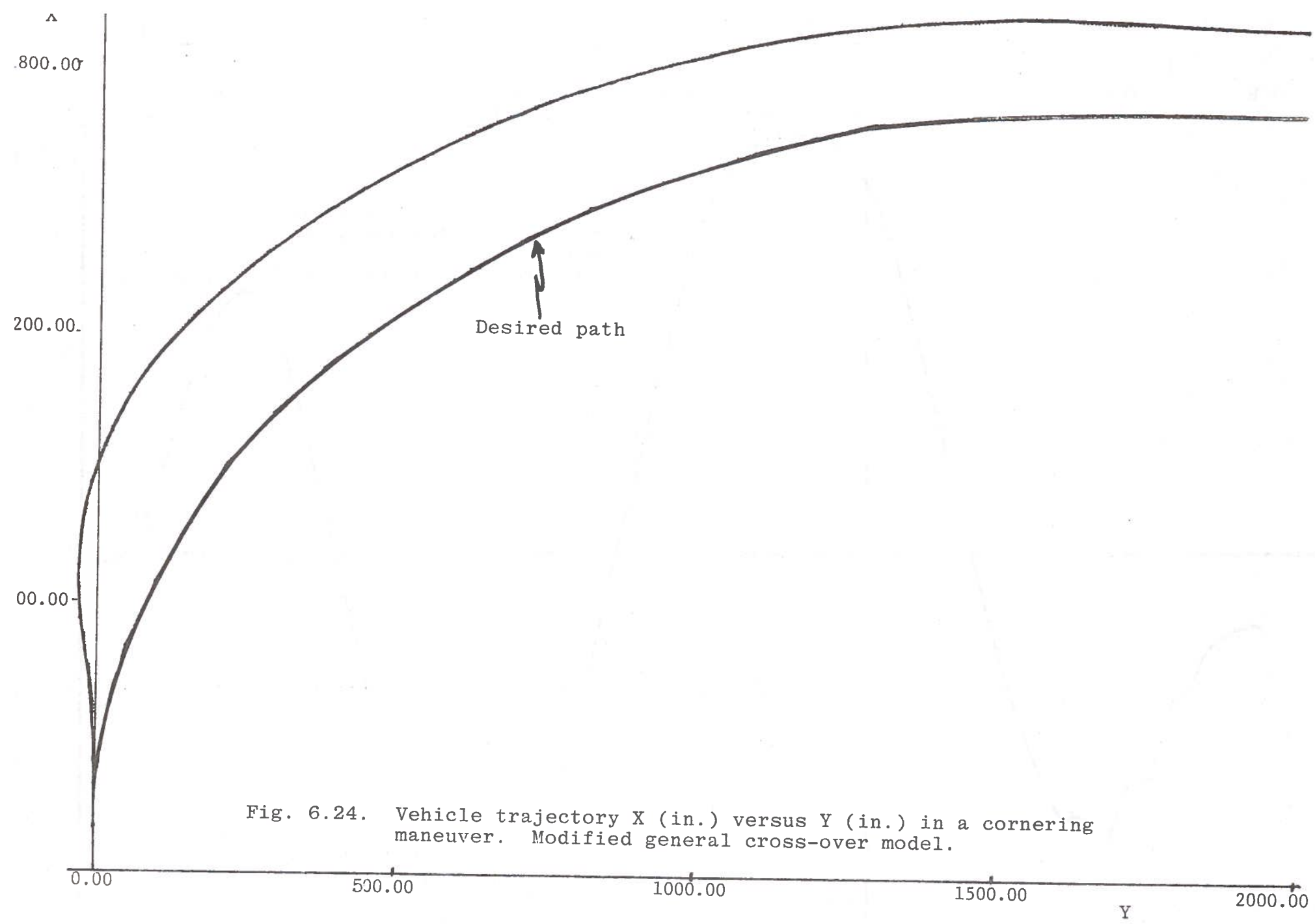

Fig. 6.24. Vehicle trajectory X (in.) versus Y (in.) in a cornering maneuver. Modified general cross-over model.

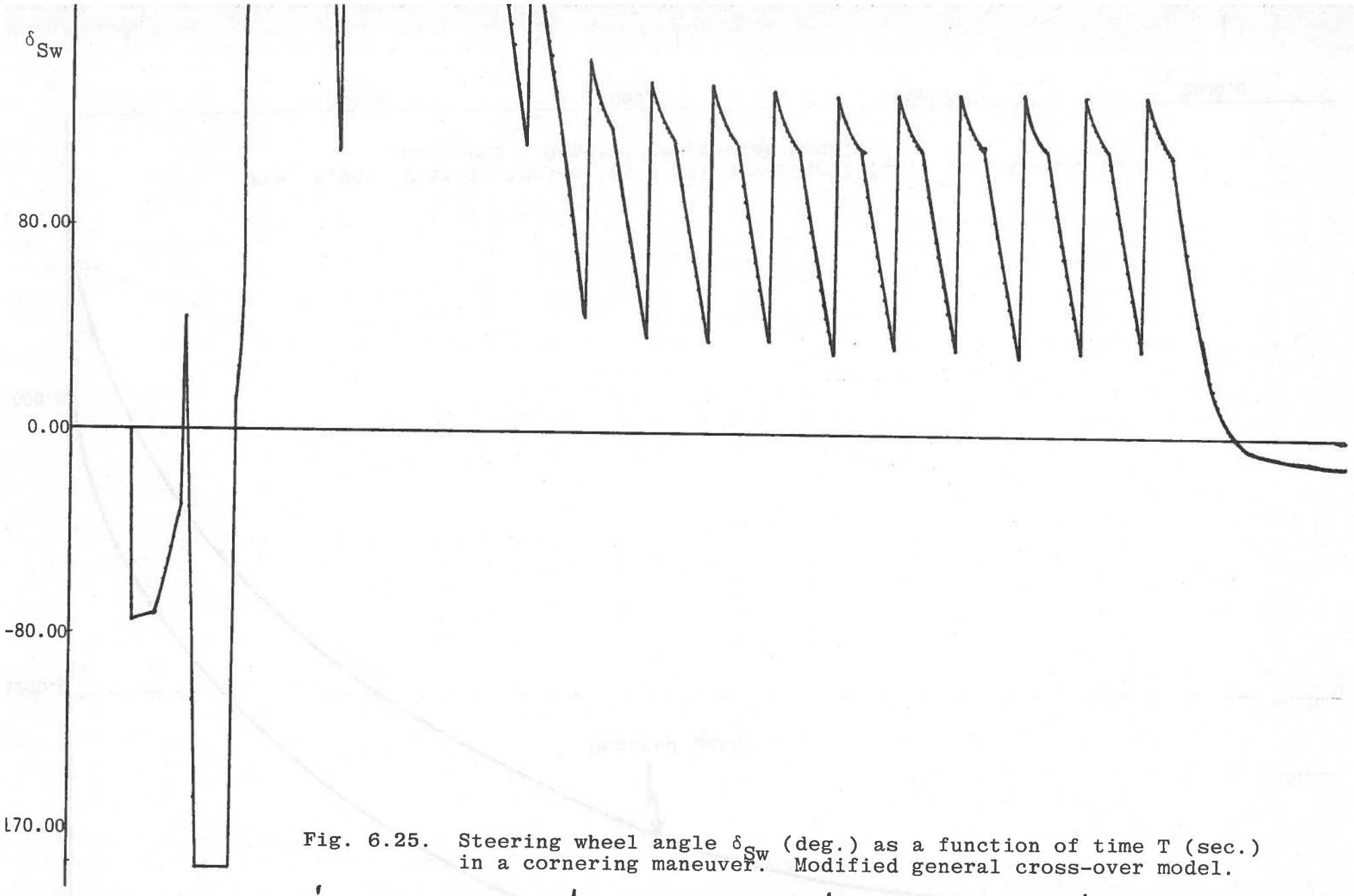

Fig. 6.25. Steering wheel angle δ_{Sw} (deg.) as a function of time T (sec.) in a cornering maneuver. Modified general cross-over model.

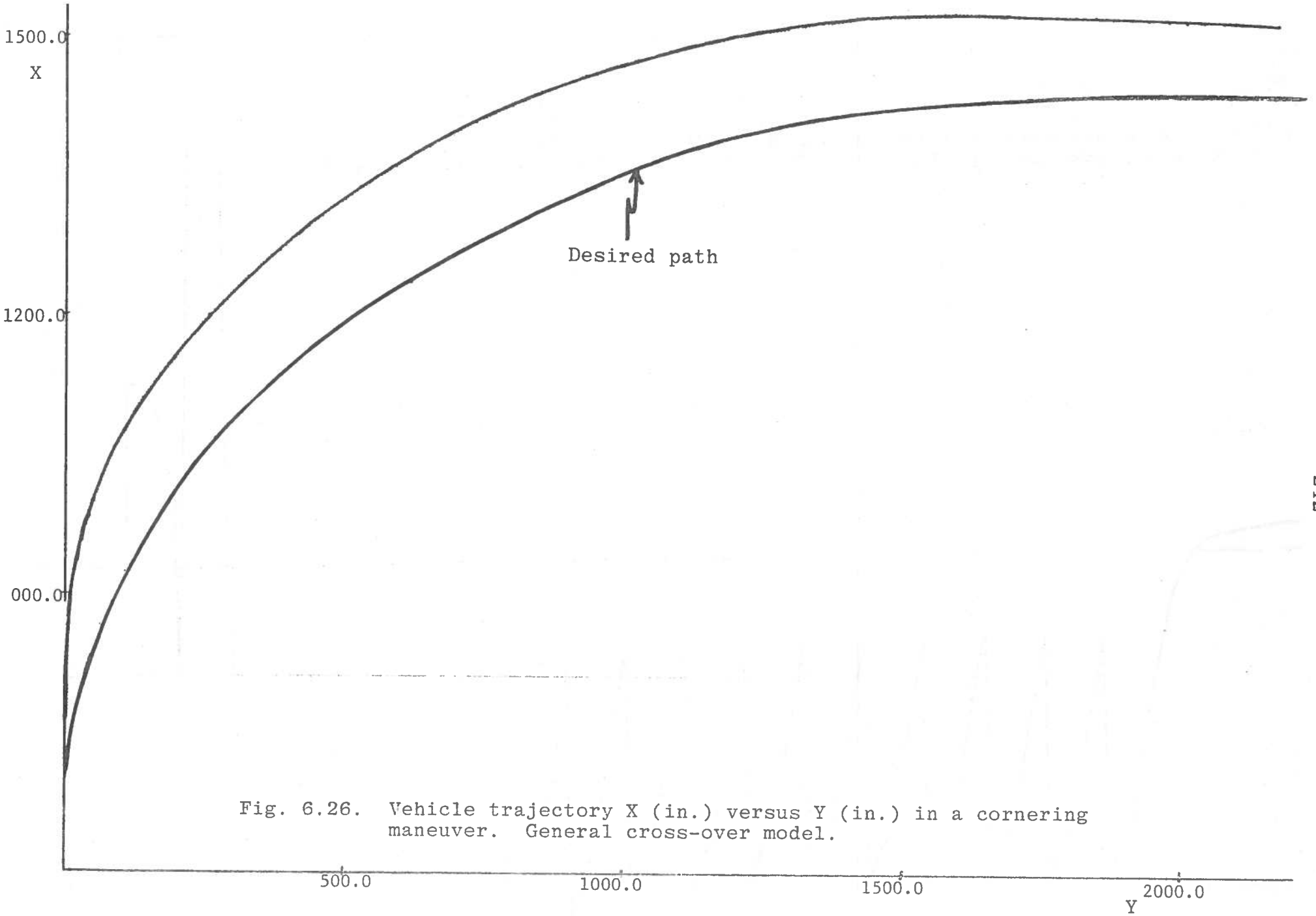

Fig. 6.26. Vehicle trajectory X (in.) versus Y (in.) in a cornering maneuver. General cross-over model.

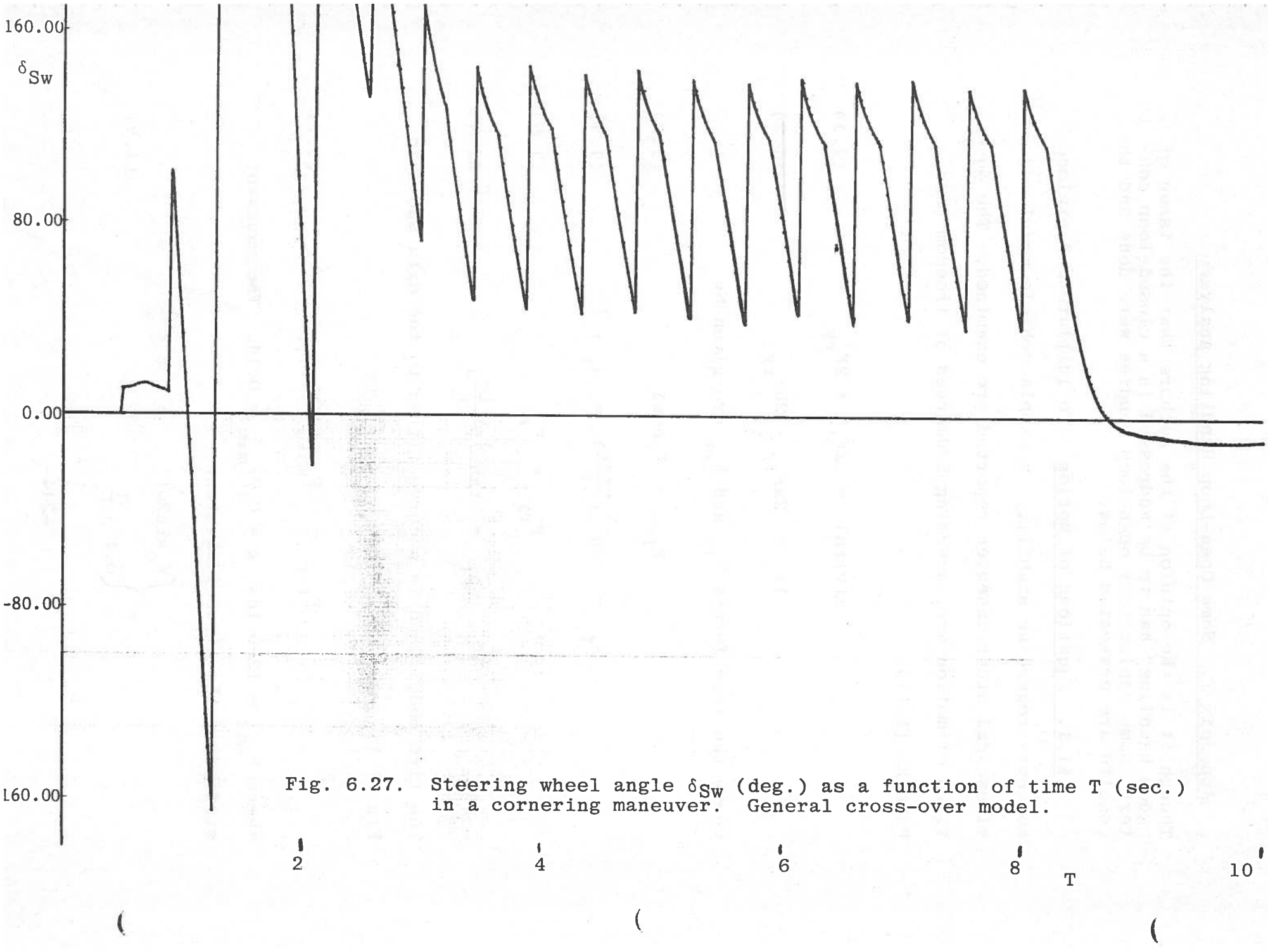

Fig. 6.27. Steering wheel angle δ_{Sw} (deg.) as a function of time T (sec.) in a cornering maneuver. General cross-over model.

Appendix I. Some Open-Loop Handling Analyses

Though it is the opinion of the authors that the issue of "good handling" has to be addressed in a closed-loop context, some exploratory open-loop studies were done and the results are presented below.

§I.1. Equations of Motion. To initiate and explore concepts regarding stability, a simple vehicle model and a sinusoidal steer maneuver reported are examined. The equations of motion are, assuming 2 degrees of freedom (see Pacejka [I.1]),

$$m(\dot{v}+ru) = 2F_{fy} + 2F_{ry} \tag{I.1}$$

$$I\dot{r} = 2aF_{fy} - 2bF_{ry} \tag{I.2}$$

where the tire forces F_{fy} and F_{ry} are given by

$$F_{fy} = F_f\cos\delta \tag{I.3}$$

$$\theta_f = \tan^{-1}\left(\frac{v+ar}{u}\right) = \alpha_f + \delta \tag{I.4}$$

$$F_{ry} = F_r \tag{I.5}$$

$$\alpha_r = \tan^{-1}\left(\frac{v-br}{u}\right) \tag{I.6}$$

The tire model used is a curve fitted to the data shown in Fig. I.1:

$$F_{f,r} = -F_{max}\tanh k\alpha_{f,r} \tag{I.7}$$

where F_{max} = 1250 lbs, $k = C_f/F_{max} = 0.14$. The maneuver studied is the sinusoidal steer

$$\delta = \begin{cases} \delta_o \sin 2\omega t, & o \leq t \leq \frac{1}{\omega} \\ o, & t > \frac{1}{\omega} \end{cases} \tag{I.8}$$

§I.2. Severity Parameters. The concept of severity parameters, i.e., input parameters that push the vehicle into the limit range, has been advanced to judge handling and a study along these lines was undertaken. The severity parameters in the maneuver are the amplitude δ_o, the frequency ω, and the forward velocity u (constant).

The system of nonlinear equations (I.1) and (I.2) were solved numerically by a Runga-Kutta scheme in the SSP/IBM. No problems were encountered in this connection.

Some typical output re handling parameters is shown in Figs. I.2, I.3 and I.4. The data was obtained for the specific vehicle with parameters

$$a = 52.9"$$
$$b = 66.1"$$
$$M = 12.7 \text{ lb-sec}^2/\text{in.}$$
$$I = 32000 \text{ lb-sec}^2\text{in.}$$

Shown in Fig. I.2 is a gain $(\dot{r}/\delta_o)$ as a function of time for the vehicle moving at 60 mph. About 12% effects are seen in the handling parameter peak gain as the severity of the maneuver is increased. Also effected is the time T_R to the first zero crossing, which is a measure of vehicle lag.

From data such as this, the plots shown in Figs. I.3 and I.4 were constructed. Fig. I.3 shows the maximum gain as a function of vehicle speed for maneuvers of increasing severity. For low speeds, a relative insensitivity to the severity parameter δ_o is seen. However, at high speeds, (8-20%) effects are observed. Fig. I.4 shows the "lag time" T_R/T, where $T = \frac{2\pi}{\omega} = 2$--a handling parameter--as a function of vehicle speed for manuevers of increasing severity. For

all cases, only 5% effects are seen and relative insensitivity to the severity parameter δ_o can be concluded.

Fig. I.5 is a plot involving the "method-of-moment" concept. Shown inside the "performance envelope" are resultant moment vs resultant force trajectories, i.e., resultant force and resultant moment as functions of time, for a vehicle traveling at 60 mph, for $\delta_o = 5°$ and $\delta_o = 15°$. Clearly the maneuver involving 15° is dangerous since the trajectory is for a considerable portion of time close to the limit capacity of the tires. However, definitive conclusions must await closed-loop studies, since whether human drivers would allow such conditions is debatable.

§I.3. Stability and Eigenvalue Analysis. To investigate the stability (asymptotic) of maneuvers, perturbations have to be given to the system. Let

$$v \to v + \xi \quad , \quad r \to r + \eta \tag{I.9}$$

where ξ and η are taken to be very small quantities. Substituting eqs. (I.9) into eqs. (I.10) and (I.11) gives

$$m(\dot{v}+\dot{\xi}+ur+u\eta) = 2F_{fy} + 2\delta F_{fy} + 2F_{ry} + 2\delta F_{ry}$$

$$I(\dot{r}+\dot{\eta}) = 2aF_{fy} + 2a\delta F_{fy} - 2bF_{ry} - 2b\delta F_{ry}$$

which reduce to

$$m(\dot{\xi}+u\eta) = 2\delta F_{fy} + 2\delta F_{ry} \tag{I.10}$$

$$I\dot{\eta} = 2a\delta F_{fy} - 2b\delta F_{ry} \tag{I.11}$$

Now

$$\delta F_{fy} = \delta F_f \cos\delta \qquad (I.12)$$

and

$$\delta F_f = \delta(-F_{max}\tanh k\alpha_f)$$

Differentiating gives

$$\delta F_f = -\frac{F_{max}k}{\cosh^2 k\alpha_f}\delta\alpha_f \qquad (I.13)$$

where

$$\delta\alpha_f = \frac{\xi+a\eta}{u}\cos^2\theta_f \qquad (I.14)$$

Substituting eqs. (I.13) and (I.14) into (I.12) yields

$$\delta F_f = -[\frac{\xi+a\eta}{u}\cos^2\theta_f\cos\delta]\frac{F_{max}k}{\cosh^2 k\alpha_f}. \qquad (I.15)$$

Similarly

$$\delta\alpha_r = \frac{\xi-b\eta}{u}\cos^2\alpha_r \qquad (I.16)$$

and

$$\delta F_{ry} = -\frac{kF_{max}}{u\cosh^2 k\alpha_r}\cos^2\alpha_r(\xi-b\eta) \qquad (I.17)$$

Substituting eqs. (I.15) and (I.16) into (I.10) and (I.11) gives

$$\begin{pmatrix}\dot{\xi}\\ \dot{\eta}\end{pmatrix} = A\begin{pmatrix}\xi\\ \eta\end{pmatrix} \qquad (I.18)$$

where

$$A = \begin{pmatrix} a_{11} & a_{12} \\ a_{21} & a_{22} \end{pmatrix}$$

and

$$a_{11} = -\frac{2kF_{max}}{mu}\left[\frac{\cos^2\theta_f\cos\delta}{\cosh^2 k\alpha_f} + \frac{\cos^2\alpha_r}{\cosh^2 k\alpha_r}\right]$$

$$a_{12} = -\frac{2kF_{max}}{mu}\left[\frac{a\cos^2\theta_f\cos\delta}{\cosh^2 k\alpha_f} - \frac{b\cos^2\alpha_r}{\cosh^2 k\alpha_r}\right] - u$$

$$a_{21} = -\frac{2kF_{max}}{Iu}\left[\frac{a\cos^2\theta_f\cos\delta}{\cosh^2 k\alpha_f} - \frac{b\cos^2\alpha_r}{\cosh^2 k\alpha_r}\right]$$

$$a_{22} = -\frac{2kF_{max}}{Iu}\left[\frac{a^2\cos^2\theta_f\cos\delta}{\cosh^2 k\alpha_f} + \frac{b^2\cos^2\alpha_r}{\cosh^2 k\alpha_r}\right]$$

Equations (I.1), (I.2), and (I.18) were integrated numerically with $\delta_o = 10°$. For all the maneuvers reported upon in §I.2, the perturbations η and ξ were found to decay with time and so those maneuvers are asymptotically stable. It would seem that the concept of asymptotic stability is of questionable applicability, since some of the maneuvers in question come so close to the force generating capacity of the tires.

An investigation was made on the role, if any, of the eigenvalues of the matrix A on the nature of the original and the perturbed maneuvers. These eigenvalues, which are functions of time, were calculated for the following

hypothetical situations: (i) understeer car (a=52.9", b=66.1") (ii) neutral steer car (a=60.5", b=59.5"--actually slightly oversteer) (iii) oversteer car (a=66.4", b=53.6"). All other vehicle parameters were kept at fixed values and the speed was taken to be 60 mph.

Shown in Fig. I.6 is the real part of the dominant eigenvalue (i.e., the eigenvalue whose real part has the largest magnitude) as a function of time for two values of the steering severity parameter δ_o. The results are for the understeer car. Such a vehicle is stable in steady, straight-line motion, the tires being treated nonlinearly (see Pacejka [I.1]). Note that for both cases the eigenvalues are always negative and settle down to a constant negative value after the steering maneuver is completed. This implies that the integral from 0 to infinity of the real part of the eigenvalue is negative. Since Cesari (Ref. [I.2], p. 48) used a similar measure to assess the asymptotic stability of systems such as the one at hand, one could speculate that a proof of asymptotic stability could indeed be constructed using such integrals. However, the role of asymptotic stability, if any, in addressing issues of controlability is questionable. Towards this end the influence of the eigenvalues on the perturbation was investigated. Shown in Figs. I.7 and I.8 are the associated velocity and yaw rate perturbation (initial values: ξ_o=10 in/sec, η_o=0) as functions of time. Unfortunately, there appears to be no discernible relationship or pattern between the magnitudes of the real part of the eigenvalues

and the peaks and rates seen in Figs. I.7 and I.8. It can be concluded however that since the perturbation decay with time, the motion is asymptotically stable. Figs. I.9, I.10, and I.11 show similar results for the neutral steer car. Even though slightly oversteer, stability is seen in the eigenvalues being always negative and the decay of the perturbations with time. Again though, no obvious correlation between the results in Fig. I.12 and those in Figs. I.13 and I.14 can be seen.

Results for the oversteer car are shown in Figs. I.15, I.16, and I.17. The vehicle in question is unstable for a straight line, steady state maneuver (see Pacejka, Ref. [I.1]) and it is interesting that for the first time, eigenvalues with a positive real part occur. Indeed, once the steering maneuver is over the real part of the dominant eigenvalue settles down to a positive constant value and asymptotic instability could be inferred. However, it is seen that the perturbations seem to be decaying to zero once the maneuver is ended. Perhaps divergences would occur for larger times, but this was not verified since the computational costs involved for the oversteer car proved to be prohibitive for such an exploratory work. In any event, one of the goals of this study, namely the establishing of correlations between eigenvalues and perturbed maneuvers again cannot be realized.

One other item that was further explored was the concept set forth in the Plan of Work and Methodology of exercising the perturbation eqs. (I.18), which are linear, to

compute neighboring trajectories, as opposed to exercising the nonlinear simulation, eqs. (I.1) and (I.2). To assess the accuracy of this procedure a comparison was made between the results so obtained (denoted by a subscript p in the sequel) and ones obtained from eqs. (I.1) and (I.2) with initial conditions set equal to the perturbations (denoted by a subscript n in the sequel). Shown in Table I.1 is a comparison of the velocities for a relatively small initial velocity perturbation: ξ_o=1 in/sec, for a neutral steer car. Very good agreement is seen, the differences being so small as to be indistinguishable graphically. Some discrepancies do occur for an initial velocity perturbation: ξ_o=10.0, as Fig. I.18 shows, but these are again small enough to be neglected. Differences in yaw rates were found in both cases to be even smaller. A more demanding situation is the oversteer car. Results for it are shown in Table I.2 and Fig. I.19 for a velocity perturbation: ξ_o=10. Table I.2 shows that acceptable differences in yaw rates are still found. However, Fig. I.19 shows that considerable differences occur in the velocities. The conclusion to be drawn is that for such unstable systems (which may be encountered as the severity parameter is increased), considerable caution must be exercised in computing neighboring trajectories from the variational equations.

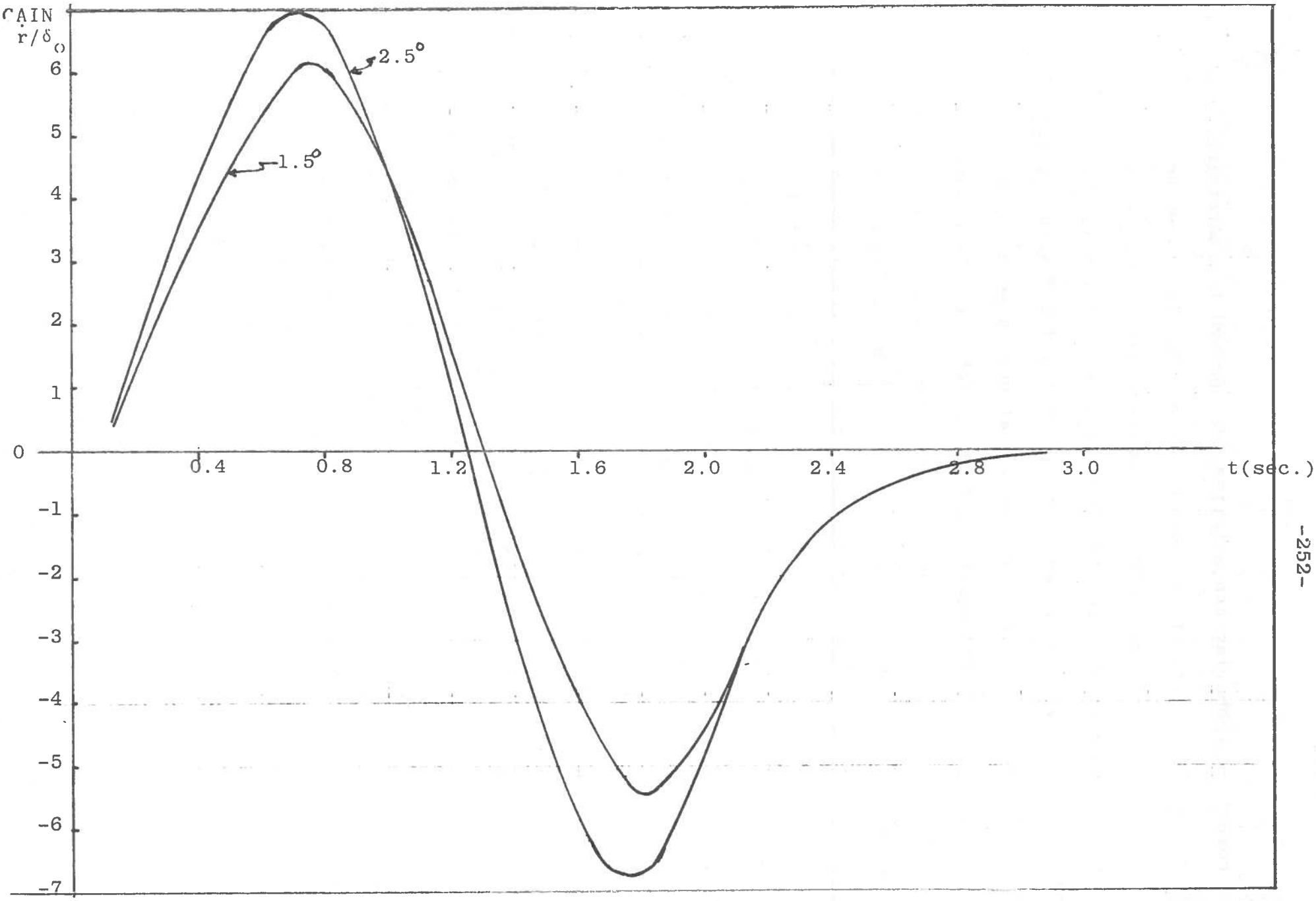

Fig. I.2 Gain as a function of time at 60 m.p.h.

SIDE FORCE VS. SLIP ANGLE

(057 E70-14 GY BB CWTP CAMBER = 0., SLIP = 0.)

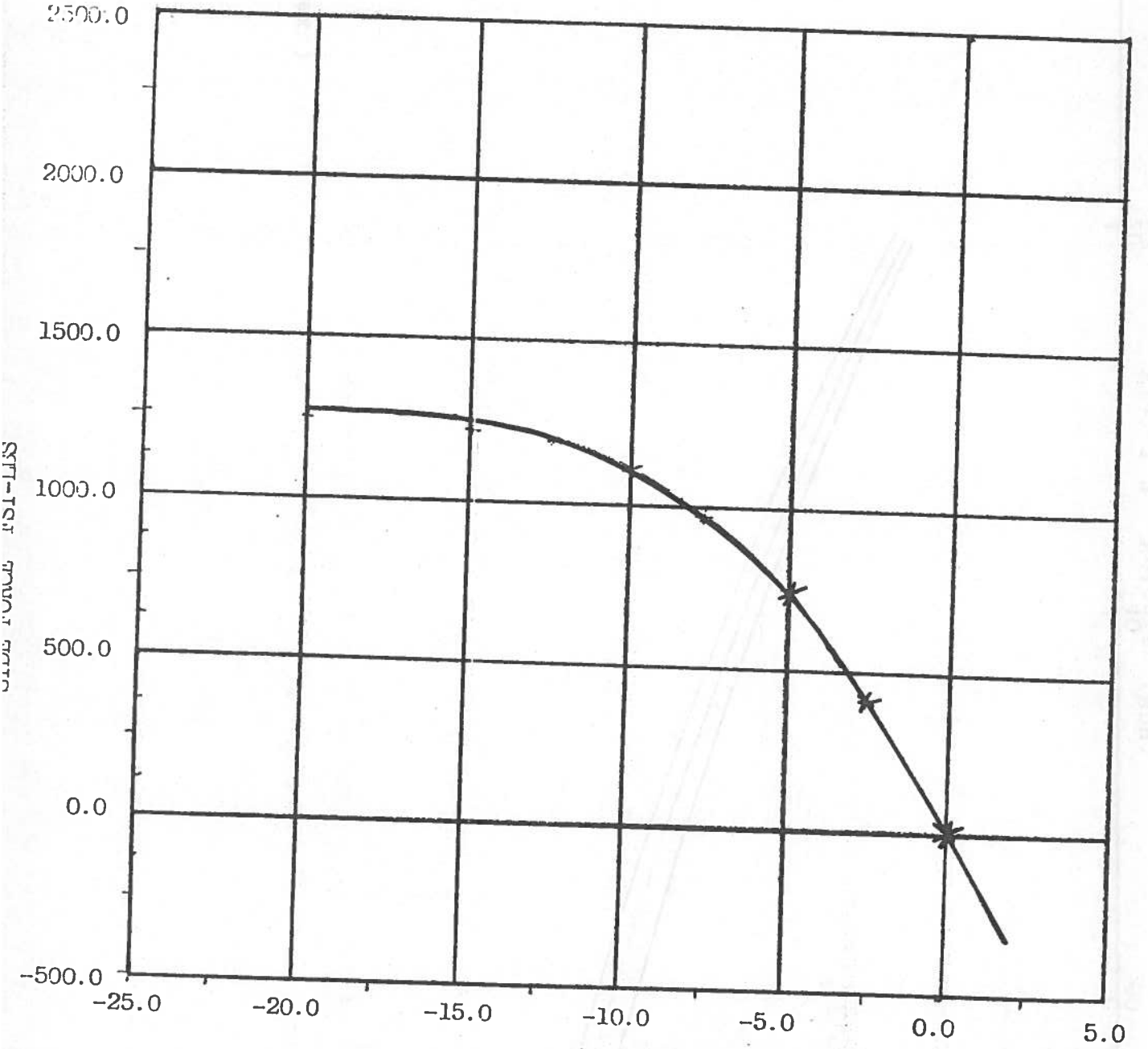

Fig.I.1.SLIP ANGLE-DEGREES

Normal Load = 1487.500 -LBS

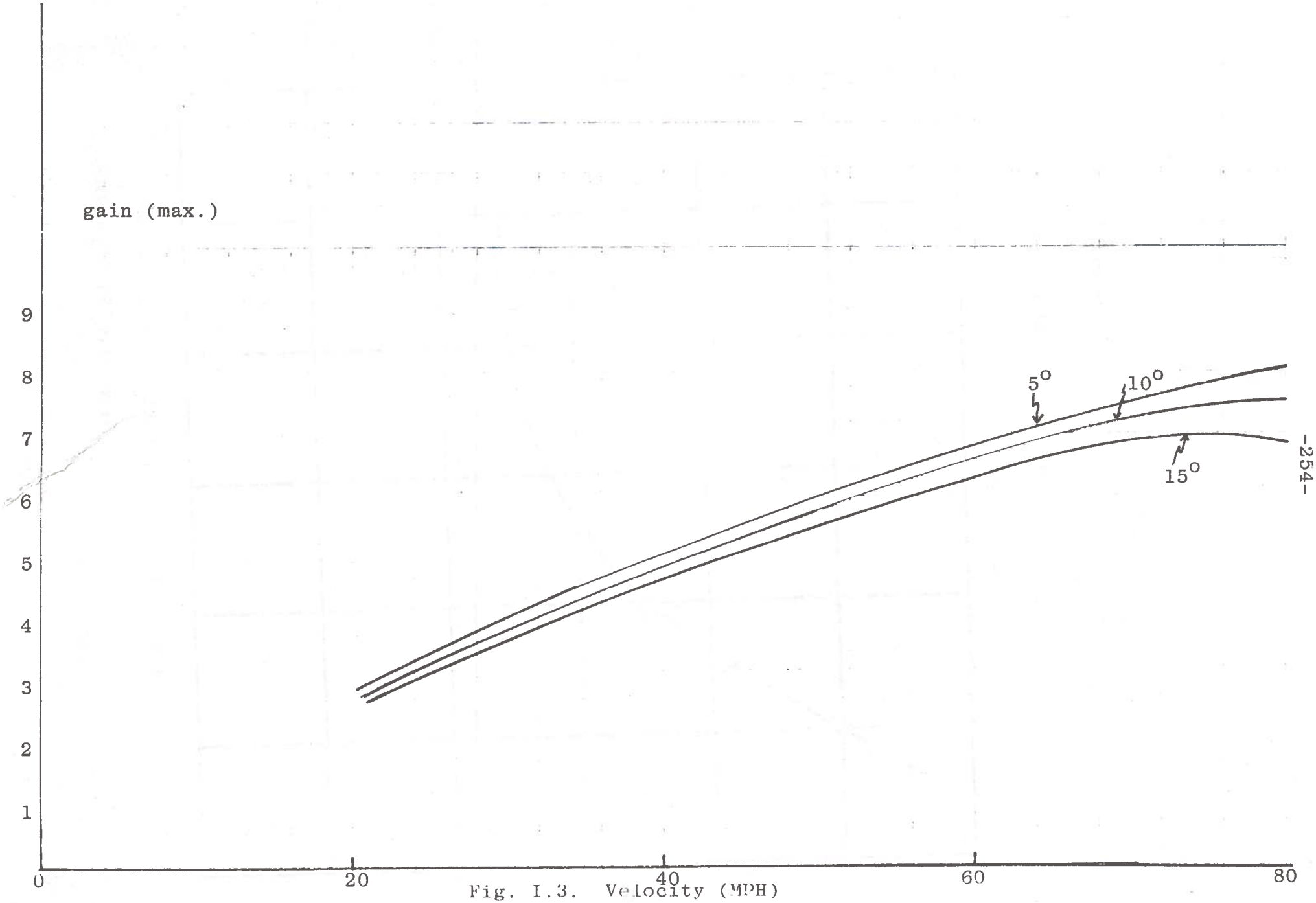

Velocity (MPH)

Fig. I.3.

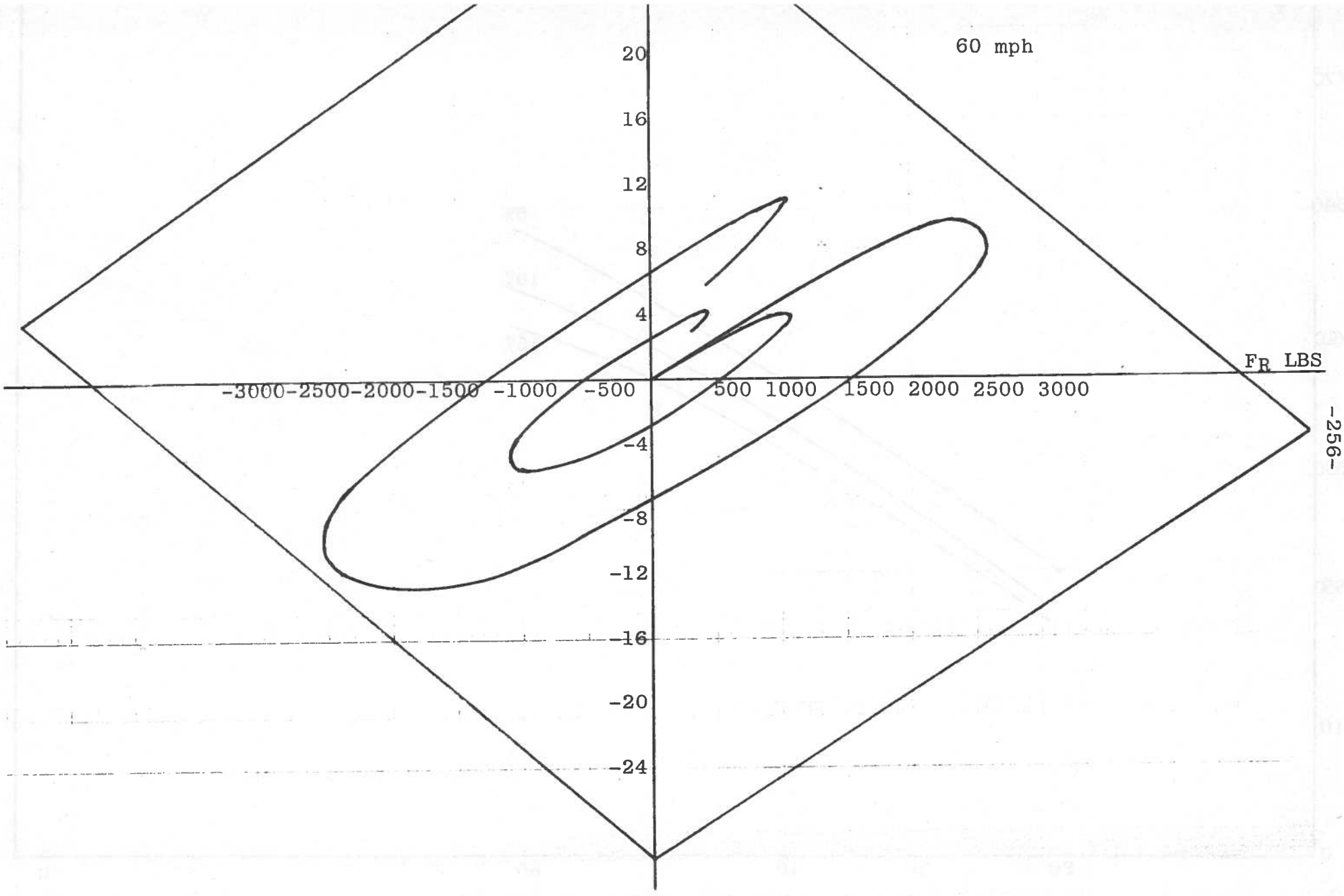

Fig. I.5. Moment M versus resultant force F_R

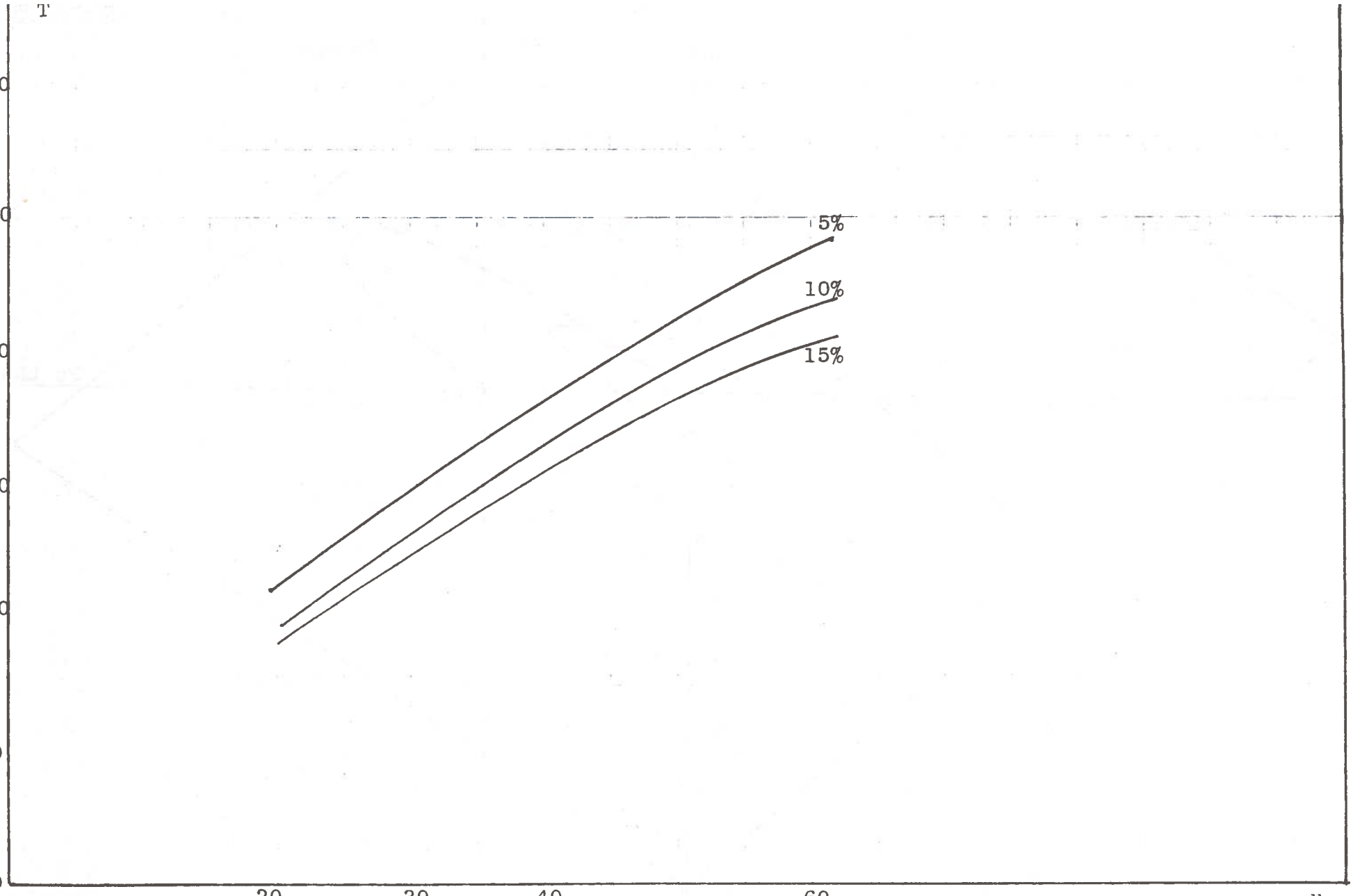

Fig. I. 4. Lag time T_R/T versus speed u.

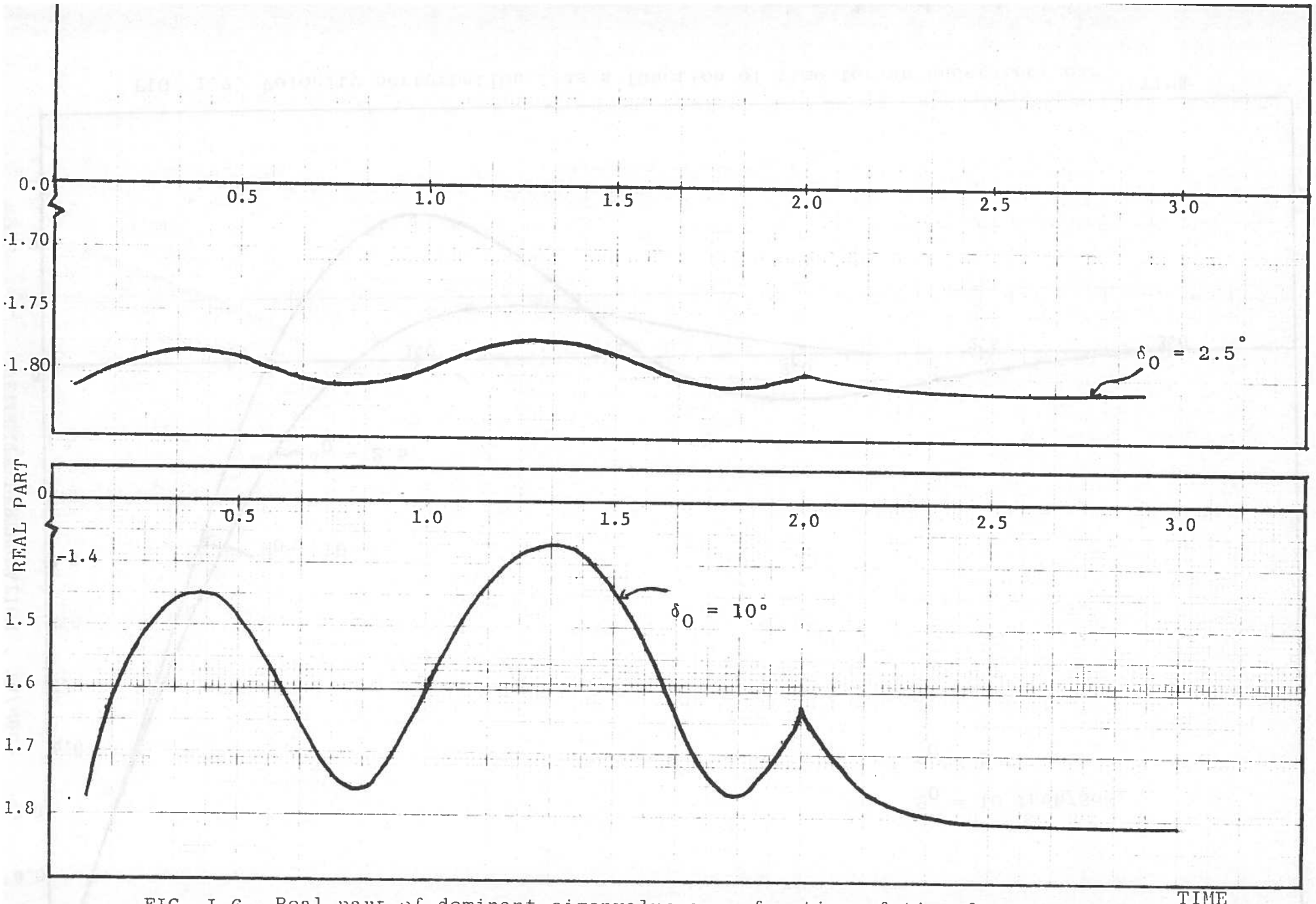

FIG. I.6. Real part of dominant eigenvalue as a function of time for an understeer car.

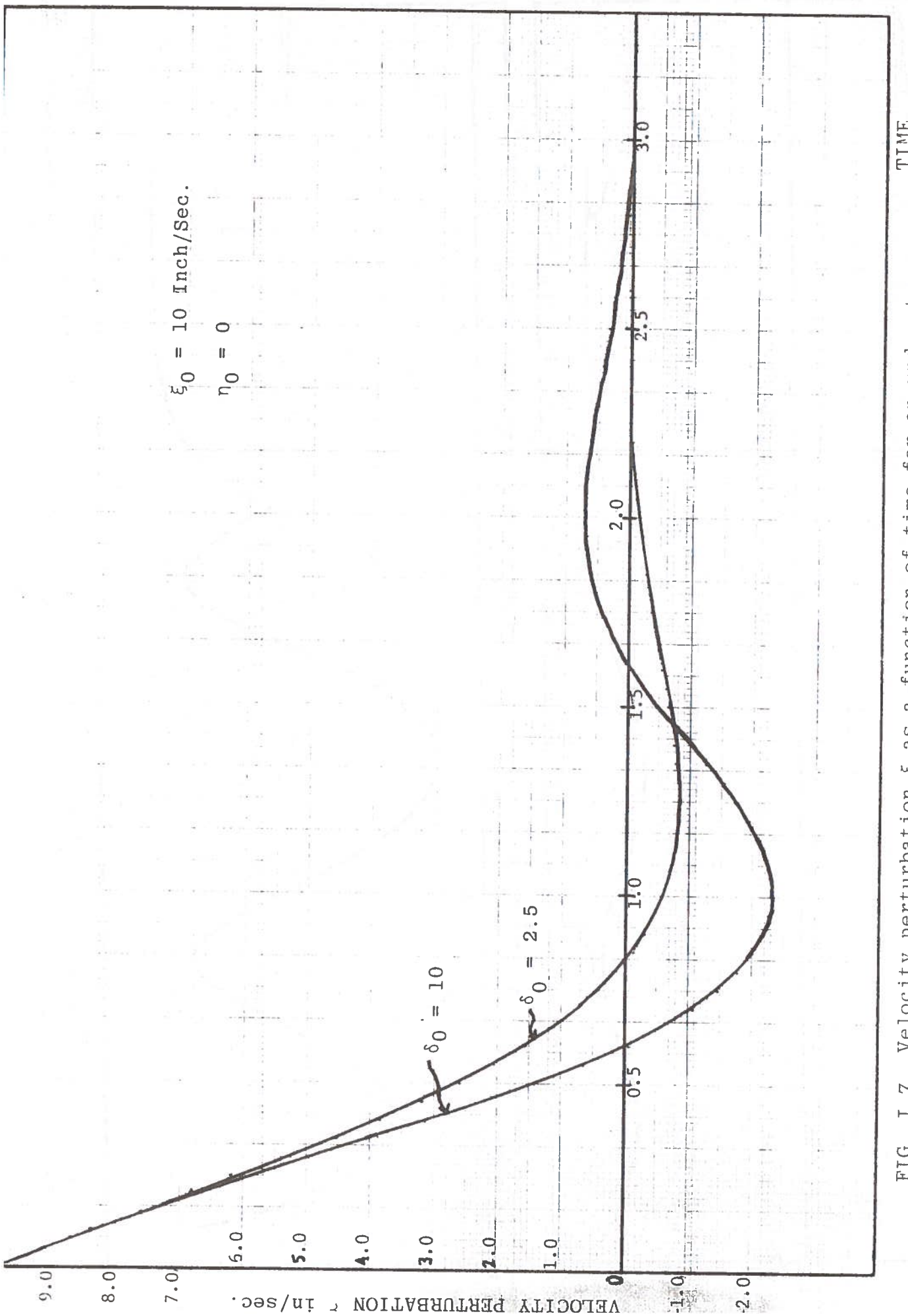

FIG. I.7. Velocity perturbation ξ as a function of time for an understeer car.

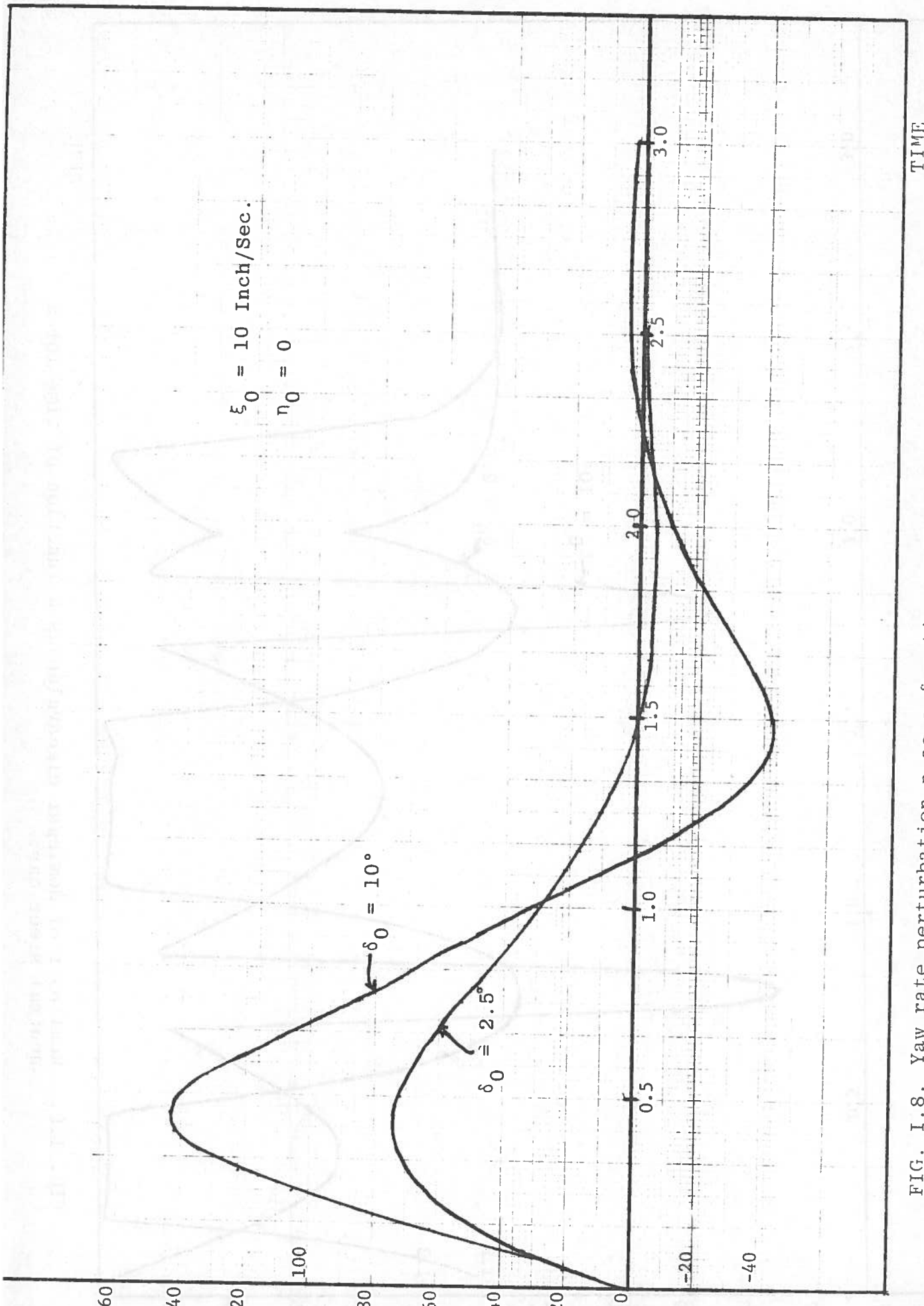

FIG. I.8. Yaw rate perturbation η as a function of time for an understeer car.

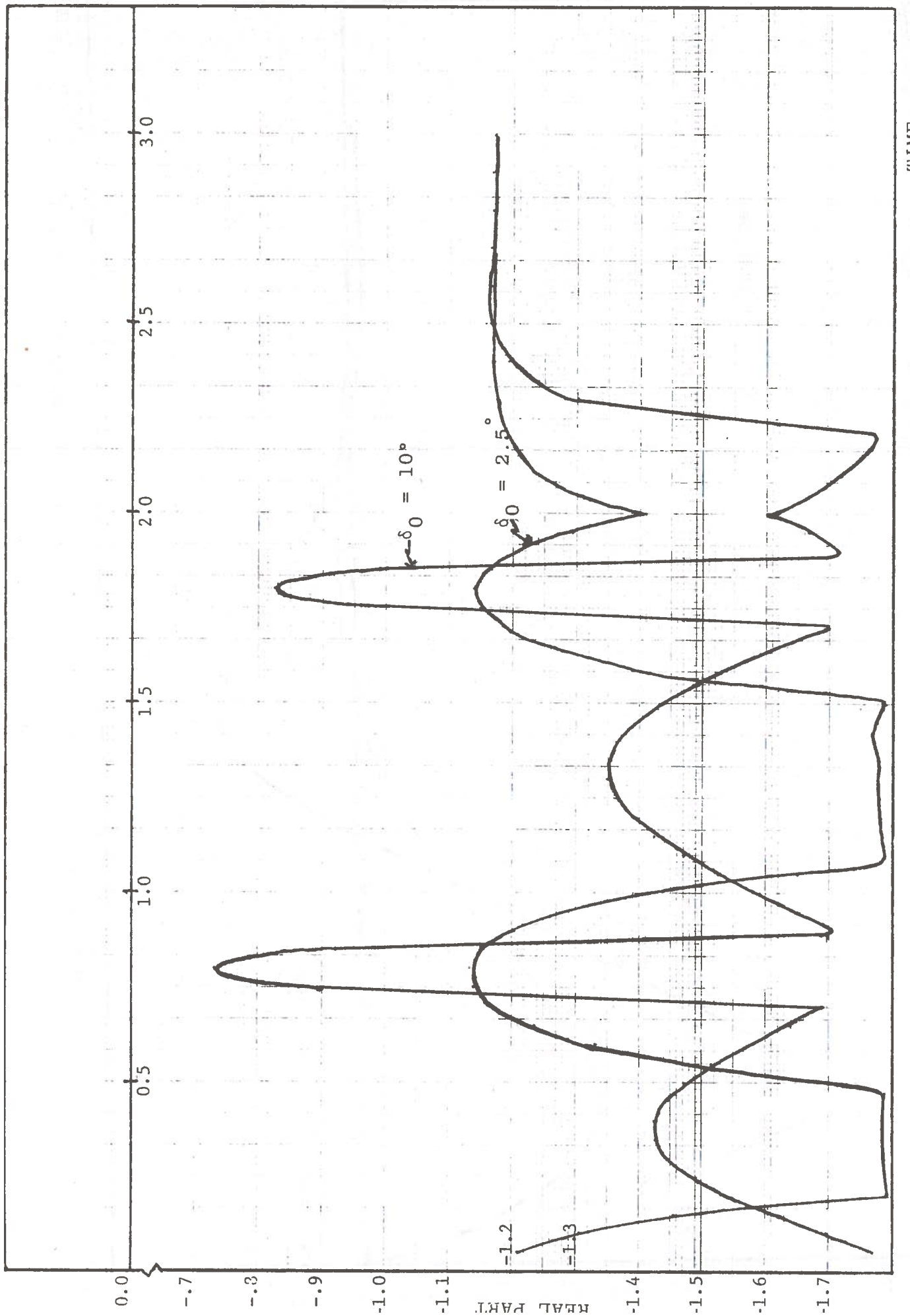

FIG. I.9. Real part of dominant eigenvalue as a function of time for a neutral steer car.

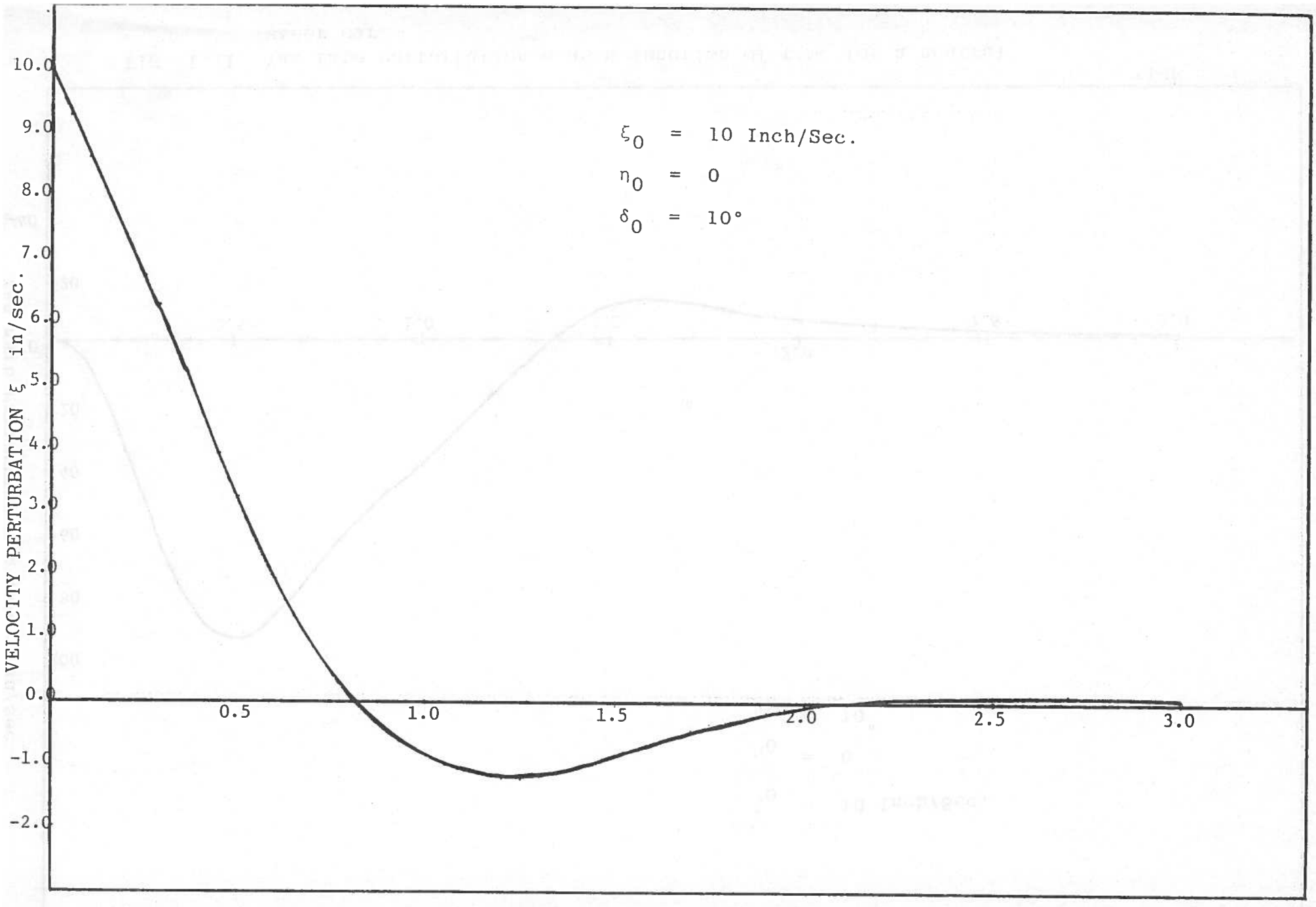

FIG. I.10. Velocity perturbation ξ as a function of time for a neutral steer car.

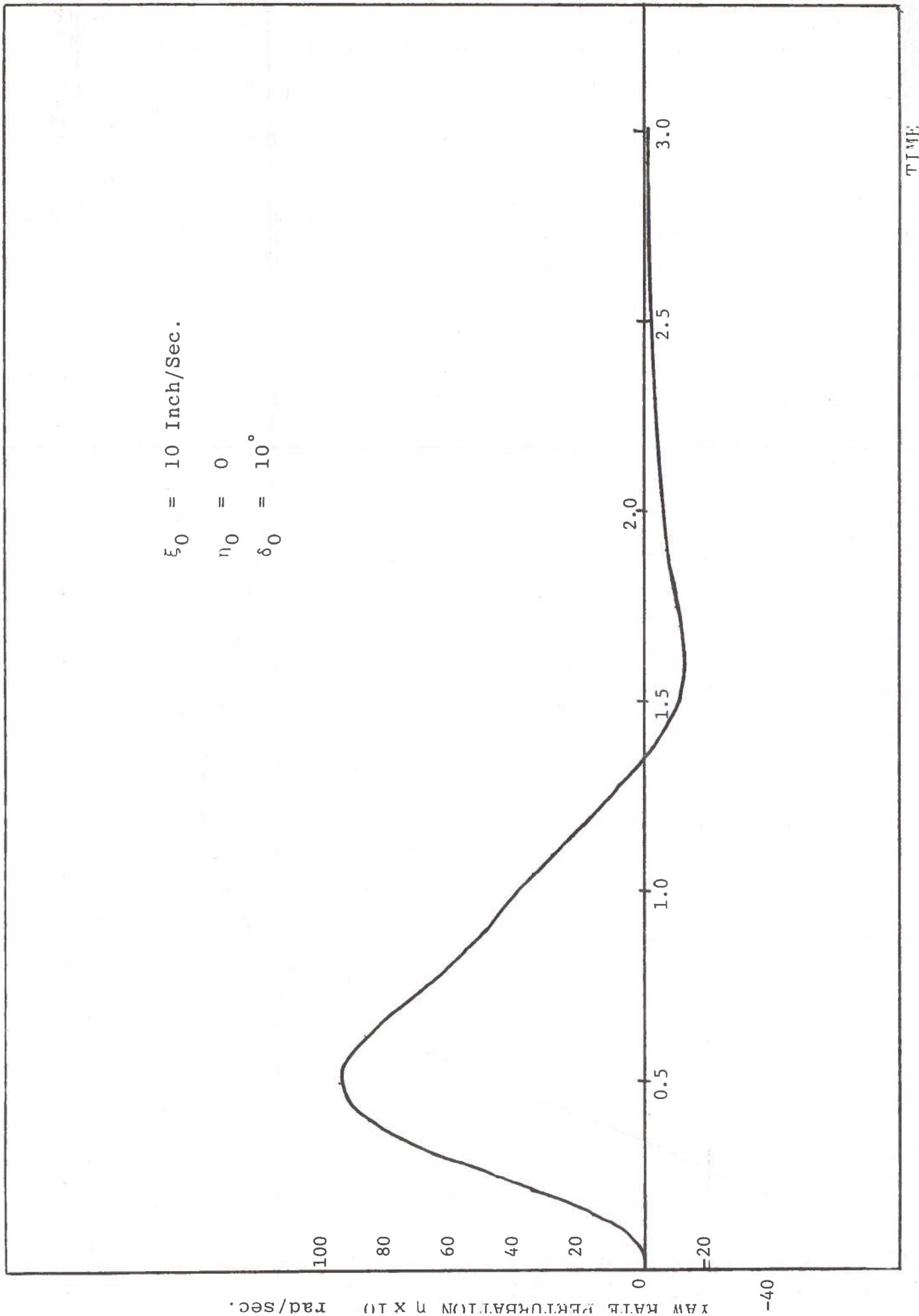

FIG. I.11. Yaw rate perturbation η as a function of time for a neutral steer car.

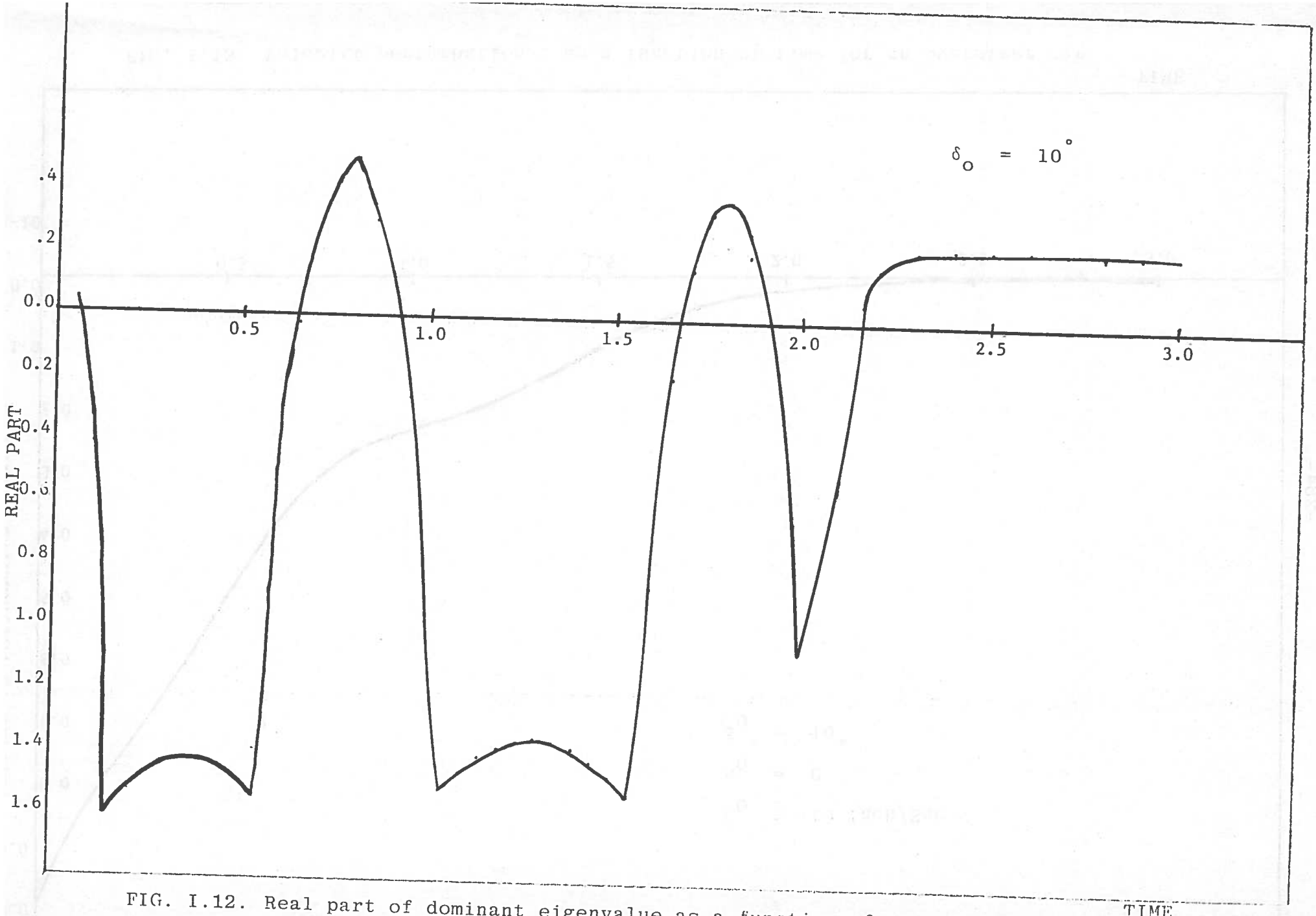

FIG. I.12. Real part of dominant eigenvalue as a function of time for an oversteer car.

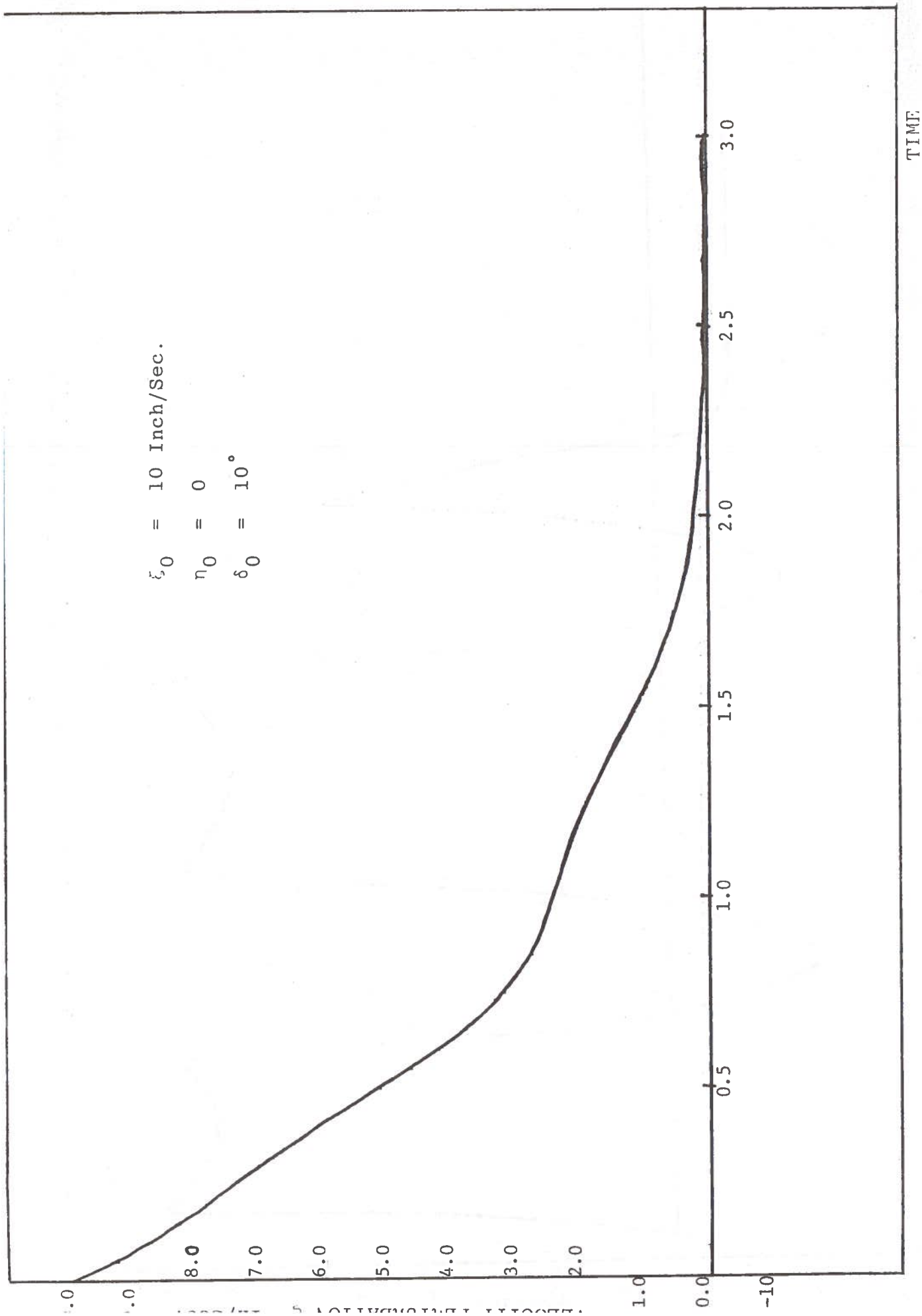

FIG. I.13. Velocity perturbation ξ as a function of time for an oversteer car.

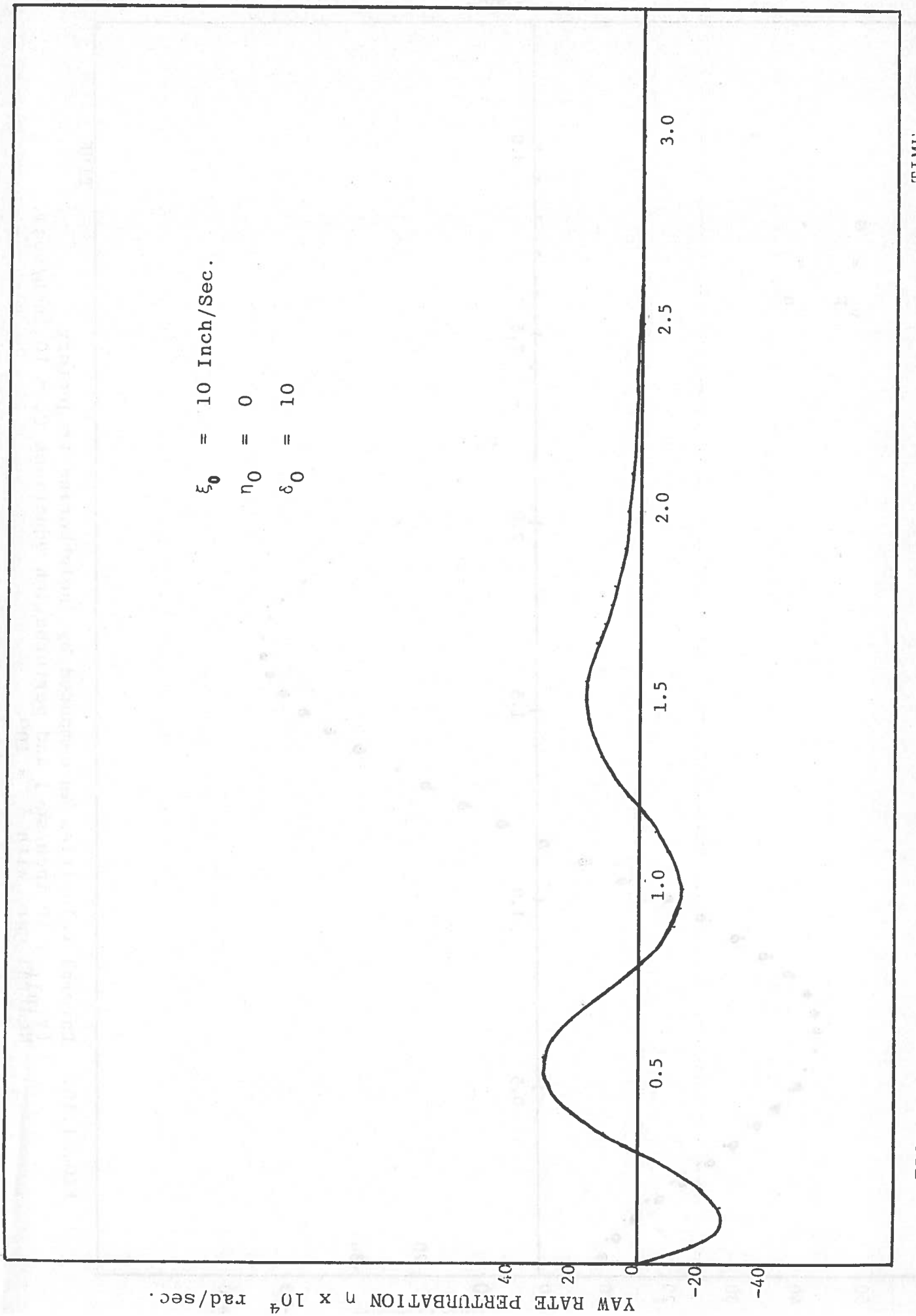

FIG. I.14. Yaw rate perturbation η as a function of time for an oversteer car.

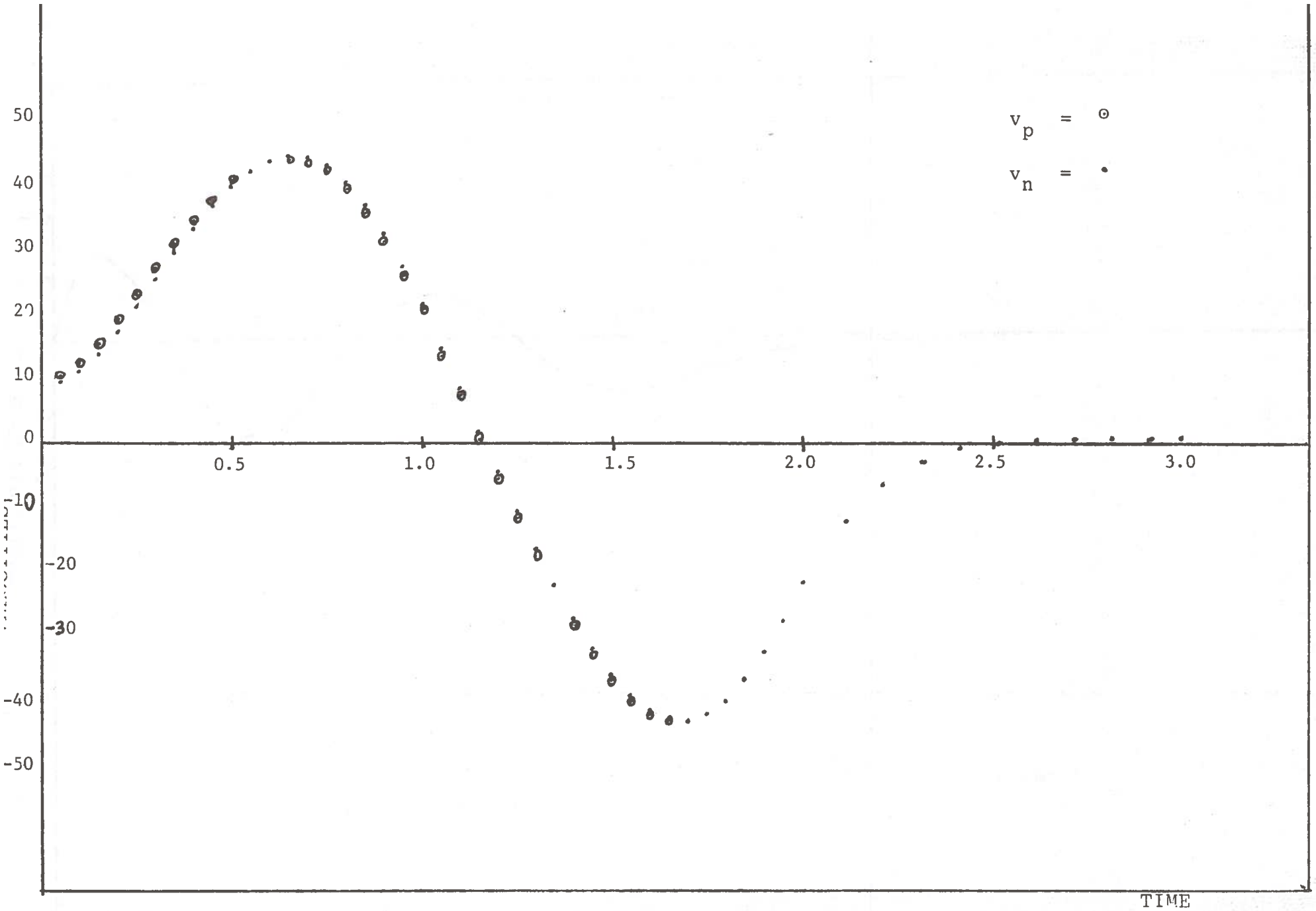

FIG. I.15. Lateral velocities as computed by "neighboring trajectory" (v_{init} = 10 inch/sec) and perturbation equations (ξ = 10 inch/sec). Neutral car, with $\delta_o = 10^o$.

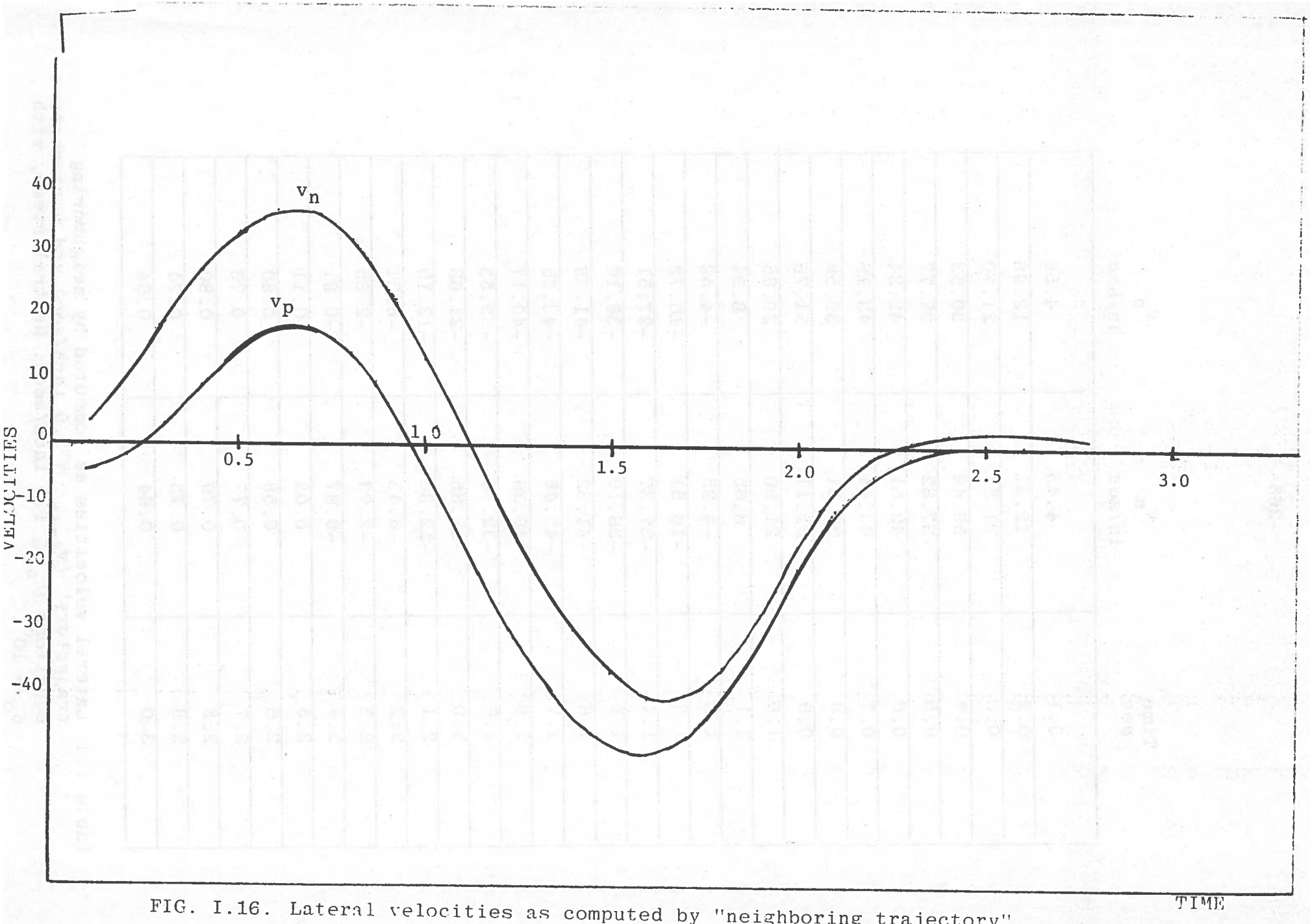

FIG. I.16. Lateral velocities as computed by "neighboring trajectory" (v_{init} = 10 inch/sec) and perturbation equations (ξ_o = 10 inch/sec). Oversteer car, with $\delta_o = 10^o$.

Time sec	v_n in/sec	v_p in/sec
0.1	4.45	4.56
0.2	12.31	12.46
0.3	21.57	21.70
0.4	30.48	30.53
0.5	37.82	37.77
0.6	42.51	42.34
0.7	43.44	43.18
0.8	39.91	39.58
0.9	32.11	31.76
1.0	21.20	20.86
1.1	8.65	8.34
1.2	-4.25	-4.52
1.3	-16.51	-16.72
1.4	-27.37	-27.51
1.5	-36.10	-36.16
1.6	-41.82	-41.78
1.7	-43.48	-43.35
1.8	-40.36	-40.17
1.9	-32.74	-32.53
2.0	-21.85	-21.65
2.1	-12.36	-12.19
2.2	-6.43	-6.31
2.3	-2.93	-2.85
2.4	-0.97	-0.91
2.5	0.08	0.11
2.6	0.58	0.60
2.7	0.77	0.78
2.8	0.79	0.80
2.9	0.73	0.74
3.0	0.64	0.64

Table I.1. Lateral velocities as computed by 'neighboring trajectory' (v_{init} = 1.0 inch/sec) and perturbation equations (ξ_o = 1.0 inch/sec). Neutral steer, with $\delta_o = 10^o$.

Time sec	r_n rad/sec	r_p rad/sec
0.1	.156	.170
0.2	.359	.378
0.3	.614	.632
0.4	.873	.887
0.5	1.098	1.108
0.6	1.253	1.263
0.7	1.307	1.314
0.8	1.236	1.254
0.9	1.045	1.067
1.0	.759	.780
1.1	.412	.428
1.2	.040	.047
1.3	-.329	-.330
1.4	-.665	-.675
1.5	-.950	-.963
1.6	-1.151	-1.163
1.7	-1.238	-1.245
1.8	-1.191	-1.194
1.9	-1.016	-1.015
2.0	-.742	-.740
2.1	-.483	-.481
2.2	-.313	-.311
2.3	-.203	-.201
2.4	-.133	-.130
2.5	-.088	-.085
2.6	-.058	-.055
2.7	-.039	-.036

Table I.2. Yaw rate as computed by "neighboring trajectory" (v_{init} = 10 inch/sec) and perturbation equations (ξ_o = 10 inch/sec). Oversteer car, with $\delta_o = 10^o$.

REFERENCES FOR APPENDIX I.

I.1. H. J. Pacejka, "Simplified Analysis of Steady-State Turning Behavior of Motor Vehicles," Vehicle Systems Dynamics, Vol. 2, 1978.

I.2. L. Cesari, Asymptotic Behavior and Stability Problems in Ordinary Differential Equations, 3rd Edition, Springer-Verlag 1971, p. 48.